TRANSPORT AND OPTICAL PROPERTIES FOR NANOSTRUCTURES UNDER THE INFLUENCE OF RASHBA SPIN ORBIT INTERACTION

Thesis

Submitted to

Delhi Technological University

In fulfilment for the requirements for the degree of

DOCTOR OF PHILOSOPHY

in

APPLIED PHYSICS

By

PRIYANKA

2K19/PHDAP/504

Under the Supervision of

PROF. RINKU SHARMA

Professor

Department of Applied Physics

Delhi Technological University, Delhi

DEPARTMENT OF APPLIED PHYSICS

DELHI TECHNOLOGICAL UNIVERSITY

DELHI-110 042, INDIA

October-2024

©Delhi Technological University-2024

All rights reserved.

Dedicated to my Maa and Bhai

DECLARATION

This is to certify that the Ph.D. thesis entitled **"*Transport and Optical Properties for Nanostructure under the Influence of Rashba Spin Orbit Interaction*"** submitted to Delhi Technological University (DTU) for the award of the degree of **"Doctor of Philosophy"** in Applied Physics is a record of bonafide work carried out by me under the guidance & supervision of ***Prof. Rinku Sharma*** at ***Atomic, Molecular and Terahertz Radiation Emission & Advance Simulation Lab***, ***Department of Applied Physics***, ***Delhi Technological University*** and has fulfilled the requirements for the submission of this thesis. The results contained in this thesis are original and have not been submitted to any other University/Institutions for the award of any degree or diploma.

Priyanka

Research Scholar

Roll No.: 2K19/Ph.D./AP/504

Department of Applied Physics

Delhi Technological University

Date:

Place: **Delhi**

DELHI TECHNOLOGICAL UNIVERSITY

Formerly Delhi College of Engineering

(Under Delhi Act 6 of 2009, Govt. of NCT of Delhi)

Shahbad Daulatpur, Bawana Road, Delhi-110042

CERTIFICATE

This is to certify that the Ph.D. thesis entitled **"*Transport and Optical Properties for Nanostructure under the Influence of Rashba Spin Orbit Interaction.*"** submitted to Delhi Technological University (DTU) for the award of the degree of **"Doctor of Philosophy"** in Applied Physics is a record of bonafide work carried out by me under the guidance & supervision of ***Prof. Rinku Sharma*** at ***Atomic, Molecular and Terahertz Radiation Emission & Advance Simulation Lab, Department of Applied Physics, Delhi Technological University*** and has fulfilled the requirements for the submission of this thesis. The results contained in this thesis are original and have not been submitted to any other University/Institutions for the award of any degree or diploma.

Priyanka

Roll No.: 2K19/Ph.D./AP/504

This is to certify that the above statement made by the candidate is correct to the best of our knowledge.

Prof. Rinku Sharma	**Prof. A. S. Rao**
Supervisor	Head of the Department
Department of Applied Physics	Department of Applied Physics
Delhi Technological University	Delhi Technological University
Delhi, India-110042	Delhi, India-110042

ACKNOWLEDGEMENTS

First and foremost, I wish to express my deepest gratitude to my parents and family, who have been the foundation of my emotional, physical, and mental well-being throughout my pursuit of this degree. Words cannot fully capture my indebtedness to them. As I write this thesis, I fondly remember my late father, ***Mr. Jai Kumar****, whose wisdom and encouragement since childhood instilled in me a love for learning and a desire for academic excellence. I am eternally grateful to him for embedding such invaluable principles in my life.*

The unwavering love, care, support, and blessings of my mother and brother, ***Mrs. Raj Bala*** *and* ***Mr. Neeraj Mann****, gave me the strength to undertake this work and see it through to the best of my abilities. Their constant belief in my potential and their encouragement during challenging times fueled my determination. I am forever indebted to their sacrifices, which allowed me to pursue my dreams without hesitation. My deepest gratitude to my beloved niece,* ***Gunika Mann****, whose innocent joy and unspoken support brought light and warmth to my journey. Her presence has been a constant reminder of the simple beauties in life, and her laughter has been a source of motivation during the most challenging moments of this work. I extend my heartfelt thanks to my sisters,* ***Mrs. Babita****,* ***Mrs. Sonia****,* ***Mrs. Monika****, and my sister-in-law,* ***Mrs. Himanshi****. I am immensely grateful to my fiancé,* ***Mr. Amit Shokeen****, whose steadfast encouragement has been my anchor, providing unwavering support. His belief in me, particularly during the final stages of my studies, has been a source of strength and motivation that I deeply cherish.*

Above all, I offer my boundless gratitude to ***Lord Krishna****, whose constant blessings empowered me to carry out this work successfully.*

Gratitude, when sincerely expressed, is a beautiful endeavour, yet no words can truly convey the depth of my appreciation. Over the past five years at Delhi Technological University, particularly within the ***Atomic, Molecular and Terahertz Radiation Emission & Advance Simulation Lab****, I have been fortunate to receive guidance and assistance from many kind souls, to whom I extend my sincere thanks.*

It is with great honor that I express my deep sense of gratitude, indebtedness, and respect to my supervisor, ***Prof. Rinku Sharma****, from the Department of Applied Physics at Delhi Technological University. It has been a privilege to work under such an enthusiastic, distinguished, and supportive mentor. Their unwavering encouragement, constant guidance, meticulous supervision, and constructive feedback have played a pivotal role in shaping this milestone in my academic journey.*

I also extend my heartfelt appreciation to ***Prof. A. S. Rao****, Head & DRC Chairperson, Department of Applied Physics, for their invaluable assistance and suggestions. I am equally grateful to* ***Prof. Vinod Singh****, DRC member, and the SRC and DRC committee members for their enduring support and thoughtful recommendations.*

I owe my sincere gratitude to ***Dr. Manoj Kumar*** *from the Department of Physics, Govt. College for Women, Jind, for his timely advice and support.*

It is my pleasure to express my sincere thanks to all the faculty members of Department of Applied Physics, DTU for their continuous encouragement and help during my research work. I am also grateful technical and non-technical staff for their timely support and cooperation whenever required.

I sincerely thank my dear former and present lab-mates whose support helped in accomplishing my work. It is my pleasure to thank my seniors ***Dr. Suman Dahiya*** *&* ***Ms. Richa***

for their support. I would also like to thank all the other research scholars of Department of Applied Physics, Delhi Technological University, Delhi for their help and advice. I wish to acknowledge the enjoyable company and suitable help rendered by my dear friends, ***Mr. Jasveer Singh, Ms. Sheetal Kumari, Ms. Vishakha Sharma, Ms. Aneesha, Dr. Mansha Kanshal, Ms. Ritu, Ms. Varnam Sherawat, Ms. Niama, Mr. Yash Pathak, Mr. Ankit Kumar, Mr. Rahul Kundara, Mr. Vishal Deswal*** *and* ***Mr. Vishnu Dubey*** *for their help and support during this tenure. Achieving a work-life balance is crucial, and it wouldn't have been possible without my friends* ***Mrs. Anjali Rana*** *and* ***Mrs. Neha****. These are my stress busters during this time.*

I gratefully acknowledge the financial assistance provided by ***University Grants Commission (UGC)*** *in the form of Junior Research Fellowship and Senior Research Fellowship during the period of my research. I extend my gratitude to* ***Delhi Technological University*** *and staff in* ***Administration****,* ***Accounts****,* ***Store & Purchase****,* ***Library*** *and* ***Computer Centre*** *for their help and services.*

I thank one and all for helping me accomplish the successful realization of the thesis.

Thank you all!!!

Priyanka

ABSTRACT

Transport and Optical Properties for Nanostructures under the Influence of Rashba Spin Orbit Interaction

Transport properties and non-linear processes via multiphoton transitions have been investigated in atomic, molecular, and bulk states theoretically and experimentally. Quantum nanostructures like quantum wells, wires and dots have been playing a key role in the investigation of transport properties and multi-photon processes as well as non-linear optical properties. These nanostructures have many important applications in optoelectronics, such as optical switching, THz multi-photon quantum well infrared photodetectors fusion of frequency up-conversion for bioimaging among other useful purposes. Much focus has recently been directed toward spin-dependent features because of the possible applications to novel generation and multifunction devices, in particular - towards spintronic type systems such as a Spin transistor or a Quantum computer. The study of spin-orbit interaction directly through this is used to perform the analysis on the basis of device functionality in a semiconductor nanostructure. To investigate the influence of this interaction on non-linear optical processes in such nanostructures, understanding is a must. It is, therefore, imperative to understand how quantum nanostructures couple and interact with strong fields in the presence of spin-orbit interaction for further developments at fundamental level as well scaling up novel devices based on spins. Moreover, parameters such as static magnetic and electric fields, the photon energy of laser field are crucial in investigating of electronic dispersion curve, ballistic conductance, linear and non-linear optical characters (referred to inter-band transitions in nanostructures).

Chapter 1 offers a concise introduction to nanostructures, external perturbations, as well as their linear and non-linear properties & transport properties, with an emphasis on multiphoton processes. It includes a brief discussion on the desired characteristics of nanostructures, specifically quantum wires and quantum dots, along with a focus on the selected material, highlighting its distinct properties.

Additionally, this chapter provides key definitions and explanations of various optical and transport properties. Optical properties describe how materials interact with light, involving processes such as absorption, reflection, and transmission. In contrast, nonlinear optical properties refer to the material's response to intense light, where the relationship between the input and output light is non-linear. Whereas, transport properties give the Ballistic conductance by the help of Landuer-Büttiker formalism.

In **Chapter 2**, we investigate the combined impacts of Rashba spin orbit-interaction, external electric field, magnetic field, and Aluminum concentration on energy dispersion and conductivity in a $Ga_{1-x}Al_xAs$ quantum wire. The Energy eigenvalues and eigenvectors are quantified using the diagonalization method and the transport properties are computed by Landuer-Büttiker formalism. It is noticed that the external electric field, magnetic field, Rashba spin-orbit interaction, and Aluminum concentration (impurity factor x) alter the energy spectra and conductivity. Hence, these parameters significantly affect the physical and transport properties.

Chapter 3 focuses on the electron quantum transport of a *GaAs* quantum wire at the nanoscale under the influence of hydrostatic pressure and temperature. The existence of spin-orbit coupling in the quantum wire has set up a propitious stage for the development of apparatus for electron transportation. Here, we analyze the impact of hydrostatic pressure and

temperature on the energy band structure as well as on the ballistic conductivity. The Energy eigenvalues and eigenvectors are found by using the diagonalization method and the ballistic conductance is computed by Landuer-Büttiker formalism. Also, we have studied the behaviour of energy concerning an external electric field, magnetic field and temperature. The system is expressed by parabolic confinement to the normal intense magnetic field and RSOI causes the collaborative impact of interior and exterior agents leading to downward/upward and lateral/vertical shifts in the dispersion. The oddity of the energy subbands results in oscillatory patterns in the ballistic conductance.

Chapter 4 provides the study of the impact of impurities on optical absorption coefficients, refractive index changes, second-harmonic generation, and third-harmonic generation for inter-subband transitions between electronic states in a $Ga_{1-x}Al_xAs$ quantum wire, driven by a symmetric parabolic potential. The system is influenced by an intense electric field, magnetic field, and Rashba spin-orbit interaction. The analytical expressions for linear and nonlinear optical absorption coefficients, refractive index changes, and both second and third harmonic generation are derived using the compact density-matrix approach.

The numerical results demonstrate that the optical properties are highly sensitive to impurity concentration and can be controlled through impurity. The shifts in peak magnitude and position due to the impurity factor reveal potential for manipulating optical non-linearity within the quantum wire and offering opportunities for tuning optical non-linearities with practical applications in devices.

Chapter 5 describes the optical properties of $In_xGa_{1-x}As$ quantum dot. First, we calculate the energy levels and wavefunctions in the presence of an impurity. Then, we examine how the impurity affects the absorption coefficients, refractive index changes, and third-harmonic

generation. The results show that as the impurity concentration increases, the absorption coefficients, refractive index changes, and third-harmonic generation peaks shift from their original positions and decrease in magnitude. This highlights the significant influence of impurity concentration on the optical properties of the nanostructure.

Chapter 6 delves into the the effect of both Rashba and Dresselhaus spin-orbit interactions in a system with double-well anharmonic confinement potential. We show that one can manipulate the energy band structure by tuning structural parameters of confinement potential and strengths of electric field, magnetic field, spin-orbit interactions. Moreover, we find that ballistic magnetoconductance oscillations are susceptible to spin-orbit induced modifications of the wire's energy dispersion in presence of magnetic and electric fields.

Chapter 7 indicates that the thesis conclusion with a summary, a brief recapitulation of the research presented in previous chapters and possible future approaches for extending work addressed.

References also form part along with bibliography at the end of each chapter.

LIST OF PUBLICATIONS

PUBLICATIONS RESULTING FROM THIS THESIS WORK (05)

Article in International Refereed Journals (05):

1. ***"Effects of impurity factor on the physical and transport properties for $Ga_{1-x}Al_xAs$ quantum wire in the presence of Rashba spin-orbit interaction";*** **Priyanka**, Rinku Sharma and Manoj Kumar, Physica B: Condensed Matter, 629 (2022), 413649.

2. ***"Effect of hydrostatic pressure and temperature on the ballistic conductance under the influence of Rashba spin-orbit coupling";*** **Priyanka**, Rinku Sharma, and Manoj Kumar, Physica B: Condensed Matter, 648 (2023), 414402.

3. ***"Hydrogenic impurity effect on the optical properties of $Ga_{1-x}Al_xAs$ quantum wire under terahertz field";*** **Priyanka**, Rinku Sharma, Manoj Kumar and Pradumn Kumar, Micro and Nanostructures, 173 (2023), 207451.

4. ***"Impact of impurity on the non-linear and linear optical properties of $In_xGa_{1-x}As$ quantum dot";*** **Priyanka** and Rinku Sharma, Solid state communication, 366–367 (2023), 115155.

5. ***"Impurity-modulated physical and transport properties in a $In_xGa_{1-x}As$ double quantum wire";*** **Priyanka** and Rinku Sharma, Physica B: Condensed Matter, 659 (2023), 414845.

PUBLICATIONS OTHER THAN THIS THESIS WORK (05)

Article in International Refereed Journals (05):

1. ***"Thermodynamic properties of $In_xGa_{1-x}N$ double quantum wire in the presence of impurity and Rashba spin-orbit interaction";*** **Priyanka** and Rinku Sharma, Physica B: Condensed Matter, 691 (2024), 416305.
2. ***"Combined effect of Rashba spin-orbit interaction, hydrostatic pressure and temperature on energy dispersion based ballistic conductance of InAs tunnel-coupled (double) quantum wire under exterior magnetic and electric field";*** Sukhvinder Kumar, **Priyanka,** Manoj Kumar and Anand Kumar, Physica B: Condensed Matter, 415715 (2024), 677.
3. ***"Hydrostatic Pressure Effect on the Thermodynamic Properties of Quantum Wire Under a Crossed Electromagnetic Field";*** Pranay Khosla, Yash Gupta, Sakshi Arora, **Priyanka** and Rinku Sharma; Journal of Low Temp. Phys, 213 (2023), 92–106.
4. ***"Impact of Impurity on the Mean Energy, Heat Capacity, Free Energy, Entropy and Magnetocaloric Effect of $Ga_{1-\chi}Al_{\chi}As$ Quantum Wire";*** Sakshi Arora, Yash Gupta, Pranay Khosla, **Priyanka** & Rinku Sharma; Journal of Low Temp. Phys, 212 (2023), 54–68.
5. ***"Thermodynamic Properties of Conical Quantum Dot Modulated by External Fields and Rashba Spin–Orbit Interaction";*** Yash Gupta, Pranay Khosla, Sakshi Arora, **Priyanka** & Rinku Sharma; Journal of Low Temp. Phys, 213 (2023,) 251–263.

International Conferences Presentation (06):

1. International Conference on ***"Nanotechnology: Opportunities & Challenges",*** Organised by Department of Applied Sciences & Humanities held on 28th-30th November 2022.
2. ***"International Conference on Physics" (ICOP-23),*** Organised by Institute for Scientific and Engineering Research (ISER) held on 8th January 2023, at Bangalore, India.
3. 2nd International Conference on ***"Advanced Functional Materials & Devices", (AFMD-2023),*** Organised by IQAC & Department of Physics, ARSD College, held on 13th -15th march 2023.
4. ***"SPIE Optics and Optoelectronics Conference",*** Organised by SPIE held on 24th- 27th April 2023 at Prague Czech Republic.
5. International Conference on ***"International Conference on Atomic, Molecular, Material, Nano and Optical Physics with Applications" (ICAMNOP–2023),*** Organised by Department of Applied Physics, Delhi Technological University held on 20th- 22th Dec 2023.
6. International Conference on ***"Frontiers in Optics + Laser Science 2024",*** Organised by FiO LS Management Optica (formerly OSA) held on 23th-26th Sept 2024.

TABLE OF CONTENTS

List of Figures

1

CHAPTER

Introduction

- *This Chapter presents a through background of the research work, with a primary emphasis on the importance of nanostructure like quantum wells, wires, and dots in the study of transport properties, multi-photon processes, and non-linear optical properties at the nanoscale.*
- *These structures have critical applications in optoelectronics, including optical switching, THz multi-photon infrared photodetectors, and bioimaging through frequency up-conversion.*
- *Spin-orbit interaction in semiconductor nanostructures is vital for understanding and enhancing the functionality of devices and analyzing linear & non-linear optical and transport properties.*
- *Parameters like static magnetic and electric fields, laser photon energy, electronic dispersion, ballistic conductance, and inter-band transitions are critical for evaluating both linear & non-linear optical and transport properties in nanostructures.*

1.1 BACKGROUND

These days, various technological improvements make it possible to fabricate semiconductor structures whose dimensions are in the nanometre range. There are two major factors responsible for the increasing interest in these semiconductor nanostructures. They are first of all scientifically interesting because they enable us to create artificial potentials for carrier electrons and holes in semiconductors at scales comparable or smaller than the de Broglie wavelength. Quantum confinement effects therefore are not only pronounced but can be designed to a large extent. Now, we are able to prepare semiconductor nanostructures with small length scales where previous theoreticians arrived at conclusions directly from theoretical considerations. Second, quantum mechanics has moved from the ideal to relevant case. Thus, confinement can enable new device concepts that alleviate constraints off the design in their absence [1–7].

In this same vein, recent theoretical works selecting different sizes of systems homogeneities down to low-dimensional geometries play a crucial role in the experience. These include confinement potentials (hard wall, harmonic oscillator and Gaussian) where the particle is localized [8–14]. Another profile is a one-dimensional double quartic-well potential, which has been studied extensively in physics and chemistry (also known as the quadratic anharmonic double well oscillator). It has been studied by quantum mechanical and semiclassical methods (WKB approximation, variational perturbation theory for calculating energy eigenvalues) this explains phenomena such as tunneling and doublet splitting. Owing to the opportunity of fabrication techniques, the double quantum structures have become remarkable systems as well as low-dimensional single structures in the last two decades. In addition, the double structures like double quantum well and double quantum wire (DQW) structures are important because

they may be used to explain the physical phenomenon's such as tunnelling and doublet splitting. Semiconductor nanostructure - in contrast to 0D materials, semiconductor structures are attractive for potential use in nanoelectronics and optoelectronics as a consequence of their tunable energy spectrum which depends on the size and shape. This tunability renders these materials interesting candidates to realize, for instance, quantum optical devices where the control of a qubit by photonic degrees of freedom is required as in many quantum information processing tasks [15–17].

The confinement can alter the energy spectrum (i.e. the set of discrete eigenenergy's) from a quantum well to wires and dots by tuning both size and shape, as well a strength of creating potential in each case. The confinement of the electron gas leads to significantly different phenomena compared to those observed in a three-dimensional electron gas. This confinement of the structures into low dimension manifests as discrete energy levels (sub-band) instead, hence Low-dimensional structures have received considerable attention due to their drastic modifications in absorption spectra and also because of the emergence of several new physical properties, such as electronic optical transportation features. These properties are crucial for various types of microelectronics devices (including resistors, capacitors, inductors transistors switches and modulators), optoelectronics devices that include LEDs laser diodes infrared emitters phototransistors solar cells etc. fluorescence device applications [18,19]. There are thousands of nanostructures (quantum dot & quantum wire) which can be a potential source for single photon emitters, here in the current thesis we concern two (nanostructure).

1.2 QUANTUM DOT

Semiconductor quantum dots are essentially artificial atoms, as they act like nanoscale zero-dimensional systems that exhibit distinct energy levels such to those of naturally occurring atom. Due to quantum confinement, they can be shaped externally (as in by semiconductor processing), controlled in terms of shape or number electrons by bands edges moving around instead. Even though they are man-made devices, these structures resemble natural atoms. Quantum dots generally are created by confining electrons in a lateral or vertical manner within semiconductor thin films, using electrostatic gates to control the number of electrons and their repartition. This forms a potential well similar to that of an empty bowl, which captures conduction electrons [20,21]. The first quantum dot material was developed in the early 80s by A. I. Ekimov et al. [22], raising a plethora of experimental and theoretical studies on its properties, nature and potential applications ultimately. There have been countless methods developed to make quantum dots but in general they can be separated into a couple of groups such as; high-energy processes (e.g. MBE, Molecular Beam Epitaxy or MOCVD, Metal-organic Chemical Vapor Deposition) and chemical synthesis via controlled nucleation and growth in solution Harmonic potential confinement is a widely studied and practical approximation used to model the movement of ions in theoretical studies [23–27]. Through electrostatic gates, changes in geometry or applied magnetic fields the properties of quantum dots can be adjusted and studies allow to have insights into Quantum effects in finite low-dimensional systems [28,29].

1.2.1 Electron States of Quantum Dot

When electrons are confined in all three spatial dimensions, a quantum dot is fully quantized in all directions. Consequently, the potential energy must be expressed as $V(\vec{r}) = V(x,y,z)$ for quantum dots. Thus, the time-independent Schrödinger equation becomes:

$$\left[-\frac{\hbar^2}{2m_e^*}\left(\frac{\partial^2}{\partial x^2}+\frac{\partial^2}{\partial y^2}+\frac{\partial^2}{\partial z^2}\right)+V(x,z)\right]\psi(x,y,z)=E\psi(x,y,z) \quad \textbf{(1.1)}$$

And the wavefunction is given by

$$\psi(x,y,z)=\phi(x,y,z)e^{i0x} \quad \textbf{(1.2)}$$

The wave function and total energy derived from solving the Schrödinger equation for various potential profiles can be expressed as:

$$\psi_{p,q,r}(x,y,z)=\phi_{p,q,r}(x,y,z), \quad \textbf{(1.4)}$$

$$\text{And } E_{p,q,r}=\varepsilon_{p,q,r}\ . \quad \textbf{(1.5)}$$

with $\phi_{p,q,r}(x,y,z)$ and $\varepsilon_{p,q,r}$ are known as quantised energy and corresponding wave function for x, y and z directions, respectively.

1.3 QUANTUM WIRE

The quantum wire is the closest thing yet to a truly one-dimensional electronic transport nanostructure, because electrons are confined by a two-dimensional (two dimensional) structure so that they can move freely only in this direction. In condensed matter physics, semiconductor quantum wires are important quasi-one-dimensional systems that have attracted considerable attention because of the applications related to spintronic technology for which they can be platform [30,31]. A droplet is a linear feature, which forms along two-dimensional electron gases at the interface of semiconductor heterostructures that restrict electrons to effective widths on the order of their de Broglie wavelength. Usually, the confinement in one dimension is assumed to be parabolic and this defines a "quantum wire". Quantum wire

experimentally and theoretical calculations have pointed out the importance of spin-dependent electronic as well as optical properties in quantum wires with their asymmetric SO coupling for future developments in practical technologies such as spintronics [32].

1.3.1 Electron States of Quantum Wire

A 2DEG exists when electrons are free to move in two dimensions (in a plane, say), but confined motion is restricted along the third dimension. This confines quantum wire formation. In order to design the quantum wire, confinement potential in two dimensions has to be achieved. If we take potential to be $V(\vec{r})$ or, for instance, $V(x,z)$ the eigenvalue equation will look as

$$\left[-\frac{\hbar^2}{2m_e^*}\left(\frac{\partial^2}{\partial x^2}+\frac{\partial^2}{\partial y^2}+\frac{\partial^2}{\partial z^2}\right)+V(x,z)\right]\psi(x,y,z)=E\psi(x,y,z) \quad \textbf{(1.6)}$$

And the wave function comes out to be

$$\psi(x,y,z)=\phi(x,z)e^{ik_y y}, \quad \textbf{(1.7)}$$

Under these conditions, the wave function of the quantum wire system can be determined as follows:

$$\psi_{p,k_y,r}(x,y,z)=\phi_{p,r}(x,z)e^{ik_y y}, \quad \textbf{(1.8)}$$

$\phi_{p,n}$ is the associated wave function and the total energy is given below

$$E_{p,r}(k_y)=\varepsilon_{p,r}+\frac{\hbar^2 k_y}{2m}. \quad \textbf{(1.9)}$$

Here, $\varepsilon_{p,r}$ is the quantized electron energy for the x and z- direction.

1.4 NANOSTRUCTURE SPINTRONICS

Electrons have spin (which is an intrinsic angular momentum) and charge. The spins of an electron system produce a total magnetic momentum. Electron spin has also been proposed as a suitable candidate for processing information in low-dimensional semiconductor structures alongside charge. This led to the emergence of spintronics (shown as in **Figure 1.1**). A very significant spintronics device is the Datta-Das Spin Field Effect Transistor. The controlling of electron spins by electric gates (electrostatic fields) is an essential for fabricating replenishable spintronic devices [33]. Among these various technologies, spin-based device concepts have emerged where in one can control the direction of its magnetic moment and such devices are believed to be more powerful compared to current pharmaceutical ion channel-like charging mechanisms [34–36].

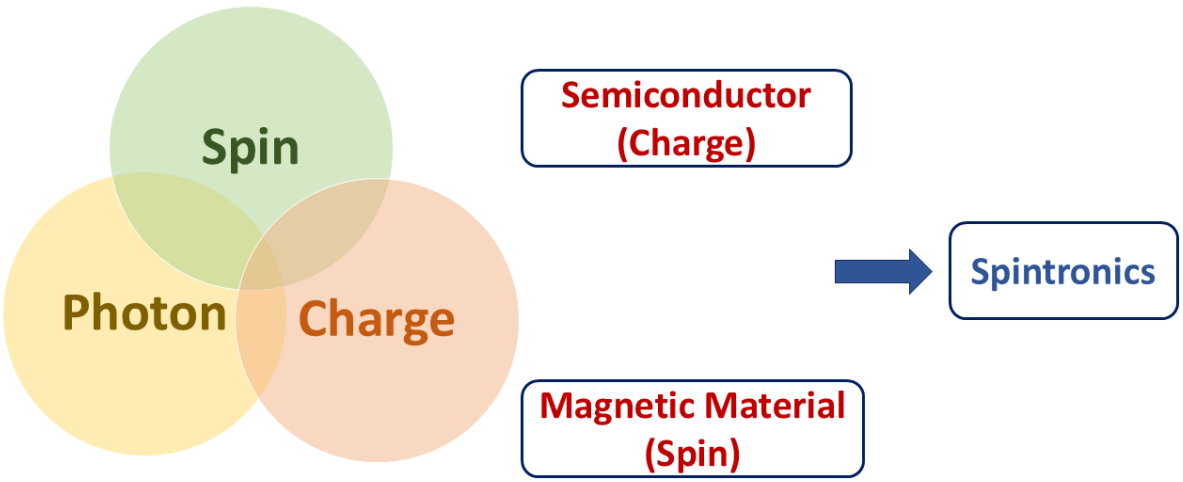

Figure 1.1 Diagram for the Spintronics

So far, conventional semiconductor devices have had to apply a relatively high number of electrons into or out the conduction band through an external electric field in order for

switching to occur. This conversion of electrons uses up energy and time. The thing is that, instead of manipulating electrons for logic gates or sensing applications like other approaches to develop sensors and circuits do, spintronic devices only need the change in orientation (up / down) of these spins. During the injection and transport of electrons in a semiconductor, while playing with most (actually not all) spin-containing structures modifying their orientation under special circumstances as usually is performed by means of SOI effects, it turns out that spins do follow to applied electric fields within very standard Si/SiGe heterostructure designs [37].

1.4.1 Dirac equation for Spin-orbit interaction

One can derive the spin-orbit interaction term by taking a non-relativistic limit of Dirac equation. For electrons, the Dirac equation is accurate and we can add a potential $V = -{e^2}/{r}$ to Hamiltonian of an electron in a hydrogen atom. For instance, the Dirac equation becomes [38]:

$$\left(c\vec{\alpha} \cdot \vec{P} + \beta mc^2 + V\right)\psi = E\psi \qquad \textbf{(1.10)}$$

Where, *c* and $\vec{P}$ are known as speed of light and momentum vector, $\vec{\alpha}$ includes Pauli spin matrix and β are written as:

$$\vec{\alpha} = \begin{pmatrix} 0 & \vec{\sigma} \\ \vec{\sigma} & 0 \end{pmatrix}\ ,\ \beta = \begin{pmatrix} 1 & 0 \\ 0 & 1 \end{pmatrix} \qquad \textbf{(1.11)}$$

For the upper (ψ) and lower (ϕ) wave function, we rewrite the eq. 1.10

$$\begin{pmatrix} E - V - mc^2 & -c\vec{\sigma} \cdot \vec{P} \\ -c\vec{\sigma} \cdot \vec{P} & E - V + mc^2 \end{pmatrix}\begin{pmatrix} \psi \\ \phi \end{pmatrix} = \begin{pmatrix} 0 \\ 0 \end{pmatrix} \qquad \textbf{(1.12)}$$

From this expression, two differential equations are coming out:

$$(E - V - mc^2)\,\psi - \left(c\vec{\sigma}\cdot\vec{P}\right)\varphi = 0, \tag{1.13}$$

$$(E - V + mc^2)\,\psi - \left(c\vec{\sigma}\cdot\vec{P}\right)\varphi = 0. \tag{1.14}$$

Using eq. (1.14) eq. in eq. (1.13), we obtain

$$(E - V - mc^2)\,\psi = \left(c\vec{\sigma}\cdot\vec{P}\right)\left(\frac{1}{E-V+mc^2}\right)\left(c\vec{\sigma}\cdot\vec{P}\right)\psi. \tag{1.15}$$

The energy eigenvalue of the Schrödinger equation, $E_s = E - mc^2$ enables us to deal with the non-relativistic situation where we require that $E_s << mc^2$. Since $V << mc^2$, we may expand the energy denominator on RHS of eq. 1.15

$$\frac{1}{E - V + mc^2} = \frac{1}{E_s + 2mc^2 - V} = \frac{1}{2mc^2}\left(1 + \frac{E_s - V}{2mc^2}\right)^{-1}$$

$$\approx \frac{1}{2mc^2}\left(1 - \frac{E_s - V}{2mc^2}\right) = \frac{1}{2mc^2} - \frac{E_s - V}{4m^2c^4} \tag{1.16}$$

If we only consider the lowest term in this expansion, we obtain the non-relativistic Schrödinger equation, represented as $1/2mc^2$. Including higher-order terms introduces the fine structure. This transformation leads us to eq. (1.15)

$$E_s\,\psi = \left(\frac{P^2}{2m} + V - \frac{\vec{\sigma}\cdot\vec{P}(E_s - V)\vec{\sigma}\cdot\vec{P}}{4m^2c^2}\right)\psi \tag{1.17}$$

To eliminate the E_s on the right side of the equation, and taking into account the commutative properties of *V* and *σ*, the following expression can be derived:

$$(E_s - V)\,\vec{\sigma}\cdot\vec{P}\psi = \vec{\sigma}\cdot\vec{P}(E_s - V)\psi + \vec{\sigma}[(E_s - V), P]\psi$$

$$= \left(\vec{\sigma}\cdot\vec{P}\right)\frac{P^2}{2m}\psi + \vec{\sigma}[\vec{P}, V]\psi. \qquad \textbf{(1.18)}$$

Put eq. 1.18 in eq. 1.17, we get

$$E_s\,\psi = \left(\frac{P^2}{2m} + V - \frac{P^4}{8m^3c^2} - \frac{(\vec{\sigma}\cdot\vec{P})\cdot(\vec{\sigma}\cdot[P,V])}{4m^2c^2}\right)\psi$$

$$= \left(\frac{P^2}{2m} + V - \frac{P^4}{8m^3c^2} - \frac{i(\vec{\sigma}\cdot\vec{P})\times[P,V]}{4m^2c^2} - \frac{\vec{P}\cdot[\vec{P},V]}{4m^2c^2}\right)\psi. \qquad \textbf{(1.19)}$$

Here, the first two terms are understood to be the Hamiltonian for the non-relativistic Schrödinger equation. The third term adds the correction to relativistic kinetic energy. The fourth term involves the spin-orbit interaction, whereas known as an energy shift from a final term. We can write out the spin-orbit interaction term with a minor bit of algebra to simplify our result.

$$\left[\vec{P}, V\right]\psi = \left(\vec{P}V - V\vec{P}\right)\psi = \left(i\hbar\nabla\frac{e^2}{r} - \frac{e^2}{r}i\hbar\nabla\right)\psi$$

$$= i\hbar e^2\left(\left(\nabla\frac{1}{r}\right)\psi + \frac{1}{r}\nabla\psi - \frac{1}{r}\nabla\psi\right) = i\hbar e^2\frac{\vec{r}}{r^3}\psi, \qquad \textbf{(1.20)}$$

$\hbar$ is known as Planck constant. The Hamiltonian for the spin-orbit interaction becomes,

$$H_{SO} = -\frac{i\vec{\sigma}\cdot\vec{P}\times\left[\vec{P}, V\right]}{4m^2c^2} = -\frac{i\vec{\sigma}\cdot\vec{P}\times(-i\hbar e^2\frac{\vec{r}}{r^3})}{4m^2c^2}$$

$$= -\frac{\hbar e^2\vec{\sigma}\cdot(\vec{P}\times\vec{r})}{4m^2c^2r^3} = \frac{e^2}{4m^2c^2r^3}\left(\frac{\hbar}{2}\vec{\sigma}\right)\cdot(\vec{r}\times\vec{P})$$

$$= \frac{e^2}{2m^2c^2r^3}\vec{S}\cdot\vec{L}. \qquad \textbf{(1.21)}$$

Here, vector operator for the spin is represented by the spin space and also called spin angular momentum and $\vec{L}$ is known as orbital angular momentum.

1.4.2 Spin-orbit interaction

The spin-orbit interaction (SOI) or spin-orbit coupling, which are both the name of an internal force that is complex and not fully understood. As its name implies, SOI relates the spin dynamics of an electron to how it orbits in space. Two energy wells are formed in SOI, which generates internal magnetic field by the direction and velocity of electron transport inside a material that causes splitting between spin-up and spin-down electrons. Solid-state systems exhibit three principle sources of SOI. One is impurities in the conduction layer that are usually unimportant for low dimensional electron gas systems [39]. The second is through the absence of bulk inversion symmetry which occurs naturally in zinc-blende structures where two face-centered cubic (fcc) lattices are occupied by different atoms. It leads to a crystal potential that has effects on electrons moving in the lattice, giving them spin-splitting up to quantum states with zero momentum. This so-called Dresselhaus SOI was already introduced in the theoretical work [40]. A third source of SOI is the structural inversion asymmetry in a heterostructure, which splits the low-lying conduction band into two nondegenerate bands. This potential generates a macroscopic electric field when two-dimensional motions of electrons are enforced. Within this field, the motion of electrons contributes to an effective magnetic field that destroys spin degeneracy in their band structure at nonzero wave vectors. This is the Rashba SOI, which was first introduced by Rashba [41] (as shown in **Figure 1.2**).

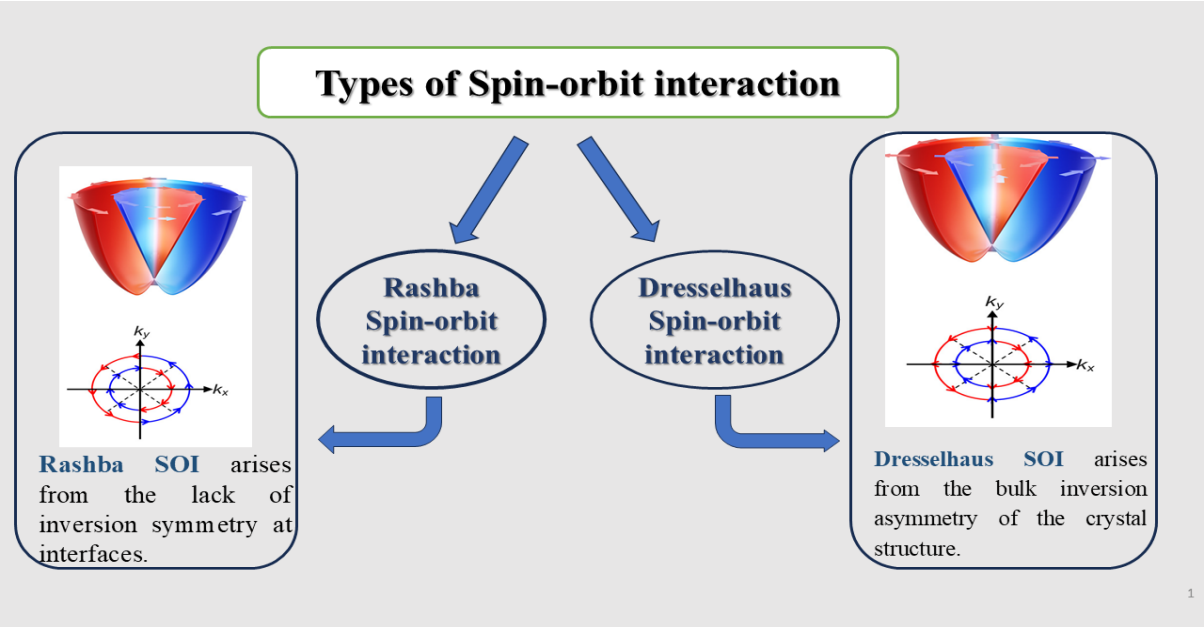

Figure 1.2 Schematic diagram for the types of Spin orbit-interaction

1.4.3 Dresselhaus Spin-Orbit Interaction

The Dresselhaus spin-orbit interaction (DSOI) comes from the microscopic electric field induced by breaking of inversion symmetry in the bulk structure semiconductor material with zinc-blende type crystal lattice. The power of the DSOI is also subjected to both thickness and effective dimension [42]. The DSOI Hamiltonian is:

$$H_D = \frac{\beta}{\hbar}\vec{\sigma}\cdot\vec{k} \tag{1.22}$$

Here, β, $\vec{\sigma}$ and $\vec{k}$ are known as DSOI coupling constant, Pauli matrices and kinematic operator components, respectively.

$$\vec{\sigma} = \sigma_x\hat{\imath} + \sigma_y\hat{\jmath} + \sigma_y\hat{\jmath} \text{ and } \vec{k} = k_x\hat{\imath} + k_y\hat{\jmath} + k_y\hat{\jmath} \tag{1.23}$$

Where,

$$\sigma_x = \begin{pmatrix} 0 & 1 \\ 1 & 0 \end{pmatrix},\ \sigma_x = \begin{pmatrix} 0 & -i \\ i & 0 \end{pmatrix}, \text{ and } \sigma_z = \begin{pmatrix} 1 & 0 \\ 0 & -1 \end{pmatrix}, \quad \textbf{(1.24)}$$

$\pi_q = p_q + eA_q$ under the influence of an external magnetic field (where and for (q = x, y, z) represent the components of momentum and the vector potential associated with the external magnetic field, respectively. Therefore, $k_x = \pi_y\pi_x\pi_y - \pi_z\pi_x\pi_z$ and the other component of kinematic operator [43,44]:

$$k_x = \frac{1}{2}\Big\{(p_x + eA_x)[\big(p_y + eA_y\big)^2 - (p_z + eA_z)^2] + [\big(p_y + eA_y\big)^2 - (p_z + eA_z)^2](p_x + eA_x)\Big\}, \quad \textbf{(1.25)}$$

$$k_y = \frac{1}{2}\big\{\big(p_y + eA_y\big)[(p_z + eA_z)^2 - (p_x + eA_x)^2] + [(p_z + eA_z)^2 - (p_x + eA_x)^2]\big(p_y + eA_y\big)\big\}, \quad \textbf{(1.26)}$$

And

$$k_x = \frac{1}{2}\Big\{(p_z + eA_z)[(p_x + eA_x)^2 - \big(p_y + eA_y\big)^2] + [(p_x + eA_x)^2 - \big(p_y + eA_y\big)^2](p_z + eA_z)\Big\}. \quad \textbf{(1.27)}$$

For the DSOI, we consider a low-dimensional system where the growth direction is [001], and an external magnetic field is applied in the z direction. Furthermore, we can approximate the operators p_z and ${p_z}^2$ along the z-direction as their expectation values, $< p_z >$ and $< {p_z}^2 >$. In contrasts, the term $\sigma_z k_z$ can be ignored as $< p_z > = 0$ and $A_z = 0$ [44]. In the case of bulk inversion symmetry, linear and trilinear contributions to the DSOI exist as a consequence of the destruction of inversion symmetry: the linear term is

$$H_D = \frac{\beta}{\hbar} < p_z{}^2 > \left[\sigma_y\left(p_y + eA_y\right) - \sigma_x(p_x + eA_x)\right], \quad \textbf{(1.28)}$$

Consider $\alpha_D = \beta < p_z{}^2 >$ where $< p_z{}^2 >$ is a constant term. The linear and the trilinear Hamiltonian term for DSOI:

$$H_D = \frac{\alpha_D}{\hbar}\left[\sigma_y\left(p_y + eA_y\right) - \sigma_x(p_x + eA_x)\right], \quad \textbf{(1.29)}$$

$$H_D{}^3 = \frac{\beta}{\hbar}\left[\sigma_x(p_x + eA_x)\left(p_y + eA_y\right)^2 - \sigma_y\left(p_y + eA_y\right)(p_x + eA_x)^2\right]. \quad \textbf{(1.30)}$$

For nanostructure, the trilinear Hamiltonian term of DSOI is neglected as a consequence of dominant linear Hamiltonian term [45].

1.4.4 Rashba Spin-orbit interaction

This SOI occurs only in semiconductors heterostructures. The RSOI originates from a macroscopic electric field that is, in turn, generated by the inversion asymmetry of the confining potential along growth direction (as seen by **Figure 1.3**). It is shown that RSOI can be controlled by a gate electric field. The characteristic beating pattern of Shubnikov-de Haas oscillations in the magnetoresistance of a two-dimensional electron gas can be used to determine the magnitude coupling parameter [35]. The RSOI Hamiltonian in configuration space for a thin system with 2D confinement only grown along the z-direction can be written as [46,47]:

$$H_R = \frac{\alpha_R}{\hbar}\left[\vec{\sigma} \times \left(\vec{p} + e\vec{A}\right)\right]_z \quad \textbf{(1.31)}$$

α_R is called as RSOI constant.

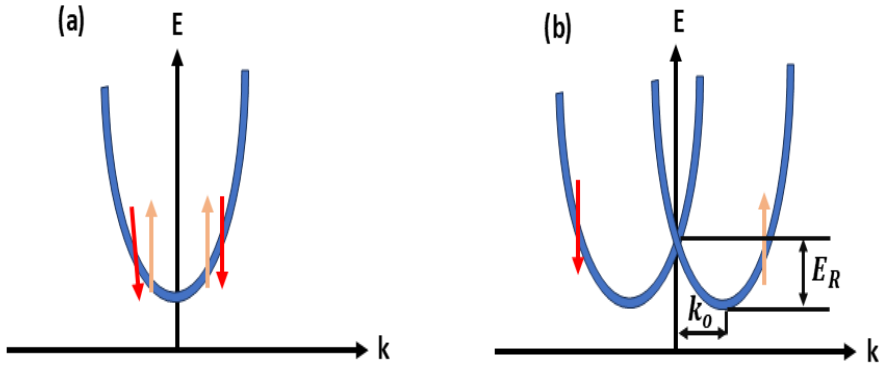

Figure 1.3 Energy dispersion curve (a) without RSOI and (b) with RSOI.

1.5 ZEEMAN EFFECT

When an atomic or molecular structure is in an external magnetic field its energy level also divides into gest of closely spaced lines. The Zeeman effect is the phenomenon where, when an object emitting or absorbing light is placed in a magnetic field, its spectrum changes. In the presence of an external magnetic field a splitting in energy occur with respect to how the atom interacts with this magnetic field [48]. The shift of atomic energy levels is given by

$$\Delta E = -\vec{\mu} \cdot \vec{B} \tag{1.32}$$

Here, $\vec{\mu}$ and $\vec{B}$ are known as magnetic dipole moment and magnetic field, respectively. The energy of this shift is orientation-dependent based on where the magnetic field and a sample's own magnetic moment are relative to each other. There are two types of magnetic moments in an atom, one due to the orbital angular momentum of electrons and other being it due to

intrinsic spin angular momentum of the electron. The spin angular momentum will be denoted as $\vec{S} = \frac{\hbar}{2}\vec{\sigma}$ and the associated magnetic moment is given by

$$\vec{\mu}_s = \frac{\mu_B g^*}{\hbar}\vec{S} \tag{1.33}$$

or

$$\vec{\mu}_s = \frac{\mu_B g^*}{\hbar}\vec{\sigma} \tag{1.34}$$

Here, μ_B is known as Bohr magneton and its value is defined by $\mu_B = \frac{e\hbar}{2m}$. g^* is known as effective Lande-*g* factor and its value for free electron is 2. In the existence of external applied magnetic field, the energy state levels are spilt into two sublevels, one corresponding to spin-up and other for the spin-down. For a single electron with only intrinsic spin angular momentum, the Zeeman Hamiltonian is given by

$$H_z = -\vec{\mu}_s \cdot \vec{B} = -\frac{\mu_B g^*}{2}\vec{\sigma} \cdot \vec{B} \tag{1.35}$$

1.6 NON-LINEAR MULTIPHOTON

Recently, a great effort, both theoretical and experimental in the field of quantum dynamics under strong nonstationary external fields has been increasing dynamically throughout this decades. The investigation of quantum mechanics with explicitly time-dependent Hamiltonians has helped uncover many otherwise hidden phenomena that are not visible via the more traditional methods based on stationary quantum mechanics [49]. Years later, the development of laser and maser technologies has led to the discovery of new phenomena in nonlinear quantum systems coupled with strong electromagnetic fields. More recently, study has been

expanded to low-dimensional semiconductor nanostructures in which strong electric fields lead to nonlinear multiphoton processes. These methods have relevance in opto-electronic device applications. Low-dimensional semiconductor heterostructure systems have demonstrated a plethora of optical characteristics superior to their 3D analogues as result of the confinement region smaller than bulk materials. [50,51].

A. K. Jaiwal et al. brought the first ideas of two-photon transitions in 1931 [52], multi-photon transitions have obsessed physicists for a while. The cross-section for multi-photon transitions is very small, so witnessing these nonlinear processes necessitates a high radiation source. Lasers, developed in the 1960s, provided physicists with this indispensable tool: an intense source of optical radiation. Kaiser and Garrett [53] first made competitive experimental observation of the nonlinear absorption in CaF2: Eu3+ with two-photon processes. In 1964, Singh and Bradley [54] observed three-photon excited fluorescence in naphthalene crystals as evidence of the dependence between nonlinear absorption and fluorescence in crystals. Ever since then, multi-photon excitation has been increasingly used for the molecular spectroscopy of many materials [55].

Quantum nanostructures have shown promising application potential as emerging nonlinear media for multiphoton processing-all-optical frequency up-conversion [56,57], ultrafast optical switching [58], THz multi-photon quantum well infrared photodetectors [59] and high-order nanocrystal based two or three-photon scanning bioimaging [60] etc. Multi-photon excitation is especially significant in the creation of ultra-sensitive quantum well infrared photodetectors (QWIPs). This advantage of multi-photon over single-photon processes was recently shown by Schneider et al. [61] who observed the photocurrent to scale quadratically with incident power when laser light illuminated two bound states and one continuum state. They also observed that

the second intermediate state contributes to optical nonlinearity, making it possible for these systems to serve as extremely sensitive low-power nonlinear devices [62].

1.7 NON-LINEAR OPTICAL PROCESSES

The study focuses on phenomena resulting from the alteration of a material system's optical properties due to the presence of intense laser light. In linear optics, the induced polarization depends linearly on the electric field, as shown by

$$\vec{P}(\omega) = \varepsilon_o \chi^{(1)} \vec{E}(\omega) \quad \textbf{(1.36)}$$

Here, ε_o and $\chi^{(1)}$ are known as permittivity in vacuum and linear susceptibility, respectively. For the nonlinear study, material's optical response is defined by the eq. (1.36) with the help of polarisation $\vec{P}(\omega)$ power series of applied electric field $\vec{E}(\omega)$ as:

$$\vec{P}(\omega) = \varepsilon_o(\chi^{(1)}\vec{E}^1(\omega) + \chi^{(2)}\vec{E}^2(\omega) + \chi^{(3)}\vec{E}^3(\omega)+\dots) \quad \textbf{(1.37)}$$

The $\chi^{(2)}$ and $\chi^{(3)}$ are called second and third order non-linear optical susceptibilities. And the terms $\vec{P}^2(\omega) = \varepsilon_o \chi^{(2)}\vec{E}^2(\omega)$ and $\vec{P}^3(\omega) = \varepsilon_o \chi^{(3)}\vec{E}^3(\omega)$ are known as second and third order non-linear polarizations, respectively. Typically, only laser light is intense enough to alter the optical properties of a material system, as nonlinear susceptibilities are generally much smaller than linear susceptibility. In linear optics, the refractive index is given by

$$n = \sqrt{\epsilon_r} = \sqrt{(1+\chi^{(1)})}, \quad \textbf{(1.38)}$$

In this context, ϵ_r represents the relative permittivity of a nonmagnetic material system. The term $1+\chi^{(1)}$ is basically nothing but the dielectric constant of medium. The linear properties

are described by the first-order susceptibility and other susceptibilities of higher order contribute non-linear effects, which depend on the molecular configuration. In silica glass $\chi^{(2)}$ is negligible. Still, the lowest-order non-linear susceptibility giving rise to macroscopic effects in optical fibres is the third order $\chi^{(3)}$. This sensitivity can cause several phenomena as the third harmonic generation, four wave mixing (FWM) and non-linear refraction. We have studied various non-linear optical properties like absorption coefficient, refractive index changes, third harmonic generation and Optical rectification using our method [63–67].

Optical rectification is a non-linear optical process in which an intense light beam incident on a second-order nonlinear medium generates (rectifies) the QPM dc polarization. Optical rectification is a second-order process with respect to optical field strengths and can be seen as the inverse of the electro-optic effect at typical intensities. The effect was first observed in 1962 [49] when radiation from a ruby laser was transmitted through potassium deuterium phosphate and potassium dihydrogen phosphate crystals. Here, the electric field strength of laser beam is given by:

$$E(t) = \frac{1}{2}\left[Ee^{i\omega t} + E^{*}e^{-i\omega t}\right] \quad \textbf{(1.39)}$$

For the crystal in which $\chi^{(2)}$ is non-zero. The value of the non-linear polarization is given by $P^2 = \chi^2 E^2(\omega)$ or expressed as $P^2 = 2\chi^2 \vec{E}\vec{E}^{*} + \chi^2 \vec{E}^2 e^{-i2\omega t} + \cdots$.

The second part of the polarization involves to terms, in which one is zero-frequency (first term) and other has frequency 2ω representation. Its zero-frequency term is optical rectification, which produces a constant electric field inside the nonlinear process. The density matrix formalism can also be used for analysing the nonlinear processes.

1.8 DENSITY MATRIX FORMALISM

This formally requires the use of density matrix, and it is particularly useful for description of relaxation effects due to interactions that have not been treated quantitatively within a many-particle approach (e.g. electron-phonon interaction in QDs or collision-induced resonance broadening in atomic vapor systems). This is in contrast to pure theoretical wave function methods, present a transparent way of describing linear and non-linear features even at properties across or close-to resonance (minimal detuning). Despite being correct for a pure state, the time-dependent Schrödinger equation (TDSE) provide no relief when it comes to describing statistical mixtures of states with classical probabilities due to all kinds of interactions are not included. This goes under the density matrix formalism, which starts with a definition of some kind of "density operator" as:

$$\rho = \sum_k p_k |\psi_k\rangle\langle\psi_k| \tag{1.40}$$

Thus, the elements of the density matrix are

$$\rho_{nm} = \langle u_n|\rho|u_m\rangle = \sum_k p_k c_n^k(t) c_m^{k^*}(t) \tag{1.41}$$

The summation over k represents the ensemble average or simply an averaging over all quantum states. The density matrix element ρ_{nn} correspondigly gives the probability that system is found in an energy eigenstate $|u_n\rangle$. The off-diagonal element $\rho_{nm} = \rho_{nm}{}^*$ corresponds to a coherent mixture of energy eigenstates $|u_n\rangle$ and $|u_m\rangle$ (and in the absence of such coherence it is zero). We can also use the density matrix to compute, <*A*> where *A* is observable represented by the Hermitian operator *A*. The expectation value of the observable, in a single state listed above is given by an ensemble average <*A*> for a system:

$$<A> = \sum_k \langle \psi_k | A | \psi_k \rangle \quad \textbf{(1.42)}$$

Or it can be written as;

$$<A> = \sum_{nm} \rho_{nm} A_{nm} \text{ or } <A> = Tr\,(\rho A). \quad \textbf{(1.43)}$$

We need to know the dynamics of the density matrix itself in order to be able describe how any observable related with the system behaves. The expression for the time variation of this density matrix is given by:

$$\dot{\rho} = \frac{1}{i\hbar}[H, \rho] + \sum_k |\Psi_k\rangle \langle \Psi_k| \frac{d}{dt} p_k \quad \textbf{(1.44)}$$

The first term on the right-hand side describes commutation of the Hamiltonian with density operator, and second one relates to relaxation. In a clean state the classical probability of these quantum states has a zero-time derivative. At the sixth order itself this derivative is zero but in a statistical mixture of states, these causes themselves being statistics (phonon-electron interactions) it will be non-zero. The confounding dynamics of the interactions cannot be written down explicitly in time, and are instead lumped into a phenomenological relaxation term which simplifies the eq. (1.44) to:

$$\dot{\rho} = \frac{1}{i\hbar}[H, \rho] - \Gamma(\rho - \rho^{eq}) \quad \textbf{(1.45)}$$

The rate of decay is shown in Γ denotes the density matrix ρ tends to its equilibrium state formed by ρ^{eq}. In the case when Hamiltonian does not contain interaction terms, diagonal elements of density matrix become stationary and oscillatory behaviour is acquired by off-diagonal ones. In addition to external fields such as electric and magnetic fields are used, in order to study the linear and non-linear optical properties of nanostructures more accurately.

Finally, we investigate relativistic effects in nanostructures, with a focus on the appearance of Rashba spin-orbit interaction.

1.9 QUANTUM TRANSPORT IN NANOSTRUCTURES SYSTEMS

The search for ever smaller structures and low-dimensional properties of materials has pushed the research to the mesoscopic regime. Material, or matter in general that is divided into three categories based on scale: macroscopic, microscopic and mesoscopic. Macroscopic systems are the ones clearly visible to the eye and microscopic ones like atoms, molecules etc. with too small size for us can't perceive them directly. Our focus of this review is on mesoscopic systems, located in a "middle-ground scale" (10^{-6}–10^{-9}m), larger than just some atoms or molecules yet small that they do not concord with classical objects. Mesoscopic systems are great for studying both macro and microscopic properties simultaneously, which is perfect when you need it to be controlled so that we can look at the most fundamental quantum mechanical features.

In macroscopic conductors, conductivity (σ) characterizes the transport properties that are material dependent. Where such a conductor is conductance obey Ohm's law with A being across-sectional area and L being length of the conductor.

$$G = \frac{A}{L}\sigma \qquad \textbf{(1.46)}$$

From eq. (1.46), if we made the length extremely short, *G* could be infinity large for a conductor. Yet, this ohmic behaviour is of a different nature than the mesoscopic one that always applies to micro and micropumps. To know this limit, you have to think about electron's quantum nature. Although electrons refer to as particles, unlike classical particles they display

properties of waves and wave-particle duality. In the mesoscopic systems, which is important for determining and identifying different transport regimes.

1.9.1 Characteristic length

Since low-dimensional quantum systems exhibit novel transport properties, we must consider important lengths other than the dimensions of a given sample to study those phenomena [68]. Here are these lengths with a short description of each.

1.9.2 Wavelength (λ)

The transport properties are dominated by quantum mechanics when a sample of material is small enough that its size causes it to affect electron movement. We define the de Broglie wavelength as

$$\lambda = \frac{2\pi\hbar}{p} = \frac{2\pi}{k} \tag{1.47}$$

where *p* represents the typical electron momentum and *k* is the electron wave vector. The Fermi wavelength λ_F is similarly defined as the de Broglie wavelength at the Fermi surface,

$$\lambda_F = \frac{2\pi}{k_F} \tag{1.48}$$

The Fermi wave vector k_F varies with dimensionality. For a two-dimensional electron gas (2DEG), $k_F = \sqrt{2\pi n_s}$, where n_s represents the electron density. The corresponding Fermi wavelength is given by:

$$\lambda_F = \sqrt{\frac{2\pi}{n_s}} \tag{1.49}$$

The current is carried among the electrons near the Fermi energy at low temperatures. As such, the Fermi wavelength is a crucial length scale for quantum features. Technically, you should use quantum mechanics for anything involving length scales as large or smaller than the Fermi wavelength.

1.9.3 Mean Free Path (L_{mf})

The mean free path quantifies the average distance travelled by an electron before experiencing scattering with phonons, impurities or other electrons [68]. These collisions change the momentum of electron when it moves from one state to another. Classically, the average speed of a conduction electron is taken to be given by the Fermi velocity $v_F = \frac{\hbar k_F}{m^*}$. The mean free path ($L_{mf}$), is the average distance an electron can cover before its momentum is significantly altered, is related to the mean relaxation time τ_{mf}between scattering events by:

$$L_{mf} = v_F \tau_{mf} \quad \textbf{(1.50)}$$

In that case, electrons will move ballistically through the structure. This state can be a yardstick to look for ballistic transport phenomena.

1.9.4 Phase-relaxation Length ($L_{\varphi r}$)

A second important scale in low-dimensional systems is the phase relaxation length. This is the length scale over which this coherence endures for a conducting electron as part of its corresponding phase in quantum mechanical wave function. The electron's motion is described by a wave function that also contains a phase in quantum mechanics. This is then called the phase relaxation length quantifying how far an electron can go before its fate changes at which

point it no longer behaves as a free particle, since inelastic scattering randomizes its phase. An electron initially in a well-defined phase state (i.e., with energy *E*) that scatters is transformed into some other possible combination of states and hence its original quantum-mechanical wavefunction undergoes "phase randomization" after the scattering event. The phase relaxation length of an electron is defined as the distance travelled by the electron before its associated phase gets randomized, and it is connected with another parameter called "phase Relaxation Time" ($\tau_{\varphi r}$), which refers to either the time between two inelastic scattering events or else reflects on how much faster temporal coherence fades.

$$L_{\varphi r} = \sqrt{D\tau_{\varphi r}} \tag{1.51}$$

Where, *D* is called diffusion constant and it is represented by;

$$D = \frac{1}{d} v_F^2 \tau_{mf} = \frac{1}{d} L_{\varphi r} v_F, \tag{1.52}$$

here, *d* is used for the dimensionality of the sample.

1.10 TRANSPORT REGIMES

By scaling analysis with the relevant length scales of a structure, information of quantum transport behaviours may be obtained. According to the ohmic (or classically) behaving conductor at sufficiently low temperatures is one in which the quantum wire sample dimensions are much larger than the Fermi wavelength (λ_F), mean free path (L_{mf})and phase relaxation length ($L_{\varphi r}$) [69–71] so if this condition revealed as: Nonetheless, this is not true in the mesoscopic scale where we have:

a. **Diffusive regime:** For the diffusive regime, where both W and are L much larger than the mean free path (W, $L > L_{mf}$), In this regime, impurities scatter the electrons effectively (shown in **Figure 1.4 (a)**).

b. **Quasi-Ballistic Regime:** The electrical resistance in this regime does not a single value, and the current transport qualitatively depends on whether ($L > L_{mf} > W$). However, the motion of electrons maybe be scattered by impurities (shown in **Figure 1.4 (b)**).

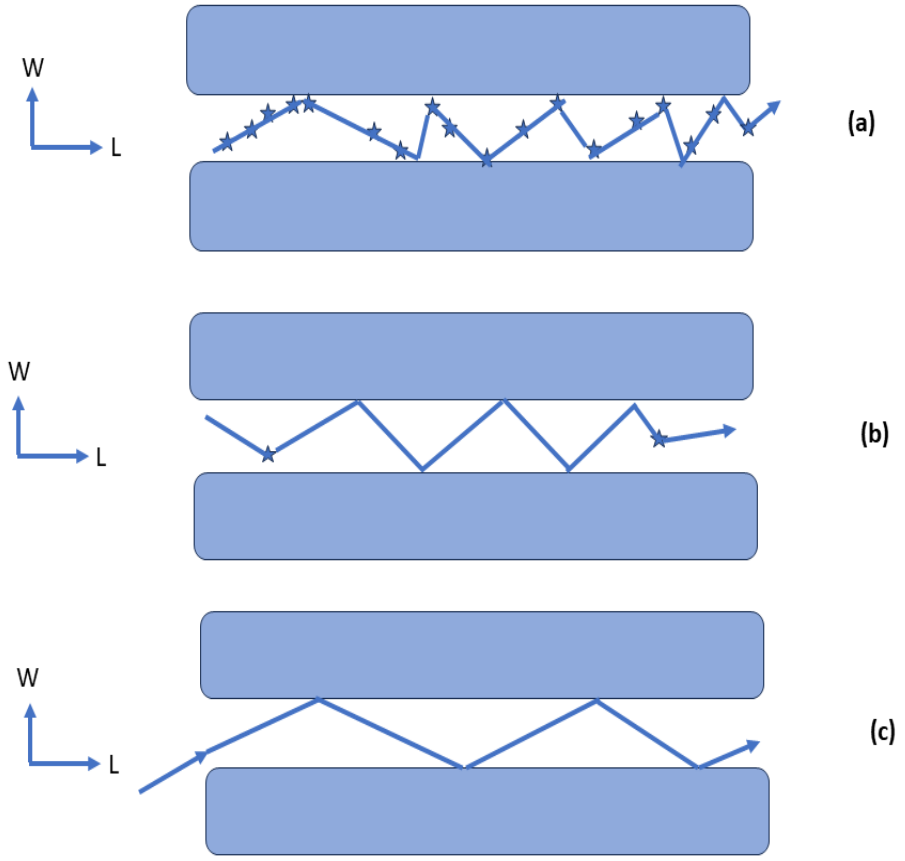

Figure 1.4 Illustration of the (a) diffusive, (b) quasi-ballistic and (c) ballistic quantum transport regimes.

c. **Ballistic Regime:** In the ballistic transport regime: In this thesis, we concentrate into the situation in which is larger than both of and ($L_{mf} > W$, L) i.e. Ballistic Regime. In

this limit impurity scattering vanishes and electron motion is dominated by specular reflection off the walls. The physical shape of the conductor is more crucial. This regime is characterized by the conductance, which is in principle independent of disorder up to effects described by Landauer's formula for an ideal wire. This formula connects the electronic transport coefficients and quantum transmission coefficients, which is highly critical for low-dimensional systems-based understanding of quantum transportation (shown in **Figure 1.4 (c)**).

1.10.1 Landauer Formalism

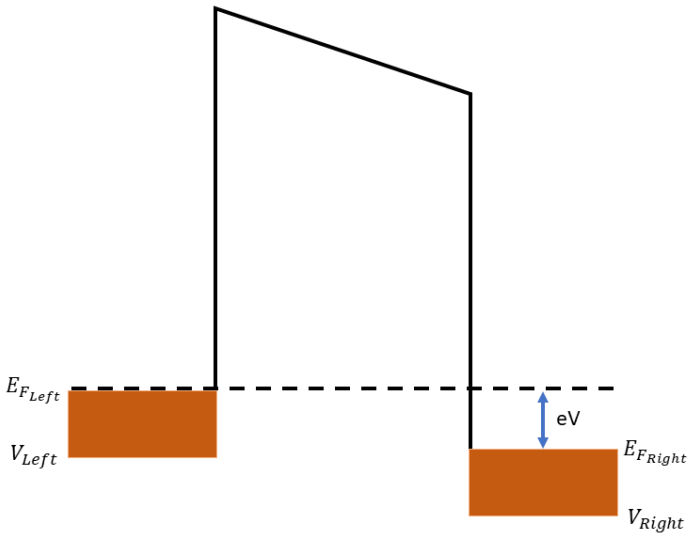

Figure 1.5 A schematic diagram of a barrier surrounded by a Fermi sea of electrons, with a positive bias applied on the left side and E_{F_L} represents the energy level on the left.

To further illustrate this, we are going to take one dimensional barrier and two Fermi seas (as shown in **Figure 1.2**). The electron distribution is modelled by a fermi-function. At

equilibrium, every lead has its own Fermi level which is, $E_{F_{left}}$ for the left and $E_{F_{right}}$ for the right. When a small bias V is applied, then the average change in Fermi energy between source and drain side becomes, $E_{F_{left}}$- $E_{F_{right}}$ = eV. We assume that at the Fermi level, in equilibrium for each lead into we have a distribution of incoming electrons described by a Fermi function. For this system, we want to compute the relationship between current and voltage. Since we are dealing with the propagating mode only, all other channels open at a higher bias voltage and therefore will not conduct in this regime so for simplicity we consider just one empty channel, i. e., lowest available subband in both leads is occupied. Our goal is to find an expression for the total current across the barrier from the bias. Let us start by calculating the current due to electrons coming from left of barrier [72,73]:

$$I_{left} = 2e \int_0^{\infty} f_{left}\big(E(k)\big) v(k) T_{left \to right}(k) \frac{dk}{2\pi} \qquad \textbf{(1.53)}$$

with spin degeneracy 2, e the electron charge, with Fermi-Dirac distribution function in left lead is defined as $f_{left}\big(E(k)\big)$ with the Fermi energy $E_{F_{left}}$ and $v(k)$ is known as velocity of electron. The Transmission coefficient $T_{left \to right}$ is the probability of an electron prepared in the left would be to pass through the barrier and reach right. The factor of $\frac{dk}{2\pi}$ is used for counting the number of states in terms for k-states.

We can accomplish this change of integration variable by:

$$dk = \frac{dk}{dE} dE = \frac{1}{\hbar v} dE \qquad \textbf{(1.54)}$$

Eq, (1.54) is put in the eq. (1.53) and consider V_L shows the lower part in the band of left lead, therefore, eq. (1.53) becomes;

$$I_{left} = 2e\int_{V_L}^{\infty} v(E) f_{left}(E) T_{Left\rightarrow right}(E)\frac{dE}{2\pi\hbar v(E)} = \frac{2e}{h}\int_{V_L}^{\infty} f_{left}(E) T_{Left\rightarrow right}(E)dE. \quad \textbf{(1.55)}$$

The current due to electrons arriving from the right can be calculated in a similar manner. The main differences are the sign reversal because the electrons are moving in the opposite direction and the adjustment of the lower limit in the energy integral.

$$I_{right} = -\frac{2e}{h}\int_{V_R}^{\infty} f_{right} T_{right\rightarrow left}(E)dE \quad \textbf{(1.56)}$$

When the biasing is very small value, the expression $T_{left\rightarrow right} = T_{right\rightarrow left}$ can be used and the lower limits for eq. (1.55) & (1.56) consider as $E_{Ci} = Min(v_L, v_R)$. Therefore, the expression of net current can be written as the addition of I_{left} and I_{right} [73];

$$I_{Total} = I_{left} + I_{right} = \frac{2e}{h}\int_{E_{Ci}}^{\infty} T(E)[f_{left}(E) - f_{right}(E)]dE. \quad \textbf{(1.57)}$$

For the small value of biasing, the difference of $f_{left}(E) - f_{right}(E)$ can be expanded by Taylor series to the lowest order around the Femi energy at the equilibrium, E_F,

$$f_{left}(E) - f_{right}(E) \approx eV\frac{\partial f(E)}{\partial E_F} = -eV\frac{\partial f(E)}{\partial E} \quad \textbf{(1.58)}$$

Therefore, the total current is given by

$$I_{Total} = \frac{2e}{h}\int_{E_{Ci}}^{\infty} T(E)\left(-eV\frac{\partial f(E)}{\partial E}\right)dE, \quad \textbf{(1.59)}$$

Thus, the conductance for the system is

$$G = \frac{I}{V} = \frac{2e^2}{h}\int_{E_C}^{\infty} T(E)\left(-\frac{\partial f(E)}{\partial E}\right)dE. \quad \textbf{(1.60)}$$

For the low temperature, $\frac{\partial \mathrm{f(E)}}{\partial \mathrm{E}} \approx -\delta(\mathrm{E} - \mathrm{E_F})$. Due to these integral collapses and we get the Landauer formula for the quantum conductance

$$G = \frac{2e^2}{h} T(E_F) \quad \textbf{(1.61)}$$

This result in Eq. (1.61) can be generalized to describe multiple propagating modes in the leads as follows [74]. An electron approaching a barrier in mode n could be transmitted to any other mode m on the rest of one electrode or reflected into another arbitrary similar single-mode state my on that same lead. Total quantum conductance by summing over all the possible modes:

$$G = \frac{2e^2}{h} \sum_{m,n} T_{mn}(E_F). \quad \textbf{(1.62)}$$

1.11 PROBLEM STATEMENT AND OBJECTIVES

The present thesis aims to investigate the transport and linear and nonlinear optical properties of quantum nanostructures with electric and magnetic fields influence, as well as Rashba spin-orbit interactions. It consists of seven separate chapters. The **chapter 1** is the introductory and describes nanostructures within the presence of spin-orbit interactions, presents transport properties, linear and nonlinear optical properties due to multiphoton processes. An overview of quantum wires and quantum dots is provided, as well as the Rashba spin-orbit interaction. The **chapter 2** analyses the transport properties of $\mathrm{Ga_{1-x}Al_xAs}$ Quantum Wire under the presence of impurity. In this chapter, combined impacts of Rashba spin orbit interaction, external electric field, magnetic field, and Aluminium concentration on energy dispersion and conductivity in a $\mathrm{Ga_{1-x}Al_xAs}$ quantum wire have been explored. The Energy eigenvalues and eigenvectors are quantified using the diagonalization method and the transport properties are

computed by Landuer-Büttiker formalism. It is noticed that the external electric field, magnetic field, Rashba spin-orbit interaction, and Aluminium concentration (impurity factor x) alter the energy spectra and conductivity. **Chapter 3** provides explanations of the impact of hydrostatic pressure and temperature on the energy band structure as well as on the ballistic conductivity. The Energy eigenvalues and eigenvectors are found by using the diagonalization method and the ballistic conductance is computed by Landuer-Büttiker formalism. The behaviour of energy concerning an external electric field, magnetic field and temperature are also focused. The system is expressed by parabolic confinement to the normal intense magnetic field and RSOI causes the collaborative impact of interior and exterior agents leading to downward/upward and lateral/vertical shifts in the dispersion. The oddity of the energy subbands results in oscillatory patterns in the ballistic conductance. **Chapter 4** is focused on the effect of impurity factor on the optical absorption coefficients, refractive index changes, second harmonic generation, and third-harmonic generation for the intersubband transitions is explored between the electronic states of $Ga_{1-x}Al_xAs$ quantum wire initiated by the symmetric parabolic potential. The system is conquered by the presence of an intense electric field, magnetic field, and Rashba spin-orbit interaction. For the linear and non-linear optical absorption coefficients, refractive index, second harmonic generation, and third harmonic generation coefficient, the analytical expressions are obtained with the assistance of the compact density-matrix approach. The arithmetical outcomes illustrate the optical properties are significantly intuitive to the concentration of impurity and can be controlled by this parameter. The variation in the magnitude and position of peaks via impurity factor indicates the opportunity in the mechanism of optical non-linearity in the quantum wire and also, helps in the optical non-linearity tuning which has device application. **Chapter 5** describes the optical properties of the $In_xGa_{1-x}As$ quantum dot. In this esteem, we first estimate the energy levels and wavefunctions in the

existence of impurity. Then, we focus on the impact of impurity on the absorption coefficients, refractive index changes, and third harmonic generation. It is found that the absorption coefficients, refractive index changes, and third harmonic generation peaks start to shift from their position with the decrement in the magnitude as the concentration of impurity enhances. As a consequence, it is cognizance that the concentration of impurity has a crucial role in the nanostructure optical properties. In **chapter 6**, the influence of the temperature, hydrostatic pressure, and impurity on the energy spectrum, and ballistic conductivity of the $In_xGa_{1-x}As$ double quantum wire are described. The system is subject to the double-well anharmonic confinement potential under the existence of an intense magnetic field, electric field, Rashba and Dresselhaus SOIs. The energy eigenvalues and the ballistic conductance are calculated with the help of the diagonalization method and Landuer-Büttiker formalism, respectively. Moreover, the exploits of energy with the applied electric field, magnetic field, and temperature are also examined. The numerical result illustrates the influence of the temperature, hydrostatic pressure and impurity causing the shifting in the energy dispersion. The oddity in the energy dispersion catalyses the swinging patterns in the ballistic conductivity, and the alteration in the energy introduces the change in the conductance. **Chapter 7** summarizes the discoveries of this study and presents some future research ideas.

1.12 REFERENCES

[1] S. Banerjee, A. Dan, D. Chakravorty, Review Synthesis of conducting nanowires, Journal of materials science 37 (2002) 4261-4271.

[2] M. Law, J. Goldberger, P. Yang, Semiconductor nanowires and nanotubes, Annu Rev Mater Res 34 (2004) 83–122.

[3] S. V Zaitsev-Zotov, Y.A. Kumzerov, Y.A. Firsov, P. Monceau, Luttinger-liquid-like transport in long InSb nanowires, 12 (1999) L303.

[4] S.A. Wolf, D.D. Awschalom, R.A. Buhrman, J.M. Daughton, S. Von Molnár, M.L. Roukes, A.Y. Chtchelkanova, D.M. Treger, Spintronics: A Spin-Based Electronics Vision for the Future 1488 magnetism and materials, Knopf, 5546 (2001) 1488-1495.

[5] L. Bouzaïene, R. Ben Mahrsia, M. Baira, L. Sfaxi, H. Maaref, Hydrostatic pressure and temperature effects on nonlinear optical rectification in a lens shape InAs/GaAs quantum dot, J Lumin 135 (2013) 271–275.

[6] A. Manchon, H.C. Koo, J. Nitta, S.M. Frolov, R.A. Duine, New perspectives for Rashba spin–orbit coupling, Nat Mater 14 (2015) 871–882.

[7] H. Bahramiyan, Strain effect on the third-harmonic generation of a two-dimensional GaAs quantum dot in the presence of magnetic field and spin–orbit interaction, Indian Journal of Physics 94 (2020) 789–796.

[8] J. Adamowski, M. Sobkowicz, B. Szafran, S. Bednarek, Electron pair in a Gaussian confining potential, Physical Review B 62.7 (2000): 4234

[9] S. Zhang, R. Liang, E. Zhang, L. Zhang, Y. Liu, Magnetosubbands of semiconductor quantum wires with Rashba and Dresselhaus spin-orbit coupling, Phys Rev B Condens Matter Mater Phys 73 (2006).

[10] S. Pramanik, S. Bandyopadhyay, M. Cahay, Energy dispersion relations of spin-split subbands in a quantum wire and electrostatic modulation of carrier spin polarization, Phys Rev B Condens Matter Mater Phys 76 (2007).

[11] J.C. León-González, R.G. Toscano-Negrette, A.L. Morales, J.A. Vinasco, M.B. Yücel, H. Sari, E. Kasapoglu, S. Sakiroglu, M.E. Mora-Ramos, R.L. Restrepo, Spin–orbit and zeeman effects on the electronic properties of single quantum rings: Applied magnetic field and topological defects, Nanomaterials 13 (2023) 1461.

[12] M. Sayrac, H. Dakhlaoui, M.E. Mora-Ramos, F. Ungan, Hydrostatic pressure and temperature effects on nonlinear optical properties in harmonic-Gaussian asymmetric double quantum wells, Phys Scr 99 (2024) 045942.

[13] T.A. Sargsian, P.A. Mantashyan, D.B. Hayrapetyan, Effect of Gaussian and Bessel laser beams on linear and nonlinear optical properties of vertically coupled cylindrical quantum dots, Nano-Structures & Nano-Objects 33 (2023) 100936.

[14] R.G. Toscano-Negrette, J.C. León-González, J.A. Vinasco, A.L. Morales, F. Koc, A.E. Kavruk, M. Sahin, M.E. Mora-Ramos, J. Sierra-Ortega, J.C. Martínez-Orozco, Optical properties in a ZnS/CdS/ZnS core/shell/shell spherical quantum dot: Electric and magnetic field and donor impurity effects, Nanomaterials 13 (2023) 550.

[15] K. Banerjee, S.P. Bhatnagar, Two-well osci&&ator 15 DECEMBER 1978, n.d.

[16] R.J.W. Hodgson, Y.P. Varshni, Splitting in a double-minimum potential with almost twofold degenerate lower levels, 22.1 (1989) 61.

[17] M.F. Manning, Energy levels of a symmetrical double minima problem with applications to the NH3 and ND3 molecules, J Chem Phys 3 (1935) 136–138.

[18] S. Banerjee, A. Dan, D. Chakravorty, Review Synthesis of conducting nanowires, 37 (2002): 4261-4271.

[19] S. Lahon, P.K. Jha, M. Mohan, Nonlinear interband and intersubband transitions in quantum dots for multiphoton photodetectors, J Appl Phys 109 (2011).

[20] Maksym, P. A., and Tapash Chakraborty. "Quantum dots in a magnetic field: Role of electron-electron interactions." Physical review letters 65.1 (1990) 108.

[21] R. Hanson, L.P. Kouwenhoven, J.R. Petta, S. Tarucha, L.M.K. Vandersypen, Spins in few-electron quantum dots, Rev Mod Phys 79 (2007) 1217–1265.

[22] A.I. Ekimov, A.A. Onushchenko, Quantum Size Effect in Three-Dimensional Microscopic Semiconductor Crystals, JETP Lett 118 (2023) S15–S17.

[23] A.D. Yoffe, Semiconductor quantum dots and related systems: Electronic, optical, luminescence and related properties of low dimensional systems, Adv Phys 50 (2001) 1–208.

[24] G.F. Quinteiro, P.I. Tamborenea, Electronic transitions in disk-shaped quantum dots induced by twisted light, Phys Rev B Condens Matter Mater Phys 79 (2009).

[25] S. Lahon, P.K. Jha, M. Mohan, Nonlinear interband and intersubband transitions in quantum dots for multiphoton photodetectors, J Appl Phys 109 (2011).

[26] C.B. Murray, C.R. Kagan, M.G. Bawendi, Synthesis and characterization of monodisperse nanocrystals and close-packed nanocrystal assemblies, Annual Review of Materials Science 30 (2000) 545–610.

[27] Que, Weiming. "Excitons in quantum dots with parabolic confinement." Physical Review B 45.19 (1992) 11036.

[28] Wagner, M., U. Merkt, and A. V. Chaplik. "Spin-singlet–spin-triplet oscillations in quantum dots." Physical Review B 45.4 (1992) 1951.

[29] P. Pietiläinen, T. Chakraborty, Energy levels and magneto-optical transitions in parabolic quantum dots with spin-orbit coupling, Phys Rev B Condens Matter Phys 73 (2006).

[30] E.A. de Andrada e Silva, G.C. La Rocca, Rashba spin splitting in semiconductor quantum wires, Phys Rev B Condens Matter Phys 67 (2003).

[31] Ray, O., Sirenko, A. A., Berry, J. J., Samarth, N., Gupta, J. A., Malajovich, I., & Awschalom, D. D. (2000). Exciton spin polarization in magnetic semiconductor quantum wires. Applied Physics Letters, 76(9), 1167-1169.

[32] Žutić, I., Fabian, J., & Sarma, S. D. (2004). Spintronics: Fundamentals and applications. Reviews of modern physics, 76 (2004), 323.

[33] S. Datta, B. Das, Electronic analog of the electro-optic modulator, Appl Phys Lett 56 (1990) 665–667.

[34] Y. Karaaslan, B. Gisi, S. Sakiroglu, E. Kasapoglu, H. Sari, I. Sokmen, Spin-orbit interaction and magnetic field effects on the energy dispersion of double quantum wire, Superlattices Microstruct 85 (2015) 401–409.

[35] T. Schäpers, J. Knobbe, V.A. Guzenko, Effect of Rashba spin-orbit coupling on magnetotransport in InGaAs/InP quantum wire structures, Phys Rev B Condens Matter Mater Phys 69 (2004).

[36] Trushin, M. (2005). Transport in low dimensional systems with spin-orbit coupling (Doctoral dissertation, Staats-und Universitätsbibliothek Hamburg Carl von Ossietzky).,

[37] Nitta, Junsaku, Tatsushi Akazaki, Hideaki Takayanagi, and Takatomo Enoki. "Gate control of spin-orbit interaction in an inverted $In_{0.53}Ga_{0.47}As/In_{0.52}Al_{0.48}$ as heterostructure." Physical Review Letters 78 (1997) 1335.

[38] Birkholz, Jens Eiko. "Spin-orbit interaction in quantum dots and quantum wires of correlated electrons-A way to spintronics?." (2008).

[39] Meijer, Frank Erik. "Rashba spin-orbit interaction in mesoscopic systems." (2005).

[40] G. DRESSELHAUst, M. Tanenbautn, H.B. Briggs, Spin-Orbit Coupling Effects in Zinc Blende Structures*, 1936.

[41] E.I. Rashba, Semiconductors with a loop of extrema, J Electron Spectros Relat Phenomena 201 (2015) 4–5.

[42] P.M. Krstajić, E. Rezasoltani, P. Vasilopoulos, Spin-dependent transport in waveguides with spatially modulated strengths of the Rashba and Dresselhaus terms of the spin-orbit interaction, Phys Rev B Condens Matter Mater Phys 81 (2010).

[43] E.I. Rashba, Electron spin operation by electric fields: Spin dynamics and spin injection, in: Physica E Low Dimens Syst Nanostruct, 2004: pp. 189–195.

[44] T.Y. Zhang, W. Zhao, X.M. Liu, Energy dispersion of the electrosubbands in parabolic confining quantum wires: Interplay of Rashba, Dresselhaus, lateral spin-orbit interaction and the Zeeman effect, Journal of Physics Condensed Matter 21 (2009).

[45] J.J. Krich, B.I. Halperin, Cubic dresselhaus spin-orbit coupling in 2D electron quantum dots, Phys Rev Lett 98 (2007).

[46] J. Nitta, T. Akazaki, H. Takayanagi, T. Enoki, Gate Control of Spin-Orbit Interaction in an Inverted In 0.53 Ga 0.47 As In 0.52 Al 0.48 As Heterostructure, 1997.

[47] Luo, J., Munekata, H., Fang, F. F., & Stiles, P. J., Effects of inversion asymmetry on electron energy band structures in GaSb/InAs/GaSb quantum wells. Physical Review B, 41.11 (1990) 7685.

[48] Sarikurt, S. Electronic structure of parabolic confining quantum wires with Rashba and Dresselhaus spin-orbit coupling in a perpendicular magnetic field (Doctoral dissertation, Dokuz Eylul Universitesi (Turkey)) (2013)..

[49] Bass, M., et al. "Optical rectification." Physical Review Letters 9.11 (1962) 446..

[50] Madarasz, F. L., Szmulowicz, F., Hopkins, F. K., & Dorsey, D. L. (1994). Prediction of giant χ (3) values from a calculation of excitonic nonlinear optical properties in rectangular GaAs quantum-well wires. Physical Review B, 49(19), 13528.

[51] Dawson, P. (1992). Low power optical nonlinearities in GaAs/AlAs quantum wells produced by spatially separated electron-hole plasmas. Journal of luminescence, 53(1-6), 293-298.

[52] Jaiswal, A. K., and G. S. Agarwal. "Photoelectric detection with two-photon absorption." JOSA 59.11 (1969) 1446-1452.

[53] Kaiser, W. G. C. G. B., and C. G. B. Garrett. "Two-photon excitation in Ca F 2: Eu 2+." Physical review letters 7.6 (1961) 229.

[54] Singh, S., and L. T. Bradley. "Three-photon absorption in napthalene crystals by laser excitation." Physical Review Letters 12.22 (1964) 612.

[55] Shreve, A. P., et al. "Two-photon excitation spectroscopy of thylakoid membranes from Phaeodactylum tricornutum: Evidence for an in vivo two-photon-allowed carotenoid state." Chemical physics letters 170.1 (1990) 51-56.

[56] Y. Fu, Y. Luo, H. Ågren, Multiple-photon spectrum of CdS semiconductor quantum dot for bioimaging, Thin Solid Films 515 (2006) 842–845.

[57] N. Thantu, Second harmonic generation and two-photon luminescence upconversion in glasses doped with ZnSe nanocrystalline quantum dots, J Lumin 111 (2005) 17–24.

[58] M. Etienne, A. Biney, A.D. Walser, R. Dorsinville, D.L.V. Bauer, V. Balogh-Nair, Third-order nonlinear optical properties of a cadmiun sulfide-dendrimer nanocomposite, Appl Phys Lett 87 (2005) 1–3.

[59] H. Schneider, O. Drachenko, S. Winnerl, M. Helm, M. Walther, Quadratic autocorrelation of free-electron laser radiation and photocurrent saturation in two-photon quantum well infrared photodetectors, Appl Phys Lett 89 (2006).

[60] S. Lahon, M. Gambhir, P. Kumar Jha, M. Mohan, Multiphoton excitation of disc shaped quantum dot in presence of laser (THz) and magnetic field for bioimaging, Phys Status Solidi B Basic Res 247 (2010) 962–967.

[61] H. Schneider, T. Maier, H.C. Liu, M. Walther, Two-photon photocurrent autocorrelation using intersubband transitions at nearly-resonant excitation, Opt Express 16 (2008) 1523–1528.

[62] H.C. Liu, C.Y. Song, A.J. SpringThorpe, J.C. Cao, Terahertz quantum-well photodetector, Appl Phys Lett 84 (2004) 4068–4070.

[63] Khordad, R., and H. Bahramiyan. "Electronic and optical properties of a lens shaped quantum dot under magnetic field: Second and third-harmonic generation." Communications in Theoretical Physics 62.2 (2014) 283.

[64] S. Sakiroglu, D.G. Kilic, U. Yesilgul, F. Ungan, E. Kasapoglu, H. Sari, I. Sokmen, Third-harmonic generation of a laser-driven quantum dot with impurity, Physica B Condens Matter 539 (2018) 101–105.

[65] Rossi, F., & Molinari, E. (1996). Linear and nonlinear optical properties of realistic quantum-wire structures: The dominant role of Coulomb correlation. Physical Review B, 53(24), 16462.

[66] R. Khordad, Optical properties of quantum wires: Rashba effect and external magnetic field, J Lumin 134 (2013) 201–207.

[67] Sauvage, S., et al. "Third-harmonic generation in InAs/GaAs self-assembled quantum dots." Physical Review B 59.15 (1999) 9830.

[68] S. Datta, Electronic transport in mesoscopic systems, Cambridge university press, 1997.

[69] R. Landauer, Can a length of perfect conductor have a resistance?, Phys Lett A 85 (1981) 91–93.

[70] Galperin, Yuri M. "Quantum Transport." Lecture Notes (Lund University Press, 1998) (1998).

[71] Beenakker, C. W. J., & van Houten, H., Quantum transport in semiconductor nanostructures, In Solid state physics 44 (1991) 1-228.

[72] J.H. Davies, The physics of low-dimensional semiconductors: an introduction, Cambridge university press, 1998.

[73] A.T. Ngo, J.M. Villas-Bôas, S.E. Ulloa, Spin polarization control via magnetic barriers and spin-orbit effects, Physical Review B—Condensed Matter and Materials Physics 78 (2008) 245310.

[74] M. Büttiker, Y. Imry, R. Landauer, S. Pinhas, Generalized many-channel conductance formula with application to small rings, Phys Rev B 31 (1985) 6207.

2

CHAPTER

Physical and Transport Properties of $Ga_{1-x}Al_xAs$ Quantum Wire Under the Presence of Impurity

- *The study focuses on the energy dispersion and ballistic conductance in a $Ga_{1-x}Al_xAs$ quantum wire using a systematic and precise approach.*
- *Parabolic confinement is employed to explore the behavior of energy dispersion and conductivity.*
- *The combined effects of Rashba Spin-Orbit Interaction (RSOI), external electric field, magnetic field, and Aluminium concentration (in $Ga_{1-x}Al_xAs$) are thoroughly investigated.*
- *Energy Eigenvalues and Eigenvectors: Computed using the diagonalization method.*
- *Ballistic conductance analysed through the Landauer-Büttiker formalism.*
- *External electric fields, magnetic fields, RSOI, and Aluminium concentration (x) significantly impact energy spectra and conductivity, thereby affecting the physical and transport properties of the quantum wire.*

2.1 INTRODUCTION

Advances in experiments and theory of semiconductor technology have given impetus to the creation of different low-dimensional structures like quantum wires (QWRs), dots (QDs) as well as wells which are known altogether by their term-Quantum nanostructures. They display distinct properties and are of great interest for microelectronics and optoelectronics as their electrical, optical, or transport characteristics can be tuned. However, they have become an important focus for technology. This causes them to localize in low dimensions with the appearance of discrete energy levels (subbands) effects drastically different responses for absorbance spectra and brings about their new functionalities. Because the nonlinearity associated with optical absorption, refractive index changes and other properties of these low-dimensional systems is of paramount interest for a range of possible applications like photodetectors, Far-IR laser amplifiers or high speed electro-optical modulators [1,2]. Since the first experimental demonstration of a quasi-one-dimensional electron system in 1986, made by dynamically confining an original two-dimension electron gas (2DEG) to form semiconductor quantum wires (QWs), enormous efforts have been devoted both experimentally and theoretically on their optical properties. In QWRs, these properties can be manipulated through the energy spectrum tuning depending on effective radius as well as external electric and magnetic fields, which makes them a promising candidate for linear or nonlinear optical devices applications [3–6]. A crucial role is played by the survey to check the dependency of physical properties for low-dimensional systems on external perturbation to develop tore investigation for QWRs. For this range we need only provide an understanding of how these system characteristics respond as external perturbations will help us understand their size. Indeed, it has not only been demonstrated that they are both sensitive to external electric

fields but also magnetic fields heavily influence the optical and transport properties of these systems according to studies [7,8].

Among these properties, transport properties play an important role. The explanation for transport properties is found by using a non-interacting electron model [9], in consonance with the Landuer-Büttiker formalism [10] in which the electrons get transferred from one reservoir to another when a small bias is applied across the channel. As they are confined in the channel transversely so they are distributed among different sub-bands according to Fermi-Dirac distribution. The number of modes of electron propagation completely specify the net conductance of a system and can be determined by the Fermi energy and energy spectrum. The experiments were accomplished independently by Yuriy et al. [11] and Quay et al. [9] that established a relation between energy dispersion and the conductance in a QWR. Using energy dispersion curves, they imposed that each sub-band contributes e^2/h to the ballistic conductance. We can predict transport properties with help of QWR due to peculiar properties shown in their band structures i.e., anti-crossing and additional extrema of sub-band under the influence of external fields along with the spin-orbit interaction (SOI).

SOI influences the spintronic development considerably in low-dimensional semiconductor systems by utilizing electron spin for storing and hauling information. One of the most alluring spintronic devices is affirmed by Datta and Das [12] i.e., Spin polarised field-effect transistor (SFET) which may be rapidly switched, unlike conventional transistor. Two types of SOI are admissible for semiconductor Devices: Rashba spin-orbit interaction (RSOI) and Dresselhaus spin-orbit interaction (DSOI) [13]. The dearth of symmetry in bulk inversion brings the former into the spotlight while the latter makes an appearance from the unsymmetric behaviour of confining quantum well electric potential along its growing direction that creates a 2DEG on a

narrow-gap semiconductor material surface. Since an external gate electrode can tune RSOI [14–20]. The impact of the RSOI on the ballistic conductance of the 2DEG and QWRs has been studied by Krstajic [21]. It is predictable, of researchers paying exceptional attention to spin-dependent transport [22–27]. Moreover, the sequel of the SOI and magnetic field influence transport characteristics of low-dimensional systems which restrain movement of charge carriers in the 2DEG [28,29].

This has become quite essential to acknowledge the electronic as well as optical characteristics of impurities in the QWRs as physical, optical, and transport characteristics of low-dimensional devices are fabricated from such materials which are strongly affected due to the existence of the trivial impurities [30–34]. In heterostructures, we can analyse the properties of impurities by using some constructive tools like intense laser field, electrostatic field, magnetic field, and hydrostatic pressure. Numerous studies have been carried out for discussion of QWRs hydrogenic-trivial impurities. A minor impurity can enlarge the conductivity of a semiconductor by a few orders of magnitude. Addition of the impurities influences the electronic properties of bulk semiconductors which have been broadly recognized since the early stage of semiconductor science [35].

Since, the thermal, optical, and transport properties of semiconductor devices are firmly affected by impurities in QWRs. It has become crucial to examine the doped nanostructure. There is a flourishing interest in the research of transportation of electrons in recent times and electronics properties have been studied both theoretically [36–38] and experimentally [39,40]. To our apprehension, no evaluation of energy dispersion and transport properties of a $Ga_{1-x}Al_xAs$ QWRs under the hydrostatic pressure, temperature, electric field, and magnetic field have been done yet. The impetus behind this paper is to scrutinize the impacts of an external

electrostatic field, magnetic field along with impurity factor on the physical and transport properties of $Ga_{1-x}Al_xAs$ QWRs using the diagonalization technique.

2.2 PARABOLIC HARMONIC POTENTIAL QUANTUM WIRE WITHIN THE PRESENCE OF IMPURITY

In **Figure 2.1**, diagrammatic view of $Ga_{1-x}Al_xAs$ QWR is shown, for 1-D $Ga_{1-x}Al_xAs$ QWR harmonic potential is given by:

$$V(X) = \frac{1}{2} m^* (x, P, T) \omega_o^2 X^2, \tag{2.1}$$

Where $m^* (x, P, T)$ is the effective mass with the dependence of *x* (also known as impurity factor) concentration of the Aluminium, pressure and temperature. For $Ga_{1-x}Al_xAs$ QWR the effective mass is described as [41]:

$$m^* (x, P, T) = m_o \left[1 + \frac{\pi^2(x)}{3}\left(\frac{2}{{E_g}^i(x,P,T)} + \frac{1}{{E_g}^i(x,P,T)+\Delta_o(x)}\right) + \delta_i(x)\right]^{-1}, \tag{2.2}$$

m_o is the mass for free electron, $\pi(x)$ and $\Delta_o(x)$ are known as inter-band matrix element and valence band spin-orbit coupling $(\pi^2(x) = (28900 - 6290x)meV)$ and $\Delta_o(x) = (341 - 66x)meV$). When remote-band effects are considered through $\delta_i(x)$ parameter given by:

$$\delta_i(x) = -3.935 + 0.488x + 4.938x^2, \tag{2.3}$$

In eq. (2.2) ${E_g}^i(x, P, T)$ is defined as an energy gap in the conduction band which is given by [42]

$${E_g}^i(x, P, T) = p_i + q_i x + r_i x^2 + s_i P - \frac{\beta_i T^2}{\gamma_i + T}. \tag{2.4}$$

where the values of parameters $p_i, q_i, r_i, s_i, \beta_i$ and γ_i are 1519.4 me, 1360 meV, 220meV, 10.7 meV/kbar, 0.5405 meV/K and 204 K respectively. These values are obtained with help of photoluminescence measurement.

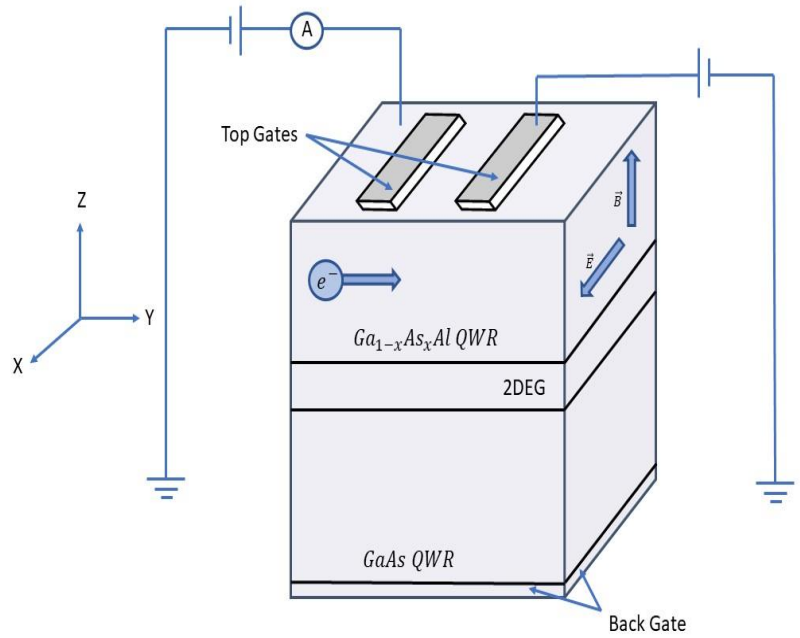

Figure 2.1 Schematic view of the *Ga$_{1-x}$Al$_x$As* QWR within the presence of 2DEG, external electric and magnetic field.

In effective-mass framework approximation, single electron Hamiltonian for a *Ga$_{1-x}$Al$_x$As* QWR in the manifestation of RSOI, under the impact of external electric and magnetic field is given as [43,44]

$$\widehat{H}_o = -\frac{1}{2m^*(x,P,T)}(\boldsymbol{p}+e\boldsymbol{A})^2 + \frac{1}{2}m^*(x,P,T)\omega_o^2 X^2 + \frac{1}{2}g^*\mu_B B\sigma_z + \frac{\alpha}{\hbar}[\sigma\times(\boldsymbol{p}+e\boldsymbol{A})]_Z \text{ , } \mathbf{(2.5)}$$

Where $\boldsymbol{p}$ exists in eq (2.1) for the momentum of an electron, e is the electronic charge, g^* is known as Landé factor. ω_o, μ_B and σ are known the oscillator frequency, Bohr magneton and Pauli matrices respectively, $\boldsymbol{B}$ is the intense magnetic field realistic in the *Z*-direction therefore

vector potential $\boldsymbol{A}$ comes out to be $BX\hat{j}$ due to symmetric gauge, last term in eq. (2.5) is known as RSOI Hamiltonian and α is the Rashba parameter.

When there is a presence of external electric field $\boldsymbol{E}$ along *X*-axis then the total Hamiltonian for this system is written as:

$$\widehat{H} = -\frac{1}{2m^*(x,P,T)}\left(p_{\boldsymbol{X}} + (p_{\boldsymbol{Y}} + eBX)^2 + \frac{1}{2}m^*(x,P,T)\omega_1^2X^2 + eEX + \frac{1}{2}g^*\mu_B B\sigma_Z\right. \frac{\alpha}{\hbar}[\sigma_X(p_{\boldsymbol{Y}} + eBX) - \sigma_Y p_{\boldsymbol{X}})], \quad \textbf{(2.6)}$$

Where $\omega_1 = (\omega_o^2 + \omega_c^2)^{\frac{1}{2}}$ known as effective cyclotron frequency and the cyclotron frequency is given by $\omega_c = \frac{eB}{m^*}$ .If there is a translation along the length of the wire then Hamiltonian remain unchanged, therefore the wavefunction is represented by:

$$\Psi(X,Y) = \varphi(X)exp\,(ik_yY), \quad \textbf{(2.7)}$$

Where k_y is the propagation constant along *Y*-direction and $k_y = p_{\boldsymbol{Y}}/\hbar$. So, we can write $\widehat{H} = \widehat{H}_q + \widehat{H}_R$ where

$$\widehat{H}_q = -\frac{p_X^2}{2m^*(x,P,T)} + \frac{1}{2}m^*(x,P,T)\omega_1^2(X - X_o)^2 - \frac{e^2E^2}{2m^*(x,P,T){\omega_1}^2} + \frac{\omega_o^2\hbar^2{k_y}^2}{{\omega_1}^2 2m^*(x,P,T)} - \frac{e^2EB\hbar k_y}{m^*(x,P,T){\omega_1}^2} + \frac{1}{2}g^*\mu_B B\sigma_Z\,, \quad \textbf{(2.8)}$$

And

$$\widehat{H}_R = \alpha(\sigma_X\left(k_y + \frac{eBX}{\hbar}\right) - i\sigma_Y\frac{d}{dX}). \quad \textbf{(2.9)}$$

Where $X_o = -(\frac{eE}{m^*(x,P,T){\omega_1}^2} + \frac{eB\hbar k_y}{{m^*}^2(x,P,T){\omega_1}^2})$ is known as guiding centre coordinate.

The energy eigenvalues and eigenvectors for $\widehat{H}_q$ is given as

$$\widehat{H}_q \Psi_{n\sigma}(X) = E_{n\sigma} \Psi_{n\sigma}(X), \quad \textbf{(2.10)}$$

Where

$$\Psi_{n\sigma}(X) = \frac{1}{(\sqrt{\pi} C_i 2^n n!)^{1/2}} H_n\left(\frac{X-X_o}{c_i}\right) exp\left(-\frac{1}{2}\left(\frac{X-X_o}{c_i}\right)^2\right) \chi_\sigma \ . \quad \textbf{(2.11)}$$

with $C_i = \sqrt{\frac{\hbar}{m^*(x,P,T)\omega_1}}$ is the characteristic length of the harmonic oscillator, n = 0 to 5 and $\sigma = \pm$. $H_n(x)$ and χ_σ are the hermite polynomial and the spinor functions for spin down ($\chi_- = \begin{pmatrix}0\\1\end{pmatrix}$) and for spin up ($\chi_+ = \begin{pmatrix}1\\0\end{pmatrix}$) respectively and energy scales corresponding to the RSOI $\Delta_{so} = \frac{m^*\alpha^2}{2\hbar^2}$. A length scale has been established to characterise the strength of lateral confining potential $l_w = \sqrt{\frac{\hbar}{m^*\omega_o}}$.The energies eigenvalues of eq. (2.10) are

$$E_{n\sigma} = \hbar\omega\left(n+\frac{1}{2}\right) - \frac{e^2E^2}{2m^*(x,P,T){\omega_1}^2} + \frac{\omega_o^2\hbar^2{k_y}^2}{{\omega_1}^2 2m^*(x,P,T)} - \frac{e^2EB\hbar k_y}{m^*(x,P,T){\omega_1}^2} + \frac{1}{2}g^*\mu_B B\sigma_Z. \quad \textbf{(2.12)}$$

If we are expanding $\varphi(X) = \sum_{n\sigma} a_{n\sigma} \Psi_{n\sigma}(X)$, the Hamiltonian $'\widehat{H}'$ eigenvalue equation can be written as:-

$$\sum_{n\sigma} a_{n\sigma}(E_{n\sigma} - E)\, \Psi_{n\sigma}(X) + \sum_{n\sigma} a_{n\sigma}\, \widehat{H}_R \Psi_{n\sigma}(X) = 0, \quad \textbf{(2.13)}$$

And via the orthogonality conditions, we have

$$(E_{n\sigma} - E)a_{n\sigma} + \sum_{n'\sigma'} \langle \Psi_{n\sigma} \left| \widehat{H}_R \right| \Psi_{n'\sigma'} \rangle = 0, \quad \textbf{(2.14)}$$

Where the 2nd term of the matrix elements of this equation are calculated as: -

$$\langle n\sigma|\widehat{H}_R|n'\sigma'\rangle = \alpha\left[\left(1-\frac{\omega_c^2}{{\omega_i}^2}\right)k_y - \frac{\omega_c eE}{\hbar{\omega_i}^2}\right]\delta_{n,n'}\delta_{\sigma,\sigma'} + \frac{\alpha}{c_i}\left[\left(\frac{\omega_c}{\omega_i}+\sigma\right)\sqrt{\frac{n+1}{2}}\,\delta_{n,n'-1} + \left(\frac{\omega_c}{\omega_i} - \sigma\right)\sqrt{\frac{n}{2}}\delta_{n,n'-1}\right]\delta_{\sigma,-\sigma}\,. \quad \textbf{(2.15)}$$

After diagonalization of eq. (2.14), we achieve the eigenfunction and the energy dispersion curve for this system.

2.3 BALLISTIC CONDUCTANCE

This part focuses on the study of independent contributions by internal and external forces to zero-temperature conductivity. The ballistic regime is understood as the case where a nanostructure connected to two large electron reservoirs allows electrons to flow without scattering and therefore the conductance can be described in terms of Landauer-Büttiker formalism at zero temperature neglecting electron-electron interactions [45]

$$G = G_i \sum_{\beta\beta'} T_{\beta\beta'}, \quad \textbf{(2.16)}$$

Here, $T_{\beta\beta'}$ is the transition probability between states $|\beta\rangle$ state to $|\beta'\rangle$ and $G_i = 2e^2/h$ is quantization constant. We follow Pershin and his colleagues and accordingly at the end of QWR, a small bias ($\mu_l > \mu_r$) is applied between the contacts (where μ_l and μ_r chemical pote ntials) [46,47]. We have assumed the non- scattering and unity of the transition probability; conductance of this system can be obtained in following way [48]:

$$G = \frac{2e^2}{h}\sum_{n,s}\sum_l \alpha_l^{n,s} f(E_m^{n,s}), \quad \textbf{(2.17)}$$

In eq. (2.17), n is defined as a level of the states and s is the level of spin whereas $E_m^{n,s}$ is the energy of extremum point in energy spectra, and $f(E_m^{n,s})$ is known as Fermi-Dirac distribution

function. $\alpha_l^{n,s}$ relates to -1 and +1 for a maximum and minimum point in the energy spectra respectively.

2.4 RESULTS AND DISCUSSION

In this present work, the energy dispersions and the ballistic conductance are described for $Ga_{1-x}Al_xAs$ quantum wire at distinct strengths of the magnetic field, external electric field, and impurity factor with $g^* = -0.44$, pressure = 15 kbar at room temperature.

This work aims to figure out the effect of energy dispersion and ballistic conductance with various strengths of an external electric field, magnetic field, RSOI, and impurity factor.

In **Figure 2.2 (a-d)**, energy dispersion is represented as a function of $k_y l_o$ with $\alpha = 25$ nm meV (RSOI factor), B = 1 T (magnetic field) and x = 0.3 (impurity factor). Here, all subsequent energy dispersion diagrams are given for more elaboration. In **Figure 2.2 (a)**, two subbands are plotted for each energy level i.e., quasi spin-up (represented by solid line) and quasi spin-down (represented by dish line). **Figure 2.2 (a)** presents the dispersion curve in absence of an electric field, E = 0 V/m in which the lower two energy levels (where n = 0, 1) are anticrossing each other due to the mixing of intraband by spin split levels and the contribution of immense diagonal elements $\langle n\sigma | H_R^i | n\sigma \rangle$ [49]. This anticrossing may lead to anomalous conductance steps. The presence of an electric field causes downward shifting of the energies and gives rise to a lateral shift along the $k_y l_o$-axis. Moreover, all spin branches descend towards lower energies as the electric field is increased. In **Figure 2.2 (b-d)**, in which electric field is varied from 0.6×10^6 V/m to 1.5×10^6 V/m, the whole spectrum gets shifted downwards to lower energies. There is more downward shifting in the spectrum observed and this is called stark shifting. Therefore, the contribution of the electric field to the energy dispersion is quadratic for downward shifts and linear for lateral displacements, as shown

clearly in eq. (2.12). The creation of camel-back morphologies, crossing and anticrossing formations is determined by the interplay between RSOI and external fields, while the electric field has a more obvious effect at the weak coupling limit (α = 25 nm meV).

Figure 2.3, shows the ballistic conductance of the $Ga_{1-x}Al_xAs$ quantum wire as a function of the chemical potential for different strengths of electric field (E = 0, $0.6\times 10^6 \mathrm{V/m}$, 1×10^6 V/m, 1.5×10^6 V/m). The conductance shows a growing stepwise profile with integer conductance plateaus. This can be well understood with the dispersion curves. **Figure 2.2 (a-d)**, presents the energy spectrum with distinct strength of the electric field. These dispersion curves have parabolic forms and are formed in pairs. However, the two lowest energy subbands in **Figure 2.2 (a-d)** are not distinguished, they consist of two curves vertically offset by a small value. Every dispersion curve in this limit would have a two-fold degeneracy. Therefore, conductance would increase $(2e^2/h)$, instead of $(2e^2/h)/2$ for a single quantum wire. This represents that the step height between two consecutive plateaus would be 1 in units of $(2e^2/h)$. However, the splitting of the subbands causes the appearance of the narrow conductance plateaus with $(2e^2/h)/2$ as shown in **Figure 2.3**. Their steps width reflects the magnitude of the subband split. The higher the subband index, the larger is the split of the subband.

In the ballistic conductance, each latest step visibly exhibits the 'turning on' of the latest mode (conducting channel) and an additional electron can travel along the wire. Ballistic conductance of quantum devices provides a new approach for designing spin filters and modulators [50]. Each sub-band has now a contribution of $2e^2/h$ to the conductance due to the impact of the field on conductance, as observed e.g. in [51]. Firstly, we will get the contribution at the lowest minimum in **Figure 2.2 (a-d)** and the second contribution when chemical potential reaches the second minima of the same sub-band. When μ is further increased and passed through the local maximum point, the conductance will decrease by $2e^2/h$. The formation of conductance peaks

is done, as shown in **Figure 2.3**. If we compare the conductance steps with the chemical potential axis, the decrease in energy with the increase in strength of the external field can be easily observed. The anticrossing is observed at the lower level for n=0 of the energy dispersion curve as shown in **Figure 2.2 (a-d)**. The presence of a camel-back formation in the energy dispersion with more than one extremum point creates narrower conductivity dips. This dip on conductance shows the steps of quantization which exhibit the monotonic increasing property, except the former.

Figure 2.4 (a-c), shows the impact on the curve of energy dispersion for various values of magnetic field and at E = 0.6×10^{6} V/m and $\alpha = 25$ nm meV . When the magnetic field is applied (in z-direction) to the $Ga_{1-x}Al_xAs$ QWR, the symmetry of time reversal is broken. A complex spectrum is obtained due to the interaction between RSOI and Zeeman splitting.

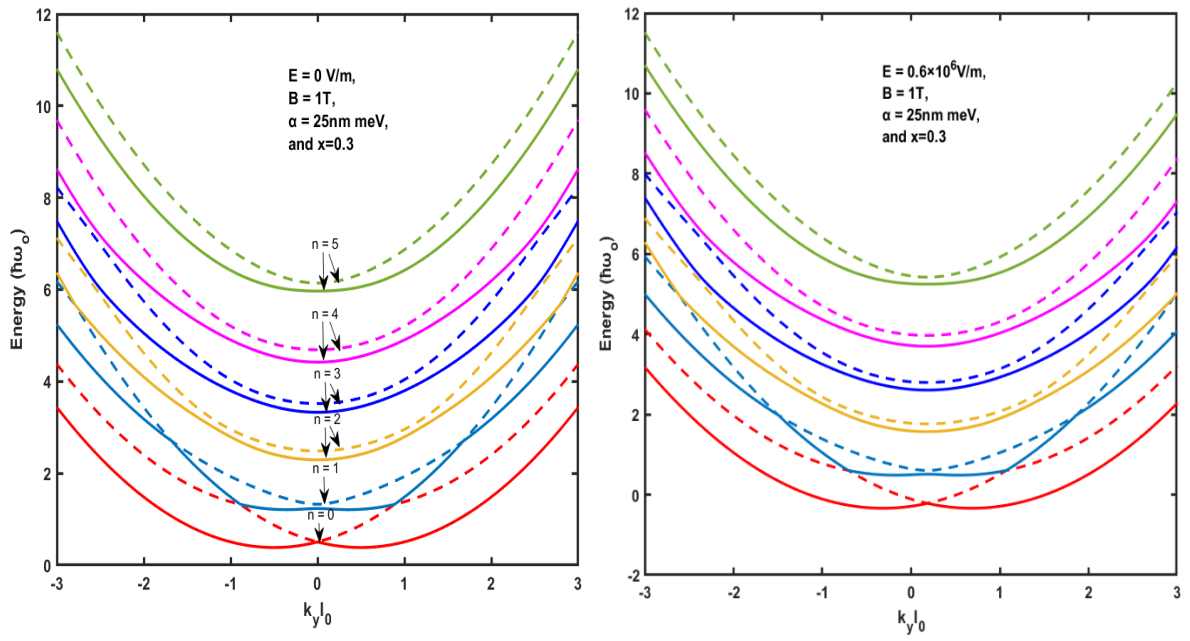

(a) **(b)**

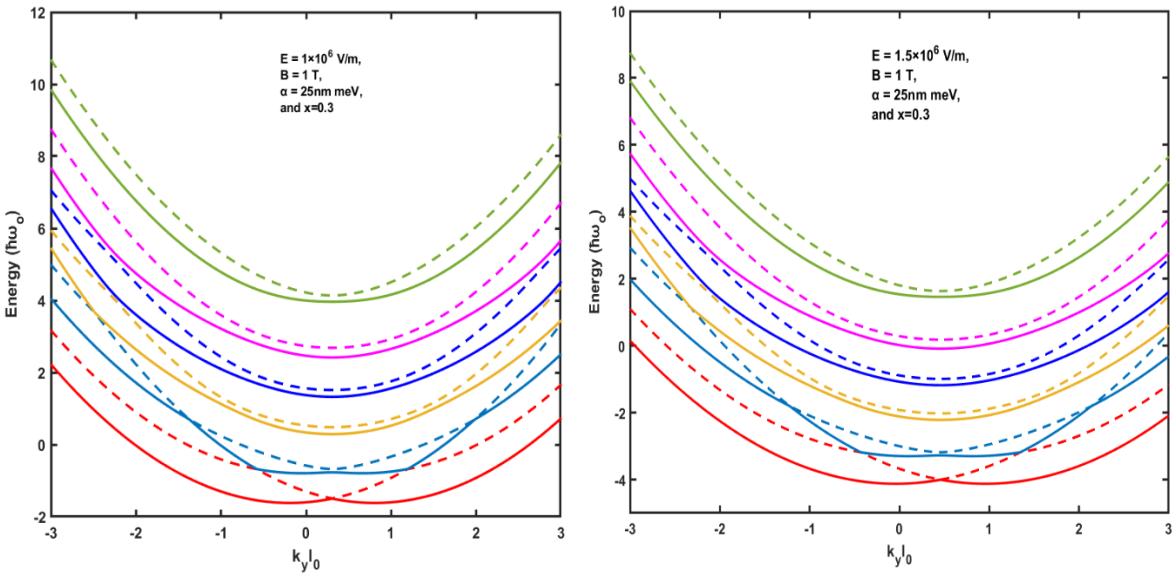

(c) **(d)**

Figure 2.2 The energy dispersion of the $Ga_{1-x}Al_xAs$ QWR at the magnetic field (B) = 1 T, RSOI (α) = 25nm meV and x = 0.3 for (a) E = 0 V/m, (b) E = 0.6× 10^6 V/m, (c) E = 1× 10^6 V/m, (d) E = 1.5× 10^6 V/m.

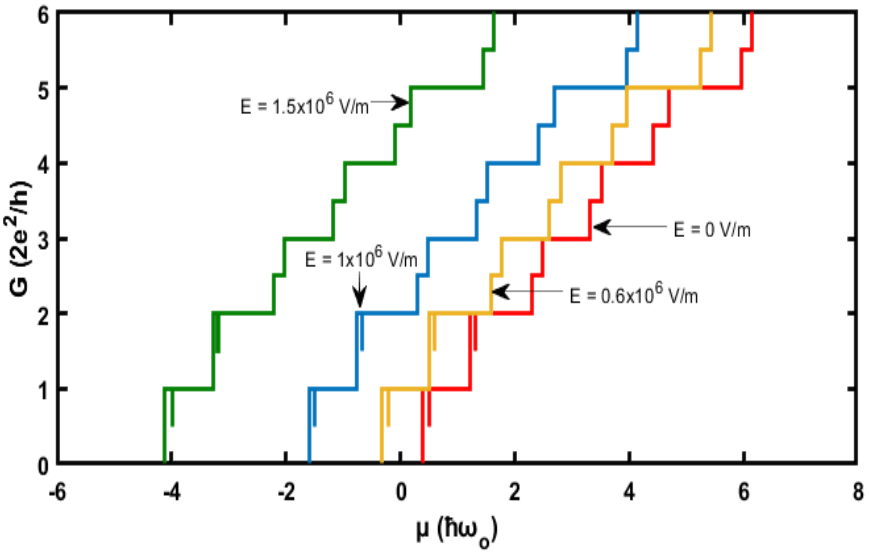

Figure 2.3 The ballistic conductivity (G) for the energy dispersions given in Fig. 2 (a-d).

Figure 2.4 (a-c), shows the impact on the curve of energy dispersion for various values of magnetic field and at E = 0.6× 10^6V/m and α = 25nm meV . When the magnetic field is

applied (in z-direction) to the $Ga_{1-x}Al_xAs$ QWR, the symmetry of time reversal is broken. A complex spectrum is obtained due to the interaction between RSOI and Zeeman splitting. Therefore, we get the variation in energy separation for the various intensities of the applied magnetic field. When the direction of the magnetic field is reversed B = -1T (B_Z to $-B_Z$), a lateral shift in energy in the subbands along k_yl_o – axis is observed towards the lower value of k_yl_o shown in **Figure 2.4 (a)**. And it is clearly seen that the gaps between the subbands are significantly dependent on the direction of applied magnetic field. This observation can help to tune the g-factor in such systems. In absence of a magnetic field i.e., B = 0 T, we obtain energy dispersion with zero lateral shift and there is no spacing between the quasi spin-up and quasi spin-down bands at $k_yl_o = 0$ represented in **Figure 2.4 (b)**. Consequently, **Figure 2.4 (c)** shows the presence of a positive magnetic field (B = 1.5 T) that induces the shifting in the dispersion graph along the positive k_yl_o-axis. This results in an increased subband separation gap which is find out by the effective oscillator energy ħω, rather than the zero field ħω. Whereas, the interplay among the Zeeman splitting and the RSOI leads to rather complex level energy dispersion, resulting in variation of energy gaps between the succeeding subbands at high external field. For an applied magnetic field, the intermixing weakens in the energy range considered. We attribute this to the enhanced effective oscillator energy ħω with reference to Δ_{so}.

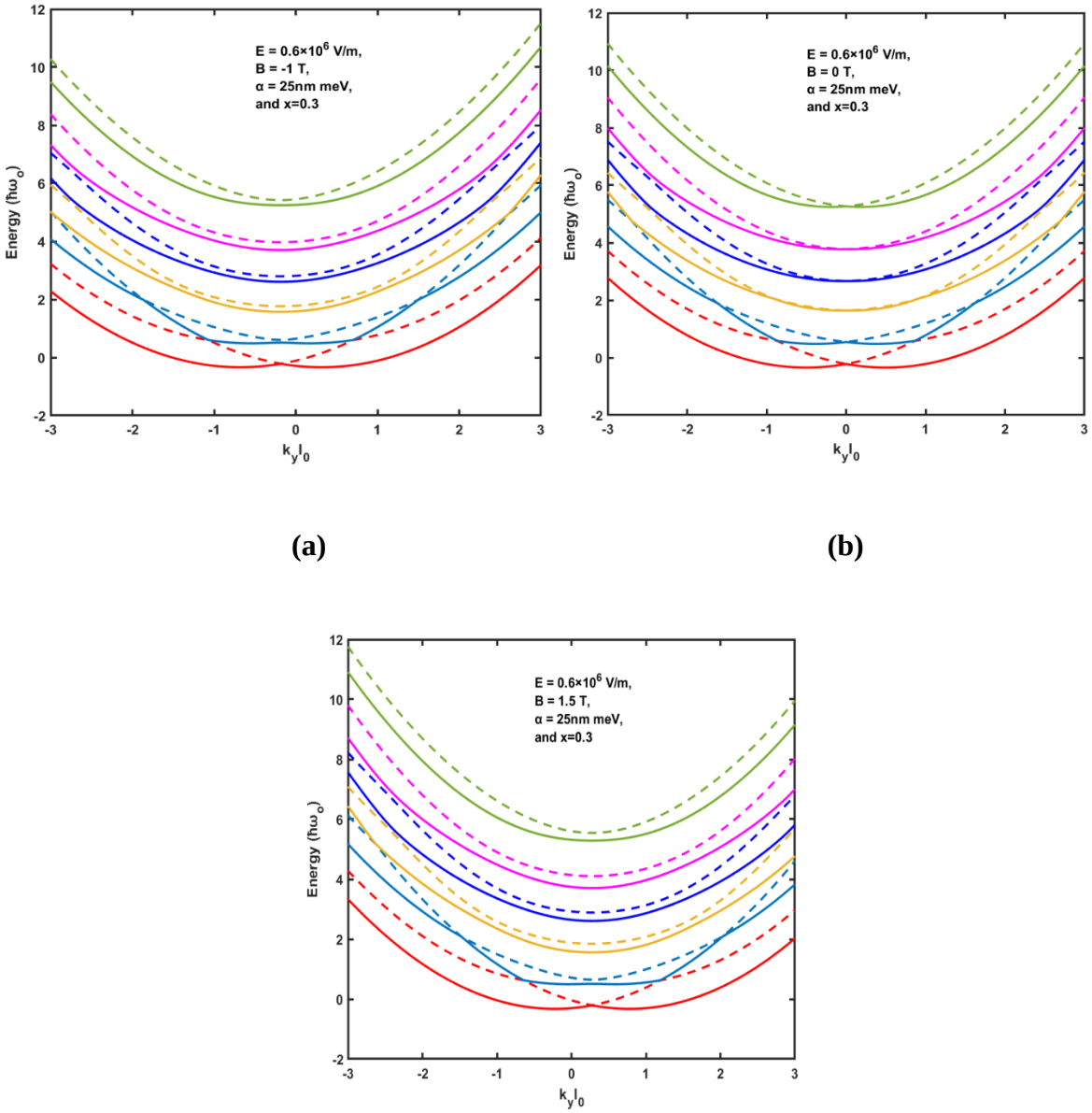

(a) **(b)**

(c)

Figure 2.4 The energy dispersion of the $Ga_{1-x}Al_xAs$ QWR at Electric field (E) = 0.6×10^6V/m, RSOI (α) = 25 nm meV and x = 0.3 for (a) B = -1 T, (b) B = 0 T, (c) B = 1.5 T.

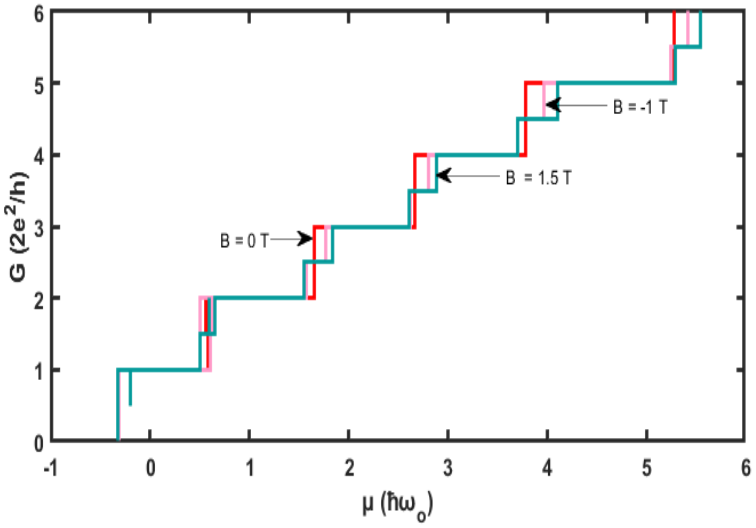

Figure 2.5 The ballistic conductivity (G) for the energy dispersions given in Fig. 2.4 (a-c).

Figure 2.5 displays that there are more propagating channels (in QWR) opened up with an increase in energy, so the G (conductivity) steps up in staircase shape. In presence of an uncertain magnetic field, there is 2-fold degeneracy i.e., state degeneracy and spin degeneracy. These propagating channels are opened up in pair with an increase in fermi-energy. Hence, the conductance for weak magnetic induction (B = -1 T, 0 T) approaches $2(2e^2/h)$, in place of $1(2e^2/h)$ for a strong magnetic field (B = 1.5 T).

Figure 2.6 (a-b) shows the effects of various values of the RSOI on the spectrum of energy dispersion. The increment in SOI value from weak to strong (from α = 30 nm meV to 55 nm meV) causes the value superimposes the lower energies and consequently, a highly intricate energy spectrum is obtained (in **Figure 2.6 (b)**) [52–54]. For strong RSOI, (α = 55 nm meV) the anticrossings between the subbands turn out to be sharper resulting in a stronger intermixing of the levels due to the coupling between the spin spilt levels. The variation of conductance with chemical potential for the various value of RSOI is represented in **Figure 2.7**. Due to the

more complex energy dispersion curves for strong coupling as compared to weak coupling, the conductivity directly depends on the energy spectrum which exhibits more exceptional steps.

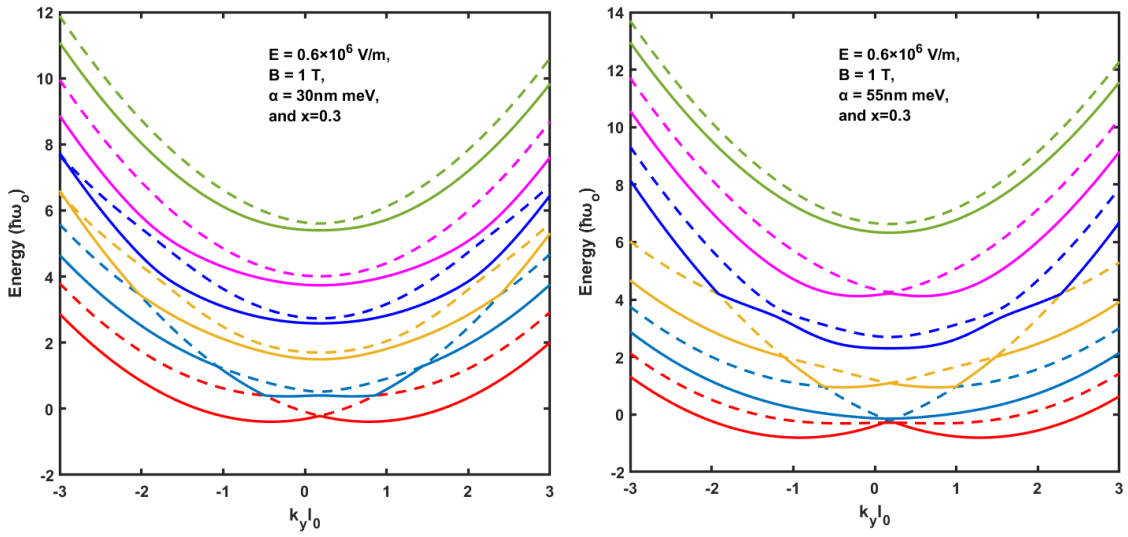

(a) **(b)**

Figure 2.6 The energy dispersion of the $Ga_{1-x}Al_xAs$ QWR at Electric field (E) = 0.6×10^6V/m, B = 1T and x = 0.3 for (a) α = 30 nm meV, & (b) α = 55 nm meV.

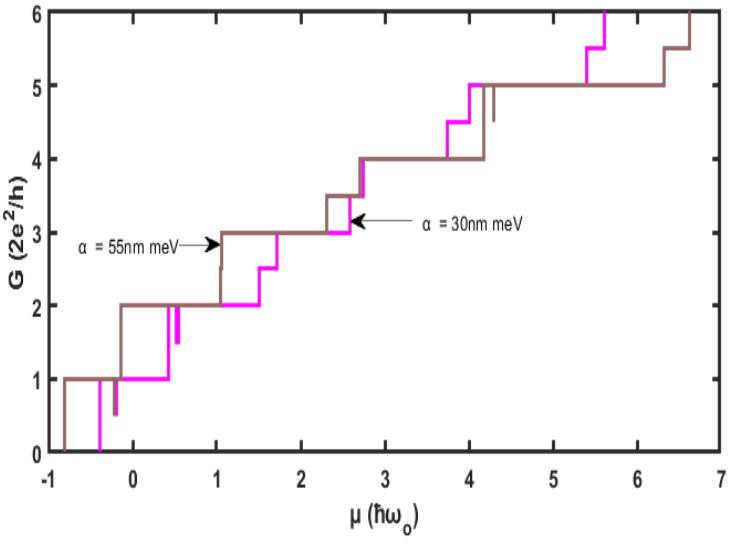

Figure 2.7 The ballistic conductivity (G) for the energy dispersions given in Fig. 2.6 (a-b).

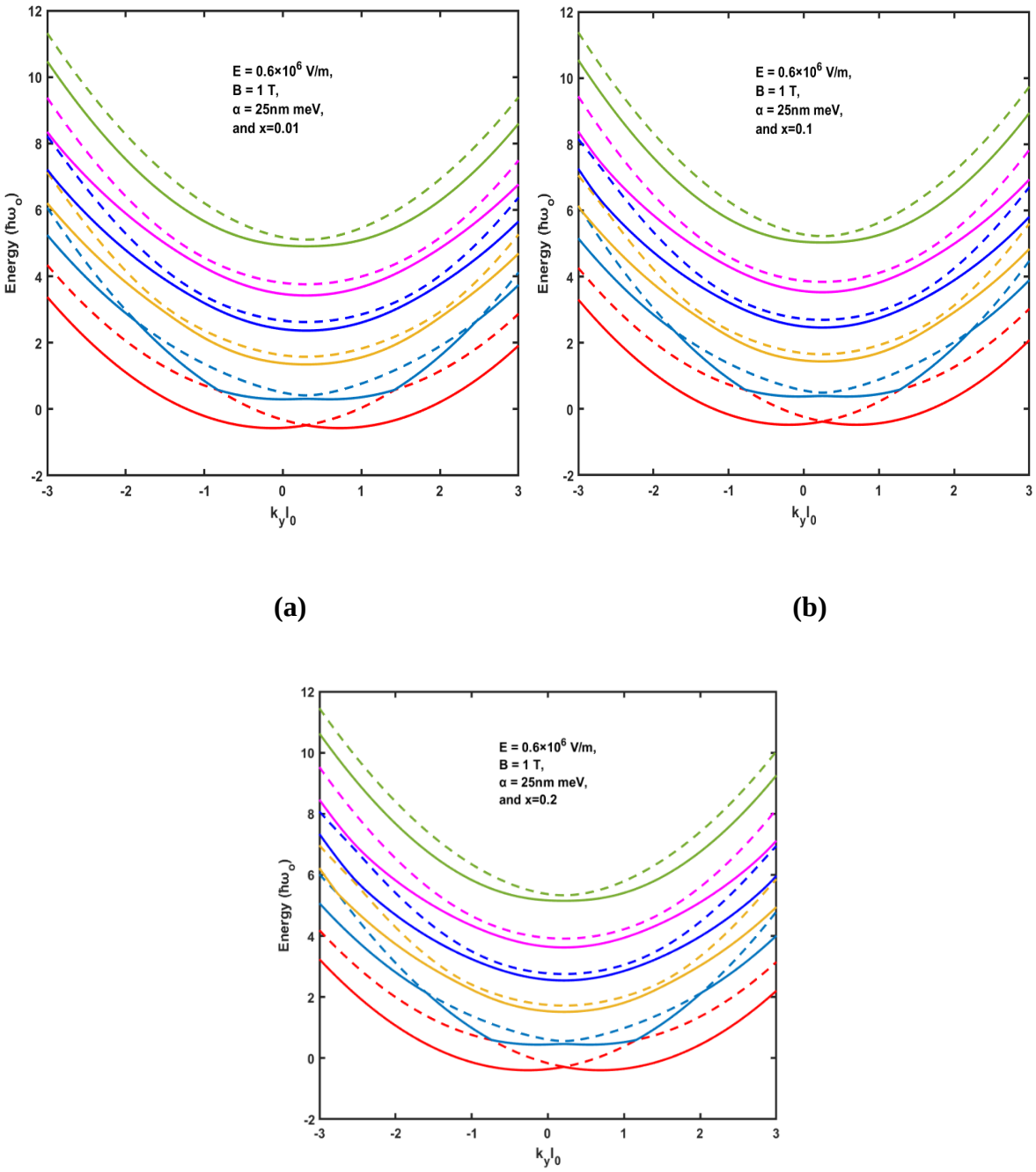

(a) **(b)**

(c)

Figure 2.8 The energy dispersion of the $Ga_{1-x}Al_xAs$ QWR at Electric field (E) = 0.6×10^6V/m, magnetic field (B) = 1 T and RSOI (α) = 25 nm meV for (a) x = 0.01, (b) x = 0.1, and (c) x = 0.2 .

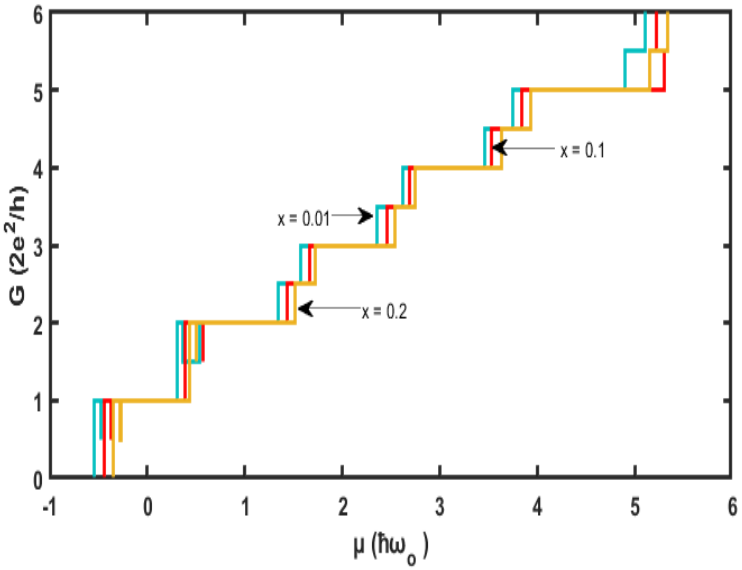

Figure 2.9 The ballistic conductivity (G) for the energy dispersions given in Fig. 2.8 (a-c).

Figure 2.8 (a-c) shows, how the energy dispersion is modified by changing the impurity factor. From the visual comparison, we find the effect of the impurity factor. The spacing between the energy subbands increases when the concentration of *Al* in QWR is increased. There is a gradual increment in splitting. As a result, conductance also changes with respect to chemical potential (μ) as shown in **Figure 2.9**. The extremum points located in energy subbands increase or decrease the conductance by e^2/h. With an increase in the *Al* concentration, the energy subbands show slight anomalies. Hence, the conductance shows generally a growth in stepwise profile with the integer conductivity.

Figure 2.10 shows the conductivity as a function of chemical potential for *GaAs* QWR (that is QWR with zero impurity) and $Ga_{1-x}Al_xAs$ QWR. We can easily see that *GaAs* QWR require a lower chemical potential for conductivity as compared to $Ga_{1-x}Al_xAs$ QWR. Also, for two lower

energy (n = 0, 1) states, conductance shows an increment of $2(2e^2/h)$ for the QWR while for higher energy states, there is an increment in conductance by $2e^2/h$.

Thus, the change in the energy dispersion leads to the variation in transport properties. Therefore, the evaluation of conductance opens the door for understanding the microscopic transport procedure. Further, it could be vital for constructing molecular and nanoscale electronic appliances.

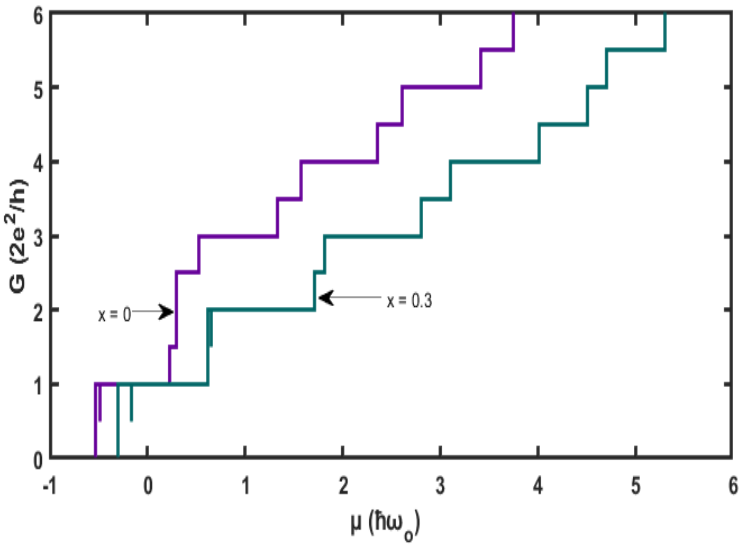

Figure 2.10 Comparison between ballistic conductivity for the *GaAs* (when x = 0) QWR with the $Ga_{1-x}Al_xAs$ (at x = 0.3) QWR.

2.5 SUMMARY

In this paper, we have scrutinized the energy dispersion and ballistic conductance for $Ga_{1-x}Al_xAs$ QWR. Collaborative impacts of the external electric field, magnetic field, SOI, as well as impurity factor on energy dispersions and ballistic conductance, have been investigated. The outcome of numerical calculation conveys that: The electric field causes the downward shifting in the spectrum of energy and ballistic conductivity steps as the chemical potential is increased.

The magnetic field and SOI altered the energy spectrum by lateral shifting that caused camel-back structures. The ballistic conductance of 1D QWR has significantly been influenced by the strengths of the external electric field, magnetic field, impurity concentration, and SOI. The extremum points in the spectrum of energy increase or decrease the conductivity steps by $2e^2/h$. The conductivity has generally a growth in stepwise profile by the factor of the integer conductivity, but due to the presence of exceptional formalism like subbands anticrossing, camelback structure, which includes more than one extremum point in the curve of energy dispersion resulted in the small trough or crest in steps of conductivity. These observations may lead to very interesting results and may be used to adjudicate the authentic character of nanostructures in transport properties and optical properties of 1D systems. To understand the microscopic transport mechanism, we need to analyze the conductance Eigen channels which are illustrated by our study in a meantime. It could perhaps be beneficial to design future molecular and nanoscale electronic devices [55].

2.6 REFERENCES

[1] S. Ghajarpour-Nobandegani, M.J. Karimi, Effects of hydrogenic impurity and external fields on the optical absorption in a ring-shaped elliptical quantum dot, Opt Mater (Amst) 82 (2018) 75–80.

[2] S. Dahiya, S. Lahon, R. Sharma, Effects of temperature and hydrostatic pressure on the optical rectification associated with the excitonic system in a semi-parabolic quantum dot, Physica E Low Dimens Syst Nanostruct 118 (2020) 113918.

[3] M. Royo, M. De Luca, R. Rurali, I. Zardo, A review on III–V core–multishell nanowires: growth, properties, and applications, J Phys D Appl Phys 50 (2017) 143001.

[4] E. Barrigón, M. Heurlin, Z. Bi, B. Monemar, L. Samuelson, Synthesis and applications of III–V nanowires, Chem Rev 119 (2019) 9170–9220.

[5] K.M. Jiang, J. Yang, R. Zhang, H. Wang, Ballistic transport properties in spin field-effect transistors, J Appl Phys 104 (2008).

[6] D. Csontos, U. Zülicke, Large variations in the hole spin splitting of quantum-wire subband edges, Physical Review B—Condensed Matter and Materials Physics 76 (2007) 073313.

[7] Y. Sun, S.E. Thompson, T. Nishida, Physics of strain effects in semiconductors and metal-oxide-semiconductor field-effect transistors, J Appl Phys 101 (2007).

[8] D. Grundler, Ballistic spin-filter transistor, Phys Rev B 63 (2001) 161307.

[9] C.H.L. Quay, T.L. Hughes, J.A. Sulpizio, L.N. Pfeiffer, K.W. Baldwin, K.W. West, D. Goldhaber-Gordon, R. De Picciotto, Observation of a one-dimensional spin–orbit gap in a quantum wire, Nat Phys 6 (2010) 336–339.

[10] Y. V Pershin, S.N. Shevchenko, I.D. Vagner, P. Wyder, Electronic transport through a nuclear-spin-polarization-induced quantum wire, Phys Rev B 66 (2002) 035303.

[11] Y. V Pershin, J.A. Nesteroff, V. Privman, Effect of spin-orbit interaction and in-plane magnetic field on the conductance of a quasi-one-dimensional system, Phys Rev B 69 (2004) 121306.

[12] J.C. Egues, G. Burkard, D. Loss, Datta-Das transistor with enhanced spin control, ArXiv Preprint Cond-Mat/0209682 (2002).

[13] R. Khordad, Optical properties of quantum wires: Rashba effect and external magnetic field, J Lumin 134 (2013) 201–207. https://doi.org/10.1016/j.jlumin.2012.08.047.

[14] R. Sharma, M. Kumar, Effects of impurity factor on the physical and transport properties for Ga1-xAlxAs quantum wire in the presence of Rashba spin-orbit interaction, Physica B Condens Matter 629 (2022) 413649.

[15] Y. Ho Park, H. Kim, J. Chang, S. Hee Han, J. Eom, H.-J. Choi, H. Cheol Koo, Separation of Rashba and Dresselhaus spin-orbit interactions using crystal direction dependent transport measurements, Appl Phys Lett 103 (2013).

[16] L. Meier, G. Salis, I. Shorubalko, E. Gini, S. Schön, K. Ensslin, Measurement of Rashba and Dresselhaus spin–orbit magnetic fields, Nat Phys 3 (2007) 650–654.

[17] S.D. Ganichev, V. V Bel'kov, L.E. Golub, E.L. Ivchenko, P. Schneider, S. Giglberger, J. Eroms, J. De Boeck, G. Borghs, W. Wegscheider, Experimental Separation of Rashba and Dresselhaus Spin Splittings<? format?> in Semiconductor Quantum Wells, Phys Rev Lett 92 (2004) 256601.

[18] S. Antil, M. Kumar, S. Lahon, S. Dahiya, A. Ohlan, R. Punia, A.S. Maan, Influence of hydrostatic pressure and spin orbit interaction on optical properties in quantum wire, Physica B Condens Matter 552 (2019) 202–208.

[19] J.M. Kikkawa, D.D. Awschalom, Resonant spin amplification in n-type GaAs, Phys Rev Lett 80 (1998) 4313.

[20] J. Nitta, T. Akazaki, H. Takayanagi, T. Enoki, Gate control of spin-orbit interaction in an inverted I n 0.53 G a 0.47 As/I n 0.52 A l 0.48 as heterostructure, Phys Rev Lett 78 (1997) 1335.

[21] P.M. Krstajić, M. Pagano, P. Vasilopoulos, Transport properties of low-dimensional semiconductor structures in the presence of spin–orbit interaction, Physica E Low Dimens Syst Nanostruct 43 (2011) 893–900.

[22] J. Nitta, F.E. Meijer, H. Takayanagi, Spin-interference device, Appl Phys Lett 75 (1999) 695–697.

[23] Q. Sun, J. Wang, H. Guo, Quantum transport theory for nanostructures with Rashba spin-orbital interaction, Physical Review B—Condensed Matter and Materials Physics 71 (2005) 165310.

[24] C.L. Romano, S.E. Ulloa, P.I. Tamborenea, Level structure and spin-orbit effects in quasi-one-dimensional semiconductor nanostructures, Physical Review B—Condensed Matter and Materials Physics 71 (2005) 035336.

[25] G. Liu, G. Zhou, A possible realization of spin filter using a quantum wire with Rashba spin-orbit coupling, J Appl Phys 101 (2007).

[26] K.J. Thomas, J.T. Nicholls, M.Y. Simmons, M. Pepper, D.R. Mace, D.A. Ritchie, Possible spin polarization in a one-dimensional electron gas, Phys Rev Lett 77 (1996) 135.

[27] R.G. Pereira, E. Miranda, Magnetically controlled impurities in quantum wires with strong Rashba coupling, Physical Review B—Condensed Matter and Materials Physics 71 (2005) 085318.

[28] F. Mireles, G. Kirczenow, Ballistic spin-polarized transport and Rashba spin precession in semiconductor nanowires, Phys Rev B 64 (2001) 024426.

[29] M. Kumar, S. Lahon, P.K. Jha, S. Gumber, M. Mohan, Spin–orbit interaction effect on nonlinear optical rectification of quantum wire in the presence of electric and magnetic fields, Physica B Condens Matter 438 (2014) 29–33.

[30] S. M'zerd, K. Rahmani, S. Janati, Y. Chrafih, I. Zorkani, A. Jorio, Stark effect of shallow donor impurities in HgS Inhomogeneous Quantum Dots, in: IOP Conf Ser Mater Sci Eng, IOP Publishing, 2017: p. 012015.

[31] L. Liu, J.-J. Liu, Binding energy of ionized-donor-bound excitons in parabolic quantum-well wires in a magnetic field, J Appl Phys 106 (2009).

[32] N.F. Raigoza Bohórquez, Á.L. Morales Aramburo, A.L. Montes Barahona, N. Porras Montenegro, C.A. Duque Echeverri, Stress effects on shallow-donor impurity states in symmetrical GaAs/AlxGa1_xAs double quantum wells, (2004).

[33] W. Xie, Impurity effects on optical property of a spherical quantum dot in the presence of an electric field, Physica B Condens Matter 405 (2010) 3436–3440.

[34] B. Çakır, Y. Yakar, A. Özmen, Linear and nonlinear absorption coefficients of spherical quantum dot inside external magnetic field, Physica B Condens Matter 510 (2017) 86–91.

[35] R. Sharma, M. Kumar, Effects of impurity factor on the physical and transport properties for Ga1-xAlxAs quantum wire in the presence of Rashba spin-orbit interaction, Physica B Condens Matter 629 (2022) 413649.

[36] C.A. Perroni, D. Bercioux, V.M. Ramaglia, V. Cataudella, Rashba quantum wire: exact solution and ballistic transport, Journal of Physics: Condensed Matter 19 (2007) 186227.

[37] I.A. Kokurin, Effect of spin–orbit coupling on spectral and transport properties of tubular electron gas in InAs nanowires, Physica E Low Dimens Syst Nanostruct 74 (2015) 264–269.

[38] P.M. Krstajić, M. Pagano, P. Vasilopoulos, Transport properties of low-dimensional semiconductor structures in the presence of spin–orbit interaction, Physica E Low Dimens Syst Nanostruct 43 (2011) 893–900.

[39] I. Cunha, L. Villegas-Lelovsky, V. Lopez-Richard, L.K. Castelano, Multichannel scattering mechanism behind the reentrant conductance feature in nanowires subject to strong spin-orbit coupling, Phys Rev B 102 (2020) 195423.

[40] K. Kolasiński, A. Mreńca-Kolasińska, B. Szafran, Transconductance and effective Landé factors for quantum point contacts: Spin-orbit coupling and interaction effects, Phys Rev B 93 (2016) 035304.

[41] H.M. Baghramyan, M.G. Barseghyan, A.A. Kirakosyan, R.L. Restrepo, C.A. Duque, Linear and nonlinear optical absorption coefficients in GaAs/Ga1− xAlxAs concentric double quantum rings: Effects of hydrostatic pressure and aluminum concentration, J Lumin 134 (2013) 594–599.

[42] E. Reyes-Gómez, N. Raigoza, L.E. Oliveira, Effects of hydrostatic pressure and aluminum concentration on the conduction-electron g factor in GaAs-(Ga, Al) As quantum wells under in-plane magnetic fields, Physical Review B—Condensed Matter and Materials Physics 77 (2008) 115308.

[43] S. Debald, B. Kramer, Rashba effect and magnetic field in semiconductor quantum wires, Physical Review B—Condensed Matter and Materials Physics 71 (2005) 115322.

[44] N. Arunachalam, A.J. Peter, C.W. Lee, Pressure induced optical absorption and refractive index changes of a shallow hydrogenic impurity in a quantum wire, Physica E Low Dimens Syst Nanostruct 44 (2011) 222–228.

[45] R. Landauer, Spatial variation of currents and fields due to localized scatterers in metallic conduction, IBM J Res Dev 1 (1957) 223–231.

[46] Y. V Pershin, J.A. Nesteroff, V. Privman, Effect of spin-orbit interaction and in-plane magnetic field on the conductance of a quasi-one-dimensional system, Phys Rev B 69 (2004) 121306.

[47] J.A. Nesteroff, Y. V Pershin, V. Privman, Influence of nuclear spin polarization on quantum wire conductance, IEEE Trans Nanotechnol 4 (2005) 141–147.

[48] I.A. Kokurin, Determination of Rashba-coupling strength for surface two-dimensional electron gas in InAs nanowires, Solid State Commun 195 (2014) 49–54.

[49] M. Kumar, S. Lahon, P.K. Jha, M. Mohan, Energy dispersion and electron g-factor of quantum wire in external electric and magnetic fields with Rashba spin orbit interaction, Superlattices Microstruct 57 (2013) 11–18.

[50] R. Rana, L. Balaghi, I. Fotev, H. Schneider, M. Helm, E. Dimakis, A. Pashkin, Nonlinear charge transport in InGaAs nanowires at terahertz frequencies, Nano Lett 20 (2020) 3225–3231.

[51] K.J. Thomas, J.T. Nicholls, M.Y. Simmons, M. Pepper, D.R. Mace, D.A. Ritchie, Possible spin polarization in a one-dimensional electron gas, Phys Rev Lett 77 (1996) 135.

[52] B. Das, S. Datta, R. Reifenberger, Zero-field spin splitting in a two-dimensional electron gas, Phys Rev B 41 (1990) 8278.

[53] A. V Moroz, C.H.W. Barnes, Effect of the spin-orbit interaction on the band structure and conductance of quasi-one-dimensional systems, Phys Rev B 60 (1999) 14272.

[54] J. Luo, H. Munekata, F.F. Fang, P.J. Stiles, Effects of inversion asymmetry on electron energy band structures in GaSb/InAs/GaSb quantum wells, Phys Rev B 41 (1990) 7685.

[55] X.-R. Zhang, X.-F. Peng, S.-H. Tan, M.-Q. Long, Ballistic electrical-thermal transport properties and their applications in graphene-nanoribbon-stacked heterojunctions, Physica E Low Dimens Syst Nanostruct 136 (2022) 115025.

3

CHAPTER

Study the Impact of Hydrostatic Pressure and Temperature on the Ballistic Conductance

- *Exploration of electron quantum transport in semiconductors on the nanoscale is enabled by the influence of electric, magnetic field and spin-orbit coupling in quantum wires offers a promising platform for developing electron transportation devices.*
- *Parabolic confinement with strong magnetic fields and Rashba spin-orbit interaction (RSOI) leads to shifts in dispersion, influencing conductance. Energy eigenvalues and eigenvectors are determined using the diagonalization method, while ballistic conductance is calculated via the Landauer-Büttiker formalism.*
- *Analysis of hydrostatic pressure and temperature effects on the energy band structure and ballistic conductivity. The study examines energy behavior under the influence of external electric and magnetic fields, as well as temperature.*
- *The unique properties of energy subbands result in oscillatory patterns in ballistic conductance.*

3.1 INTRODUCTION

The studies of spin-orbit interaction (SOI) have been growing interest in low-dimensional semiconductor devices made of III-V materials. The SOI is seen as an opportunity to control and manipulate the electron states through gate voltages [1]. Various research activities are activated by SOI on both theoretical and practical grounds, promoted by fundamental physics as well as application aspects [2,3]. Latterly, many papers have studied the effect of SOI along with the presence of the magnetic field and electric field for low-dimensional devices i.e., 2D, 1D and 0D nanostructures. In 2D nanostructures, the presence of SOI and external fields like electric and magnetic field change the optical, mechanical, optical and electronic properties. These changes help the finding pave the way for setting up the real application in optoelectronics [4,5]. Moreover, they have exclusive properties as well as excellent lubricity, chemical inertness and thermal conductivity [6]. Whereas, 0D nanostructures are enchantingly attractive in quantum-information properties due to their beneficial properties and 1D nanostructures are beneficial to be used in electro-optic devices and electronics. There are many researches theoretically and experimental in which electric, magnetic field and SOI play an important role in analysing the physical and electronic properties of 2D, 1D and 0D nanostructures [7–14]. The SOI may evince itself in a novel device either as a consequence of splitting of reversal symmetry of the entire structure, mentioned as Rashba spin-orbit interaction (SOI) term or because of insufficient reversal symmetry in the crystal structure, resorted to as Dresselhaus spin-orbit interaction (SOI) term [15]. For low dimensional nanostructure, spin-orbit plays an essential role in the physical properties and transport properties of the charge carrier. The consequences of Rashba SOI on the band structures spin

accumulation and transport properties of quantum wire (QW) are researched by S. Debald and B. Kramer [16].

The pursuit of understanding the considerable effect due to electron spin on transportation properties has significantly captivated interest during the last few years. The description for transport properties like ballistic conductance quantisation is established by using a model of the non-interacting electron [17]. In which small biasing is exhausted over the channel then electrons start moving from one reservoir to another. On account of transverse confinement in the Channel of the device given by Landauer-B$\ddot{u}$tricker formalism, the electrons are dispensed like fermi-distribution, amid various energy subdivisions of bands in the channel. Each of the energy subdivision bands gives the contribution of $2e^2$/h to the conductance [17,18]. The experiments proficient independently by Yuriy et al. [19] and Quay et al. [20] gave a relation of energy dispersion with ballistic conductance. Using energy band structure, they inflict that each subband gives rise to $2e^2/h$ steps in the ballistic conductance. Some theoretical and experimental works explore the study of ballistic conductance under the presence of external fields like a magnetic field, electric field and Rashba SOI.

We know that outwardly restrained parameters like hydrostatic pressure and temperature are capable of manipulating the optical characteristics of quantum nanostructures. In a confined system, the electric band structure is altered due to hydrostatic pressure causing amendment in electron and hole actual masses, which results in numerous unusual optical as well as physical reactions [21–25]. Hydrostatic pressure and temperature have an impact on the semiconductor devices variables like energy gap, dielectric constant, effective mass, lattice vibration and so on. The hydrostatic pressure makes a great impact on the physical along with transport characteristics of QW. B. S. Ma et al. [26] examined that temperature also affects the physical

properties of semiconductors. Also, a lot of work is done on the collaborative effect of hydrostatic pressure and temperature on the physical characteristics of semiconductor devices [27–31].

To scrutinize the properties in the field of spintronics devices further, we focus on the pressure and temperature's effect on the electronic energy spectrum, and ballistic conductance. Also, study the energy's behaviour with the electrostatic field, magnetic field and temperature. For this, we define parabolic confinement when QW is placed under external electric, intense magnetic field and also taking into account the presence of RSOI. Following is the consortium of our task. First of all, the system is described by analysing the strategy in a nutshell in Sec. 3.2 and Sec. 3.3 is dedicated to mathematical outcomes succeeded by a brief terminating segment.

3.2 PARABOLIC HARMONIC POTENTIAL QUANTUM WIRE

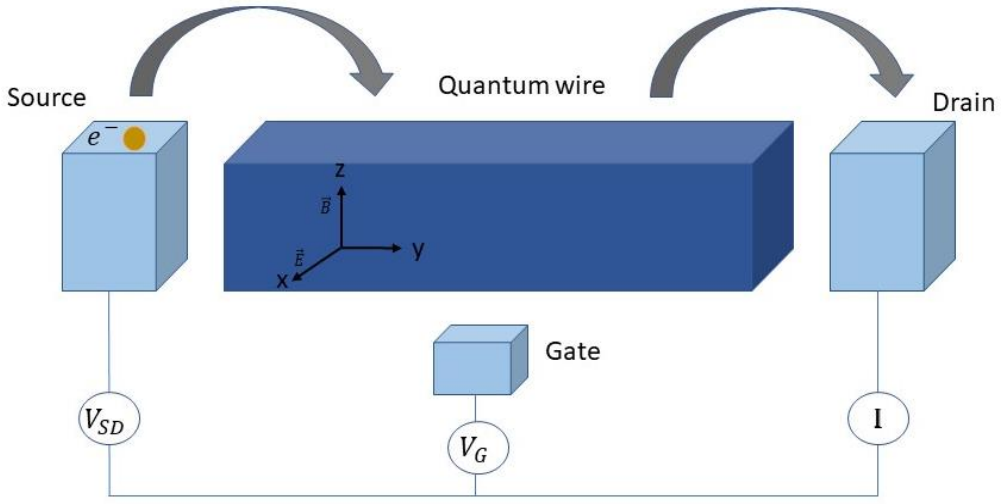

Figure 3.1 Schematic view of the *GaAs* QW which is connected to drain and source reservoirs through tunnel barriers in the presence of electric and magnetic field.

We assume an electron-bound system for the *GaAs* QW. The electron motion is confined only in x direction and the magnetic force field B is applied across QW along the z direction i.e. (0, 0, B) as shown in **Figure 3.1**. Therefore, the analogous vector potential (***A***) in landau gauge can be written as $Bx\hat{j}$ .The Hamiltonian for a single electron is given by [32,33]

$$H = \frac{(p+e\vec{A})^2}{2m_e^*(P,T)} + \frac{1}{2}m_e^*(P,T)\omega_{os}{}^2(P)x^2 + \frac{1}{2}gU_B\vec{\sigma}\cdot\vec{B} + H_R^j \qquad \textbf{(3.1)}$$

Where $\omega_{os}(P)$ is the oscillator strength, $m_e^*(P,T)$ is the pressure and temperature-dependent effective mass for an electron in Eq. (3.1). And g is known as Lande's g-factor, U_B is the Bohr magnetron and Pauli matrix is given by σ. For *GaAs* QW, $m_e^*(P,T)$ is written as [34,35]

$$m_e^*(P,T) = \left[1 + E_P^\Gamma\left(\frac{2}{E_g^\Gamma(P,T)} + \frac{1}{E_g^\Gamma(P,T)+\Delta_0}\right)\right]^{-1} m_o, \qquad \textbf{(3.2)}$$

Where m_o represents the free electron mass, $\Delta_0 = 0.341eV$ & $E_P^\Gamma = 7.51eV$. $E_g^\Gamma(P,T)$ pressure and temperature-dependent energy band gap at Γ-point for GaAs QW, written as

$$E_g^\Gamma(P,T) = E_g^\Gamma(0,0) - \frac{\alpha_i T^2}{T+204} + \beta_i P + \gamma_i P^2, \qquad \textbf{(3.3)}$$

Here,

$E_g^\Gamma(0,0) = 1.519eV, \alpha_i = 5.405\times10^{-4}eV/K, \beta_i = 1.26\times10^{-2}eV/kbar$ and $\gamma_i = 3.771.26\times10^{-2}eV/kbar^2$.

For *GaAs* QW effective width is dependent on hydrostatic pressure, given by

$$W(P) = W(0)\,[1 - 2P\,(S_{11} + S_{12})]^{1/2}, \qquad \textbf{(3.4)}$$

Here, S_{11} and S_{12} are compliance tensor components of *GaAs* and their values are 1.16×10^{-3} kbar^{-1} and -3.7×10^{-4} kbar^{-1} respectively. *W (0)* is known as effective width at zero hydrostatic pressure. Confinement potential is related to effective width as

$$W(P) = \sqrt{\frac{\hbar}{m_e^*(P,T)\omega_{os}(P)}}, \tag{3.5}$$

In eq. 3.1, H_R^j is the Hamiltonian term for Rashba SOI in presence of an external magnetic force field.

$$H_R^j = \frac{\alpha_R}{\hbar}(\vec{\sigma} \times (\vec{p} + e\vec{A})). \tag{3.6}$$

Where, α_R the Rashba SOI factor and varied by the gate voltage.

When an external electric field in *x*-direction i.e., $\vec{E}$ *= (0, 0, E)* is applied to a quantum wire then the system's Hamiltonian transform from eq. (3.1):

$$H_e = \frac{(p_x^2+(p_y+eBx)^2)}{2m_e^*(P,T)} + \frac{1}{2}m_e^*(P,T){\omega_{os}}^2(P)x^2 + eEx + \frac{1}{2}gU_B\vec{\sigma}\cdot\vec{B} + \frac{\alpha_R}{\hbar}(\sigma_x(p_y + eBx) - \sigma_y p_x). \tag{3.7}$$

Under translation, Hamiltonian remain unchanged along the wire and the Hamiltonian energy eigenstate is written as a solution of the plane wave as:

$$\Psi(x,y) = \varphi(x)\, exp(ik_y y). \tag{3.8}$$

Where k_y is the propagation constant for the plane wave in the *y*-direction. On substituting k_y instead of p_y , Reduces H_e into $H_e = H_e^j + H_R^j$ such that

$$H_e^j = \frac{p_x^2}{2m_e^*(P,T)} + \frac{1}{2}m_e^*(P,T)\omega^2(P)(x-x_i)^2 - \frac{e^2E^2}{2m_e^*(P,T)\omega^2(P)} + \frac{\omega_o^2(P)\hbar^2{k_y}^2}{\omega^2(P)2m_e^*(P,T)} - \frac{e^2EB\hbar k_y}{m_e^*(P,T)\omega^2(P)} + \frac{1}{2}gU_B\sigma_z B, \quad \textbf{(3.9)}$$

And

$$H_R^j = \alpha_R(\sigma_x\left(k_y + \frac{eBx}{\hbar}\right) - i\sigma_y\frac{d}{dx}), \quad \textbf{(3.10)}$$

Where $\omega(P) = \sqrt{\omega_o^2(P) + \omega_c^2(P)}$ and $\omega_c(P) = \frac{eB}{m_e^*(P,T)}$ known as effective cyclotron frequency and cyclotron frequency respectively and $x_i = -(\frac{eE}{m_e^*(P,T)\omega^2(P)} + \frac{eB\hbar k_y}{m_e^{*2}(P,T)\omega^2(P)})$ the coordinate of the guiding centre.

From eq (3.5), energy eigenvalues and eigenvectors of H_e^j are given as: -

$$H_e^j\Psi_{n\sigma}(x) = E_{n\sigma}\Psi_{n\sigma}(x) \quad \textbf{(3.11)}$$

And

$$\Psi_{n\sigma}(x) = \frac{1}{(\sqrt{\pi}C_i 2^n n!)^{1/2}}H_n\left(\frac{x-x_i}{c_i}\right)exp\left(-\frac{1}{2}\left(\frac{x-x_i}{c_i}\right)^2\right)\chi_\sigma, \quad \textbf{(3.12)}$$

With $C_i = \sqrt{\frac{\hbar}{m_e^*(P,T)\omega(P)}}$ is known characteristic length of the harmonic oscillator, n=0, 1, 2… and $\sigma = +$ or $-$. $H_n(x)$ is the Hermite polynomial and χ_σ is the spinor function for a spin down and spin up ($\chi_- = \begin{pmatrix}0\\1\end{pmatrix}$) or $\chi_+ = \begin{pmatrix}1\\0\end{pmatrix}$) respectively. The energies eigenvalues of eq. (3.11) are

$$E_{n\sigma} = \hbar\omega\left(n + \frac{1}{2}\right) - \frac{e^2E^2}{2m^*(x,P,T){\omega_i}^2} + \frac{\omega_o^2\hbar^2{k_y}^2}{{\omega_i}^2 2m^*(x,P,T)} - \frac{e^2EB\hbar k_y}{m^*(x,P,T){\omega_i}^2} + \frac{1}{2}g^*\mu_B B\sigma_z. \quad \textbf{(3.13)}$$

As the lateral confining potential $l_o = \sqrt{\frac{\hbar}{m_e^*(P,T)\omega_o(P)}}$ defines by the length scale characterizing.

Confining potential introduces energy scales $E_P = \hbar\omega_O(P)$ and Rashba SOI $\Delta_{SO} = \frac{m_e^*(P,T)\alpha^2}{2\hbar^2}$.

The energy eigenvalues are shown in **Figure 3.2**.

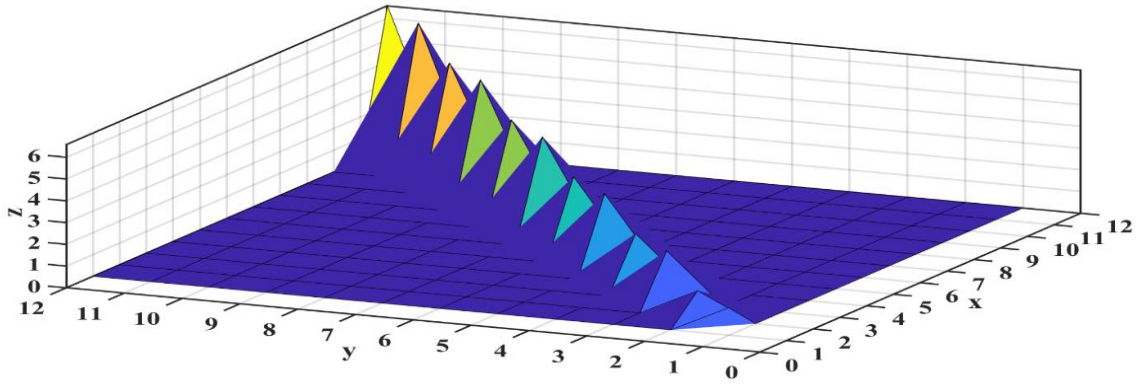

Figure 3.2 Energy eigenvalues of *GaAs* QW when mass is dependent on pressure and temperature.

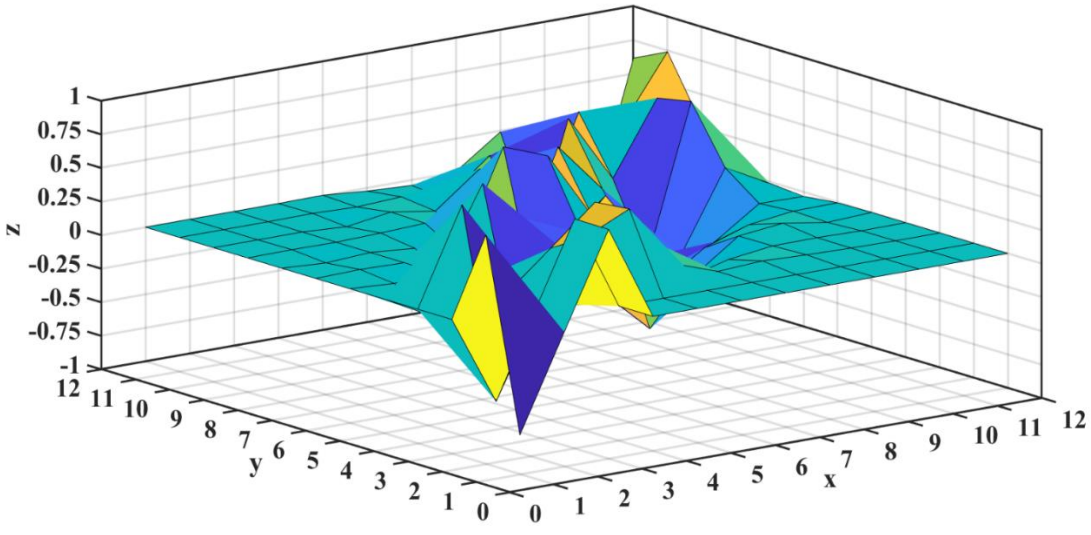

Figure 3.3 Energy eigenvectors of *GaAs* QW when mass is dependent on pressure and temperature.

If we are expanding $\varphi(x) = \sum_{n\sigma} a_{n\sigma}\, \Psi_{n\sigma}(x)$, the Hamiltonian $'\mathrm{H_e}'$ eigenvalue equation can be written as: -

$$\sum_{n\sigma} a_{n\sigma}(E_{n\sigma} - E)\, \Psi_{n\sigma}(x) + \sum_{n\sigma} a_{n\sigma}\, H_R^j \Psi_{n\sigma}(x) = 0, \quad \textbf{(3.14)}$$

$$(E_{n\sigma} - E)a_{n\sigma} + \sum_{n'\sigma'} \langle \Psi_{n\sigma} \left| H_R^j \right| \Psi_{n'\sigma'} \rangle = 0, \quad \textbf{(3.15)}$$

Where the 2nd term of matrix elements of Eq. (3.11) is calculated as:

$$\langle n\sigma | H_R^j | n'\sigma' \rangle = \alpha \left[\left(1 - \frac{\omega_c^2(P)}{\omega^2(P)} \right) k_y - \frac{\omega_c(P) eE}{\hbar \omega^2(P)} \right] \delta_{n,n'} \delta_{\sigma,\sigma'} + \frac{\alpha}{c_i} \left[\left(\frac{\omega_c(P)}{\omega(P)} + \sigma \right) \sqrt{\frac{n+1}{2}}\, \delta_{n,n'-1} + \left(\frac{\omega_c(P)}{\omega(P)} - \sigma \right) \sqrt{\frac{n}{2}} \delta_{n,n'-1} \right] \delta_{\sigma,-\sigma'}, \quad \textbf{(3.16)}$$

After diagonalization of Eq. (3.14), we obtain the eigenfunction, eigenvectors (shown in Fig. 3.3) and the energy dispersion of the subbands in *GaAs* QW for various values of pressure and temperature.

For the calculation of Ballistic conductance, we are using further a philosophized form of Landuer-Büttiker formula, which considers energy bands as erratic local exterior points and spin dependence is formulated as [36–38]:

$$G' = \sum_{i,n} C_{i,n}\, f_o(\varepsilon_{i,k_n}), \quad \textbf{(3.17)}$$

where the aggregate is deliberated over the exterior points of all subbands. The quantity $\varepsilon_{\mathrm{i,k_n}}$ is the energy at the peak points $k_y = k_{i,n}$, $C_{i,n} = 1$*(or* $C_{i,n} = -1$*)* for a local energy extremum points for the given ith spin split subband. The association of physical conductance G with G' for spin-split subbands is given as

$$G = \left(\frac{2e^2}{h} \right) G'. \quad \textbf{(3.18)}$$

And *G* is known as ballistic conductance.

3.3 RESULT AND DISCUSSION:

Here, we have performed the numerical computation for *GaAs* Quantum wire with the mass dependence on temperature and pressure at the static electric field (E = 0.6×10^{6}V/m), magnetic field (B = 1T) and Rashba SOI ($\alpha = 25\text{nm meV}$). In the residence of pressure and temperature in GaAs Quantum wire, we want to study the spectrum of the energies (in sec. A) and ballistic conductance's (G) behaviour (in sec. B) and we also demonstrate the energy dependence on external electric field (E), the intensity of magnetic field (B) and temperature of mass dependence at $k_y = 0$ (in sec. C).

Section A: *Energy Spectra*

In this Sec., we focus on the energy dispersions curve for the various value of pressure and temperature. **Figure 3.4 (a)** shows the energy dispersion for 2 kbar pressure at temperature 300K. In which there are some anti-crossing subbands structures (where solid line represents quasi spin-up state and dotted line presents quasi spin-down state) seen at lower energies state (n = 0,1) due to large value off-diagonal elements of Rashba spin-orbit contribution. And the separation between the subbands is non-uniform due to the effect of symmetric breaking when Rashba SOI and an intense magnetic field are applied at the same time. Therefore, the contribution of magnetic field and Rashba SOI interaction gives rise to varying remarkable separation in spin-up and spin-down branches of the energy states. This separation is known as spin-orbit gap. The energy dispersion used in spintronics application for the confirmation of spin transport. This could be achieved either through direct detection of the spin current or through the detection of spin accumulation at the two ends of the device [36,37]. **Figure 3.4**

(b), there is shifting in two directions of energy dispersions due to the increment in the pressure from 2kbar to 15 kbar.

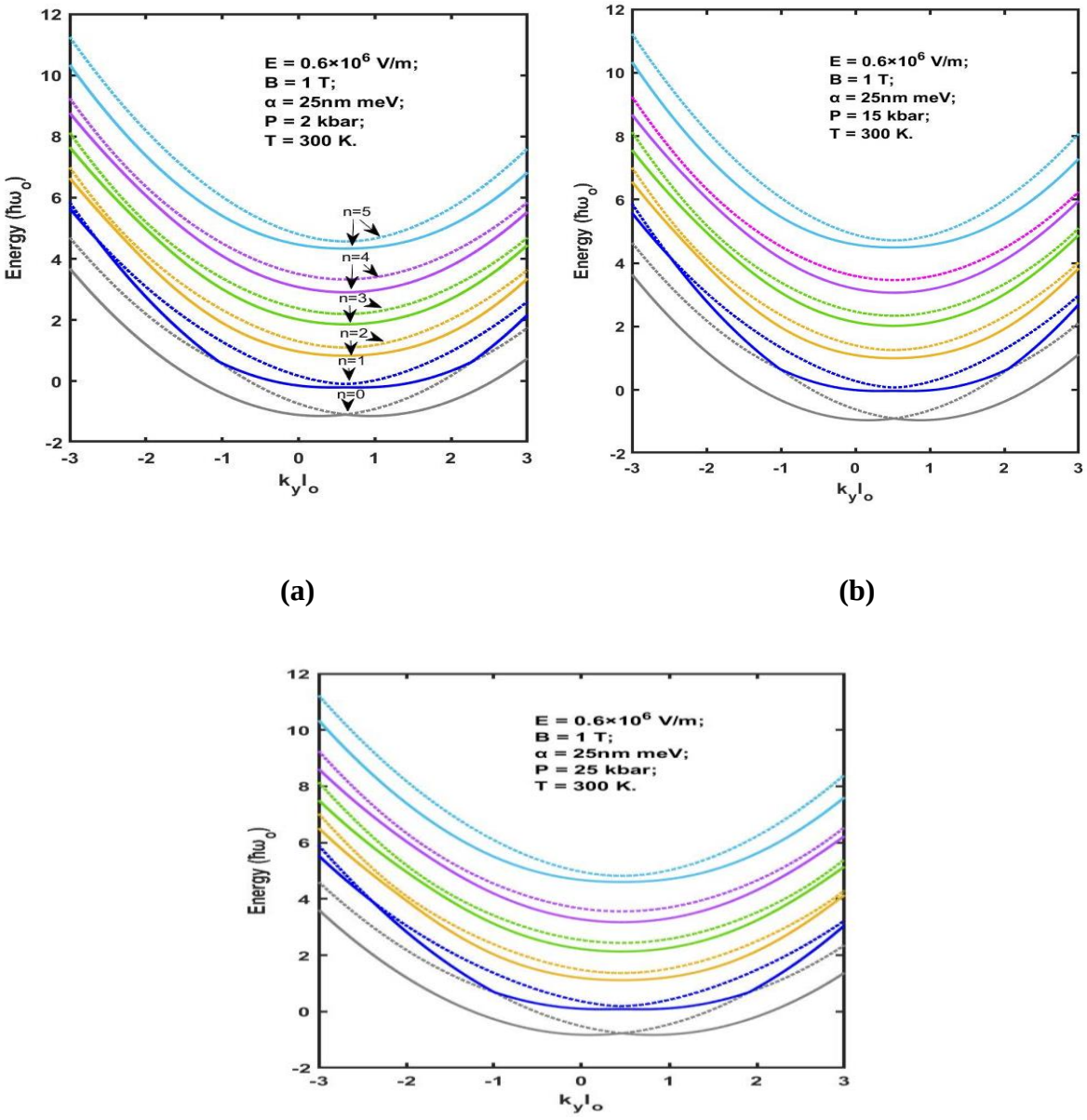

Figure 3.4 Energy dispersion as a function of $k_y l_o$ potential at B = 1 T; E=0.6× 10^6 V/m and Rashba SOI = 25 nm meV for (a) P = 2 kbar, (b) P = 15 kbar and (c) P =1 5 kbar at temperature = 300 K.

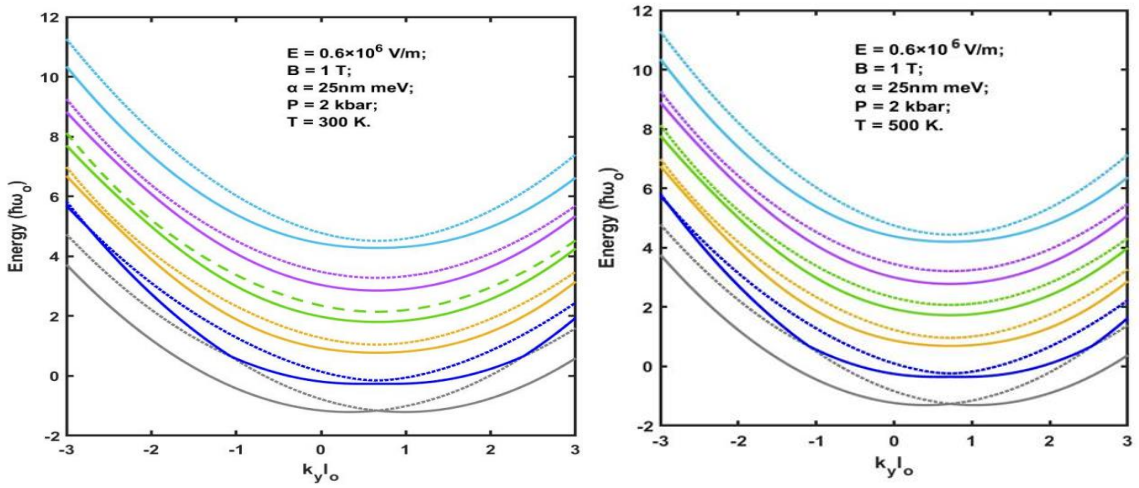

(a) **(b)**

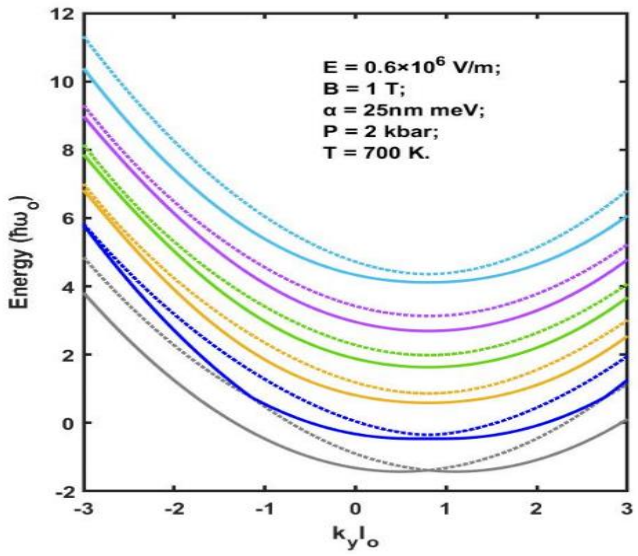

(c)

Figure 3.5 Energy dispersion as a function of $k_y l_o$ at B = 1 T; E = 0.6× 10^6 V/m and Rashba SOI = 25 nm meV (a) T = 300 K, (b) T = 500 K and (c) T = 700 K at Pressure = 2 kbar.

First is the laterally shift along the negative $k_y l_o$ direction and the second shift in an upward direction (shown in **Figure 3. 4 (b)**). As we increase the pressure by 25 kbar at temperature

100K (shown in **Figure 3.4 (c)**), the shifting in the lateral direction and upward direction also increases. We observe from **Figure 3.4 (a-c)** that the energy spectrum shifts as the pressure increases. The reason for this shifting is the increase in the effective mass of the electron, eq. (3.2), as the pressure increases. It is worth mentioning that by increasing the pressure, the wave function associated with the electron is more compressed and localized.

It is fruitful to examine the extent to which temperature and pressure of mass dependence interact to influence the system at this level. In **Figure 3.5**, three energy dispersion curves are plotted for the distinct temperature at constant pressure (2 kbar). In the case of 300K temperature (**Figure 3.5 (a)**), spin degeneracy is removed only for higher energies while intense anticrossing /crossings for states of least energy are visible. When the temperature rises from 300K to 700K, subbands get modified considerably by shifting in the downward direction and as well as in the lateral direction along the positive $k_y l_o$ axis (in **Figure 3.5 (b-c)**), the total shifting depends on the temperature values. Shifting is higher for a large value of the temperature of mass dependence.

Section B: *Ballistic Conductance*

In this section, our aim is to find the impact of pressure and temperature on ballistic conductance. According to Landuer-Bütter formalism, the conductivity of a ballistic *GaAs* quantum wire is associated with two electron reservoirs of macroscopic level (by ignoring the electron-electron reciprocation). And the extremum points in the energy subbands give rise to an increment or decrement in the conductance by $2e^2/h$. Increment in energy causes the opening of more propagating channels so the conductance steps up in the staircase shape. In **Figure 3.6** ballistic conductivity of *GaAs* quantum wire is related to chemical potential. When we apply pressure (2 kbar, 15kbar and 25kbar) the ballistic conductivity shows a stepwise

increment. From **Figure 3.4 (a-c)** and **Figure 3.5 (a-c)**, each minimum point and maximum point in the spectrum of energies provide increment and decrement of $2e^2/h$ to the ballistic conductance, respectively [39]. Each step in the ballistic conductance curve displays the 'turning on' of the latest mode called conducting channel therefore an additional electron can move laterally. For designing modulators and spin filters, ballistic conductance offers a new approach. Each of the subbands contributes $2e^2/h$ to the conductance as a consequence of external field and conditions as observed in experimental research also e.g., in [38,39]. The chemical potential grows as the energy bands are split; the first contribution in conductance comes from the lowest minimum in **Figures 3.4 (a-c)** and **3.5 (a-c)** and the second contribution comes when the chemical potential reaches the second minimum of the same subband. Whenever the chemical potential is further raised and passes through the local maximum point, the conductance will decrease by $2e^2/h$ factor. The peaks in conductance are created by this mechanism, as shown in **Figure 3.6**. Higher pressure requires higher chemical potential and it's vice-versa for temperature. The monotonic increasing characteristic is shown by the dips on ballistic conductance steps which are noticeable in energy spectra. This situation is more pronounced in lower energy states. When we differ in temperature and pressure then more than one extreme point is obtained in the energy state, as a result, narrow dips are induced in ballistic conductance steps (**Figure 3.6**).

In **Figure 3.7**, the variation of ballistic conductance with chemical potential is shown for two cases. Firstly, when temperature and pressure are 300K and 2kbar respectively. And secondly, when temperature and pressure both are zero. The ballistic conductance study helps in the manufacturing of electronic and spintronic devices and it also gives a new strategy for designing a spin filter [40–42].

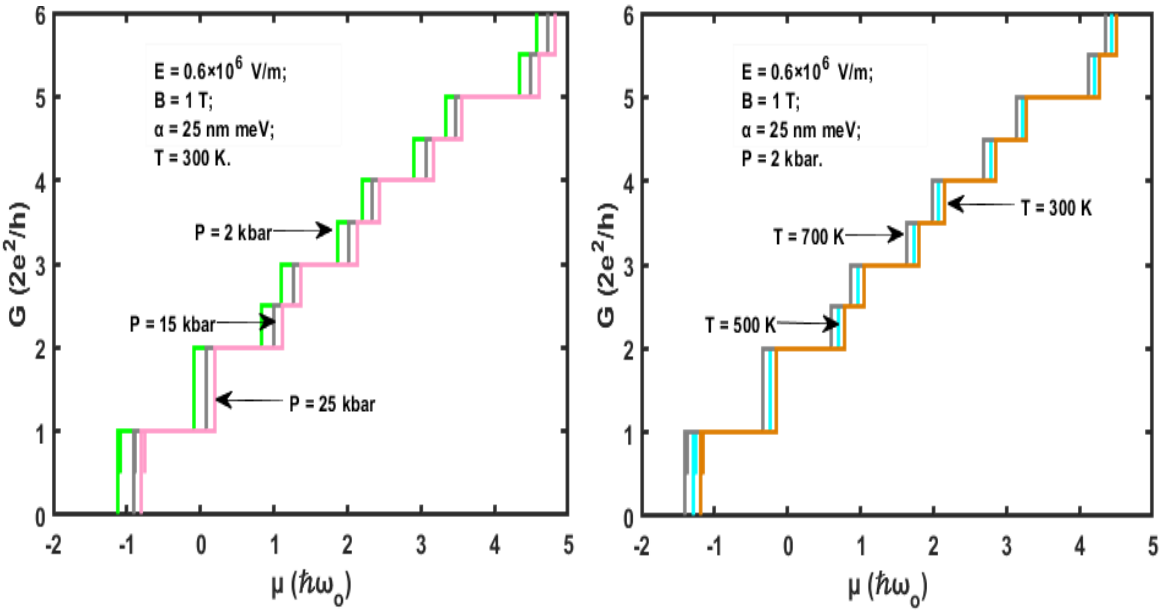

(a) **(b)**

Figure 3.6 (a & b) Conductance (G) as a function of chemical potential (μ) for energy dispersions curve given in Fig. 3.4 (a-c) and Fig. 3.5 (a-c) respectively.

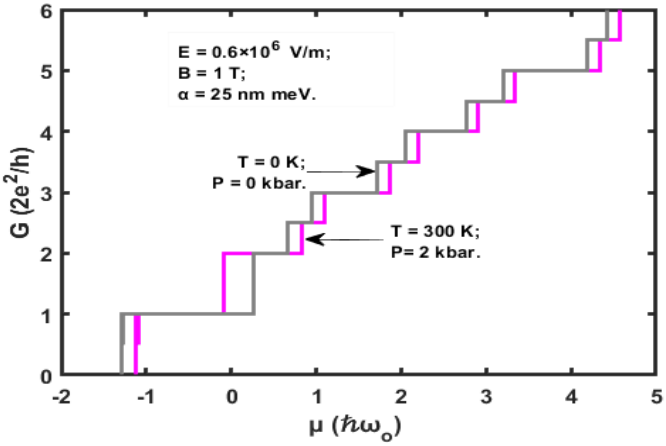

Figure 3.7 Ballistic conductance as a function of chemical potential at B = 1 T; E = 0.6× 10^6 V/m and Rashba SOI = 25 nm meV when T = 0 K; P = 0 kbar and T = 300 K; P = 2 kbar.

Section C: *Energy as a Function of E, B and Temperature*

In **Figure 3.8**, we imply that energy dispersion depends on the external electric field This is a sighting that negative and positive values of the external electrostatic field give rise to uniform structure and have the peak at zero electric fields. Furthermore, the subbands splitting inflate and all spin branches sink towards low energy states as the external field strength increases. This is evident that the system's efficacious configuration significantly alters the spectrum of energy. Consequently, in **Figure 3.9** we manifest the contrast of the energy subbands along the magnetic field and we observe that energies of all the spin branches increase when there is an increment in magnetic field intensity. **Figure 3.10** shows the energy dependence on the applied temperature for a lower energy state (n = 0) at two fixed values of pressure of mass dependence i.e., 2 kbar and 4 kbar. We easily observe that the energy curves move towards lower energy states with a rise in the applied temperature of mass dependence. For pressure 4 kbar of mass dependence, the values of lower state energies are high as compared with energy values for pressure 2 kbar.

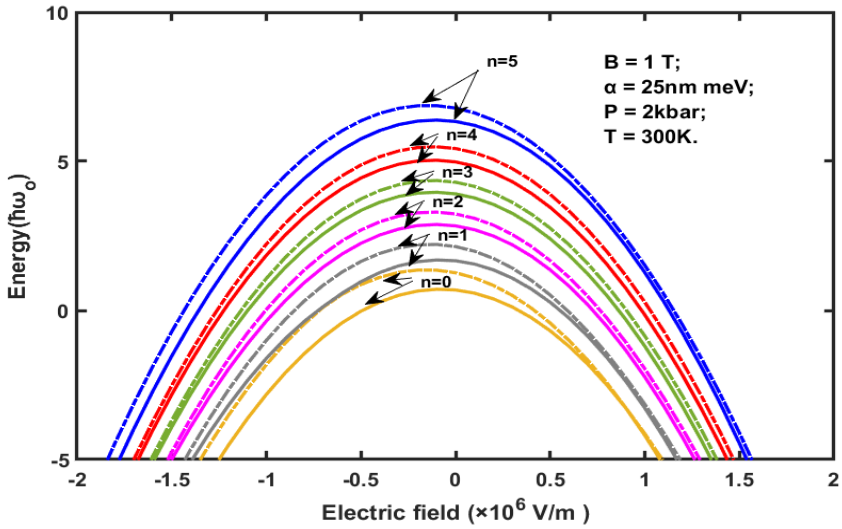

Figure 3.8 The Energy dependence on the electric strength.

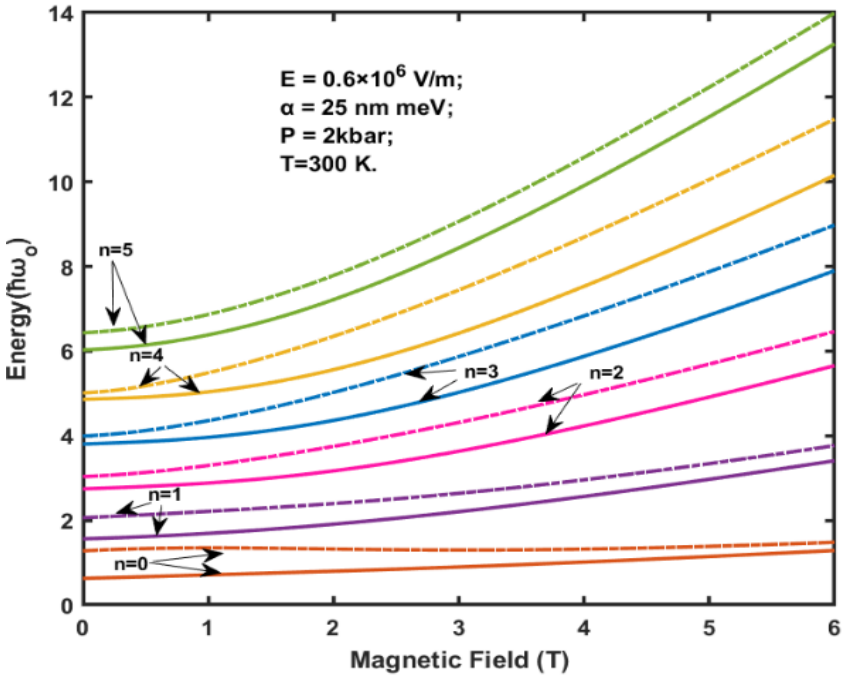

Figure 3.9 The Energy dependence on the field magnetic field.

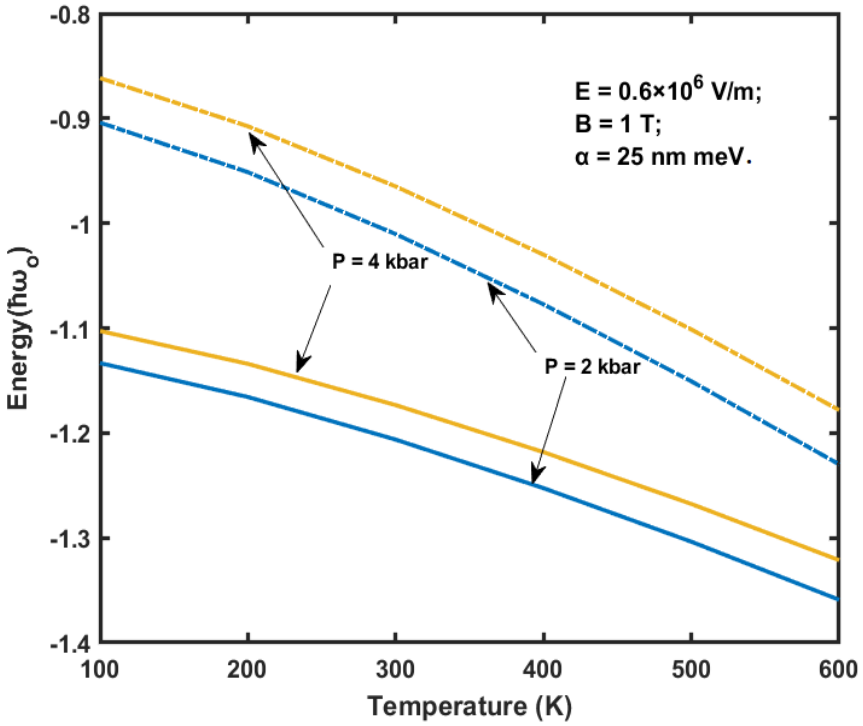

Figure 3.10 The energy dependence on the temperature for lower energy state (n=0).

3.4 SUMMARY

Hydrostatic pressure and temperature, the effect on the energy dispersions and ballistic conductance for a *GaAs* quantum wire is studied in this paper. The energy dispersions can be regulated by pressure and temperature of mass dependence according to the numerical results. Moreover, we conclude that ballistic conductance is sensitive to pressure and temperature of mass dependence. An anomaly is shown by the total conductance G for low energies due to the anticrossing of subbands. In addition, we study energy as a function of the external electric field, magnetic field and temperature of mass dependence which present regular patterns. In recent times, there are latest and enthralling viewpoints, as there is a logical relevance of conductance in topological insulators as well as Majorana fermions in hybrid superconductivity- semiconducting heterostructures, which are drawing attention enormously not merely in condensed matter community. In future, we assure prosperity in this area of investigation. The latest electronic and spin transport electronic devices will hold the market with a utility which will be associated with the physics of transport features. Alternatively, for the Majorana quasiparticle research case, conductance can overlay way for essential investigation for sake of inspecting unusual phenomenon which could be impressed by quantum simulators achieved in a system of solid state.

3.5 REFERENCES

[1] J.C. Egues, G. Burkard, D. Loss, Rashba Spin-Orbit Interaction and Shot Noise for Spin-Polarized and Entangled Electrons, Phys Rev Lett 89 (2002) 176401.

[2] E.I. Rashba, Al.L. Efros, Orbital Mechanisms of Electron-Spin Manipulation by an Electric Field, Phys Rev Lett 91 (2003) 126405.

[3] I. Žutić, J. Fabian, S. Das Sarma, Spintronics: Fundamentals and applications, Rev Mod Phys 76 (2004) 323.

[4] P.T.T. Le, M. Yarmohammadi, Perpendicular electric field effects on the propagation of electromagnetic waves through the monolayer phosphorene, J Magn Magn Mater 491 (2019) 165629.

[5] P.T.T. Le, T.C. Phong, M. Yarmohammadi, β_{12} -Borophene becomes a semiconductor and semimetal *via* a perpendicular electric field and dilute charged impurity, Physical Chemistry Chemical Physics 21 (2019) 21790–21797.

[6] P. T. T. Le, M. Davoudiniya, M. Yarmohammadi, Interplay of orbital hopping and perpendicular magnetic field in anisotropic phase transitions for Bernal bilayer graphene and hexagonal boron-nitride, Physical Chemistry Chemical Physics 21 (2019) 238–245.

[7] S. Cao, C. Cao, S. Tian, J.-H. Chen, Enhancement of spin-orbit coupling and magnetic scattering in hydrogenated graphene, Phys Rev B 104 (2021) 125422.

[8] H. Liu, T. Zhang, K. Wang, F. Gao, G. Xu, X. Zhang, S.-X. Li, G. Cao, T. Wang, J. Zhang, X. Hu, H.-O. Li, G.-P. Guo, Gate-Tunable Spin-Orbit Coupling in a Germanium Hole Double Quantum Dot, Phys Rev Appl 17 (2022) 044052.

[9] J. Sonehara, M. Kammermeier, D. Sato, D. Iizasa, U. Zülicke, S. Karube, J. Nitta, M. Kohda, Anisotropic spin dynamics in semiconductor narrow wires from the interplay between spin-orbit interaction and planar magnetic field, Phys Rev B 105 (2022) 094434.

[10] V.T. Pham, H. Yang, W.Y. Choi, A. Marty, I. Groen, A. Chuvilin, F.S. Bergeret, L.E. Hueso, I. V. Tokatly, F. Casanova, Large spin-charge interconversion induced by interfacial spin-orbit coupling in a highly conducting all-metallic system, Phys Rev B 104 (2021) 184410.

[11] M. Inglot, V.K. Dugaev, A. Dyrdał, J. Barnaś, Graphene with Rashba spin-orbit interaction and coupling to a magnetic layer: Electron states localized at the domain wall, Phys Rev B 104 (2021) 214408.

[12] H. Yang, Q. Wang, J. Fu, Interface involved Dresselhaus spin-orbit coupling in GaInAs/AlInAs heterostructures, Phys Rev B 104 (2021) 125426.

[13] S.M. Frolov, S. Lüscher, W. Yu, Y. Ren, J.A. Folk, W. Wegscheider, Ballistic spin resonance, Nature 458 (2009) 868–871.

[14] Y. Sun, S.E. Thompson, T. Nishida, Physics of strain effects in semiconductors and metal-oxide-semiconductor field-effect transistors, J Appl Phys 101 (2007).

[15] D. Grundler, Ballistic spin-filter transistor, Phys Rev B 63 (2001) 161307.

[16] S. Debald, B. Kramer, Rashba effect and magnetic field in semiconductor quantum wires, Phys Rev B 71 (2005) 115322.

[17] Priyanka, R. Sharma, M. Kumar, Effects of impurity factor on the physical and transport properties for Ga1-xAlxAs quantum wire in the presence of Rashba spin-orbit interaction, Physica B Condens Matter 629 (2022) 413649.

[18] Y. Ho Park, H. Kim, J. Chang, S. Hee Han, J. Eom, H.-J. Choi, H. Cheol Koo, Separation of Rashba and Dresselhaus spin-orbit interactions using crystal direction dependent transport measurements, Appl Phys Lett 103 (2013).

[19] Y. V. Pershin, J.A. Nesteroff, V. Privman, Effect of spin-orbit interaction and in-plane magnetic field on the conductance of a quasi-one-dimensional system, Phys Rev B 69 (2004) 121306.

[20] C.H.L. Quay, T.L. Hughes, J.A. Sulpizio, L.N. Pfeiffer, K.W. Baldwin, K.W. West, D. Goldhaber-Gordon, R. de Picciotto, Observation of a one-dimensional spin–orbit gap in a quantum wire, Nat Phys 6 (2010) 336–339.

[21] S. Zhang, R. Liang, E. Zhang, L. Zhang, Y. Liu, Magnetosubbands of semiconductor quantum wires with Rashba and Dresselhaus spin-orbit coupling, Phys Rev B 73 (2006) 155316.

[22] F. Malet, M. Pi, M. Barranco, L. Serra, E. Lipparini, Exchange-correlation effects on quantum wires with spin-orbit interactions under the influence of in-plane magnetic fields, Phys Rev B 76 (2007) 115306.

[23] Z. Zeng, C.S. Garoufalis, S. Baskoutas, G. Bester, Electronic and optical properties of ZnO quantum dots under hydrostatic pressure, Phys Rev B 87 (2013) 125302.

[24] F. Ungan, R.L. Restrepo, M.E. Mora-Ramos, A.L. Morales, C.A. Duque, Intersubband optical absorption coefficients and refractive index changes in a graded quantum well under intense laser field: Effects of hydrostatic pressure, temperature and electric field, Physica B Condens Matter 434 (2014) 26–31.

[25] F. Mireles, G. Kirczenow, Ballistic spin-polarized transport and Rashba spin precession in semiconductor nanowires, Phys Rev B 64 (2001) 024426.

[26] B.S. Ma, X.D. Wang, F.H. Su, Z.L. Fang, K. Ding, Z.C. Niu, G.H. Li, Photoluminescence from self-assembled long-wavelength InAs/GaAs quantum dots under pressure, J Appl Phys 95 (2004) 933–938.

[27] L. Bouzaïene, R. Ben Mahrsia, M. Baira, L. Sfaxi, H. Maaref, Hydrostatic pressure and temperature effects on nonlinear optical rectification in a lens shape InAs/GaAs quantum dot, J Lumin 135 (2013) 271–275.

[28] F. Segovia-Chaves, H. Vinck-Posada, The effect of the hydrostatic pressure and temperature on the defect mode in the band structure of one-dimensional photonic crystal, Optik (Stuttg) 156 (2018) 981–987.

[29] L. Bouzaiene, H. Alamri, L. Sfaxi, H. Maaref, Simultaneous effects of hydrostatic pressure, temperature and electric field on optical absorption in InAs/GaAs lens shape quantum dot, J Alloys Compd 655 (2016) 172–177.

[30] W. Xie, Hydrostatic pressure and temperature effects of an exciton–donor complex in quantum dots, Physica B Condens Matter 407 (2012) 1134–1138.

[31] A. Sivakami, M. Mahendran, Hydrostatic pressure and temperature dependence of correlation energy in a spherical quantum dot, Superlattices Microstruct 47 (2010) 530–537.

[32] E. Kasapoglu, F. Ungan, H. Sari, I. Sökmen, The hydrostatic pressure and temperature effects on donor impurities in cylindrical quantum wire under the magnetic field, Physica E Low Dimens Syst Nanostruct 42 (2010) 1623–1626.

[33] M.G. Barseghyan, A. Hakimyfard, S.Y. López, C.A. Duque, A.A. Kirakosyan, Simultaneous effects of hydrostatic pressure and temperature on donor binding energy and photoionization cross section in pöschl–teller quantum well, Physica E Low Dimens Syst Nanostruct 42 (2010) 1618–1622.

[34] U. Yesilgul, S. Şakiroğlu, E. Kasapoğlu, H. Sari, I. Sökmen, The effects of temperature and hydrostatic pressure on the photoionization cross-section and binding energy of impurities in quantum-well wires, Superlattices Microstruct 48 (2010) 106–113.

[35] R. Arulmozhi, A.J. Peter, C.W. Lee, Optical absorption in a CdS/CdSe/CdS asymmetric quantum well, Chem Phys Lett 742 (2020) 137129.

[36] Y. V. Pershin, J.A. Nesteroff, V. Privman, Effect of spin-orbit interaction and in-plane magnetic field on the conductance of a quasi-one-dimensional system, Phys Rev B 69 (2004) 121306.

[37] B.H. Mehdiyev, A.M. Babayev, S. Cakmak, E. Artunc, Rashba spin–orbit coupling effect on a diluted magnetic semiconductor cylinder surface and ballistic transport, Superlattices Microstruct 46 (2009) 593–602.

[38] G. Gumbs, A. Balassis, D. Huang, Energy bands, conductance, and thermoelectric power for ballistic electrons in a nanowire with spin-orbit interaction, J Appl Phys 108 (2010).

[39] C.H.L. Quay, T.L. Hughes, J.A. Sulpizio, L.N. Pfeiffer, K.W. Baldwin, K.W. West, D. Goldhaber-Gordon, R. de Picciotto, Observation of a one-dimensional spin–orbit gap in a quantum wire, Nat Phys 6 (2010) 336–339.

[40] S. Kumar, K.J. Thomas, L.W. Smith, M. Pepper, G.L. Creeth, I. Farrer, D. Ritchie, G. Jones, J. Griffiths, Many-body effects in a quasi-one-dimensional electron gas, Phys Rev B 90 (2014) 201304.

[41] C.H.L. Quay, T.L. Hughes, J.A. Sulpizio, L.N. Pfeiffer, K.W. Baldwin, K.W. West, D. Goldhaber-Gordon, R. de Picciotto, Observation of a one-dimensional spin–orbit gap in a quantum wire, Nat Phys 6 (2010) 336–339.

[42] L. Gen-Hua, Z. Guang-Hui, Conductance for a quantum wire with weak Rashba spin-orbit coupling, Chinese Physics Letters 22 (2005) 3159.

4

CHAPTER

Impurity Effect on the Optical Properties of $Ga_{1-x}Al_xAs$ *Quantum Wire*

- *This study investigates how impurity factors influence various optical properties, including optical absorption coefficients, refractive index changes, and both second and third harmonic generation, within* $Ga_{1-x}Al_xAs$ *quantum wires.*
- *Using the compact density-matrix approach, the study derives analytical expressions for linear and non-linear optical absorption, refractive index changes, and harmonic generation coefficients.*
- *The results demonstrate that the optical properties are highly sensitive to impurity concentration. The impurity factor significantly influences the magnitude and position of peaks, offering opportunities for tuning optical non-linearity.*
- *The control over optical non-linearity via impurity factor has potential applications in device development, particularly for systems requiring precise optical property manipulation.*

4.1 INTRODUCTION

In the few last years, low-dimensional nanostructures like: quantum dots, quantum wires, and quantum well have considerable devotion for their alluring potential applications in optical and laser technology [1–5]. In these nanostructures, the charge carrier having quantum confinement accompany the formation of energy states in the discrete form and enhance the density of states at definite energies which leads to variation in the optical spectra and helps in the evolution of novel properties. The optical properties viz. absorption spectra and refractive index changes (RICs) in the low-dimensional nanostructures take fascinated courtesy due to their high-level performance. One of the most arduously explored low-dimension nanostructures is quantum wire, especially in the theoretical and experimental research of the impurity effect on their optical properties [6–11]. Moreover, the tunability of the energy dispersion by the intense magnetic field, electric field, impurity factor, and Rashba spin-orbit interaction in the quantum wire has made a fruitful role in examining non-linear and linear properties for applications of novel devices [12,13].

A region of large potency is the spin-based phenomena in quantum wire for its profusion of the physically observable phenomena and has an encouraging future for spin-related electronic devices with a high degree of functionality, fast speed, and low power consumption [14–16]. Fortunately, spin physics in low-dimension nanostructures utilizes electron spin degree of freedom as a chunk of information instead of an electron-charge and assurance potential for imminent spin-based application devices that are smaller, faster, and more influential ergo those that are presently available. Specifically, the spin-orbit interaction (SOI) has fascinated enthusiasm as it permits optical spin detection and spin orientation. Moreover, SOI is assumed

as an opportunity for controlling and manipulating the state of an electron via gate voltage. The type of SOI, eminent in a certain quantum wire heterostructure is the Rashba SOI. The Rashba SOI comes out in the picture due to the confinement potential which explains the quantum wire is a function perpendicular to the 2-dimension electron gas (2 DEG). This conjectures a structural inversion symmetry that easily can be tweaked by the external gate potential and also control the spin-related phenomena [17–20].

Although more study has been admiring to research the effect of Rashba SOI on the optical and physical properties of the quantum wire. The optical properties have been explored by lots of investigators in both theoretical and experimental [21–30]. Some external constraints like the intense electric field, magnetic field, Rashba SOI, impurity factor (x), etc play a significant role to influence the optical properties of quantum wire [31–35]. M. Santhi et al. [36] have vastly explored the effects of hydrogenic impurity on the linear and third-order nonlinear optical absorption coefficients (ACs), and third harmonic generation (THG) optical properties of GaAs/GaAlAs quantum wire. However, when the electron is bound with the impurity atom within the presence of external perturbations shows rudimental character in grasping the electro-optical properties of hydrogenic impurities in nanostructures. The inclusion of hydrogenic impurities in nanostructures will excessively change the electrical and optical properties and affect the quantum device concert.

Martinez et al.[37] have explored the hydrostatic pressure and temperature effects on the hydrogenic impurity which relates cross-section of photoionization and impurity binding energy in $Ga_{1-x}Al_xAs/GaAs$ quantum wire. Zeiri et al. [38]discussed the linear and nonlinear susceptibility of self-organized in $GaN/Ga_{1-x}Al_xN$ quantum wire. Embroidering the energy dispersion is enthusiastic to yield the expedient optoelectronic device from the belief of confinement in the low-dimension nanostructures, transmission properties, and tunable

emission are assumed to be significant features for them. Moreover, the optical properties are studied by many researchers.

With this motivation, the current chapter aims to represent the behavior of linear and third-order nonlinear optical (ACs), an absolute change in refractive index coefficients (RICs), second harmonic generation (SHG), and THG associated with the $Ga_{1-x}Al_xAs$ Quantum wire. The following is the work's alignment: In a nutshell, Section 4.2 represents the theoretical model of our system. The corresponding outcomes and discussion are noted in Section 4.3. Belatedly, Section 4.4 covers the study's foremost conclusions.

4.2 PARABOLIC HARMONIC POTENTIAL $Ga_{1-x}Al_xAs$ QUANTUM WIRE

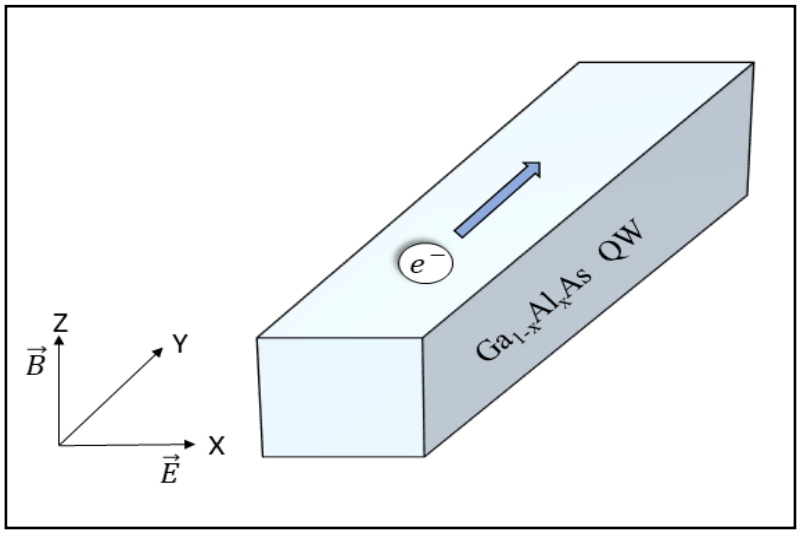

Figure 4.1 The diagram of *$Ga_{1-x}Al_xAs$* quantum wire within the existence of an external magnetic electric field, and Rashba SOI.

The Hamiltonian equation for *$Ga_{1-x}Al_xAs$* quantum wire under the influence of electric field (***E***) along *X*-direction, intense magnetic field (***B***) along *Z*-direction (shown in **Figure 4.1**), and Rashba SOI, respectively is written by

$$\widehat{H}_{oe} = -\frac{1}{2m_e^*(x,P,T)}\left(p_X + (p_Y + eBX)^2 + \frac{1}{2}m_e^*(x,P,T)\omega_{1e}^2X^2 + eEX + \frac{1}{2}g^*\mu_B B\sigma_Z + \frac{\alpha}{\hbar}[\sigma_X(p_Y + eBX) - \sigma_Y p_X)\right], \quad \textbf{(4.1)}$$

Where p_X and p_Y represents the momentum component of an electron in *X* and *Y* direction. ω_{1e} is called effective cyclotron frequency. α, $g^*, \mu_B, \sigma_X, \sigma_Y,$ and σ_z are known as Rashba SOI factor, Landé factor, Bohr magneton and Pauli matrices along x, y and z direction, respectively. $m_e^*(x,P,T)$ is known effective mass represented by [39]:

$$m_e^*(x,P,T) = m_o\left[\left(\frac{1}{\Delta_{oj}(x)+E_g^j(x,P,T)} + \frac{2}{E_g^j(x,P,T)}\right)\frac{\pi_j^2(x)}{3} + \delta_j(x) + 1\right]^{-1}, \quad \textbf{(4.2)}$$

Here, m_o is known as free electron mass, x is used for impurity factor, $\Delta_{oj}(x)$ and $\pi_j(x)$ are known as valence band spin-orbit coupling and inter-band matrix element, respectively ($\pi_j^2(x) = (-6290x + 28900)$meV and $\Delta_{oj}(x) = (-66x + 341)$meV). When the remote-band effects are examined over $\delta_j(x)$ the parameter is given by [40]:

$$\delta_j(x) = 4.938x^2 + 0.488x - 3.935, \quad \textbf{(4.3)}$$

In eq. (4.2), $E_g^j(x,P,T)$ is called conduction band's an energy gap and is expressed via

$$E_g^j(x,P,T) = p_j + q_j x + r_j x^2 + s_j P - \frac{\beta_j T^2}{\gamma_j + T}. \quad \textbf{(4.4)}$$

where the parameters' values $p_j, q_j, r_j, s_j, \gamma_j$ and β_j are given by 1519.4 meV, 1360 meV, 220meV, 10.7 meV/kbar, 204 K and 0.5405 meV/K, respectively. And the values of these parameters are determined with the assistance of photoluminescence.

Eq. (4.1) can be rewritten as write $\widehat{H}_{oe} = \widehat{H}_i + \widehat{H}_R$, where

$$\widehat{H}_i = -\frac{p_X^2}{2m_e^*(x,P,T)} + \frac{1}{2}m_e^*(x,P,T)\omega_{1e}^2(X - X_{oe})^2 - \frac{e^2E^2}{2m_e^*(x,P,T){\omega_{1e}}^2} + \frac{\omega_0^2\hbar^2{k_y}^2}{{\omega_{1e}}^2 2m_e^*(x,P,T)} -$$

$$\frac{e^2EB\hbar k_y}{m_e^*(x,P,T){\omega_{1e}}^2} + \frac{1}{2}g^*\mu_B B\sigma_Z \quad \textbf{(4.5)}$$

And

$$\widehat{H}_R = \alpha(\sigma_X\left(k_y + \frac{eBX}{\hbar}\right) - i\sigma_Y\frac{d}{dX}). \quad \textbf{(4.6)}$$

Where $X_{oe} = -\left(\frac{eE}{m_e^*(x,P,T){\omega_1}^2} + \frac{eB\hbar k_y}{m_e^{*2}(x,P,T){\omega_1}^2}\right)$ is recognized as guiding centre coordinate.

For the complete solution within the presence of external fields and Rashba SOI. As a consequence of complex coupling in the $\widehat{H}_{oe}$, we assume that there is no analytic solution of the Schrödinger can be coming out, aside from the some trival limits. Consequently, we must solve the Schrödinger equation numerically to achieve an insight about the interplay of SOI. So, expanding the $\varphi(x) = \sum_{n\sigma} a_{n\sigma}\Psi_{n\sigma}(x)$, the Hamiltonian $'\mathrm{H_{oe}}'$ eigenvalue equation can be written as: -

$$\sum_{n\sigma} a_{n\sigma}(E_{n\sigma} - E)\Psi_{n\sigma}(x) + \sum_{n\sigma} a_{n\sigma}\Psi_{n\sigma}(x) = 0, \quad \textbf{(4.7)}$$

$$(E_{n\sigma} - E)a_{n\sigma} + \sum_{n'\sigma'}\langle\Psi_{n\sigma}\left|\widehat{H}_R\right|\Psi_{n'\sigma'}\rangle = 0, \quad \textbf{(4.8)}$$

Where the matrix elements' 2nd term of Eq. (4.8) is calculated as:

$$\langle n\sigma|\widehat{H}_R|n'\sigma'\rangle = \alpha\left[\left(1 - \frac{\omega_c^2}{{\omega_{1e}}^2}\right)k_y - \frac{\omega_c eE}{\hbar{\omega_{1e}}^2}\right]\delta_{n,n'}\delta_{\sigma,\sigma'} + \frac{\alpha}{c_i}\left[\left(\frac{\omega_c}{\omega_{1e}} + \sigma\right)\sqrt{\frac{n+1}{2}}\,\delta_{n,n'-1} +\right.$$

$$\left.\left(\frac{\omega_c}{\omega_{1e}} - \sigma\right)\sqrt{\frac{n}{2}}\delta_{n,n'-1}\right]\delta_{\sigma,-\sigma'}, \quad \textbf{(4.9)}$$

4.3 LINEAR AND NON-LINEAR OPTICAL PROPERTIES

Now, our problem reduces to finding an appropriate numerical procedure for finding the various quantum states. The energies eigenvalues and their corresponding eigenvectors are obtained, and we can apply the analytical expressions via the perturbation method and density matrix approach for optical ACs, RICs and THG. For calculating these optical properties, we assume a circularly polarised electromagnetic (EM) field having incident photon frequency (ω) along the *Z*-direction, then the interaction within the system is given by [41,42]:

$$\boldsymbol{E}(t') = \frac{E_0(t')}{\sqrt{2}}(\hat{e}_X \pm \hat{e}_Y), \tag{4.10}$$

Here, the terms $\hat{e}_X$ and $\hat{e}_Y$ represents unit vector for X and Y directions respectively, and $\mathrm{E}_0(\mathrm{t}')$ is

$$E_0(t') = E_0\, cos(\,\omega t') = \tilde{E}e^{-\omega t\prime} + \tilde{E}e^{\omega t\prime}, \tag{4.11}$$

Therefore, the system is excited through an electromagnetic field. By applying, the Bloch theorem for symmetry, for $\Psi_{\,nm,k}$ and $\Psi_{\,n\prime m\prime,q\prime}$ states the dipole transition moment can be written

$$\left\langle \Psi_{\,nm,k} \left| qX \right| \Psi_{\,n\prime m\prime,k\prime} \right\rangle = \delta_{k,k\prime} \left\langle \varphi_{n,m} \left| qX \right| \varphi_{n\prime,m\prime} \right\rangle, \tag{4.12}$$

Where δ is known as the Kronecker delta function.

With the help of a compact iterative procedure and density-matrix method, we will drive the mien of THG susceptibility for the 2D model of the isotropic harmonic oscillator. The term $\bar{\rho}$ represents the electron density matrix. And the time-dependent Liouville-equation is

$$\frac{\partial\, \bar{\rho}_{ij}}{\partial t} = \frac{1}{i\hbar}[H_o - qXE(t'), \bar{\rho}]_{\,ij} - \lceil_{ij}(\bar{\rho} - \bar{\rho}^{(o)})_{ij} \tag{4.13}$$

$\bar{\rho}^{(o)}$ is known as a density-matrix operator for an unperturbed system, $\lceil_{ij}$ called as phenomenological operator. It is hypothesized that $\lceil_{ij}$ is a diagonal matrix known as relaxation rate. Equation (4.13) can be resolved with the help of the standard iterative method [42,43] then

$$\bar{\rho}(t') = \sum_n \bar{\rho}^{(n)}(t'), \tag{4.14}$$

With

$$\frac{\partial \bar{\rho}^{(n+1)}}{\partial t'} = \frac{1}{i\hbar}\{\left[H_o, \bar{\rho}^{(n+1)}\right]_{ij} - i\hbar\lceil_{ij}\bar{\rho}_{ij}^{(n+1)}\} - \frac{1}{i\hbar}[qr, \bar{\rho}^{(n)}]_{ij}E(t'). \tag{4.15}$$

The system's electronic polarization can also be expanded phenomenologically as an electric field series. Therefore, the three orders of electronic polarization $P(t')$ are expressed by

$$P(t') = \left(\epsilon_o\chi_\omega^{(1)}\tilde{E}e^{-i\omega t'} + \epsilon_o\chi_o^{(2)}\left|\tilde{E}\right|^2 + \epsilon_o\chi_{2\omega}^{(2)}\tilde{E}^2e^{-2i\omega t'} + \epsilon_o\chi_{3\omega}^{(3)}\left|\tilde{E}\right|^2\tilde{E}e^{-i\omega t'} + \epsilon_o\chi_{3\omega}^{(3)}\tilde{E}^3e^{-3i\omega t'}\right) + c.c., \tag{4.16}$$

Where $\chi_\omega^{(1)}$, $\chi_{2\omega}^{(2)}$, $\chi_o^{(2)}$and $\chi_{3\omega}^{(3)}$ are the linear susceptibility, SHG, optical rectification, and THG, respectively. The ϵ_o is known as Vaccum dielectric constant. For nth-order electronic polarization is written by

$$P^{(n)}(t') = \frac{1}{V}Tr\left(\bar{\rho}^{(n)}qr\right), \tag{4.17}$$

The term V is used for volume of interaction and Tr (trace) represents the summation over diagonal elements of the matrix $\bar{\rho}qX$. The trace (Tr) and susceptibility $\chi(\omega)$ are correlated to absorption coefficient $\alpha(\omega)$:

$$\alpha(\omega) = \omega\sqrt{\frac{\mu}{\epsilon_r}}Im[\epsilon_o\chi\,(\omega)]\ , \tag{4.18}$$

Where ϵ_o and μ is known as the real part of the relative permittivity (ϵ_r) and permeability, respectively. Now, the linear and non-linear optical AC expression can be written as [44–47];

$$\alpha^{(1)}(\omega) = \hbar\omega\sqrt{\frac{\mu}{\epsilon_r}}\frac{N_c\Gamma_{if}|M_{if}|^2}{\hbar^2\left\{(\omega_{fi}-\omega)^2+{\Gamma_{if}}^2\right\}}, \tag{4.19}$$

And

$$\alpha^{(3)}(\omega,I) = -\hbar\omega\sqrt{\frac{\mu}{\epsilon_r}}\frac{I}{2\epsilon_o n_r c}\times\frac{4N_c\Gamma_{if}|M_{if}|^2}{\hbar^4\left\{(\omega_{fi}-\omega)^2+{\Gamma_{if}}^2\right\}}\times$$

$$\left[\frac{|M_{if}|^2}{(\omega_{fi}-\omega)^2+{\Gamma_{if}}^2}+\frac{(M_{ff}-M_{ii})^2\left(3{\omega_{fi}}^2-4\omega_{fi}\omega\right)\left(\omega_{fi}^2-\Gamma_{if}^2\right)}{4\left(\omega_{fi}^2+\Gamma_{if}^2\right)\left\{(\omega_{fi}-\omega)^2+{\Gamma_{if}}^2\right\}}\right] \tag{4.20}$$

In eq. (4.11), $\hbar\omega$ and I are the energy of incident photon and intensity of incident light respectively, N_c is the carrier density and n_r represents the refractive index of quantum wire material, Γ_{if} is called relaxation time & the subscript i and f are used for initial and final states. $\omega_{if} = (E_f - E_i)/\hbar$ is known as transition frequency (where, E_i and E_f is the energy for the initial and final state). M_{if} is known as transition matrix element and determined by $M_{if} = |\langle\varphi_i|X|\varphi_f\rangle|$.

The total optical absorption coefficient is written as [48]

$$\alpha_T(\omega,I) = \alpha^{(1)}(\omega) + \alpha^{(3)}(\omega,I). \tag{4.21}$$

The linear and third-order nonlinear refractive index for optical transitions are obtained by

$$\frac{\Delta n_r^{(1)}}{n_r} = \frac{N_c}{2n_r^2\epsilon_o}\frac{|M_{if}|^2(\omega_{fi}-\omega)}{\hbar\left\{(\omega_{fi}-\omega)^2+{\Gamma_{if}}^2\right\}}\ , \tag{4.22}$$

$$\frac{\Delta n_r^{(3)}(\omega,I)}{n_r} = \frac{N_c}{2{n_r}^3\epsilon_o}\frac{I\mu c|M_{if}|^2(\omega_{fi}-\omega)}{\hbar^3(\omega_{fi}-\omega)^2+\Gamma_{if}^2}\times$$

$$\left[\frac{|M_{if}|^2}{(\omega_{fi}-\omega)^2+\Gamma_{if}^2}+\frac{2\Gamma_{if}(M_{ff}-M_{ii})}{(\omega_{fi}-\omega)^2+\Gamma_{if}^2}\times\{(\omega_{fi}-\omega)[\omega_{fi}(\omega_{fi}-\omega)+\Gamma_{if}^2]-\Gamma_{if}^2(2\omega_{fi}-\omega)\}\right] \quad \textbf{(4.23)}$$

The total refractive index is

$$\frac{\Delta n_r(\omega,I)}{n_r}=\frac{\Delta n_r^{(1)}}{n_r}+\frac{\Delta n_r^{(3)}(\omega,I)}{n_r} \quad \textbf{(4.24)}$$

And now, we focus on the SHG and THG (i.e., from the term of oscillating with *4ω*, we only cogitate the third-order contribution). With the help of the iterative method and compact density-matrix approach, the SHG and THG per unit volume are given as [48–50];

$$\chi_{2\omega}^{(2)}=-\frac{e^3n_o}{\varepsilon_o\hbar^3}\frac{M_{12}M_{23}M_{31}}{(\omega-\omega_{21}+i\Gamma_{21})(2\omega-\omega_{32}+i\Gamma_{32})}, \quad \textbf{(4.25)}$$

$$\chi_{3\omega}{}^{(3)}=-\frac{e^4n_o}{\varepsilon_o\hbar^3}\frac{M_{12}M_{23}M_{34}M_{41}}{(\omega-\omega_{21}+i\Gamma_{21})(2\omega-\omega_{31}+i\Gamma_{31})(3\omega-\omega_{41}+i\Gamma_{41})}. \quad \textbf{(4.26)}$$

The results and their implications are presented in the next section.

4.4 RESULT AND DISCUSSION

In this investigation, the effects of hydrogenic impurity on the linear and the third-order nonlinear optical ACs, RICs, SHG, and THG in a typical $Ga_{1-x}Al_xAs$ within the presence 2-DEG have been studied. The physical constraints used for arithmetical computation are [51]: $n_o = 10^{16}$ cm^{-3}, $n_r = 3.2$, $\Gamma_{12} = 1/\mathrm{T}_{12}$ where $T_{12} = 0.2$ ps and $\mu = 4\pi \times 10^{-7}$ Hm^{-1}.

In **Figure 4.2 (a-b)**, the changes in the effective mass with the variation in impurity factor (x) for different values of temperature and pressure viz. 100 K, 200 K, and 300 K and 10 kbar, 15 kbar and 20 kbar respectively, are presented. As the impurity factor (x) increases, the effective mass is also increased for each value of temperature and pressure. This is due to the strong dependence of impurity on the effective mass. When the impurity factor (x) is changed from 0 to 0.3, the behaviour of the quantum wire in terms of effective mass is counter-intuitive when

the rise in impurity factor probably enhances the effective mass. This nature helps in the study of the influences of hydrogenic impurity (x) on optical properties.

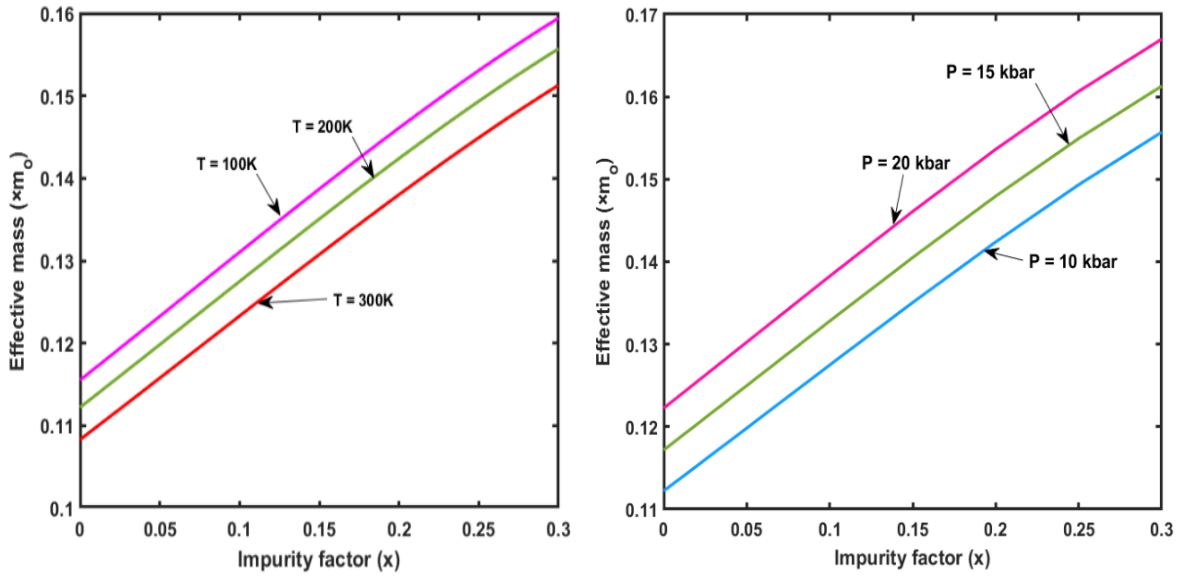

(a) **(b)**

Figure 4.2 (a and b) Effective mass variation with the hydrogenic impurity (x) for the $Ga_{1-x}Al_xAs$ quantum wire at T= 100 K, 200 K and 300 K and P = 10 kbar, 15 kbar and 20 kbar, respectively.

In **Figure 4.3 (a)**, energy gap variation with impurity factor (x) has been shown. As the hydrogenic impurity increases, the energy gap between the two subsequent levels is also increased. This enhancement in the energy gap due to impurity yields the change in optical properties of the $Ga_{1-x}Al_xAs$ quantum wire. **Figure 4.3 (b)** shows the matrix elements variation with the impurity factor (x). The matrix elements reduce with an increment in hydrogenic impurity factor (x). From the eqs. (4.19-4.25), we can easily see the dependence of matrix elements on the linear and third-order nonlinear ACs, RICs and THG therefore, when the matrix element changes these parameters also changes.

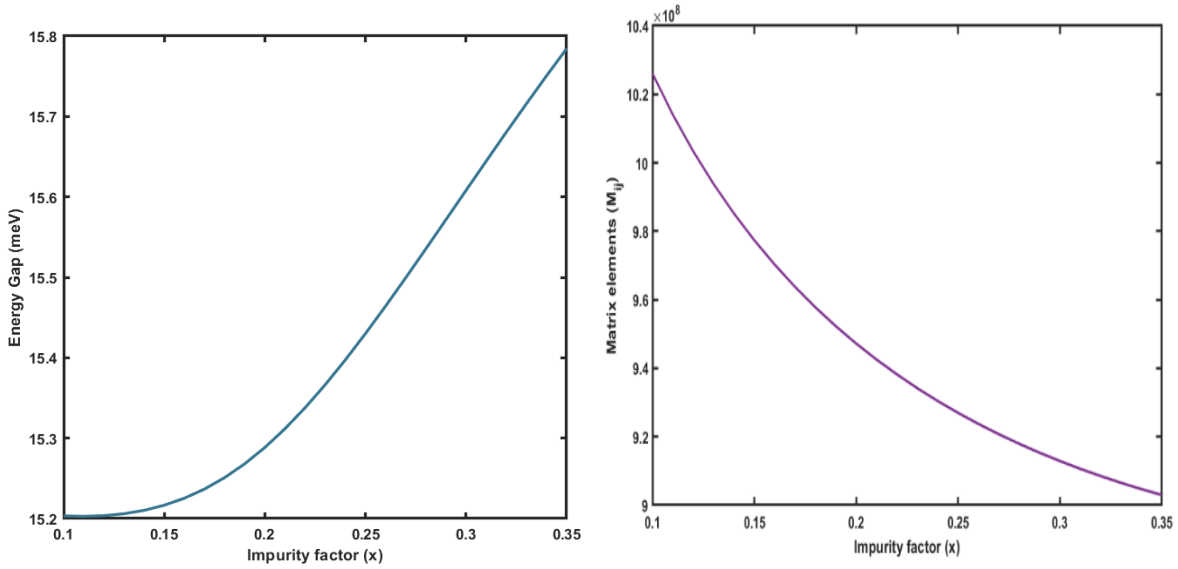

(a) **(b)**

Figure 4.3 (a) Energy gap between the two subsequent levels as a function of impurity factor (x), and (b) Matrix element as a function of impurity factor (x) for the $Ga_{1-x}Al_xAs$ quantum wire.

Figure 4.4 (a-c), demonstrates the linear $\alpha^{(1)}$, the third-order nonlinear ACs $\alpha^{(3)}$ and the total optical ACs $\alpha^{(T)}$ as a function of the incident photon energy for the various value of the hydrogenic impurity factor (x). The magnetic field, electric field, Rashba SOI, and incident laser intensity are fixed at 1 T, 50 kV/m, 35 meV and $2.04\times 10^7\,\mathrm{W/m^{-2}}$, respectively. Generally, the $\alpha^{(1)}$ illustrations resonance at the zero thwarts which denotes when the energy difference between the subsequent states becomes cognate with an incident photon. Similarly, in the case of $\alpha^{(3)}$ with a negative sign. It is initiated that when the x is raised from 0.1 to 0.3, the maxims of $\alpha^{(1)}$ and $\alpha^{(3)}$ shows blue shifting. However, this effect is abetted via the decrement in the value of $\alpha^{(1)}$ and $\alpha^{(3)}$, with $\alpha^{(3)}$ entity effected firmly as compared to linear optical AC ($\alpha^{(1)}$). Whereas, the blue shifting takes place due to the enrichment in the energy gap between the subsequent states of energy which can easily be understood by **Figure 4.4 (a)**.

This in turn consequences in further energy spacing between the ensuing states. Moreover, the impurity factor (x) effect on the $\alpha^{(3)}$ strongly as compared to $\alpha^{(1)}$ whose results illustrate the rare shape in the $\alpha^{(T)}$ curve. It can be noted that with an increment in the value of x there is a decrement in the height of peak maxims. This happened as a consequence of the small value of dipole matrix elements (M_{ij}) when the x rise. In accordance, with the eq. (4.19) and eq. (4.20) the $\alpha^{(1)}$ and $\alpha^{(3)}$ resonant peaks values are proportional to $M_{12}^2 E_{12}$ and $M_{12}^4 E_{12}$, respectively. Therefore, the consequence of M_{12} is dominant, resulting in a decrease in the magnitude of the $\alpha^{(3)}$ term more than the $\alpha^{(1)}$. It is manifest that the $\alpha^{(1)}$, $\alpha^{(3)}$ and $\alpha^{(T)}$ peaks diminution and shifts in the direction of the higher energies as the impurity boosts.

In the optical studies of quantum wire, RICs play a significant role. In **Figure 4.5 (a-c)**, the linear, third order non-linear, and total RICs are plotted as a function of the incident photon energy for various hydrogenic impurity factor (x). As demonstrated from these plots, the linear RICs increase gradually with the incident photon energy and come to an extreme value. This brings out to the normal dispersion for any frequency of incident photo where $\frac{dn}{d\omega} > 0$. However, the energy of the photon approaches threshold energy, the dispersion $\frac{dn}{d\omega}$ in the RICs change its sign. At every resonant frequency of a quantum wire, this anomalous dispersion is defined by $\frac{dn}{d\omega} < 0$. In this area, photons are sturdily absorbed and behave like an absorption band. In **Figure 4.5 (a-c)**, the anomalous dispersion region moves towards large photon energies (i.e; blueshift) as a contrast to the low value of impurity factor cases. The root cause for the resonance shifting is an enhancement in the energy gap between the two electronic states among which an optical transition takes place. As the third-order nonlinear RIC has a negative sign therefore it takes an enfeebling effect on the total RIC. Therefore, it has been discovered that the impurity, as a tunable parameter plays a significant role in supervising the optical properties of quantum wire.

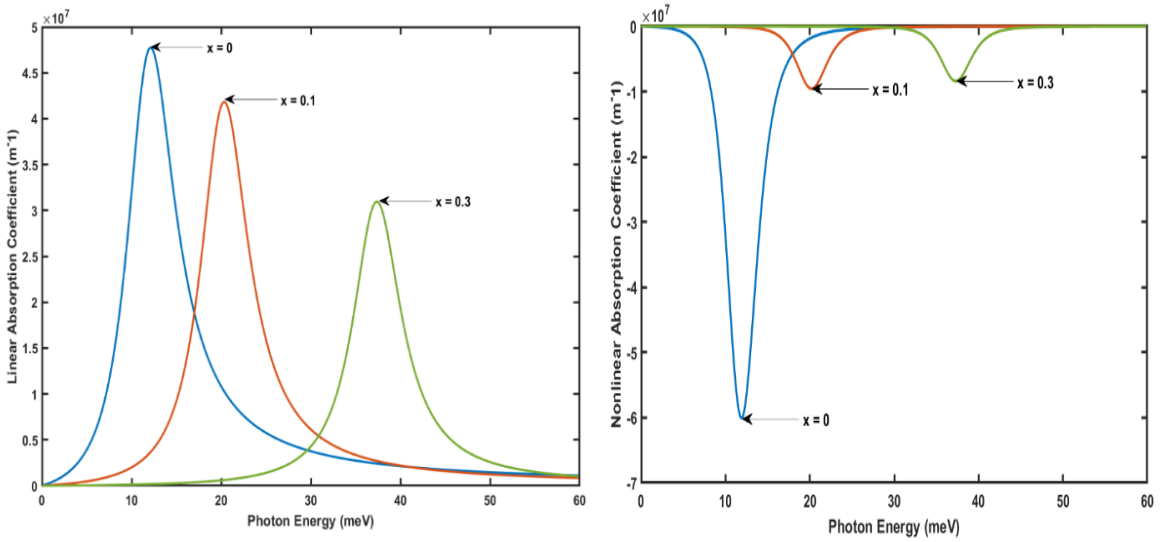

(a) **(b)**

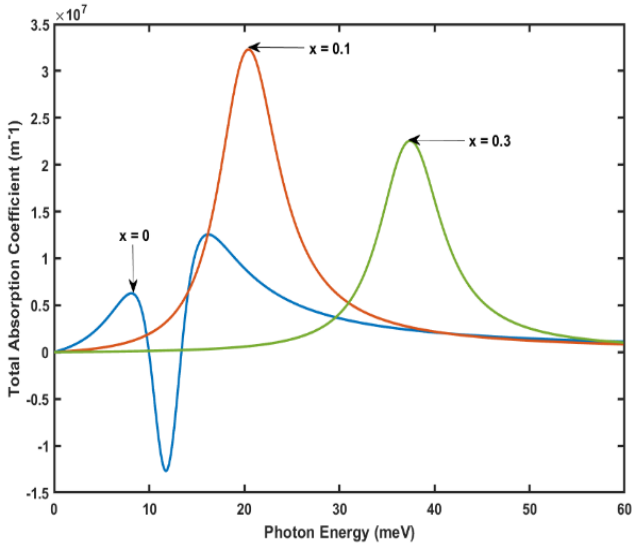

(c)

Figure 4.4 (a) Linear optical ACs, (b) Third-order nonlinear optical ACs, and (c) total optical ACs as a function of Photon energy with the various values of the impurity.

Figure 4.6, represents the SHG as a function of incident photon energy for the various value of impurity (x = 0.1, 0.2, and 0.3). It can be perceived from the plot that the resonant peaks of the SHG decrease and shift towards large value of photon energy (blue shift) when the impurity factor (x) increases. SHG figure has only one resonant peak due to the equally spaced energy spectrum. Additionally, the intensity in Fig 4.6 is much larger with the comparison of resonant peaks in the situation of unequal spacing of the energy spectrum. The changes in the amplitude and position of the peaks are due to the change in the geometric factor of the quantum wire such as energy gap and matrix elements.

Figure 4.7 shows that, for various values of the hydrogenic impurity factor x = 0, x = 0.1, and x = 0.3, the THG is plotted as a function of incident photon energy. For the low energy region, the triple resonance condition is not perfectly achieved due to the weaker confinement cause the energy separation between the states unequally and additionally, for high energy the transition energy between subbands decreases, and the overlaps of states will rise. When the hydrogenic impurity (x) is considered, the peaks of the THG coefficients show a blue shift. The magnitude of the peak for each curve reduces with the rise in impurity factor (x), due to allied with the product of matrix elements. This is due to the energy gap between two states containing hydrogenic impurity being larger than the energy gap between two states containing no hydrogenic impurity. This means that the THG drops and moves towards higher energies when the effect of impurity is taken into account.

The THG coefficient as a function of hydrogenic temperature and pressure when x = 0.1, 0.2, and x = 0.3 are illustrated in **Figure 4.8 (a)** and **(b)**, respectively. From **Figure 4.8 (a)**, it can be observed that as the temperature enhances there is an increment in height of the resonant peaks for x = 0.1, 0.2, and 0.3. When the hydrogenic impurity (x) rises from 0.1 to 0.3 the resonant peak amplitude reduces. In **Figure 4.8 (b)**, as the pressure enhances then the THG

coefficient value decreases, unlike in the previous case. The enhancement in the impurity factor (x) parameter for supplementing values of P is reflected in the fall of the resonance peak amplitude. The amplitude of the resonant peak is calculated by the product of the transition matrix elements. These optical effects can be exploited as a probe for the precise mechanism such as optical nonlinearity in quantum wires and also, used in optical-magneto instruments.

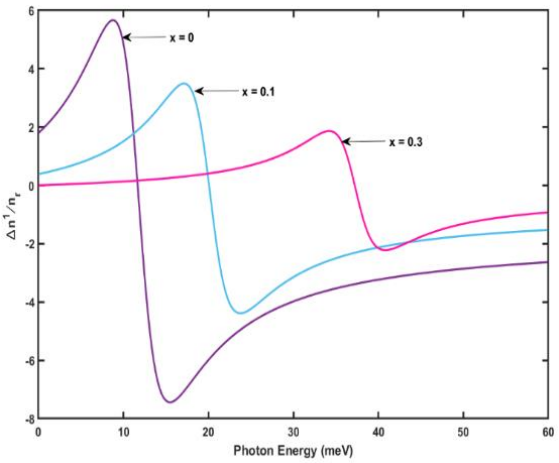

(a)

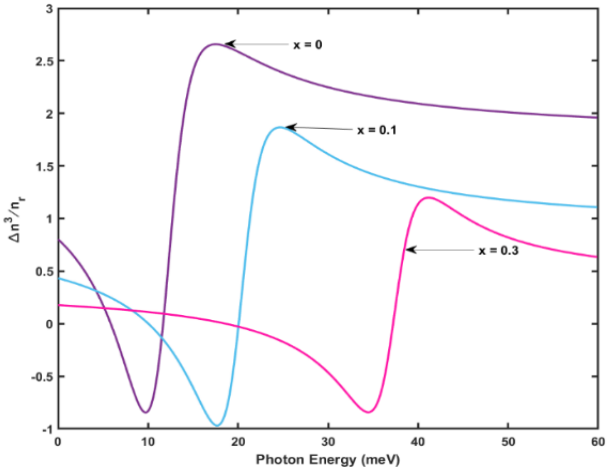

(b)

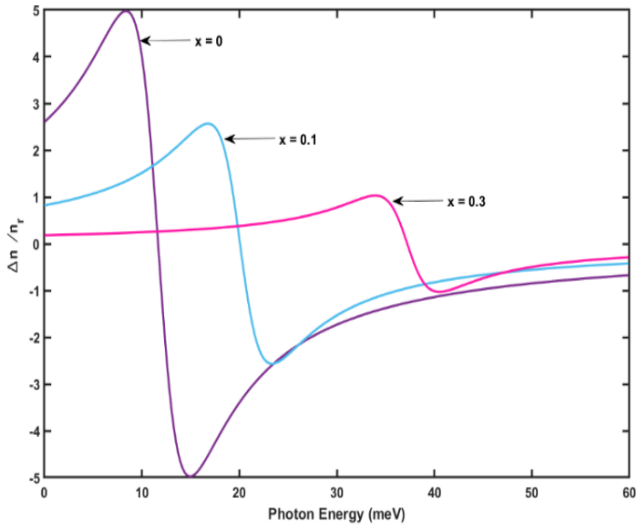

(c)

Figure 4.5 (a)The linear RIC, (b) non-linear RIC, and (c) total RIC as a function of the incident photon energy for the various value of hydrogenic impurity.

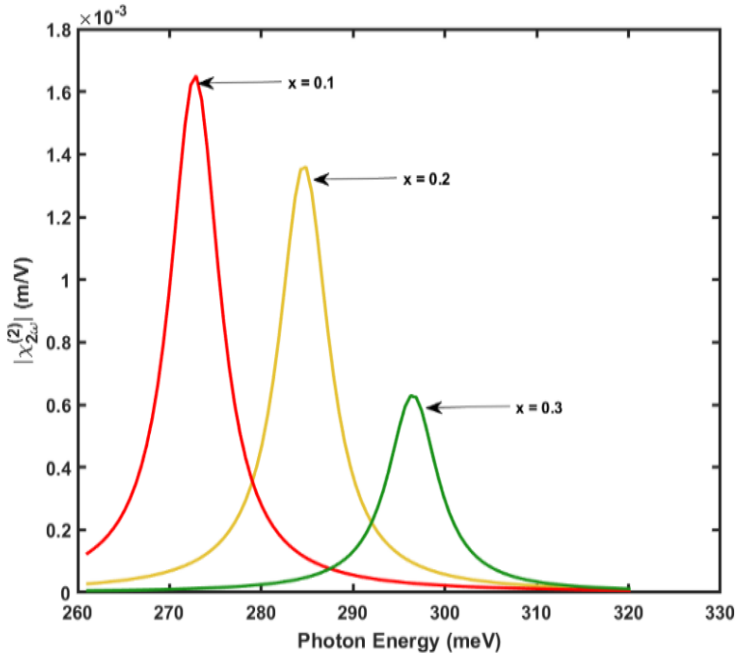

Figure 4.6 SHG as a function of photon energy when x = 0.1, 0.2, and 0.3.

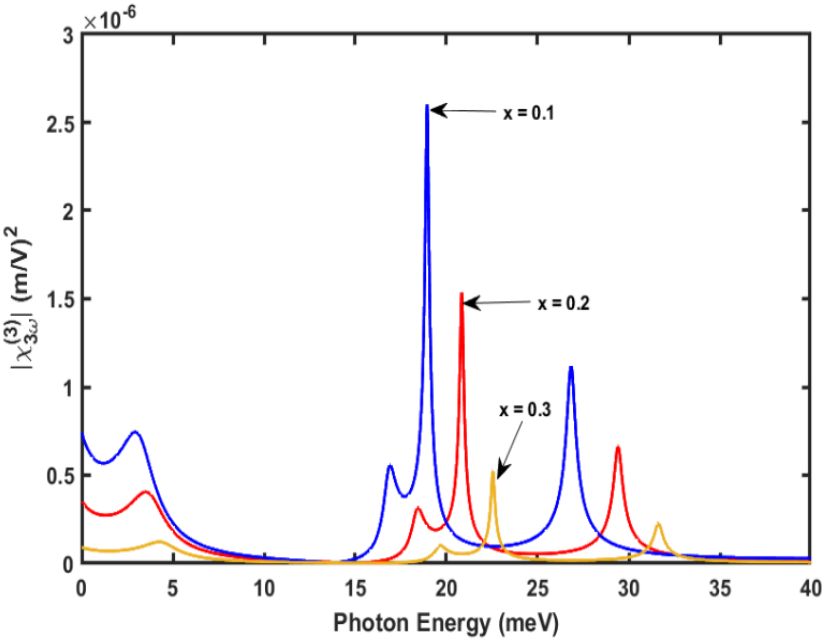

Figure 4.7 THG as a function of incident photon energy for the various value of hydrogenic impurity.

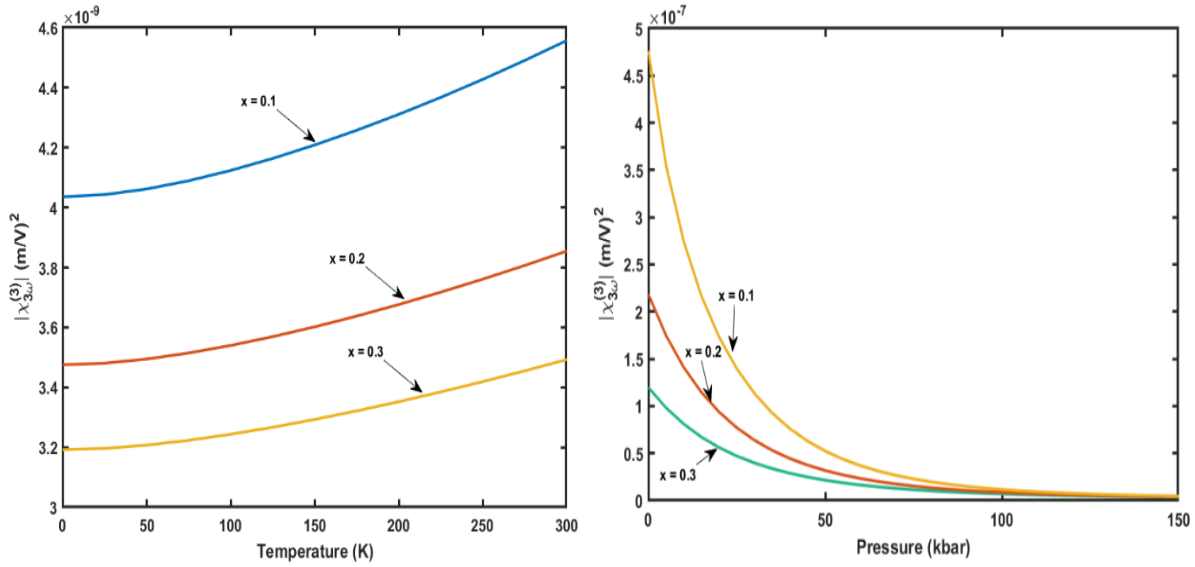

(a) **(b)**

Figure 4.8 (a) THG coefficient for the $Ga_{1-x}Al_xAs$ quantum wire as a function of hydrogenic temperature with x = 0.1, 0.2 and 0.3 at P=15 kbar, and (b) THG coefficient as a function of pressure with x = 0.1, 0.2 and 0.3 at T = 300 K.

4.5 SUMMARY

In this paper, we attention to the behaviour of optical properties for the $Ga_{1-x}Al_xAs$ quantum wire and how its changes with the various value of hydrogenic impurity. The alteration in linear and third-order nonlinear optical ACs, RICs, SHG, and THG by the impurity factor under the presence of the intense magnetic field, electric field, and Rashba SOI are demonstrated. We experiential the energy gap and the dipole moment matrix element (M_{12}), are strongly affected by the hydrogenic impurity. Due to this optical ACs, RICs, SHG, and THG of the system change. It was noticed that the enhancement in hydrogenic impurity produces blue shifts in optical properties. However, hydrogenic impurity increases the energy gap and decreases the matrix elements, therefore as a result, the peaks of optical ACs, RICs, SHG, and third harmonic

generation shift to higher photon energy. It is also concluded that the impurity factor can be explored as tunning tool for varying the optical properties via the introduction of spacing between the confined energy levels. It is presumed that impurity can show a significant role in the optical properties of semiconductor quantum wire. Therefore, the tunability and detuning of the terahertz laser in low-dimension nanostructure takes place due to the variation in hydrogenic impurity. These varieties of aspects would be beneficial for the evolution of tunable optoelectronic devices.

4.6 REFERENCES

[1] E. Kasapoglu, F. Ungan, H. Sari, I. Sökmen, Binding energies of donor impurities in modulation-doped double quantum wells under an electric field, Superlattices Microstruct 45 (2009) 618–623.

[2] R. Khordad, S.K. Khaneghah, Intersubband optical absorption coefficients and refractive index changes in a V-groove quantum wire, Physica Status Solidi (b) 248 (2011) 243–249.

[3] Y. V. Pershin, J.A. Nesteroff, V. Privman, Effect of spin-orbit interaction and in-plane magnetic field on the conductance of a quasi-one-dimensional system, Phys Rev B 69 (2004) 121306.

[4] U. Yesilgul, F. Ungan, E. Kasapoglu, H. Sarı, I. Sökmen, The linear and nonlinear intersubband optical absorption coefficients and refractive index changes in a V-shaped quantum well under the applied electric and magnetic fields, Superlattices Microstruct 50 (2011) 400–410.

[5] S. Zhang, R. Liang, E. Zhang, L. Zhang, Y. Liu, Magnetosubbands of semiconductor quantum wires with Rashba and Dresselhaus spin-orbit coupling, Phys Rev B 73 (2006) 155316.

[6] W. Xie, The nonlinear optical rectification of a confined exciton in a quantum dot, J Lumin 131 (2011) 943–946.

[7] W. Xie, The nonlinear optical rectification coefficient of quantum dots and rings with a repulsive scattering center, J Lumin 143 (2013) 27–30.

[8] S. Lahon, M. Kumar, P.K. Jha, M. Mohan, Spin–orbit interaction effect on the linear and nonlinear properties of quantum wire in the presence of electric and magnetic fields, J Lumin 144 (2013) 149–153.

[9] R. Khordad, Optical properties of quantum wires: Rashba effect and external magnetic field, J Lumin 134 (2013) 201–207.

[10] R. Khordad, S. Tafaroji, Third-harmonic generation in a quantum wire with triangle cross section, Physica E Low Dimens Syst Nanostruct 46 (2012) 84–88.

[11] P.K. Jha, M. Kumar, S. Lahon, S. Gumber, M. Mohan, Rashba spin orbit interaction effect on nonlinear optical properties of quantum dot with magnetic field, Superlattices Microstruct 65 (2014) 71–78.

[12] Y.-Y. Zhang, G.-R. Yao, Performance enhancement of blue light-emitting diodes with AlGaN barriers and a special designed electron-blocking layer, J Appl Phys 110 (2011).

[13] T. Sugaya, K.-Y. Jang, C.-K. Hahn, M. Ogura, K. Komori, A. Shinoda, K. Yonei, Enhanced peak-to-valley current ratio in InGaAs⁄InAlAs trench-type quantum-wire negative differential resistance field-effect transistors, J Appl Phys 97 (2005).

[14] I. Žutić, J. Fabian, S. Das Sarma, Spintronics: Fundamentals and applications, Rev Mod Phys 76 (2004) 323–410.

[15] S. Datta, B. Das, Electronic analog of the electro-optic modulator, Appl Phys Lett 56 (1990) 665–667.

[16] M. Kumar, S. Lahon, P.K. Jha, M. Mohan, Energy dispersion and electron g-factor of quantum wire in external electric and magnetic fields with Rashba spin orbit interaction, Superlattices Microstruct 57 (2013) 11–18.

[17] I. Žutić, J. Fabian, S. Das Sarma, Spintronics: Fundamentals and applications, Rev Mod Phys 76 (2004) 323.

[18] Doyeol Ahn, Shun-lien Chuang, Calculation of linear and nonlinear intersubband optical absorptions in a quantum well model with an applied electric field, IEEE J Quantum Electron 23 (1987) 2196–2204.

[19] M. Şahin, Third-order nonlinear optical properties of a one- and two-electron spherical quantum dot with and without a hydrogenic impurity, J Appl Phys 106 (2009).

[20] Y.-B. Yu, K.-X. Guo, Exciton effects on nonlinear electro-optic effects in semi-parabolic quantum wires, Physica E Low Dimens Syst Nanostruct 18 (2003) 492–497.

[21] J. Ganguly, S. Saha, S. Pal, M. Ghosh, Noise-driven optical absorption coefficients of impurity doped quantum dots, Physica E Low Dimens Syst Nanostruct 75 (2016) 246–256.

[22] S. Saha, S. Pal, J. Ganguly, M. Ghosh, Exploring optical refractive index change of impurity doped quantum dots driven by white noise, Superlattices Microstruct 88 (2015) 620–633.

[23] İ. Karabulut, S. Baskoutas, Linear and nonlinear optical absorption coefficients and refractive index changes in spherical quantum dots: Effects of impurities, electric field, size, and optical intensity, J Appl Phys 103 (2008).

[24] Gh. Safarpour, A. Zamani, M.A. Izadi, H. Ganjipour, Laser radiation effect on the optical properties of a spherical quantum dot confined in a cylindrical nanowire, J Lumin 147 (2014) 295–303.

[25] B. Gisi, S. Sakiroglu, E. Kasapoglu, H. Sari, I. Sokmen, Spin–orbit interaction effects on the optical properties of quantum wires under the influence of in-plane magnetic fields, Superlattices Microstruct 86 (2015) 166–172.

[26] A. Bouazra, S.A.-B. Nasrallah, M. Said, Theory of electronic and optical properties for different shapes of InAs/In0.52Al0.48As quantum wires, Physica E Low Dimens Syst Nanostruct 75 (2016) 272–279.

[27] S. Sakiroglu, B. Gisi, Y. Karaaslan, E. Kasapoglu, H. Sari, I. Sokmen, Optical properties of double quantum wires under the combined effect of spin-orbit interaction and in-plane magnetic field, Physica E Low Dimens Syst Nanostruct 81 (2016) 59–65.

[28] N. Arunachalam, A. John Peter, C. Woo Lee, Pressure induced optical absorption and refractive index changes of a shallow hydrogenic impurity in a quantum wire, Physica E Low Dimens Syst Nanostruct 44 (2011) 222–228.

[29] C. V. Nguyen, N. Ngoc Hieu, C.A. Duque, D. Quoc Khoa, N. Van Hieu, L. Van Tung, H. Vinh Phuc, Linear and nonlinear magneto-optical properties of monolayer phosphorene, J Appl Phys 121 (2017).

[30] E. Kasapoglu, F. Ungan, C.A. Duque, U. Yesilgul, M.E. Mora-Ramos, H. Sari, I. So¨kmen, The effects of the electric and magnetic fields on the nonlinear optical properties in the step-like asymmetric quantum well, Physica E Low Dimens Syst Nanostruct 61 (2014) 107–110.

[31] M.G. Barseghyan, A.A. Kirakosyan, C.A. Duque, Hydrostatic pressure, electric and magnetic field effects on shallow donor impurity states and photoionization cross section in cylindrical GaAs–Ga 1– *x* Al *x* As quantum dots, Physica Status Solidi (b) 246 (2009) 626–629.

[32] L.E. Oliveira, L.M. Falicov, Energy spectra of donors and acceptors in quantum-well structures: effect of spatially dependent screening, Phys Rev B 34 (1986) 8676.

[33] N. Porras-Montenegro, S.T. Pérez-Merchancano, A. Latgé, Binding energies and density of impurity states in spherical GaAs-(Ga,Al)As quantum dots, J Appl Phys 74 (1993) 7624–7626.

[34] A. Montes, C.A. Duque, N. Porras-Montenegro, Density of shallow-donor impurity states in rectangular cross section GaAs quantum-well wires under applied electric field, Journal of Physics: Condensed Matter 10 (1998) 5351.

[35] M.G. Barseghyan, M.E. Mora-Ramos, C.A. Duque, Hydrostatic pressure, impurity position and electric and magnetic field effects on the binding energy and photo-ionization cross section of a hydrogenic donor impurity in an InAs Pöschl-Teller quantum ring, Eur Phys J B 84 (2011) 265–271.

[36] M. Santhi, A. John Peter, C. Yoo, Hydrostatic pressure on optical absorption and refractive index changes of a shallow hydrogenic impurity in a GaAs/GaAlAs quantum wire, Superlattices Microstruct 52 (2012) 234–244.

[37] J.C. Martínez-Orozco, M.E. Mora-Ramos, C.A. Duque, Electron-related optical properties in T-shaped AlxGa1−xAs/GaAs quantum wires and dots, Eur Phys J B 88 (2015) 115.

[38] N. Zeiri, N. Sfina, S.A.-B. Nasrallah, M. Said, Linear and non-linear optical properties in symmetric and asymmetric double quantum wells, Optik (Stuttg) 124 (2013) 7044–7048.

[39] Priyanka, R. Sharma, M. Kumar, Effects of impurity factor on the physical and transport properties for Ga1-xAlxAs quantum wire in the presence of Rashba spin-orbit interaction, Physica B Condens Matter 629 (2022) 413649.

[40] R. Khordad, B. Mirhosseini, Optical properties of GaAs/Ga 1-Al As ridge quantum wire: Third-harmonic generation, Opt Commun 285 (2012) 1233–1237.

[41] R. Khordad, Second and third-harmonic generation of parallelogram quantum wires: electric field, Indian Journal of Physics 88 (2014) 275–281.

[42] G. Wang, Third-harmonic generation in cylindrical parabolic quantum wires with an applied electric field, Phys Rev B 72 (2005) 155329.

[43] F. Rossi, E. Molinari, Coulomb-induced suppression of band-edge singularities in the optical spectra of realistic quantum-wire structures, Phys Rev Lett 76 (1996) 3642.

[44] F. Zaouali, A. Bouazra, M. Said, A theoretical evaluation of optical properties of InAs/InP quantum wire with a dome cross-section, Optik (Stuttg) 174 (2018) 513–520.

[45] S. Antil, M. Kumar, S. Lahon, S. Dahiya, A. Ohlan, R. Punia, A.S. Maan, Influence of hydrostatic pressure and spin orbit interaction on optical properties in quantum wire, Physica B Condens Matter 552 (2019) 202–208.

[46] R. Khordad, Optical properties of quantum wires: Rashba effect and external magnetic field, J Lumin 134 (2013) 201–207.

[47] M.J. Karimi, M. Hosseini, Electric and magnetic field effects on the optical absorption of elliptical quantum wire, Superlattices Microstruct 111 (2017) 96–102.

[48] K. Chernoutsan, V. Dneprovskii, S. Gavrilov, V. Gusev, E. Muljarov, S. Romanov, A. Syrnicov, O. Shaligina, E. Zhukov, Linear and nonlinear optical properties of excitons in semiconductor–dielectric quantum wires, Physica E Low Dimens Syst Nanostruct 15 (2002) 111–117.

[49] R. Khordad, Second and third-harmonic generation of parallelogram quantum wires: electric field, Indian Journal of Physics 88 (2014) 275–281.

[50] G. Wang, Third-harmonic generation in cylindrical parabolic quantum wires with an applied electric field, Phys Rev B 72 (2005) 155329.

[51] N. Zeiri, A. Bouazra, S.A.-B. Nasrallah, M. Said, Linear and nonlinear susceptibilities in GaN/Al *x* Ga 1− *x* N quantum wire, Phys Scr 95 (2020) 045801.

5

CHAPTER

Non-linear and Linear Optical Properties of $In_xGa_{1-x}As$ Quantum Dot

- *The study focuses on exploring the optical properties of $In_xGa_{1-x}As$ quantum dots, with a particular emphasis on the role of impurity concentration.*
- *The energy levels and wavefunctions of the quantum dot system are first estimated in the presence of impurity, forming the basis for subsequent analysis.*
- *The research examines the effects of impurity on key optical properties, including absorption coefficients, refractive index changes, and third harmonic generation.*
- *Results reveal that as impurity concentration increases, the peaks of the absorption coefficients, refractive index changes, and third harmonic generation shift position and decrease in magnitude.*
- *The study highlights that impurity concentration plays a pivotal role in altering the optical properties of nanostructures, indicating its importance in the design and optimization of quantum dot-based devices.*

5.1 INTRODUCTION

The most significant role of hydrogenic impurity on the behavior of semiconductor plays vital importance when one study with nanodevices in order to extend its utility for practical applications, and thereby impact a major part towards manifesting the demonstration about semiconductivity in condensed matter physics [1,2]. Hydrogenic impurity states in low-dimensional semiconductors as quantum dots, quantum wire and well have been extensively investigated for the last years [3,4]. These results reveal that the optical and physical properties in presence of hydrogenic impurity can be directly managed through proper size, geometry, doping location or material selection. Recently, much of interest has focused on the inter-subband optical absorptions in low-dimensional semiconductors. In this work, the inter-subband optical absorptions (OAs) in nanodevices are considered to compare with those found from experiments. Consequently, the linear and nonlinear inter-subband OAs can be employed in feasible applications of high-speed electro-optical devices as well as photodetectors. In addition, externally introduced perturbations such as electric and magnetic fields as well appointments Rashba spin-orbit coupling (RSOC) represent powerful tools for investigating the impurity effect in low-dimensional semiconductors [5–7]. In contrast, hydrogenic impurity, externally applied field and RSOC impact on quantum dot optical properties have been the subject of considerable interest both from device applications and fundamental physics for a long time [8–11].

The impurity present in the semiconductor modifies the feast of the wave function, especially in strong spatial confinement. The external field and RSOC in the low-dimensional semiconductor break the symmetry of the system. As is well known, the RSOC and its consequence on the non-linear and linear optical properties of the quantum dot have sustained

and persisted in the last decade. The RSOC arise due to structural inversion symmetry [12–14]. The strength of the RSOC depends on the external field and the characteristics of the material. In the realistic problem of optical properties of quantum dots, RSOC plays a vital role on account of their potential applications in quantum computers [15–17]. It is esteemed the spin of electrons plays a significant role in the spin phenomena namely spin relaxation, spintronics and quantum computer [18,19]. During the last eras, much research has investigated the optical properties and electronic of low-dimensional semiconductors under the presence of RSOC theoretically and experimentally [20–26].

Linear and nonlinear optical phenomena in semiconductors become enormously significant to design the photonic and electronic nanodevices applications like high-speed electro-optical modulators, laser amplifiers and so on [27]. As a result, much theoretical research has been done to recognize the exploitation of optical properties with different concentrations of impurity. However, the linear and nonlinear absorption coefficient (ACs), refractive index changes (RICs), and third harmonic generation (THG) are the most important property among optical properties of quantum dots [28–30]. Liu et al. focus on the cylindrical core-shell nanostructure's THG non-linear susceptibility under the existence electric field [31]. The electric field and hydrogenic impurity influence on the optical properties of the 3D quantum dots are studied by E. Sadeghi [32]. Linear and non-linear optical ACs and RICs based on the inter-subband optical transition of the quantum dots are also calculated in [33,34].

In this chapter, our purpose is to study the impact of impurity on the ACs, RICs and THG of the quantum dot underneath the influence of externally applied field and RSOC by numerical calculations. For this persistence, we find the wavefunctions and energy levels in the effectiv e mass approximation numerically via the density matrix approach. The pattern of this paper is

followed as: In Section 5.2 and 5.3, the calculation for energy eigenvalues and wave functions through the density matrix approach. In section 5.4, the result and discussion about $In_xGa_{1-x}As$ quantum dot are mentioned. In the end, we represent the summary part in section 5.5.

5.2 PARABOLIC HARMONIC POTENTIAL $In_xGa_{1-x}As$ QUANTUM DOT WITHIN THE PRESENCE OF IMPURITY

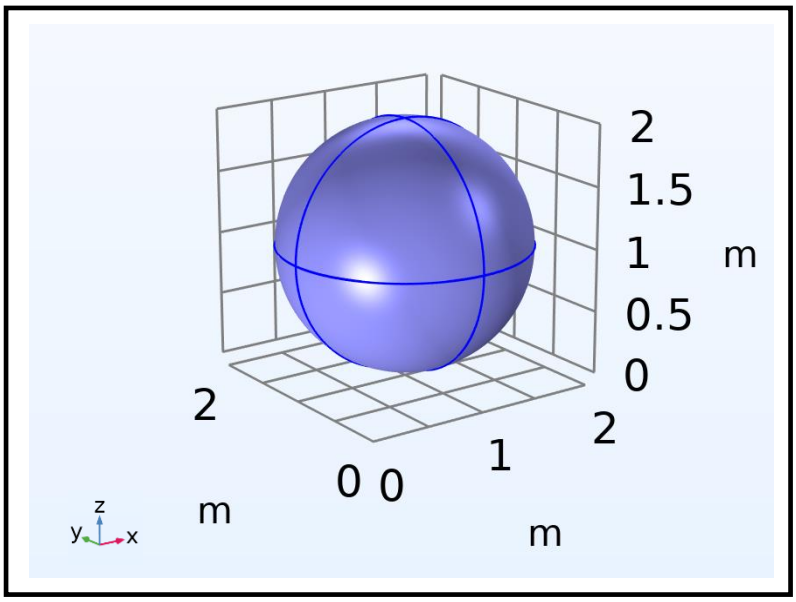

Figure 5.1 $In_xGa_{1-x}As$ quantum dot systematic diagram.

Consider the $In_xGa_{1-x}As$ quantum dot (seen in **Figure 5.1**) with parabolic confinement potential under the presence of magnetic field along z-axis $\boldsymbol{B} = (0, 0, B)$, therefore the symmetric gauge comes out to be $\boldsymbol{A} = (-y/2, x/2, 0)$. The Hamiltonian for single electron mass is given by

$$H_i(r) = \frac{1}{2m_e(x,P,T)}(\boldsymbol{p} + e\boldsymbol{A})^2 + \frac{1}{2}m_e(x,P,T)\omega_o(x^2+y^2) + \frac{1}{2}g^*\mu_B B\sigma_i \qquad \textbf{(5.1)}$$

Here, $\boldsymbol{p}$ and $\boldsymbol{A}$ are the momentum and vector potential, ω_o is known as oscillator frequency, $g^*$is the Lande factor and σ_i is the Pauli spin matrix. $m_e(x,P,T)$ is the effective mass for $In_xGa_{1-x}As$ quantum dot expressed as [35,36]:

$$m_e(x,P,T) = m_o\left[7.51\left(\frac{1}{0.341+{E_g}^i(x,P,T)}+\frac{2}{{E_g}^i(x,P,T)}\right)+1\right]^{-1}, \quad \textbf{(5.2)}$$

m_o is called free electron mass. ${E_g}^i$ is the energy bandgap for the $In_xGa_{1-x}As$ given by

$${E_g}^i(x,P,T) = {E_g}^{GaAs}(P,T) + \left[{E_g}^{InAs}(P,T) - {E_g}^{GaAs}(P,T)\right]x - 0.475x(1-x) \quad (5.3)$$

Where ${E_g}^{GaAs}(P,T) = qP - \frac{rT^2}{T+s} + {E_g}^0$,

and ${E_g}^{InAs}(P,T) = aP - \frac{bT^2}{T+c} + {E_{gi}}^0$.

The parameters values: ${E_g}^0$ = 1.52 eV (named as energy gap at P = 0 kbar and T = 0 K), q = 1.08×10^{-2} eV/kbar, r = 50.4×10^{-5} eV/K, and s = 204 K are the pressure coefficient and temperature coefficients, respectively for GaAs semiconductors. And ${E_{gi}}^0$ = 0.42 eV (named as energy gap at P = 0 kbar and T = 0 K), a = 7.7×10^{-3} eV/kbar, b = 41.9×10^{-5} eV/K and c = 271 K are the pressure coefficient and temperature coefficients, respectively for InAs semiconductors.

When the RSOC is introduced in the system the total Hamiltonian becomes

$$H_T = \frac{p^2}{2m_e(x,P,T)} + \frac{e}{m_e(x,P,T)}\boldsymbol{A}.\boldsymbol{p} + \frac{e^2A^2}{2m_e(x,P,T)} + + \frac{1}{2}m_e(x,P,T)\omega_o(x^2+y^2) + \frac{1}{2}g^*\mu_B B\sigma_i + \frac{\alpha}{\hbar}[\sigma\times\boldsymbol{p}]_z + \frac{e\alpha}{\hbar}[\sigma\times\boldsymbol{A}]_z \quad \textbf{(5.4)}$$

The last two terms in eq. (5.4) corresponds to RSOC. In which α is known as the Rashba constant and σ is the electron spin. Moreover, the energy wave function and eigen energies correspond to eq. (5.4) are

$$\varphi_{nl\sigma} = \frac{1}{\sqrt{2\pi}} e^{il\varphi} R_{nl}(r) \chi_{\sigma} \tag{5.5}$$

and

$$E^{T}_{nl\sigma} = (2n + |l| + 1)\hbar\Theta^{2}_{\sigma} + \frac{\hbar}{2} l\omega_c + \sigma\left(\frac{1}{2} g^{*}\mu_B B + l\alpha m_e(x,P,T)\omega_o^2\right) \tag{5.6}$$

Where $R_{nl}(r) = \frac{\sqrt{2}}{a}\sqrt{\frac{n!}{(n+|l|)!}} exp\left(-\frac{r^2}{2a^2}\right)\left(\frac{r^2}{a^2}\right)^{|l|/2} L_n^{|l|}\left(\frac{r^2}{a^2}\right)$, n = 0,1,2,…, and l = 0,±1, ±2,… .

a is the Bohr radius ($a = \left(\frac{\hbar}{m_e(x,P,T)\omega_o}\right)^{1/2}$), and $\Theta^{2}_{\sigma} = \omega_o^2 + \frac{\omega_c^2}{4} + \frac{\sigma\alpha m_e(x,P,T)\omega_o^2\omega_c}{\hbar}$ with $\omega_c = \frac{eB}{m_e(x,P,T)}$ called cyclotron frequency. χ_{σ} is called the spinor function.

5.3 LINEAR AND NON-LINEAR OPTICAL PROPERTIES

For the scheming of optical properties of the $In_xGa_{1-x}As$ quantum dot, the perturbation expansion and density matrix approach are used. The expression for the linear, nonlinear and total ACs are written as [37]

$$\alpha^{(1)}(\omega) = \omega\sqrt{\frac{\rho}{\rho_r}}\frac{\sigma_s\Gamma_{if}|M_{if}|^2}{\hbar\left\{(\omega_{fi}-\omega)^2+\Gamma_{if}{}^2\right\}}, \tag{5.7}$$

And

$$\alpha^{(3)}(\omega, I) = -\hbar\omega\sqrt{\frac{\rho}{\rho_r}}\frac{I}{2\epsilon_o n_r c} \times \frac{4\sigma_s\Gamma_{if}|M_{if}|^2}{\hbar^4\left\{(\omega_{fi}-\omega)^2+\Gamma_{if}{}^2\right\}} \times$$

$$\left[\frac{|M_{if}|^2}{(\omega_{fi}-\omega)^2+\Gamma_{if}{}^2}+\frac{(M_{ff}-M_{ii})^2(3\omega_{fi}{}^2-4\omega_{fi}\omega)(\omega_{fi}^2-\Gamma_{if}^2)}{4(\omega_{fi}^2+\Gamma_{if}^2)\{(\omega_{fi}-\omega)^2+\Gamma_{if}{}^2\}}\right] \quad \textbf{(5.8)}$$

The parameters used in eq. (5.7) and (5.8), ρ is known as permeability, ρ_r is the real part of permittivity and $\hbar\omega$ is the incident photon energy. *I*, σ_s and n_r are the intensity of incident light, carrier density and refractive index of the $In_xGa_{1-x}As$ quantum dot, respectively. Γ_{if} and ω_{if} named as relaxation time and transition frequency. $M_{if} = |\langle\varphi_i|r|\varphi_f\rangle|$ known as the transition matrix element. The total ACs are given by

$$\alpha_T(\omega, I) = \alpha^{(1)}(\omega) + \alpha^{(3)}(\omega, I). \quad \textbf{(5.9)}$$

The linear and non-linear RICs for the optical transition are written as [38]

$$\frac{\Delta n_r^{(1)}}{n_r} = \frac{\sigma_s}{2n_r^2\epsilon_o}\frac{|M_{if}|^2(\omega_{fi}-\omega)}{\hbar\{(\omega_{fi}-\omega)^2+\Gamma_{if}{}^2\}}\ , \quad \textbf{(5.10)}$$

$$\frac{\Delta n_r^{(3)}(\omega,I)}{n_r} = -\frac{\sigma_s}{2n_r{}^3\epsilon_o}\frac{I\rho c|M_{if}|^2(\omega_{fi}-\omega)}{\hbar^3(\omega_{fi}-\omega)^2+\Gamma_{if}^2}\times$$

$$\left[\frac{|M_{if}|^2}{(\omega_{fi}-\omega)^2+\Gamma_{if}^2}+\frac{2\Gamma_{if}(M_{ff}-M_{ii})}{(\omega_{fi}-\omega)^2+\Gamma_{if}^2}\times\{(\omega_{fi}-\omega)[\omega_{fi}(\omega_{fi}-\omega)+\Gamma_{if}^2]-\Gamma_{if}^2(2\omega_{fi}-\omega)\}\right] \quad \textbf{(5.11)}$$

The total RICs represented as

$$\frac{\Delta n_r(\omega,I)}{n_r} = \frac{\Delta n_r^{(1)}}{n_r} + \frac{\Delta n_r^{(3)}(\omega,I)}{n_r}. \quad \textbf{(5.12)}$$

For the oscillation with 4ω, we consider a third-order contribution. Therefore, the THG per unit volume is obtained with the help of the density matrix approach, and written as [39]

$$\chi_{3\omega}{}^{(3)} = -\frac{q^4\vartheta}{\varepsilon_o\hbar^3}\frac{M_{12}M_{23}M_{34}M_{41}}{(\omega-\omega_{21}+i\Gamma_{21})(2\omega-\omega_{31}+i\Gamma_{31})(3\omega-\omega_{41}+i\Gamma_{41})}. \quad \textbf{(5.13)}$$

Here, q and ϑ are known as the charge on an electron and electron density, respectively.

In the result section, the behaviour of the ACs, RICs and THG are studied.

5.4 RESULT AND DISCUSSION

In this work, the impact of the hydrogenic impurity (x) on the ACs, RICs and THG of the $In_xGa_{1-x}As$ quantum dot under the influence of RSOC are examined. The constraints used in this paper are: $\vartheta = 10^{16}\ \mathrm{cm}^{-3}$, $n_r = 3.2$, $\Gamma_{12} = 1/T_{12}$ where $T_{12} = 0.14$ ps and $\rho = 4\pi \times 10^{-7}\ \mathrm{Hm}^{-1}$.

The linear, non-linear and total ACs of the $In_xGa_{1-x}As$ quantum dot with the different concentrations of the hydrogenic impurity (x = 0, 0.1, 0.2 and 0.3) are shown in **Figure 5.2,** respectively. As it is easily noticeable that the position and magnitude of the peaks depend on the concentration of x. In such a way, the increase in the value of x the position of peaks towards a higher value of incident energies (blue shift) and the magnitude of peaks decreases. The blue shifting occurs as a consequence of an increment in the energy difference between the successive levels of the energy with the concentration of impurity. Moreover, the impurity (x) influences the total AC firmly as compared to the linear AC causing the erratic shape in the total AC. The magnitude decreases with the increment in the impurity happens on account of the small value of the dipole matrix element (M_{ij}). The linear and non-linear ACs depend on the $M_{12}^2 E_{12}$ and $M_{12}^4 E_{12}$, respectively present in the eqs. (5.7) and (5.8). As the M_{12} is dominant the magnitude of the non-linear peak becomes larger than linear AC. It is obvious the linear, non-linear and total ACs peaks decrease and move towards higher energies as impurity increases.

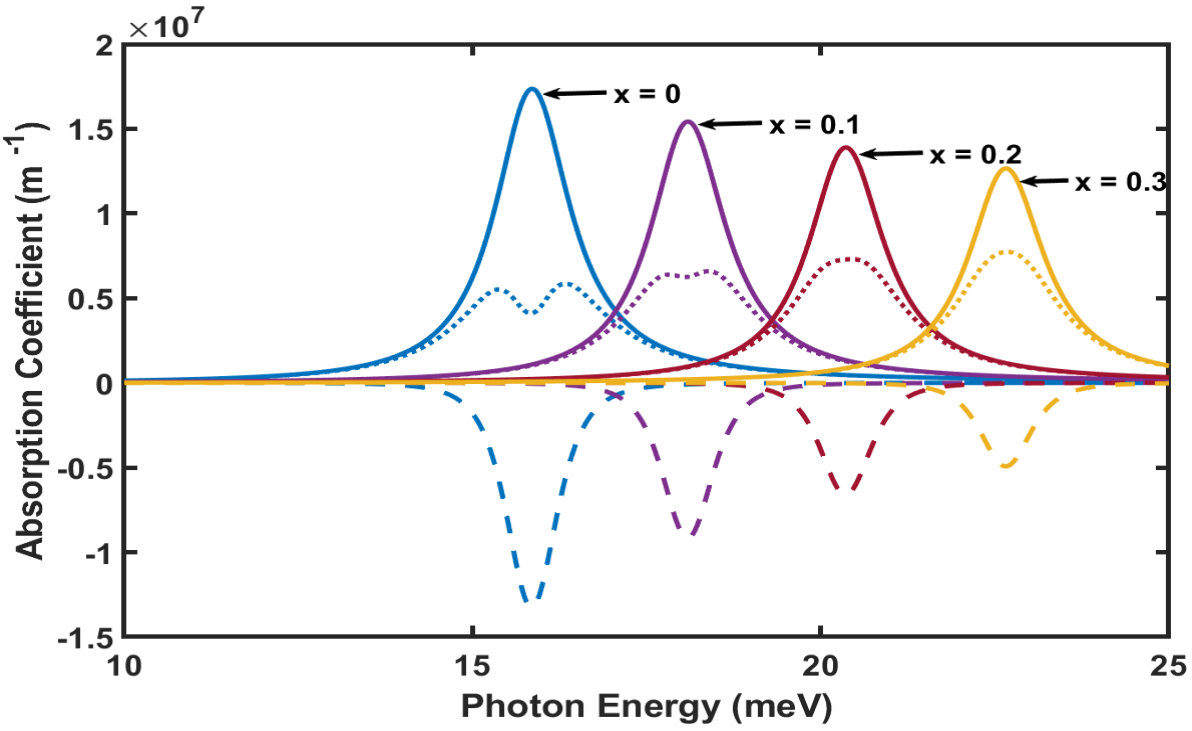

Figure 5.2 Change of linear (solid line), non-linear (dashed line), and total ACs (solid dashed line) with the incident photon energy for x = 0, 0.1, 0.2 and 0.3.

Figure 5.3 (a-c) represents the varation in the linear, non-linear and total RICs with the incident energy under the influence of impurity (x = 0, 0.1, 0.2 and 0.3). From the figure, the linear RIC start to rise with the incident photon energy and attains the maximum point which is called normal dispersion reason. Whenever the incident photon energy avenue the threshold energy, the sign of the $dn/d\omega$ vary and the anomalous dispersion occurs in the resonant frequency of the $In_xGa_{1-x}As$ quantum dot. With the concentration of the hydrogenic impurity, the resonant frequency moves towards a higher frequency (blue shift) with a decrement in the magnitude of the peaks. The nonlinear RIC eq. (5.11) contains a negative sign whereas the linear RIC eq. (5.10) have positive signs hence the total RIC is reduced by it. Thereby, the non-linear must be used for the high optical intensity devices.

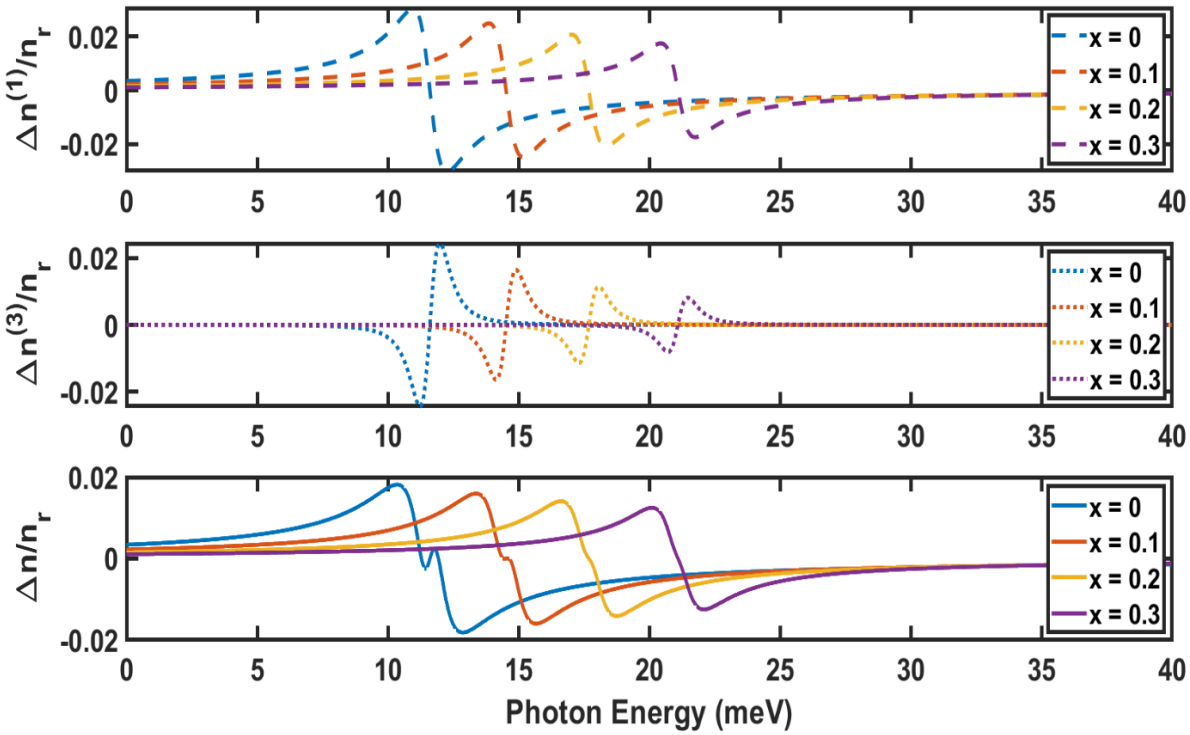

Figure 5.3 Change of (a) linear, (b) non-linear, and (c) total RICs with the incident photon energy for x = 0, 0.1, 0.2 and 0.3.

In **Figure 5.4**, the change in the THG with the photon energies under the impact of impurity (x=0, 0.1, 0.2 and 0.3). With the concentration of the impurity (x), the peaks of the THG shift towards a high value of energies and indicate blue shifting. THG peak magnitude decreases with the increment in impurity as a consequence of matrix elements product. However, the gap between the two states becomes large when we introduce impurity into our system. Therefore, the THG peak reduces its magnitude and shifts towards higher photon energies as the impurity increases.

Figure 5.5 (a and b) shows the Bohr radius variation with different hydrogenic impurity factors for different values of pressure and temperature. It is observed that the Bohr radius decreases with increases in impurity due to mass dependence on the impurity factor. Whenever

the pressure rises Bohr radius starts to decrease with the smaller value and vice versa for temperature rises as seen in **Figure 5.5 (a)** and **(b).**

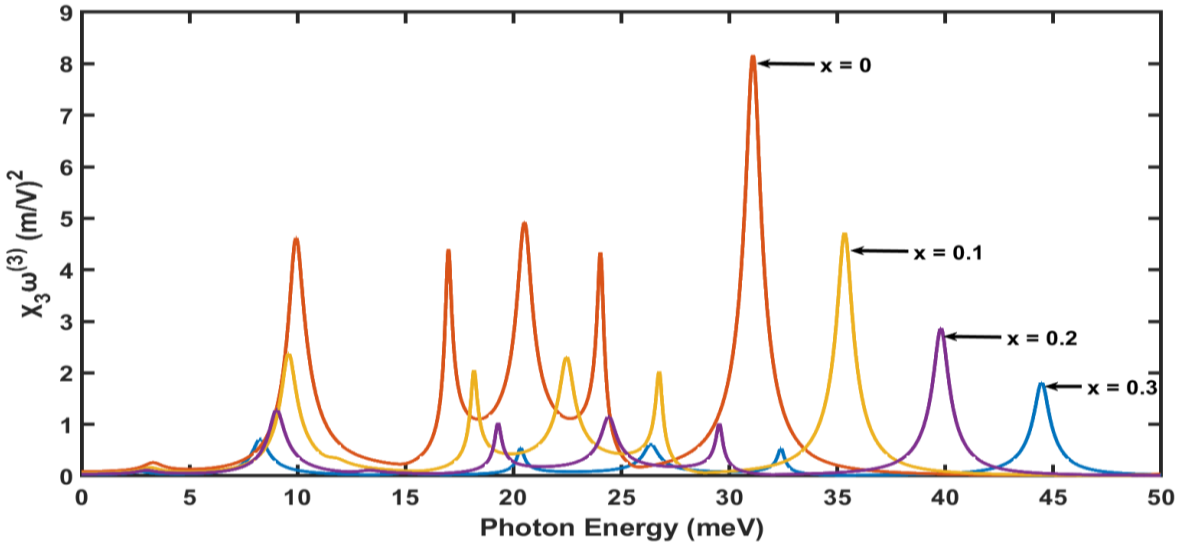

Figure 5.4 Change of THG with the incident photon energy for x = 0, 0.1, 0.2 and 0.3.

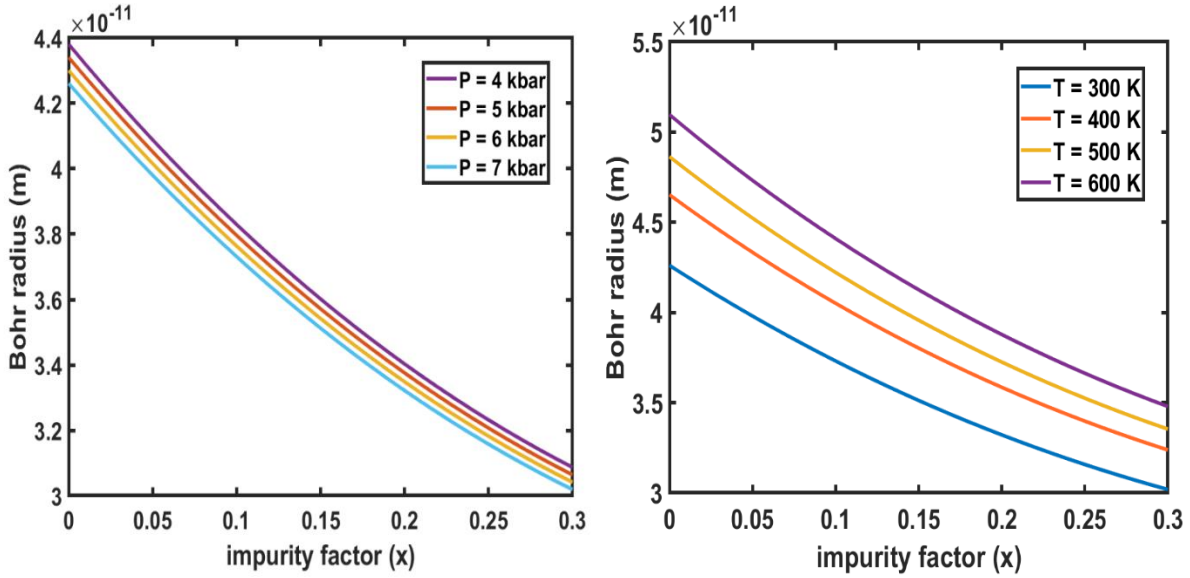

(a) **(b)**

Figure 5.5 Bohr radius variation with the impurity at a different range of (a) pressure and (b) temperature.

5.5 SUMMARY

In this paper, the influence of hydrogenic impurity on the linear and non-linear optical properties of $In_xGa_{1-x}As$ quantum dot under the presence of an external applied field are demonstrated. It is observed that the dipole matrix elements and the transition energy both are strongly affected by the presence of impurities. Similarly, effects are shown in the case of RICs and THG. Hydrogenic impurity factor (x) inceases the energy gap between two states as a result, the peaks of ACs, RICs and THG shift towards higher incident energies. Whereas, impurity decreases the dipole matrix elements due to which the magnitude of the ACs, RICs and THG peaks decreases. Therefore, it was found that the impurity value caused the blue shifts and decrease in the peaks of linear and non-linear optical properties.

5.5 REFRENCES

[1] L. Jiang, H. Wang, H. Wu, Q. Gong, S. Feng, External electric field effect on the hydrogenic donor impurity in zinc-blende GaN/AlGaN cylindrical quantum dot, J Appl Phys 105 (2009).

[2] S.-S. Li, J.-B. Xia, Electronic structure and binding energy of a hydrogenic impurity in a hierarchically self-assembled GaAs⁄AlxGa1−xAs quantum dot, J Appl Phys 100 (2006).

[3] G. Rezaei, S. Shojaeian Kish, Linear and nonlinear optical properties of a hydrogenic impurity confined in a two-dimensional quantum dot: Effects of hydrostatic pressure, external electric and magnetic fields, Superlattices Microstruct 53 (2013) 99–112.

[4] E. Kasapoglu, H. Sari, I. Sökmen, Binding energy of impurity states in an inverse parabolic quantum well under magnetic field, Physica B Condens Matter 390 (2007) 216–219.

[5] F.K. Boz, S. Aktas, Magnetic field effect on the binding energy of a hydrogenic impurity in coaxial GaAs/ AlxGa1−xAs quantum well wires, Superlattices Microstruct 37 (2005) 281–291.

[6] C.A. Duque, A. Montes, A.L. Morales, Binding energy and polarizability in GaAs–(Ga, Al) As quantum-well wires, Physica B Condens Matter 302 (2001) 84–87.

[7] E. Niculescu, A. Gearba, G. Cone, C. Negutu, Magnetic field dependence of the binding energy of shallow donors in GaAs quantum-well wires, Superlattices Microstruct 29 (2001) 319–328.

[8] Y.-X. Li, J.-J. Liu, X.-J. Kong, The effect of a spatially dependent effective mass on hydrogenic impurity binding energy in a finite parabolic quantum well with a magnetic field, J Appl Phys 88 (2000) 2588–2592.

[9] Y.J. Wang, Y.A. Leem, B.D. McCombe, X.-G. Wu, F.M. Peeters, E.D. Jones, J.R. Reno, X.Y. Lee, H.W. Jiang, Strong three-level resonant magnetopolaron effect due to the intersubband coupling in heavily modulation-doped GaAs/AlxGa1-xAs single quantum wells at high magnetic fields, Phys Rev B 64 (2001) 161303.

[10] S. Paul, J.B. Roy, P.K. Basu, Empirical expressions for the alloy composition and temperature dependence of the band gap and intrinsic carrier density in Ga *x* In1− *x* As, J Appl Phys 69 (1991) 827–829.

[11] E. Sadeghi, Electric field and impurity effects on optical property of a three-dimensional quantum dot: A combinational potential scheme, Superlattices Microstruct 50 (2011) 331–339.

[12] R. Khordad, H. Bahramiyan, The second and third-harmonic generation of modified Gaussian quantum dots under influence of polaron effects, Superlattices Microstruct 76 (2014) 163–173.

[13] U. Merkt, J. Huser, M. Wagner, Energy spectra of two electrons in a harmonic quantum dot, Phys Rev B 43 (1991) 7320.

[14] P.K. Jha, M. Kumar, S. Lahon, S. Gumber, M. Mohan, Rashba spin orbit interaction effect on nonlinear optical properties of quantum dot with magnetic field, Superlattices Microstruct 65 (2014) 71–78.

[15] I. Žutić, J. Fabian, S. Das Sarma, Spintronics: Fundamentals and applications, Rev Mod Phys 76 (2004) 323.

[16] D. Sanjeev Kumar, S. Mukhopadhyay, A. Chatterjee, Effect of Rashba interaction and Coulomb correlation on the ground state energy of a GaAs quantum dot with parabolic confinement, Physica E Low Dimens Syst Nanostruct 47 (2013) 270–274.

[17] Li, Shu-Shen, et al. "Spin-dependent transport through Cd 1− x Mn x Te diluted magnetic semiconductor quantum dots." Physical Review B 68.24 (2003) 245306.

[18] J.E. Hirsch, Spin hall effect, Phys Rev Lett 83 (1999) 1834.

[19] S.A. Wolf, A.Y. Chtchelkanova, D.M. Treger, Spintronics—A retrospective and perspective, IBM J Res Dev 50 (2006) 101–110.

[20] M. Wierzbicki, Thermoelectric properties of magnetic configurations of graphene-like nanoribbons in the presence of Rashba and spin–orbit interactions, Physica E Low Dimens Syst Nanostruct 87 (2017) 220–227.

[21] H. Hassanabadi, H. Rahimov, L. Lu, C. Wang, Nonlinear optical properties of a three-electron quantum dot with account of the Rashba spin–orbit interaction, J Lumin 132 (2012) 1095–1100.

[22] R. Khordad, Optical properties of wedge-shaped quantum dots under Rashba spin–orbit interaction, Int J Mod Phys B 31 (2017) 1750055.

[23] H. Hassanabadi, H. Rahimov, L. Lu, C. Wang, Nonlinear optical properties of a three-electron quantum dot with account of the Rashba spin–orbit interaction, J Lumin 132 (2012) 1095–1100.

[24] K. Premasiri, S.K. Radha, S. Sucharitakul, U.R. Kumar, R. Sankar, F.-C. Chou, Y.-T. Chen, X.P.A. Gao, Tuning Rashba Spin–Orbit Coupling in Gated Multilayer InSe, Nano Lett 18 (2018) 4403–4408.

[25] T. Koga, J. Nitta, T. Akazaki, H. Takayanagi, Rashba Spin-Orbit Coupling Probed by the Weak Antilocalization Analysis in <math display="inline"> <mi>InAlAs</mi> <mi>/</mi> <mi>InGaAs</mi> <mi>/</mi> <mi>InAlAs</mi> </math> Quantum Wells as a Function of Quantum Well Asymmetry, Phys Rev Lett 89 (2002) 046801.

[26] A. Gharaati, Lande g-factor in semiconductor cylinder quantum dots under magnetic fields and spin-orbit interaction, Solid State Commun 258 (2017) 17–20.

[27] L. Zhuang, L. Guo, S.Y. Chou, Silicon single-electron quantum-dot transistor switch operating at room temperature, Appl Phys Lett 72 (1998) 1205–1207.

[28] M. Kirak, S. Yilmaz, Third harmonic generation of spherical multilayered quantum dot: effects of quantum confinement, impurity, electric and magnetic fields, Applied Physics A 128 (2022) 459.

[29] R.L. Restrepo, E. Kasapoglu, S. Sakiroglu, F. Ungan, A.L. Morales, C.A. Duque, Second and third harmonic generation associated to infrared transitions in a Morse quantum well under applied electric and magnetic fields, Infrared Phys Technol 85 (2017) 147–153.

[30] H. Bahramiyan, Strain effect on the third-harmonic generation of a two-dimensional GaAs quantum dot in the presence of magnetic field and spin–orbit interaction, Indian Journal of Physics 94 (2020) 789–796.

[31] L. Liu, J. Li, G. Xiong, Studies of the third-order nonlinear optical susceptibility for InxGa1−xN/GaN cylinder quantum dots, Physica E Low Dimens Syst Nanostruct 25 (2005) 466–471.

[32] E. Sadeghi, Electric field and impurity effects on optical property of a three-dimensional quantum dot: A combinational potential scheme, Superlattices Microstruct 50 (2011) 331–339.

[33] C.-J. Zhang, K.-X. Guo, Z.-E. Lu, Exciton effects on the optical absorptions in one-dimensional quantum dots, Physica E Low Dimens Syst Nanostruct 36 (2007) 92–97.

[34] W. Xie, Linear and nonlinear optical properties of a hydrogenic donor in spherical quantum dots, Physica B Condens Matter 403 (2008) 4319–4322.

[35] P. Başer, I. Altuntas, S. Elagoz, The hydrostatic pressure and temperature effects on hydrogenic impurity binding energies in GaAs/InxGa1-xAs/GaAs square quantum well, Superlattices Microstruct 92 (2016) 210–216.

[36] S. Paul, J.B. Roy, P.K. Basu, Empirical expressions for the alloy composition and temperature dependence of the band gap and intrinsic carrier density in Ga *x* In1− *x* As, J Appl Phys 69 (1991) 827–829.

[37] G. Rezaei, S. Shojaeian Kish, Linear and nonlinear optical properties of a hydrogenic impurity confined in a two-dimensional quantum dot: Effects of hydrostatic pressure, external electric and magnetic fields, Superlattices Microstruct 53 (2013) 99–112.

[38] G. Rezaei, S. Shojaeian Kish, Linear and nonlinear optical properties of a hydrogenic impurity confined in a two-dimensional quantum dot: Effects of hydrostatic pressure, external electric and magnetic fields, Superlattices Microstruct 53 (2013) 99–112.

[39] R. Khordad, H. Bahramiyan, Optical properties of a GaAs cone-like quantum dot: Second and third-harmonic generation, Opt Spectrosc 117 (2014) 447–452.

6

CHAPTER

Physical and Transport Properties in $In_xGa_{1-x}As$ Double Quantum Wire

- *The study investigates the effects of temperature, hydrostatic pressure, and impurities on the energy spectrum and ballistic conductivity of $In_xGa_{1-x}As$ double quantum wire rings.*
- *The system is subject to a double-well anharmonic confinement potential, intense magnetic and electric fields, and Rashba and Dresselhaus spin-orbit interactions.*
- *Energy eigenvalues are calculated using the diagonalization method.*
- *Ballistic conductance is evaluated through the Landauer-Büttiker formalism.*
- *Shifts in energy dispersion are caused by variations in temperature, pressure, and impurities.These shifts lead to changes in ballistic conductivity patterns.*
- *Applied electric and magnetic fields, as well as temperature, influence the energy behavior and modify conductance.*

6.1 INTRODUCTION

The inspection of physical and transport properties of nanostructures viz. quantum well (QW), quantum wire (QWR) and quantum dot (QD), have an intense curiosity for the high-performance devices over the past decades in their confining potential applications [1,2]. The scrutiny of the physical and transport properties of nanostructures like QW, QD and QWR, formed by the constrictive charge's motion in bulk structures, offers noteworthy participation to the sprouting invention technology of today. Restricting the motion of charge carriers develops the discrete energy dispersion consequently the optical properties of nanostructures modify [3,4]. The movement of the charge carriers is restricted by the confinement potential which is generally presumed as a harmonic oscillator, gaussian potential, and hard wall potential. Although, there is illustrious problem potential in physics and chemistry which is dealt with under the quartic-well potential and potential profile. Moreover, the double quartic-well potential has been used to illuminate some physical aspects like the occurrence of the doublet, and tunnelling with the help of semi-classical methods and quantum mechanics [5,6]. In this kind of study, energy eigenvalues have been calculated with the assistance of mainly variational perturbation method, WKB approximation etc. Therefore, some engrossing physical appearances of the double-well potential structures have been illustrated by many researchers' notable bulging of the subordinate energy eigenvalues for a system in which two-wells are effectively apart from each other [7–9]. Shi et al. illustrated the double QW structure with enough height potential barrier [10]. Moreover, there are many influences of external perturbative fields which deals with the transport and electronic phenomena related to coupled double-QW that have been focused theoretically [11–13] and experimentally [14,15]. Korepov

and Liberman [16] have investigated the theory of two parallel QWs coupled by tunnelling within the existence of a perpendicular magnetic field. Lyo and his colleagues [17] examined the magnetoresistance, conductivity, and mobility of the coupled double-QW within the existence of an externally applied magnetic field. For window-coupled double-QW, the magneto-transport properties have been deliberated by Tang et al [18].

Furthermore, there is a growing curiosity about the utilisation of the electron spin instead of its information processing and charge storage. The spin and charge of an electron have been used for information processing in the exploration of nanostructures recently. Most of the devices initiate the electron spin via spin-orbit interaction (SOI) [19]. The paradigmatic device among all the devices is the "spin field effect transistor" (SFET) designed by Datta Das[20]. Wherein the Rashba SOI helps in controlling the rotation of the electron spin when they pass through the device. Moreover, the Rashba SOI can be modulated by the gate voltage. This kind of interaction arises via the inversion asymmetry of the confining potential within two-dimensional electron gas (2DEG) [21]. Omitting Rashba SOI, the Dresselhaus interaction also subsidizes the spin-orbit interaction. This classification of interaction arises in the crystal lattice structure due to the bulk inversion asymmetry and having the zinc-blende structure. Dresselhaus interaction has two part which includes linear and the cubic term wise to wave vector (k) of an electron whereas, the cubic term is mainly avoided due to the effective linear term. Dresselhaus SOI strength is associated with the sample thickness [22,23]. There is a lot of research has been done along with the Rashba and Dresselhaus SOIs making an impact on the various properties of the nanostructures like physical, optical and transport properties[24–26] .

Amid these properties, the transport properties show a pivotal role. The transport properties can be explained by the non-interacting model accordance with the Landuer-Büttiker formalism, the movement of charge carrier gets shifted from one reservoir to the other in the presence of a small biasing across the channel [27,28]. Whenever the electrons are confined in the channel along a transversal direction the distribution of electrons is done by the Fermi-Dirac distribution amongst different sub-bands. The number of modes for the propagation of electrons shows the net ballistic conductivity for the system which can be find out by the fermi-energy and the energy dispersion [29]. Quay et al. [30] established the connection between energy dispersion and the conductance of nanostructure devices. The energy dispersion executed that every sub-band subsidizes $2e^2/h$ to the ballistic conductivity. Moreover, the impact of externally applied fields, SOIs and other parameters like impurity, pressure and temperature on the transport properties of the nanostructure devices have been examined by many researchers [31–34].

The outwardly controlled parameters like temperature, hydrostatic pressure and impurity can manipulate the physical, optical, and electronic characteristics of nanostructures. In the quantum system, the energy spectrum and ballistic conductance can be shifted due to these parameters. As, the temperature, hydrostatic pressure and impurity influence the nanostructure devices' variables like effective mass, energy gap, lattice vibration, dielectric constant and so on [35–37]. Abundant studies have been explored for the discussion of the QWRs under the presence of temperature, pressure, and hydrogenic-trivial impurities. It has become vital to study the doped nanostructure [38,39].

In this current study, the influence of temperature, hydrostatic pressure, and impurity on energy dispersion and ballistic conductance in the presence of Rashba and Dresselhaus SOIs have been

investigated. Moreover, we examine the energy exploits along the electric field, magnetic field, and temperature at x = 0 and 0.3. The paper is ordered in this way: Firstly, in section 6.2 and 6.3 we illustrate the theoretical framework. Formerly, in section 6.4 we describe the numerical result and discussion, and finally, the summary of the chapter is represented in section 6.5.

6.2 DOUBLE QUANTUM WIRE-WELL POTENTIAL

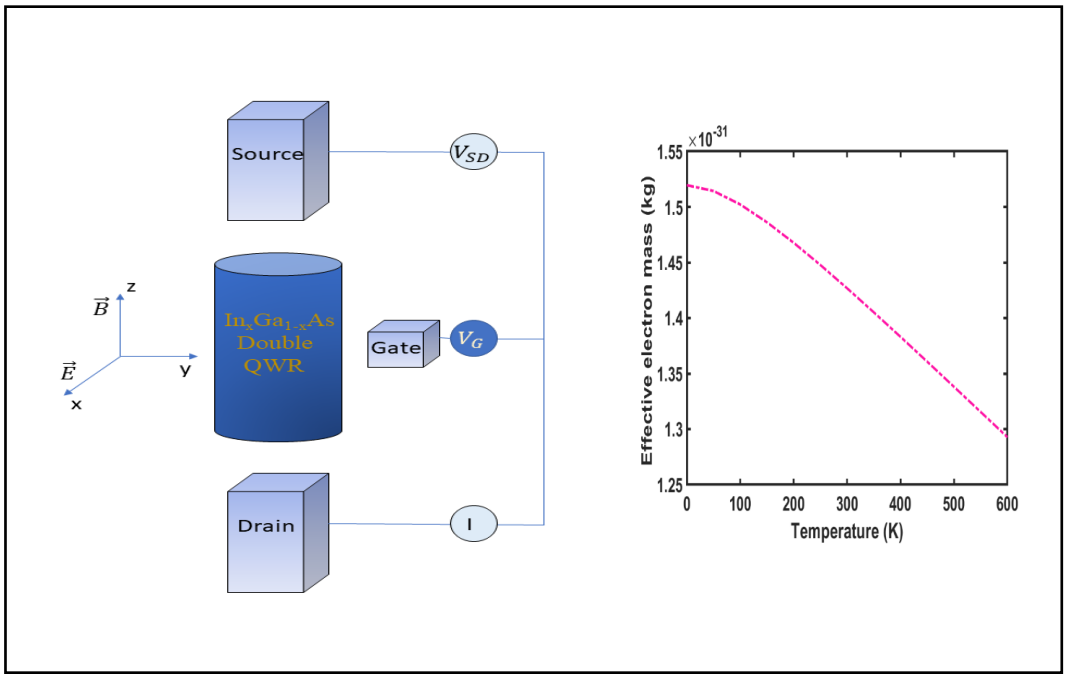

Figure 6.1 Schematic view of the $In_xGa_{1-x}As$ double QWR which is coupled to the source and drain reservoirs via tunnel barriers under the presence of external fields and effective mass dependence on the temperature at P = 2 kbar & x = 0.3.

A quasi-one-dimensional $In_xGa_{1-x}As$ double QWR (**Figure 6.1**) is considered in which 2DEG and magnetic field applied along the x-y plane and z-direction, respectively. The $In_xGa_{1-x}As$ double QWR is confined by the double-well potential which is written by [40]

$$V(x)=\frac{1}{4}\rho\left(x^2-\frac{\beta^2}{\rho}\right)^2. \quad \textbf{(6.1)}$$

Where ρ and β are the positive versatile structural parameters which help in adjusting the barrier's height between the wells and the width of the wells. Assume the double QWR is lie on the *x*-*y* plane and the electrons are allowed to move without any restrictions along the *y*-direction. The intense magnetic and electric field are applied along the z-direction *(0, 0, B)* and *x*-direction *(E, 0, 0*), respectively. The Hamiltonian for the single-particle electron under the occurrence of Rashba and Dresselhaus SOIs in double QWR is written as

$$H=\frac{1}{2m_e(x,P,T)}\left[p_x^2+(p_y^2+eBx)^2\right]\sigma_m+V(x)\sigma_m+eEx\sigma_m+\frac{1}{2}g\mu_B B\sigma_z+H_R+H_D \quad \textbf{(6.2)}$$

Where $m_e(\mu,P,T)$ is known as the effective mass of an electron and having dependence on the impurity, pressure and temperature, *e* is the electron charge, p_x and p_y are the *x* and *y*-components of the momentum, respectively. σ_m is a 2×2-unit matrix. g is used for the Lande *g*-factor, μ_B is called Bohr magneton and σ_z is the Pauli matrix for *z*-component. The first and second terms in eq. (6.2) represents kinetic and confining potential contribution, respectively. Electric field contribution in energy and Zeeman energy splitting is given by the third and fourth terms in eq. (6.2). The last two terms are known as Rashba and Dresselhaus spin-orbit interaction terms. The expression for $m_e(x,P,T)$, $\mathrm{H_R}$, and H_D are given by [41]

$$m_e(x,P,T)=m_o\left[1+7.51\left(\frac{2}{{E_g}^j(x,P,T)}+\frac{1}{0.341+{E_g}^j(x,P,T)}\right)\right]^{-1}, \quad \textbf{(6.3)}$$

m_o is the free electron mass, The energy bandgap (${E_g}^j$) for the $In_xGa_{1-x}As$ in terms of *x, P* and *T* is:

$${E_g}^j(x,P,T)={E_g}^{GaAs}(P,T)+\left[{E_g}^{InAs}(P,T)-{E_g}^{GaAs}(P,T)\right]x-0.475x(1-x) \quad \textbf{(6.4)}$$

Where $E_g{}^{GaAs}(P,T) = E_g{}^0 + aP - \frac{bT^2}{T+c}$, and $E_g{}^{InAs}(P,T) = E_{gi}{}^0 + uP - \frac{vT^2}{T+w}$.

The values of $E_g{}^0$ = 1.52 eV (known as energy gap at P = 0 kbar and T = 0 K), a = 1.08× 10^{-2} eV/kbar, b = 50.4× 10^{-5} eV/K, and c = 204 K are the pressure coefficient, temperature coefficients, respectively for *GaAs*. And $E_{gi}{}^0$ = 0.42 eV (known as energy gap at P = 0 kbar and T = 0 K), u = 7.7× 10^{-3} eV/kbar, v = 41.9× 10^{-5} eV/K and w = 271 K are the pressure coefficient, and temperature coefficients, respectively for InAs [42].

And,

$$H_R = \frac{\alpha_R}{\hbar}[\sigma_x(p_y + eBx) - \sigma_y p_x], \tag{6.5}$$

$$H_D = \frac{\alpha_D}{\hbar}[\sigma_y(p_y + eBx) - \sigma_x p_x]\,. \tag{6.6}$$

Here α_R and α_D are the Rashba and Dresselhaus SOIs parameters. σ_x and σ_y are the Pauli matrix for x & y-component, respectively.

Moreover, as a result of the transitional invariance movement along the y-direction, the energy eigenfunctions of Hamiltonian in form of a plane wave are given by

$$\psi(x,y) = \emptyset(x)exp\ (ik_y y), \tag{6.7}$$

Here, k_y is known as wave number for the plane wave. If the Hamiltonian in eq. (6.2) becomes separated in the x and y form, the Hamiltonian ($H = H_I + H_{II} + H_R + H_D$) are given by

$$H_I = \left[-\frac{\hbar^2}{2m_e(x,P,T)}\frac{d^2}{dx^2} + \frac{1}{2}m_e(x,P,T)\omega^2(x - x_j)^2 + \frac{\hbar^2 k_y^2}{2m_e(x,P,T)} - \frac{1}{2}m_e(x,P,T)\omega^2 x_j^2\right]\sigma_m + \frac{1}{2}g\mu_B B\sigma_z,$$

$$H_{II} = \left[-\frac{1}{2}\left(m_e(x,P,T)\omega_j^2 + \beta^2\right)x^2 + \frac{1}{4}\rho x^4 + \frac{1}{4}\frac{\mu^4}{\lambda}\right]\sigma_m,$$

$$H_R = \alpha_R\left[\sigma_x\left(k_y + \frac{eB}{\hbar}x\right) + i\sigma_y\frac{d}{dx}\right],$$

$$H_D = \alpha_D\left[\sigma_y\left(k_y + \frac{eB}{\hbar}x\right) + i\sigma_x\frac{d}{dx}\right]. \quad \textbf{(6.8)}$$

The variable introduced in the above equation is as follows: $\omega = \sqrt{\omega_j^2 + \omega_c^2}$ is known as effective oscillator frequency and $\omega_c = \frac{eB}{m_e(x,P,T)}$ is the cyclotron frequency. $x_j = -l_j\omega_{jw}^2(\omega_{cj} + el_jE/\hbar\omega_j)$ called guiding centre coordinate with the characteristic length $l_j = \sqrt{\hbar/\, m_e(x,P,T)\omega_j}$ and the diminutive $\omega_{jw} = \omega_j/\omega$, ω_{cj}=ω_c/ω_j, and $k_o = l_jk_y$.

The eigenfunctions of Hamiltonian H_I achieve with the help of the Schrödinger equation $H_I\varphi_{n\sigma} = E_{n\sigma}^l\varphi_{n\sigma}$ are written as

$$\varphi_{m\sigma} = \frac{1}{\sqrt{l_j\sqrt{\pi\omega_{jw}}2^n n!}}H_n\left(\frac{x-x_j}{l_j\sqrt{\omega_{jw}}}\right)exp\left(-\frac{1}{2}\left(\frac{x-x_j}{l_j\sqrt{\omega_{jw}}}\right)^2\right)\chi_\sigma, \quad \textbf{(6.9)}$$

With m = 0, 1, 2, 3, … and so on, $\sigma = \pm$, $H_n(x)$ is known as nth order of Hermite polynomial, χ_σ are the spinor function for the spin-up $\chi_+ = \begin{pmatrix}1\\0\end{pmatrix}$ and spin-down $\chi_- = \begin{pmatrix}0\\1\end{pmatrix}$ along *z*-direction. Eigenenergies for the H_I are given by

$$E_{n\sigma}^l = \frac{1}{\omega_{jw}}\left(n + \frac{1}{2}\right) + \frac{\omega_{j\omega}^2}{2}(k_j^2 - 2k_o\tilde{E}\omega_{cj} - \tilde{E}^2) \pm \frac{\Delta y}{2}. \quad \textbf{(6.10)}$$

In recent work, we consider l_j as length scale and $\hbar\omega_j$ is the energy scale. $\tilde{E} = el_jE/\hbar\omega_j$ and $\Delta y = g\mu_BB/\hbar\omega_j$ are the contribution of electric field and Zeeman energy in the scaled forms,

respectively. As we expand $\emptyset(x) = \sum_{n,\sigma} A_{n\sigma}\varphi_{n\sigma}(x)$ in the form of H_I's eigenfunction therefore the Schrödinger equation corresponding to eq. (6.9) becomes

$$(E^{l}_{n\sigma} - E)A_{n\sigma} + \sum_{b,\sigma'=\sigma}(H_{II})^{\sigma\sigma'}_{nb} A_{b\sigma'} + \sum_{b,\sigma'\neq\sigma}(H_R)^{\sigma\sigma'}_{nb} A_{b\sigma'} + \sum_{b,\sigma'\neq\sigma}(H_D)^{\sigma\sigma'}_{nb} A_{b\sigma'} = 0. \quad \textbf{(6.11)}$$

Where $(H_{II})^{\sigma\sigma'}_{nb} = \langle\varphi_{n\sigma}|H_{II}|\varphi_{b\sigma'}\rangle$ and the matrix elements for this term are expressed as follows

$$(H_{II})^{\sigma\sigma'}_{nb} = P_{b4}\delta_{n.b-4} + P_{b3}\delta_{n.b-3} + P_{b2}\delta_{n.b-2} + P_{b1}\delta_{n.b-1} + P_0\delta_{n.b} + P_{a1}\delta_{n.b+1} + P_{a2}\delta_{n.b+2} + P_{a3}\delta_{n.b+3} + P_{a4}\delta_{n.b+4}. \quad \textbf{(6.12)}$$

Where *P* factors in the above eq. are given by

$$P_{b4} = \tfrac{1}{16}\tilde{\rho}\omega^2_{jw}\sqrt{(n+1)(n+2)(n+3)(n+4)},$$

$$P_{b3} = \tfrac{1}{4}\tilde{\rho}\tilde{x}_J\omega_{jw}\sqrt{2\omega_{jw}(n+1)(n+2)(n+3)},$$

$$P_{b2} = \tfrac{1}{4}\omega_{jw}\sqrt{(n+1)(n+2)}\left[\tilde{\rho}\left(3\tilde{x}_J^{\,2} + \left(n+\tfrac{3}{2}\right)\right) - (1+\tilde{\beta}^2)\right],$$

$$P_{b1} = \tfrac{1}{2}\tilde{\rho}\sqrt{2\omega_{jw}(n+1)}\left[\tilde{\rho}\left(\tilde{x}_J^{\,2} + \tfrac{3}{2}\omega_{jw}(n+1)\right) - (1+\tilde{\beta}^2)\right],$$

$$P_0 = \tfrac{1}{4}\tilde{\rho}\left[\tilde{x}_J^{\,4} + 3\omega_{jw}\tilde{x}_J^{\,2}(2n+1) + \frac{\tilde{\beta}^4}{\tilde{\rho}^2}\right] + \tfrac{1}{4}\tilde{\rho}\left[\tfrac{3}{2}\omega^2_{jw}(n^2+n+\tfrac{1}{2})\right] - \tfrac{1}{2}(1+\tilde{\beta}^2)\left[\tilde{x}_J^{\,2} + \omega_{jw}\left(n+\tfrac{1}{2}\right)\right],$$

$$P_{a1} = \tfrac{1}{2}\tilde{x}_J\sqrt{2\omega_{jw}n}\left[\tilde{\rho}\left(\tilde{\beta}^2 + \tfrac{3}{2}\omega_{jw}n\right) - (1+\tilde{\beta}^2)\right],$$

$$P_{a2} = \tfrac{1}{4}\omega_{jw}\sqrt{n(n-1)}\left[\tilde{\rho}\left(3\tilde{\beta}^2 + (n-\tfrac{1}{2})\right) - (1+\tilde{\beta}^2)\right],$$

$$P_{a3} = \frac{1}{4}\widetilde{x_j}\tilde{\beta}\omega_{jw}\sqrt{2\omega_{jw}n(n-1)(n-2)},$$

$$P_{a4} = \frac{1}{16}\widetilde{x_j}\omega_{jw}^2\sqrt{n(n-1)(n-2)(n-3)},$$

With $\widetilde{x_j} = \frac{x_j}{l_j}$, $\tilde{\beta} = \frac{\beta}{\sqrt{m_e(x,P,T)\omega_j}}$ and $\tilde{\rho} = \frac{\rho}{\hbar\omega_j}$.

The matrix element of Rashba and Dresselhaus Hamiltonian from the eq. (6.12) $(H_R)_{nb}^{\sigma\sigma'} = \langle\varphi_{n\sigma}|H_R|\varphi_{b\sigma'}\rangle$ and $(H_D)_{nb}^{\sigma\sigma'} = \langle\varphi_{n\sigma}|H_D|\varphi_{b\sigma'}\rangle$, are given by

$$(H_R)_{nn}^{\pm\mp} = \sqrt{2\tilde{\Delta}_R}\left[k_j\left(1-\omega_{cj}^2\omega_{jw}^2\right) - \omega_{cj}\omega_{jw}^2\tilde{E}\right], \quad \textbf{(6.13)}$$

$$(H_R)_{nb}^{\pm\mp} = \sqrt{\frac{2\tilde{\Delta}_R}{\omega_{jw}}}\left[(\omega_{cj}\omega_{jw} \pm 1)\sqrt{\frac{(n+1)}{2}}\delta_{n,b-1} + ((\omega_{cj}\omega_{jw} \mp 1)\sqrt{\frac{n}{2}}\delta_{n,b+1}\right], \quad \textbf{(6.14)}$$

$$(H_D)_{nn}^{\pm\mp} = \mp i\sqrt{2\tilde{\Delta}_D}\left[k_j\left(1-\omega_{cj}^2\omega_{jw}^2\right) - \omega_{cj}\omega_{jw}^2\tilde{E}\right], \text{ and} \quad \textbf{(6.15)}$$

$$(H_R)_{nb}^{\pm\mp} = \mp i\sqrt{\frac{2\tilde{\Delta}_D}{\omega_{jw}}}\left[(\omega_{cj}\omega_{jw} \mp 1)\sqrt{\frac{(n+1)}{2}}\delta_{n,b-1} + ((\omega_{cj}\omega_{jw} \pm 1)\sqrt{\frac{n}{2}}\delta_{n,b+1}\right]. \quad \textbf{(6.16)}$$

The scaled Rashba and Dresselhaus SOIs energies are defined as $\tilde{\Delta}_R = \Delta_{SO}^R/\hbar\omega_j$ and $\tilde{\Delta}_D = \Delta_{SO}^D/\hbar\omega_j$ with $\Delta_{SO}^R = m_e(x,P,T)\alpha_R^2/2\hbar^2$ and $\Delta_{SO}^D = m_e(x,P,T)\alpha_D^2/2\hbar^2$.

The energy function and energy dispersion relation of the $In_xGa_{1-x}As$ Double QWR under the existence of Rashba and Dresselhaus SOIs can be found by the diagonalization of eq. (6.11).

6.3 TRANSPORT PROPERTIES

For the two microscopic electron reservoirs, the ballistic conductance is calculated with the help of the Landuer-Büttiker formalism [43]

$$G = G_j \sum_{\beta\beta'} T_{\beta\beta'}, \quad \textbf{(6.17)}$$

Where, $T_{\beta\beta'}$ called the transition probability from the $|\beta\rangle$ state to $|\beta'\rangle$ state. The G_j is equal to the $2e^2/h$ which is known quantization constant. Considering at the end of the QWR a small bias is applied in between the contacts [44]. Also, assume the non-scattering condition with the unity transition probability. Therefore, the conductance for those systems is written as [45]:

$$G = \frac{2e^2}{h} \sum_{n,s} \sum_{l} \gamma_l^{n,s} f(E_m^{n,s}), \quad \textbf{(6.18)}$$

In above equation, *n* is the level states number, and *s* is the spin level, $E_m^{n,s}$ is the extremum's point energy, and $f(E_m^{n,s})$ is called Fermi-Dirac distribution function. $\gamma_l^{n,s}$ relays to +1 and -1 for the minimum and maximum points in the energy dispersion respectively.

6.4 RESULT AND DISCUSSION

In this paper, the numerical constant for calculation of the physical and transportation properties follows as the structural parameter $\tilde{\rho} = 1$, $\tilde{\beta} = 1.5$, $\tilde{\Delta}_R = 0.2$ and $\tilde{\Delta}_D = 0.3$ considering the strong constant Rashba and Dresselhaus coupling limit by which tunnelling of an electron in the quantum wire is possible.

In **Figure 6.2**, the energy dispersion plots for the variegated temperature i.e.; for *T* = 0 K, 400 K, 700 K and 900 K with B = 1T, E = 0.6× 10^6V/m, α = 25nm meV, and P = 4kbar. For a better understanding, Here and all consequent energy dispersion is plotted with a different colour in which each energy level contains two sub-bands via two-fold degeneracy: one is presented by the solid line and another one is presented by the dashed line. All solid lines show the quasi spin-down and the dashed line show the quasi spin-up state. **Figure 6.2 (a)**, shows the energy dispersion in the absence of temperature (T = 0 K), the dispersion curve not

intertwined with all the branches at the k_y = 0 consequently the existence of the electric field, magnetic field, Rashba and Dresselhaus SOIs. Furthermore, the anti-crossing between the sub-bands is a consequence of the off-diagonal term present in the SOI energy contribution term. And the gap between the two sub-bands is non-uniform by the result of symmetric broken when we applied the magnetic field and SOIs field at the one-time [46]. So that the contribution of magnetic field and SOIs induces the notable separation among the quasi spin-down and spin-up sub-bands. The separation is called the spin-orbit gap. Moreover, the temperature enhances from T = 0 K to 400 K, cause downward (~0.1 $\hbar\omega_j$) and lateral shifting (~0.12) along the positive value of $k_y l_o$ in the energy dispersion as seen in **Figure 6.2 (b)**. Further enhancement in the temperature (T = 400 K to 900 K) as represented in **Figure 6.2 (b-d)**, give rise to more downward and laterally shifting due to the dependence of the mass on the temperature. We perceive from **Figure 6.2 (a-d)** that energy dispersion shifts as the temperature increase. The cause of these variations is the dependence of the effective mass of the electron on the temperature, given in eq. (6.3). It is assistance citing that by enhancing the temperature, the wave function associated with the electron becomes more scattered.

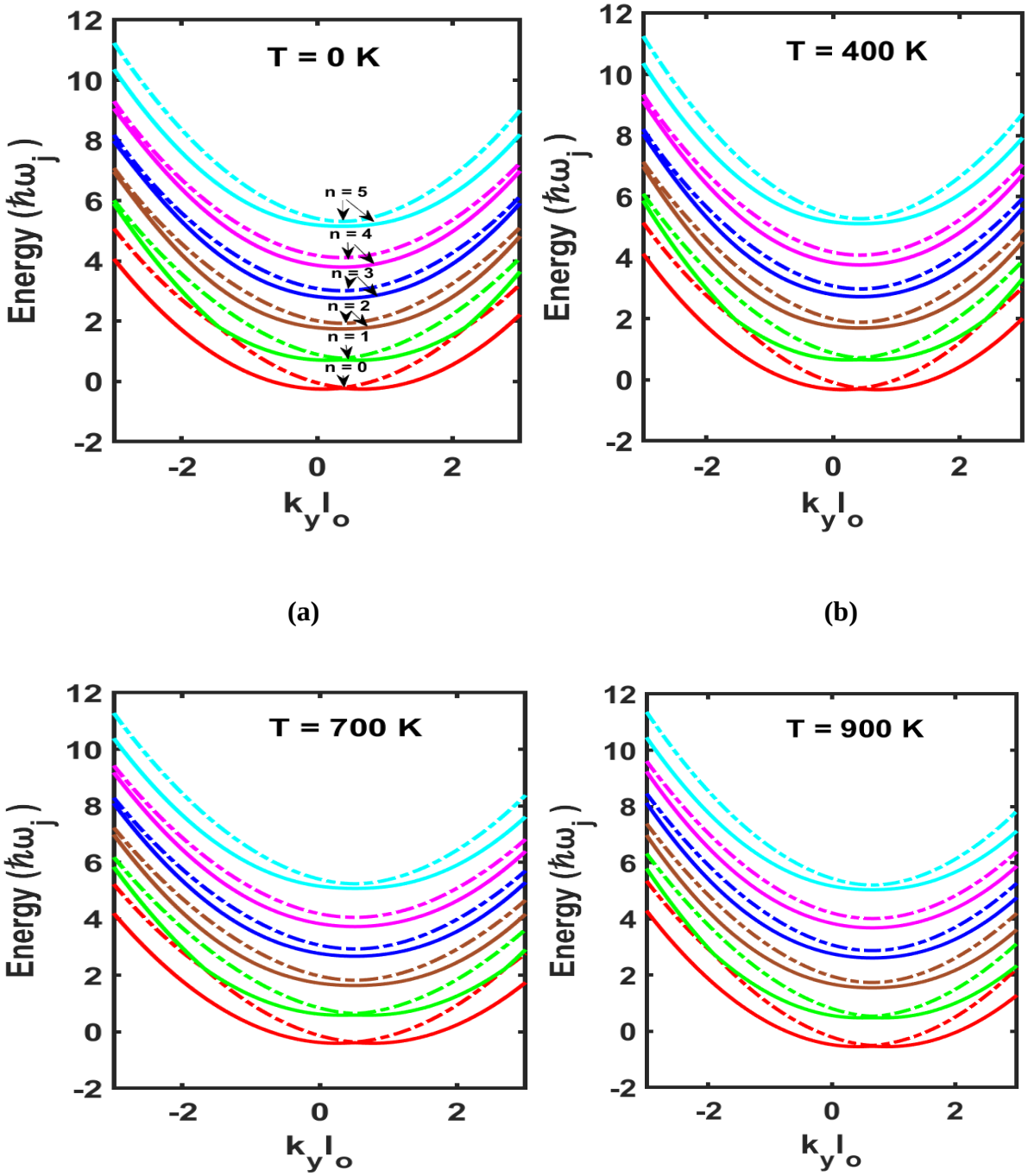

Figure 6.2 Energy dispersion curve at the (a) T = 0 K, (b) T = 400K, (c) T = 700K, and (d) T = 900 K with P = 4 kbar.

Scrutiny of the $In_xGa_{1-x}As$ QWR with the external perturbation is influential for the administration of the physical and transport properties. And is fruitful to inspect the influence of the temperature and pressure on the dispersion curves. Therefore, in **Figure 6.3 (a-d)** we concentrate on the effect of pressure on energy dispersion with T = 300 K. When the pressure is enhanced from P = 0 to 70 kbar the energy dispersion shows two types of shifting first one is upward shifting (~0.12 $\hbar\omega_j$) and the other one is laterally shifting (~0.11) along the negative value of $k_y l_o$. The shifting in the energy dispersion with an increase in pressure determines the effective geometry of the QWR. The total shifting in the dispersion depends on the pressure values. Shifting is large when we provide high pressure in the system. Whereas, the interplay between the external fields and SOIs regulates the advent of camel-back shapes, anti-crossing and crossing formations.

To show the influence of impurity on energy dispersion, we begin the study of the energy dispersion in the absence of impurities after that we introduce and enhance the impurity in the system at P = 4 kbar and T = 300 K. It is shown from **Figure 6.4 (a-d)** that when the impurity is introduced the dispersion starts to shift upward and the negative value of $k_y l_o$. The separation between the sub-bands is used to determine the chemical potential value required for the conductance. And the anti-crossing in the dispersion generates a dip in the conductance curve. Therefore, the variation in the energy dispersion as a result of impurity produces the variation in the conductance also.

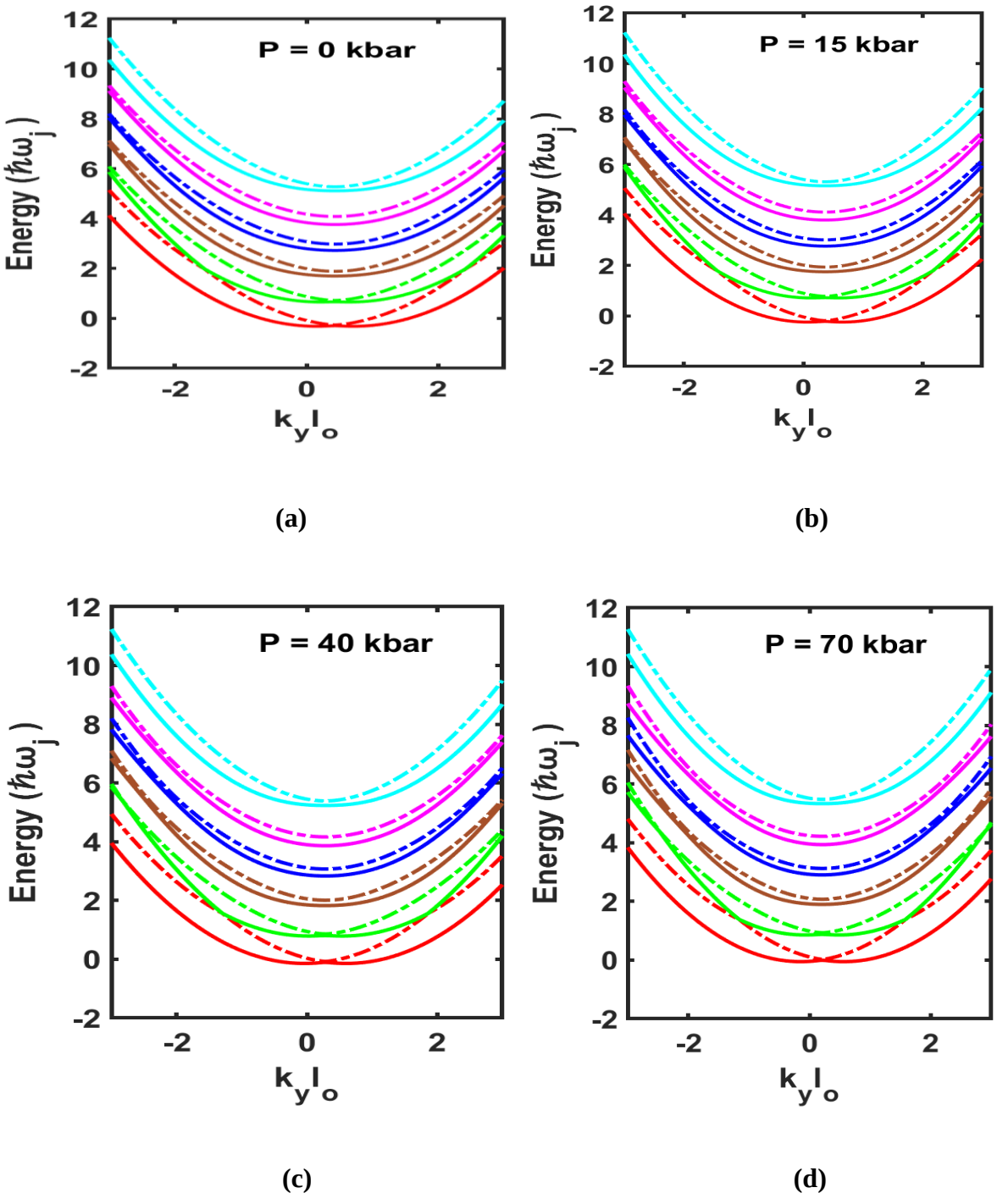

Figure 6.3 Energy dispersion curve at the (a) P = 0 kbar, (b) P = 15 kbar, (c) P = 40 kbar, and (d) P = 70 kbar with T = 300 K.

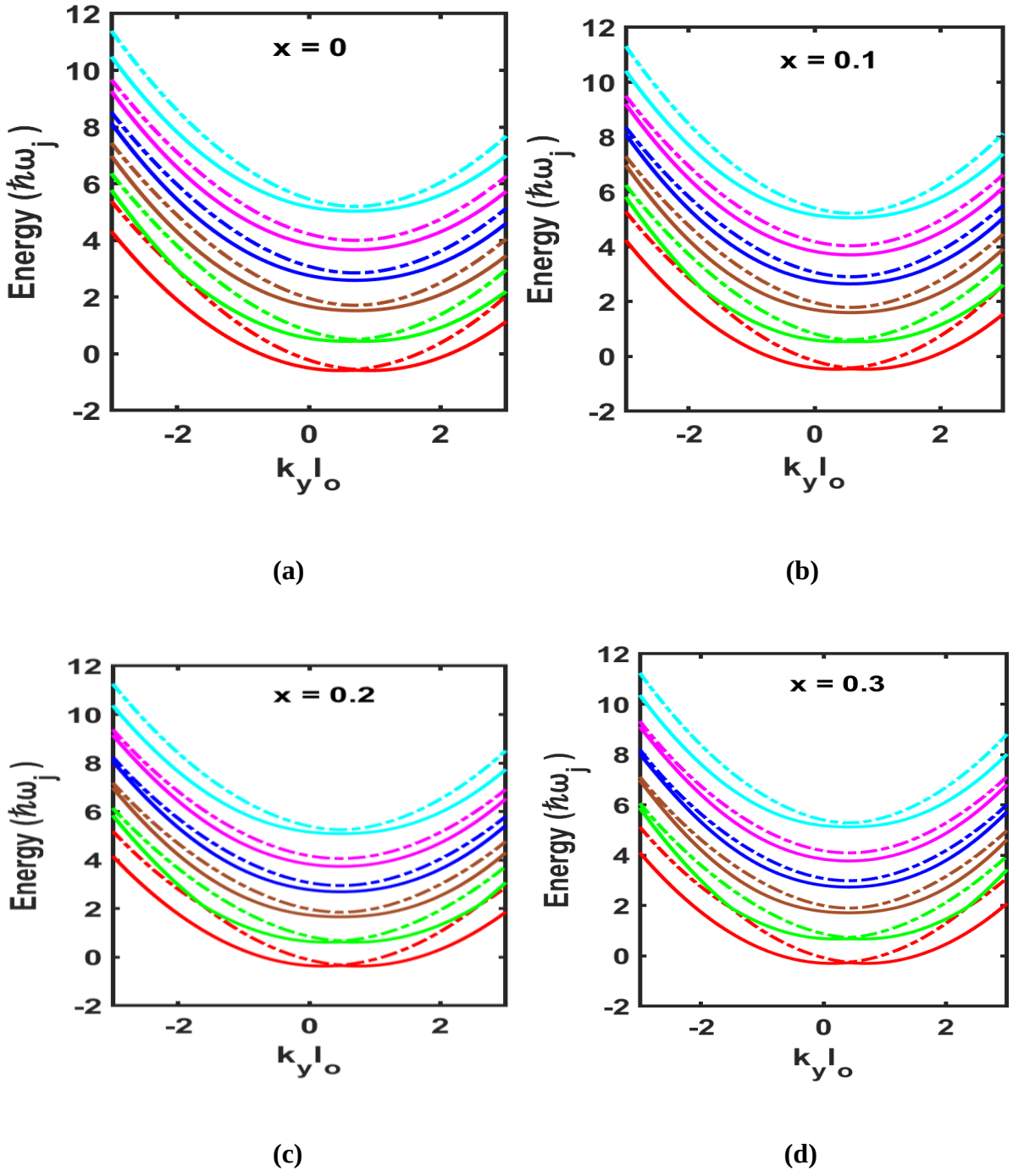

Figure 6.4 Energy dispersion curve at the (a) x = 0, (b) x = 0.1, (c) x = 0.2, and (d) x = 0.3 with P = 4 kbar and T = 300 K.

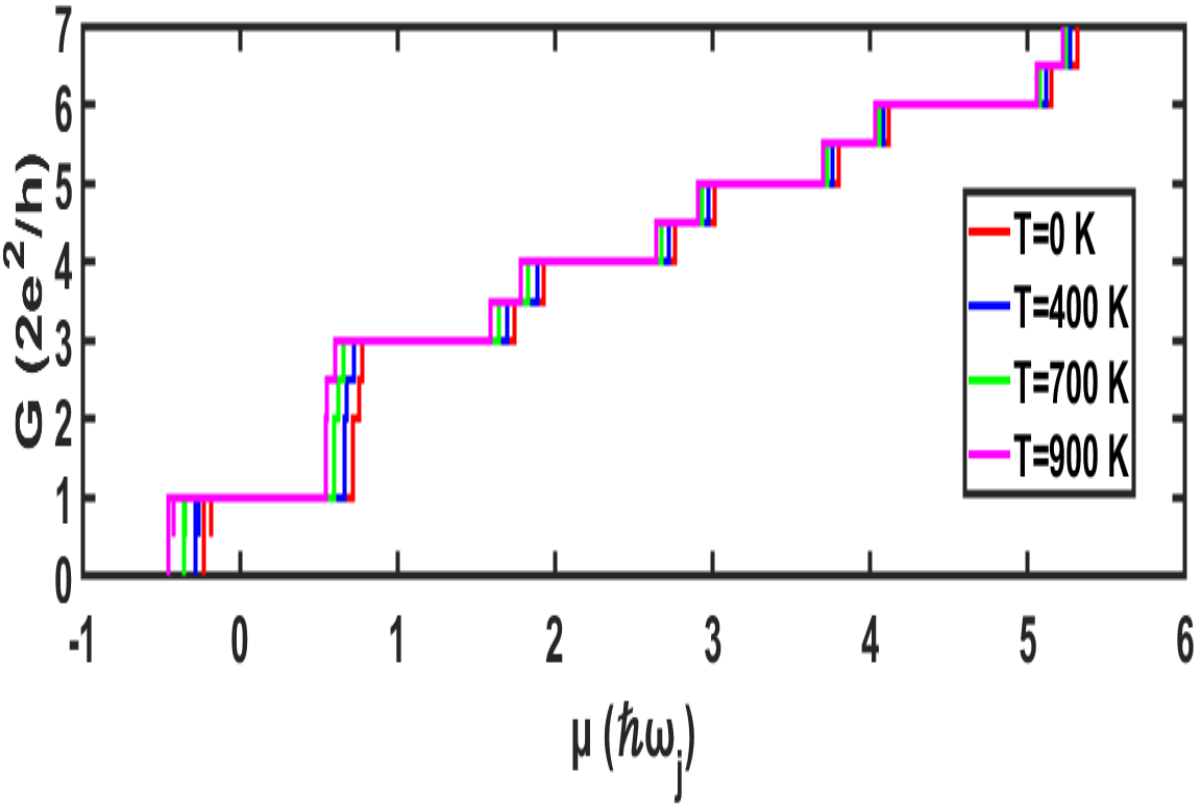
G (2e²/h)
μ (ħω_j)
T=0 K
T=400 K
T=700 K
T=900 K

(a)

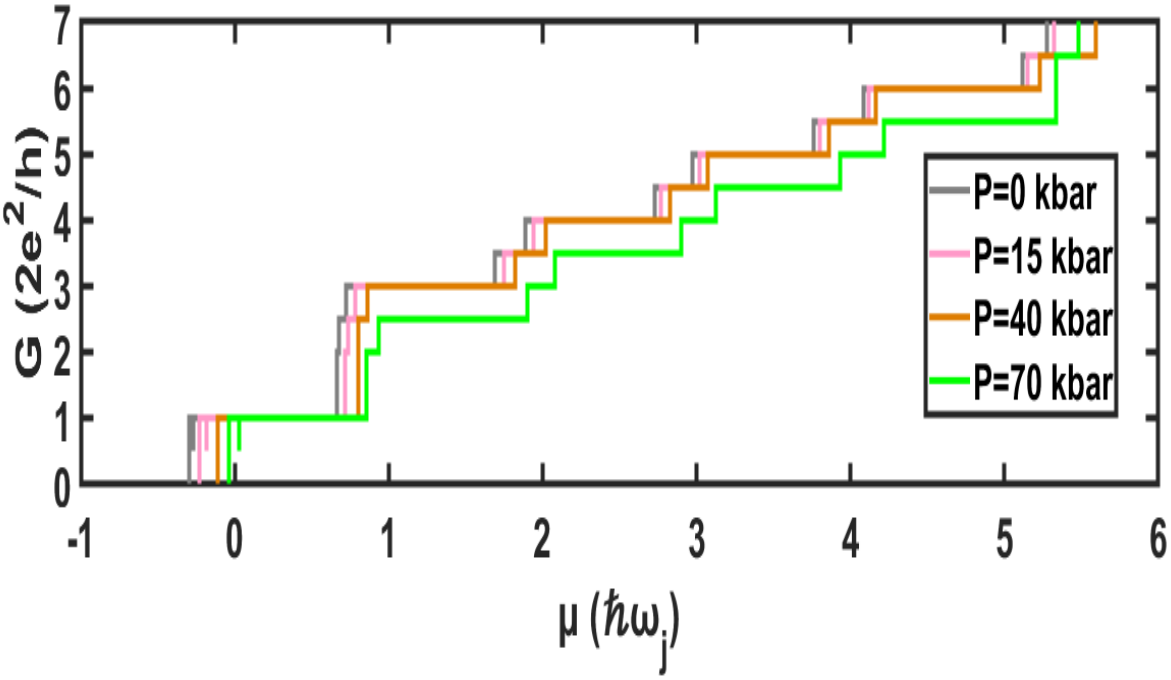
G (2e²/h)
μ (ħω_j)
P=0 kbar
P=15 kbar
P=40 kbar
P=70 kbar

(b)

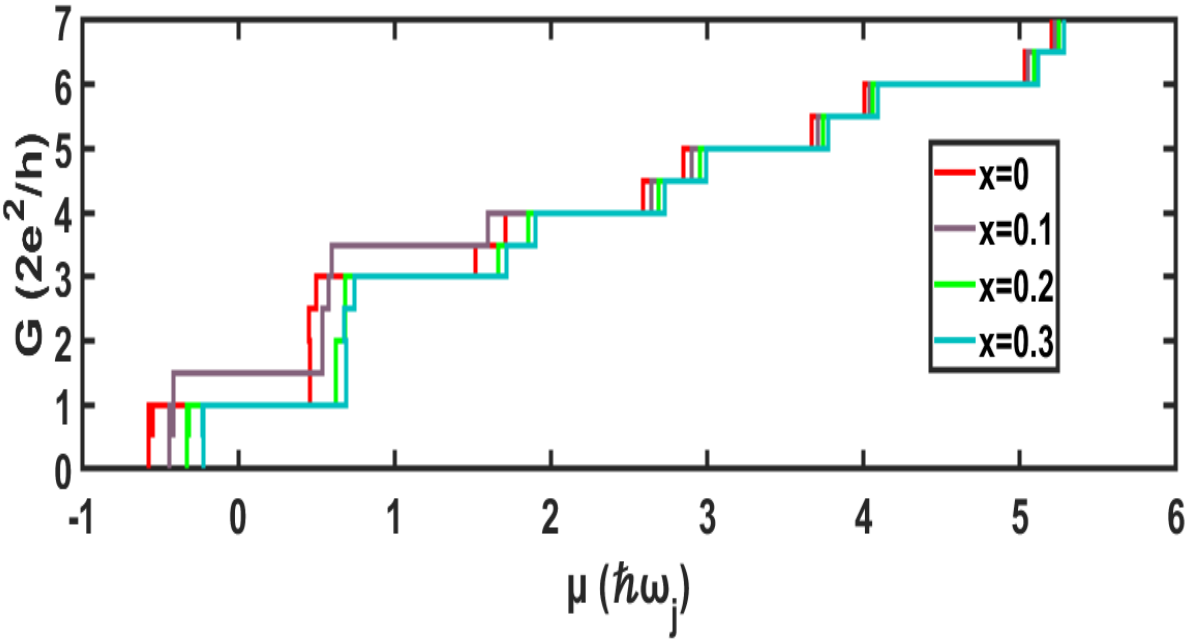

(c)

Figure 6.5 (a-c) Ballistic Conductance (G) as a function of chemical potential (μ) for the energy dispersions plot shown in Figs 6.2 (a-c), Figs. 6.3 (a-c), and Figs. 6.4 (a-c) respectively.

In **Figure 6.5 (a-c)**, we represent the consequence of temperature, hydrostatic pressure, and impurity factor on the ballistic conductivity of the $In_xGa_{1-x}As$ double QWR. Following the Landuer-Bütter formalism, the ballistic conductivity of a 1D nanostructure is linked with the two electrons reservoir at the microscopic level where we must neglect the electron-electron repulsion. Furthermore, the extreme points (maximum/minimum points) present in the energy spectrum cause the staircase structure (decrement/increment) in the conductance with the step size of $2e^2/h$. The increment in the energy spectrum opens more propagating channels due to which ballistic conductance has a staircase shape. From the **Figure 6.2 (a-d)**, **6.3 (a-d)** and **6.4**

(a-d), each extremum points in the energy dispersion create the decrement and increment of an integer $2e^2/h$ in the ballistic conductance [47]. Whenever the energy sub-bands split the conductance's chemical potential starts to grow. The foremost contribution in the conductivity arises from the lowest minimum point in these energy dispersion curves whereas, the second contribution arises due to the 2^{nd} minimum point of the same sub-band. At each time when chemical potential passes through the local maximum points, the conductivity of the system decreases by the integer factor $2e^2/h$. The staircase structure is generated in **Figure 6.5 (a-c)** by using these mechanics. Therefore, when we provide the temperature: 0 K, 400 K, 700 K, and 900 K, the ballistic conductance is represented by the stepwise increment shown in Fig. 6.5 (a). The temperature rise requires a low chemical potential for conductivity. Whereas, when we increase the pressure (P = 0 kbar to 70 kbar) and impurity (x = 0 to 0.3) higher value of chemical potential is required represented by **Figure 6.5 (b, c)**.

In **Figure 6.6 (a-b)**, the energy dispersion versus electric field plot is shown for x = 0 and 0.3. This is noticeable that the positive and negative values of the electric field give escalation to a uniform structure. Moreover, the splitting between the sub-bands bloat and whole the spin branches basin in the direction of the small energy states. Whenever we introduce impurity the energy plot with an electric field starts to shift in the downward direction. Subsequently, **Figure 6.7 (a and b)**, represents the spectra of energy sub-bands with the magnetic field for the x = 0 and x = 0.3. It is observed that all the branches of the energy spectrum increase with the increment in the intense magnetic field. And when the impurity is introduced, the whole spectrum shifts towards high energy. Therefore, the confinement potential enhances with the separation between the sub-bands while lifting degeneracy in every sub-bands. Simultaneous, contribution of magnetic field and impurity familiarize the remarkable separation in spin-up and spin-down of the energy levels. **Figure 6.8 (a and b)**, represents the energy necessity on

the applied temperature for the x = 0 and 0.3. It is easily espied that the energy for the lower energy state (n = 0 and 1) starts decreasing with the rise in the temperature.

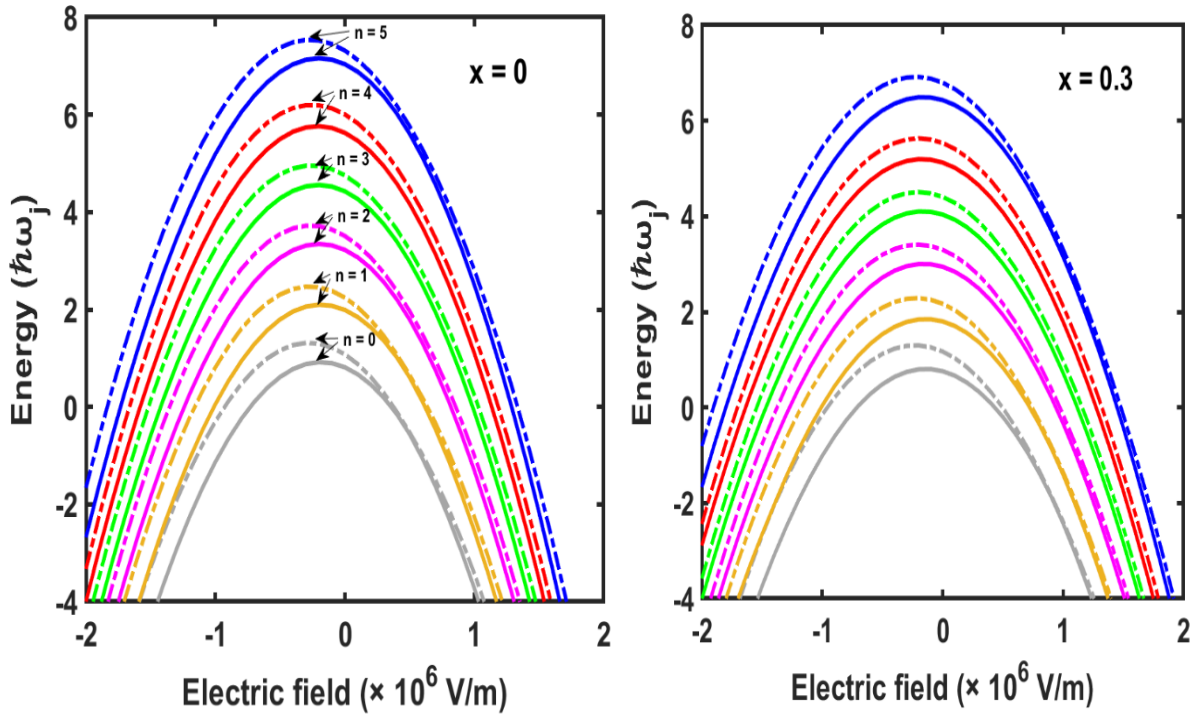

(a) **(b)**

Figure 6.6 Energy dependency on the Electric field at (a) x = 0 and (b) x = 0.3.

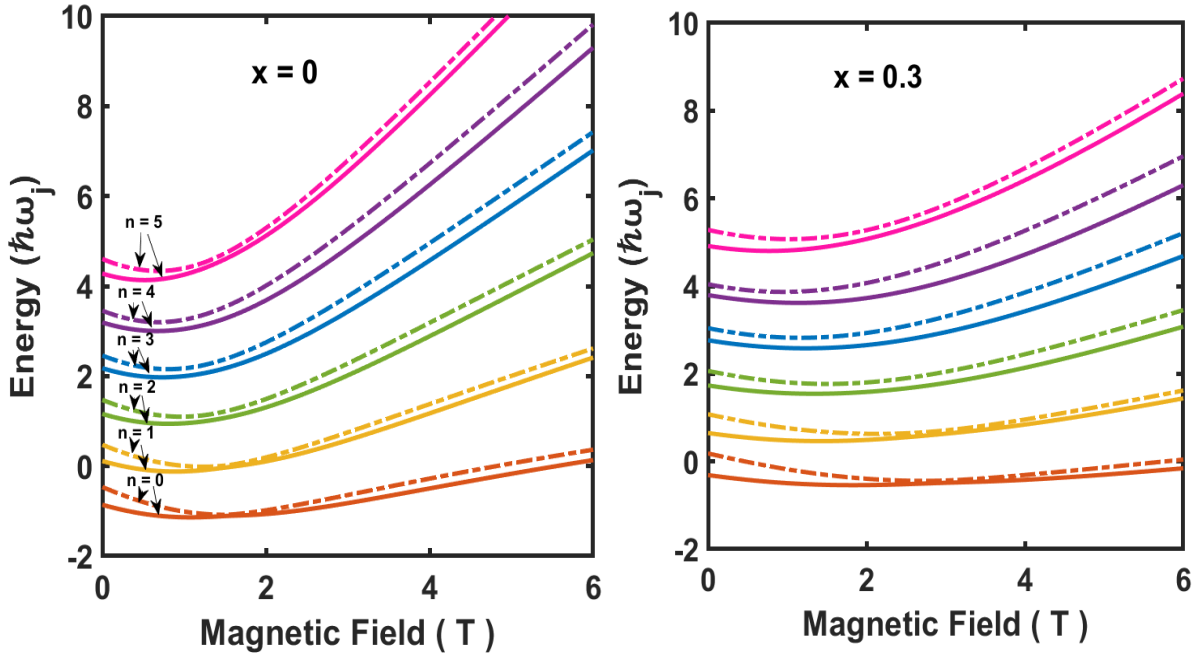

(a) **(b)**

Figure 6.7 Energy dependence on the Magnetic field at (a) x = 0 and (b) x = 0.3.

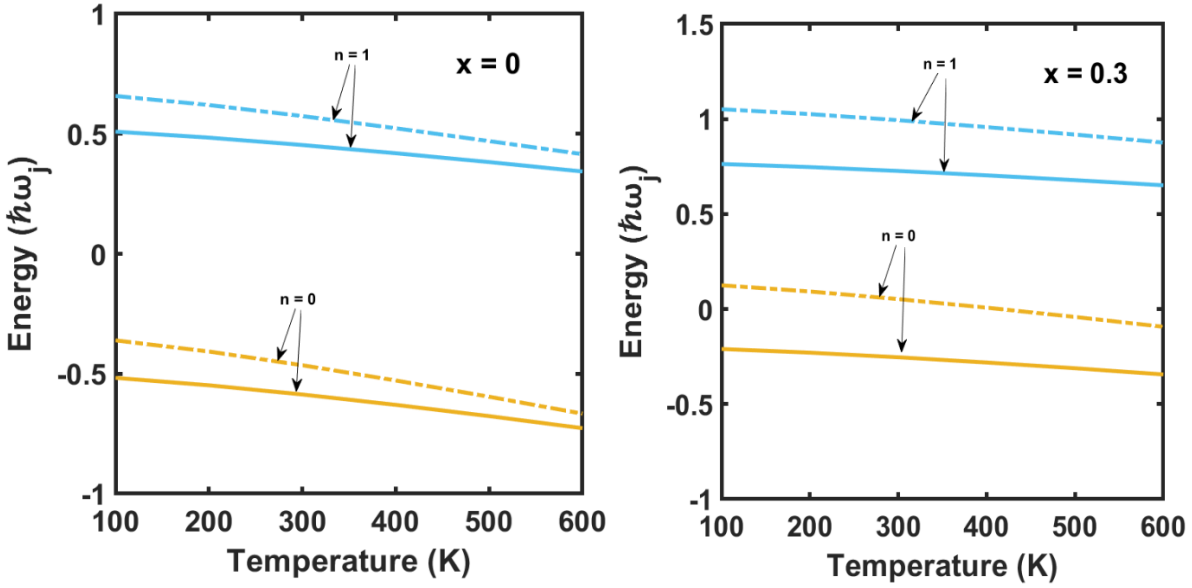

(a) **(b)**

Figure 6.8 Energy dependency on the temperature at (a) x = 0 and (b) x = 0.3.

6.5 SUMMARY

In this research, we focused on the energy spectrum and ballistic conductivity for the $In_xGa_{1-x}As$ QWR. The effect of temperature, hydrostatic pressure and SOIs fields along with the impurity on the energy spectrum and ballistic conductance have been examined. The results of our arithmetical scheming bear that: the variation in the temperature shifts the energy dispersion in the downward direction and the ballistic conductance steps along with the axis of chemical potential start shifting towards a lower value of chemical potential as a consequence of the reduction in energy with the rise in temperature easily noticeable. The effect of the variation in the pressure causes the upward shifting in the energy dispersion as a result conductivity of the QWR starts changing. Furthermore, the change in the impurity factor causes the variation in the energy dispersion and in the ballistic conductance of the $In_xGa_{1-x}As$ QWR. Whereas, the conductivity of the QWR is influenced by the strength of the externally applied field, confinement potential shape, SOIs and impurity concentration. The extremum points (maximum and minimum) in the energy dispersion create the changes (rise and deduction) in the steps of conductivity by the factor of $2e^2/h$. Moreover, the growth in the ballistic conductance has mainly in the form of a stepwise profile along with the integer conductivity, omitting the existence of abnormal formalism viz. camelback-like structure, sub-bands anti-crossing generates numerous extreme points in the energy spectrum as a consequence of this the small dips, troughs or crests are created in the steps of ballistic conductance. The outcomes of these expedite significant results and are used for adjusting the characterisation of nanostructures, optical, physical, and transport properties of the QWR system. It is also useful for the manufacturing of nanoscale electronic devices, spin filters and future molecules. For a better understanding of the transport mechanism at microscopic level, we must securitize the

Eigen channels of conductivity which is demonstrated by other studies in a meantime. Therefore, the study of transport properties of nanostructures has attracted vast activity due to high potentiality for the design of optoelectronic devices applications, spin filter and far infrared laser amplifiers, high- speed electrooptical modulators and photodetectors.

6.6 REFERENCES

[1] T. Sugaya, K.-Y. Jang, C.-K. Hahn, M. Ogura, K. Komori, A. Shinoda, K. Yonei, Enhanced peak-to-valley current ratio in InGaAs⁄InAlAs trench-type quantum-wire negative differential resistance field-effect transistors, J Appl Phys 97 (2005).

[2] M.G. Barseghyan, M.E. Mora-Ramos, C.A. Duque, Hydrostatic pressure, impurity position and electric and magnetic field effects on the binding energy and photo-ionization cross section of a hydrogenic donor impurity in an InAs Pöschl-Teller quantum ring, Eur Phys J B 84 (2011) 265–271.

[3] S. Banerjee, A. Dan, D. Chakravorty, Review synthesis of conducting nanowires, J Mater Sci 37 (2002) 4261–4271.

[4] K.I. Kolokolov, S.D. Beneslavski, N.Ya. Minina, A.M. Savin, Far-infrared intersubband absorption in p-type GaAs/AlxGa1− xAs single heterojunctions under uniaxial compression, Phys Rev B 63 (2001) 195308.

[5] Sitnitsky, A. E. "Exact solution of Schr\" odinger equation with symmetric double-well potential versus WKB: accuracy for ground state splitting." arXiv preprint arXiv:1801.03733 (2018).

[6] K.S.U. Kansanen, Theory for polaritonic quantum tunneling, Phys Rev B 107 (2023) 035405.

[7] S.C. Arapan, S. V. Korepov, M.A. Liberman, B. Johansson, Conductance of a disordered double quantum wire in a magnetic field: Boundary roughness scattering, Phys Rev B 67 (2003) 115328..

[8] Y. Karaaslan, B. Gisi, S. Sakiroglu, E. Kasapoglu, H. Sari, I. Sokmen, Electric and magnetic field modulated energy dispersion, conductivity and optical response in double quantum wire with spin-orbit interactions, Phys Lett A 382 (2018) 507–515.

[9] G. Thorgilsson, C.-S. Tang, V. Gudmundsson, Time-dependent magnetotransport of a wave packet in a quantum wire with embedded quantum dots, Phys Rev B 76 (2007) 195314.

[10] J.-R. Shi, B.-Y. Gu, Magnetoconductance oscillations of two parallel quantum wires coupledthrough a potential barrier, Phys Rev B 55 (1997) 9941.

[11] N.R. Abdullah, C.-S. Tang, V. Gudmundsson, Time-dependent magnetotransport in an interacting double quantum wire with window coupling, Phys Rev B 82 (2010) 195325.

[12] G.R. Aizin, N.J.M. Horing, L.G. Mourokh, V.M. Kovalev, Current driven electromagnetic wave amplification by double quantum wire superlattice, J Appl Phys 96 (2004) 4225–4232.

[13] N.R. Abdullah, C.-S. Tang, V. Gudmundsson, Time-dependent magnetotransport in an interacting double quantum wire with window coupling, Phys Rev B 82 (2010) 195325.

[14] B. Brun, F. Martins, S. Faniel, B. Hackens, G. Bachelier, A. Cavanna, C. Ulysse, A. Ouerghi, U. Gennser, D. Mailly, S. Huant, V. Bayot, M. Sanquer, H. Sellier, Wigner and Kondo physics in quantum point contacts revealed by scanning gate microscopy, Nat Commun 5 (2014) 4290.

[15] S. Bandyopadhyay, W. Porod, Double quantum wire Aharonov-Bohm interferometers for possible LN2 temperature operation, Superlattices Microstruct 5 (1989) 239–245.

[16] S. V Korepov, M.A. Liberman, Tunnel-coupled double quantum wires in a magnetic field: electron scattering on impurities and boundary roughness, Physica B Condens Matter 322 (2002) 92–109.

[17] L.W. Smith, W.K. Hew, K.J. Thomas, M. Pepper, I. Farrer, D. Anderson, G.A.C. Jones, D.A. Ritchie, Row coupling in an interacting quasi-one-dimensional quantum wire investigated using transport measurements, Phys Rev B 80 (2009) 041306.

[18] C.-S. Tang, V. Gudmundsson, Coherent magnetotransport spectroscopy in an edge-blocked double quantum wire with window and resonator coupling, Phys Rev B 74 (2006) 195323.

[19] X.F. Wang, P. Vasilopoulos, Magnetotransport in a two-dimensional electron gas in the presence of spin-orbit interaction, Phys Rev B 67 (2003) 085313.

[20] A. Łusakowski, J. Wróbel, T. Dietl, Effect of bulk inversion asymmetry on the Datta-Das transistor, Phys Rev B 68 (2003) 081201.

[21] A. Manchon, H.C. Koo, J. Nitta, S.M. Frolov, R.A. Duine, New perspectives for Rashba spin–orbit coupling, Nat Mater 14 (2015) 871–882.

[22] D. V. Bulaev, D. Loss, Spin relaxation and anticrossing in quantum dots: Rashba versus Dresselhaus spin-orbit coupling, Phys Rev B 71 (2005) 205324.

[23] M.K. Jana, R. Song, H. Liu, D.R. Khanal, S.M. Janke, R. Zhao, C. Liu, Z. Valy Vardeny, V. Blum, D.B. Mitzi, Organic-to-inorganic structural chirality transfer in a 2D hybrid perovskite and impact on Rashba-Dresselhaus spin-orbit coupling, Nat Commun 11 (2020) 4699.

[24] R. Khordad, Optical properties of quantum wires: Rashba effect and external magnetic field, J Lumin 134 (2013) 201–207.

[25] V. Galitski, I.B. Spielman, Spin–orbit coupling in quantum gases, Nature 494 (2013) 49–54.

[26] S. Pramanik, S. Bandyopadhyay, M. Cahay, Energy dispersion relations of spin-split subbands in a quantum wire and electrostatic modulation of carrier spin polarization, Phys Rev B 76 (2007) 155325.

[27] Yu. V. Pershin, S.N. Shevchenko, I.D. Vagner, P. Wyder, Electronic transport through a nuclear-spin-polarization-induced quantum wire, Phys Rev B 66 (2002) 035303.

[28] Y. V. Pershin, J.A. Nesteroff, V. Privman, Effect of spin-orbit interaction and in-plane magnetic field on the conductance of a quasi-one-dimensional system, Phys Rev B 69 (2004) 121306.

[29] Y. v. Pershin, J.A. Nesteroff, V. Privman, Effect of spin-orbit interaction and in-plane magnetic field on the conductance of a quasi-one-dimensional system, Phys Rev B Condens Matter Mater Phys 69 (2004).

[30] C.H.L. Quay, T.L. Hughes, J.A. Sulpizio, L.N. Pfeiffer, K.W. Baldwin, K.W. West, D. Goldhaber-Gordon, R. de Picciotto, Observation of a one-dimensional spin–orbit gap in a quantum wire, Nat Phys 6 (2010) 336–339.

[31] J.A. Nesteroff, Y. V. Pershin, V. Privman, Polarization of Nuclear Spins from the Conductance of Quantum Wire, Phys Rev Lett 93 (2004) 126601.

[32] Y. V. Pershin, J.A. Nesteroff, V. Privman, Effect of spin-orbit interaction and in-plane magnetic field on the conductance of a quasi-one-dimensional system, Phys Rev B 69 (2004) 121306.

[33] P. Dahan, I.D. Vagner, Nuclear spin relaxation rate of magnetic impurities in quantum Hall effect systems, Phys Rev B 72 (2005) 115328.

[34] F. Segovia-Chaves, H. Vinck-Posada, The effect of the hydrostatic pressure and temperature on the defect mode in the band structure of one-dimensional photonic crystal, Optik (Stuttg) 156 (2018) 981–987.

[35] L. Bouzaïene, R. Ben Mahrsia, M. Baira, L. Sfaxi, H. Maaref, Hydrostatic pressure and temperature effects on nonlinear optical rectification in a lens shape InAs/GaAs quantum dot, J Lumin 135 (2013) 271–275.

[36] W. Xie, Impurity effects on optical property of a spherical quantum dot in the presence of an electric field, Physica B Condens Matter 405 (2010) 3436–3440.

[37] E. Sadeghi, Electric field and impurity effects on optical property of a three-dimensional quantum dot: A combinational potential scheme, Superlattices Microstruct 50 (2011) 331–339.

[38] Al, E. B., et al. "Effects of applied electric and magnetic fields on the nonlinear optical properties of asymmetric GaAs/Ga1-xAlxAs double inverse parabolic quantum well." Optical Materials 47 (2015): 1-6.

[39] P. Başer, I. Altuntas, S. Elagoz, The hydrostatic pressure and temperature effects on hydrogenic impurity binding energies in GaAs/InxGa1-xAs/GaAs square quantum well, Superlattices Microstruct 92 (2016) 210–216.

[40] E. Gildener, A. Patrascioiu, Pseudoparticle contributions to the energy spectrum of a one-dimensional system, Physical Review D 16 (1977) 423.

[41] S. Paul, J.B. Roy, P.K. Basu, Empirical expressions for the alloy composition and temperature dependence of the band gap and intrinsic carrier density in Ga *x* In1− *x* As, J Appl Phys 69 (1991) 827–829.

[42] S. Paul, J.B. Roy, P.K. Basu, Empirical expressions for the alloy composition and temperature dependence of the band gap and intrinsic carrier density in GaxIn 1-xAs, J Appl Phys 69 (1991) 827–829.

[43] Imry, Yoseph, and Rolf Landauer. "Conductance viewed as transmission." Reviews of Modern Physics 71.2 (1999) S306..

[44] G. Möller, R. Moessner, Magnetic multipole analysis of kagome and artificial spin-ice dipolar arrays, Phys Rev B Condens Matter Mater Phys 80 (2009).

[45] I.A. Kokurin, Determination of Rashba-coupling strength for surface two-dimensional electron gas in InAs nanowires, Solid State Commun 195 (2014) 49–54.

[46] Priyanka, R. Sharma, M. Kumar, Effect of hydrostatic pressure and temperature on the ballistic conductance under the influence of Rashba spin-orbit coupling, Physica B Condens Matter 648 (2023).

[47] B.H. Mehdiyev, A.M. Babayev, S. Cakmak, E. Artunc, Rashba spin-orbit coupling effect on a diluted magnetic semiconductor cylinder surface and ballistic transport, Superlattices Microstruct 46 (2009) 593–602.

7

CHAPTER

Conclusion, Future Scope of Work and Social Impact

- *This chapter conclude the research conducted in this thesis.*
- *Additionally, it briefly discusses the key conclusions drawn from the results.*
- *Finally, the chapter highlights the potential future directions for research and the societal impact that could be explored to build on this study.*

7.1 Conclusion

Nowadays, quantum nanostructures, such as quantum wells, quantum wires, and quantum dots, have emerged as a new class of nonlinear materials for studying multi-photon phenomenon as well as nonlinear optical properties, and possess some unique potential applications in optoelectronic devices including optical switches, THz multi-photon quantum well infrared photodetectors, multi-photon bioimaging, and frequency up conversion, among others. Moreover, there has been a shift in semiconductor physics towards exploring effect of external factors such as hydrostatic pressure, temperature, electric field, magnetic field as well as spin-dependent phenomena as they offer vast potential applications in spin transistors, spin filters, and quantum computing. The study of spin-related effects in semiconductor nanostructures typically involves considering spin-orbit interaction. Understanding effect of such external factors is crucial for investigating its impact on nonlinear optical processes in quantum nanostructures. This thesis focuses on studying the physical, transport and linear and non-linear optical properties of quantum nanostructures in the presence of external factors such as Rashba impurity factor, hydrostatic pressure, temperature, electric and magnetic fields, as well as considering the Rashba spin-orbit interaction.

Chapter 1 starts with an overview of nanostructures, spin–orbit interaction is treated as the key component that could affect linear & non-linear properties and transport properties due to external perturbations. The first part outlines the most common quantum dot and quantum wire nanostructures touching on crucial features of these structures as well their unique properties. The chapter also gives a short account of the materials employed and special features characterizing them. They are the Rashba spin-orbit interaction and external perturbations as electric field, magnetic field, hydrostatic pressure and temperature. The chapter then provides information on the particular classes of low-dimensional semiconductor structures which

include quantum dots as well as two dimensional and one-dimensional systems. All of the structures are introduced, explained as to what they have unique and then detailed how this structure works. Also, the introduction in Chapter 1 has definitions and explanations of different light-behavior, nonlinear properties and ballistic conductance. Optical properties describe the interaction between light and matter, e.g., absorption reflection or transmission. In contrast, in the case of nonlinear optical properties we consider how materials behave when irradiated with intense light i.e. between input and output light is non-linear relationship. Transport properties show how an electron can travel in nanostructure system.

Chapter 1 is a fundamental introduction of various concepts, structures and properties concerning low-dimensional semiconductors as well as their optical and transport behavior with which one could get oriented to the later topics raised by each chapter together.

Chapter 2 examines the transport properties of a $Ga_{1-x}Al_xAs$ quantum wire in the presence of impurities. This analysis explores the combined effects of Rashba spin-orbit interaction, an external electric field, a magnetic field, and varying concentrations of aluminum on the energy dispersion and conductivity of the wire. The energy eigenvalues and eigenvectors are determined using the diagonalization method, while transport properties are calculated through the Landauer-Büttiker formalism. The results reveal that external fields, Rashba spin-orbit interaction, and aluminium concentration (impurity factor x) significantly influence the energy spectra and conductivity.

Chapter 3 discusses the effects of hydrostatic pressure and temperature on the energy band structure and ballistic conductivity. The energy eigenvalues and eigenvectors are obtained through the diagonalization method, while ballistic conductance is calculated using the Landauer-Büttiker formalism. Additionally, the chapter examines how energy behaves in response to external electric and magnetic fields, as well as temperature variations. The system

is modeled using parabolic confinement under a strong magnetic field, and the Rashba spin-orbit interaction (RSOI) creates a combined effect of internal and external factors, resulting in upward/downward and lateral/vertical shifts in the energy dispersion. The peculiarities in the energy subbands lead to oscillatory patterns in ballistic conductance.

Chapter 4 examines the impact of the impurity factor on optical properties such as absorption coefficients, refractive index changes, second-harmonic generation, and third-harmonic generation during intersubband transitions between electronic states in a $Ga_{1-x}Al_xAs$ quantum wire, driven by a symmetric parabolic potential. The system is influenced by an intense electric field, magnetic field, and Rashba spin-orbit interaction. Analytical expressions for the linear and non-linear optical absorption coefficients, refractive index changes, second-harmonic generation, and third-harmonic generation are derived using the compact density-matrix approach. The numerical results reveal that the optical properties are highly sensitive to impurity concentration and can be modulated by this parameter. Variations in the magnitude and position of the peaks with changes in the impurity factor highlight opportunities for controlling optical non-linearity in the quantum wire, offering potential for device applications.

Chapter 5 focuses on the optical properties of $In_{1-x}Ga_xAs$ quantum dot. The energy levels and wavefunctions are first determined in the presence of impurities. The chapter then examines the effects of impurity on absorption coefficients, refractive index changes, and third-harmonic generation. The results indicate that as impurity concentration increases, the absorption coefficients, refractive index changes, and third-harmonic generation peaks shift from their original positions and decrease in magnitude. This highlights the significant role impurity concentration plays in influencing the optical properties of the nanostructure.

In **Chapter 6**, the effects of temperature, hydrostatic pressure, and impurity on the energy spectrum and ballistic conductivity of the $In_{1-x}Ga_xAs$ double quantum wire are discussed. The system is modeled with a double-well anharmonic confinement potential in the presence of an intense magnetic field, electric field, and both Rashba and Dresselhaus spin-orbit interactions. Energy eigenvalues and ballistic conductance are computed using the diagonalization method and Landauer-Büttiker formalism, respectively. The chapter also explores how energy responds to applied electric and magnetic fields, as well as temperature variations. The numerical results show that temperature, hydrostatic pressure, and impurities lead to shifts in the energy dispersion. These irregularities in the energy spectrum result in oscillatory patterns in ballistic conductivity, with changes in energy affecting the conductance.

The main objective of this Ph.D. dissertation is to study the impacts of Rashba spin-orbit interaction and impurity on the transport and linear and nonlinear optical responses in quantum wire and quantum dot, through three potential environmental conditions, i.e., hydrostatic pressure and temperature effects. Besides, the Rashba spin-orbit interaction (SOI) impact factor and study of energy dispersion, ballistic conductance, second and third harmonic generation in quantum wire are also investigated. The study additionally includes the computation of changes in optical rectification coefficient and absorption processes at quantum wire and quantum dot under electric field, hydrostatic pressure, temperature, impurity etc. The knowledge of these topics is not only interesting from the fundamental point of view but it may have practical applications such as quantum dot lasers, systems for processing information using bandgap device, quantum properties (quantum computers) or devices utilising effects at the interplay between optics and spintronics. Moreover, this work will serve as a motivation for further experimental and theoretical studies in the field of transport and non-linear optical properties in nanosystems with spin-orbit interaction.

7.2 FUTURE SCOPE OF THE WORK

➢ Study of Effect of impurity with hydrostatic pressure, temperature and electric field on the optical properties of transition metal dichalcogenide (TMD) quantum nanostructure with spin-orbit interaction.

➢ Study of Effect of impurity with hydrostatic pressure, temperature and magnetic field on the optical properties of transition metal dichalcogenide (TMD) quantum nanostructure with spin-orbit interaction.

➢ Electric field, Hydrostatic pressure, Temperature & impurity effect on SHG and linear and non-linear optical properties of transition metal dichalcogenide (TMD) quantum nanostructure with spin-orbit interaction.

➢ Impurity, Electric field, Hydrostatic pressure & Temperature effect on THG in transition metal dichalcogenide (TMD) quantum nanostructure with spin-orbit interaction.

7.3 SOCIAL IMPACT

The research on quantum nanostructures, as presented in the thesis, holds the potential for substantial social impact across various technological fields. Below are key areas where the societal benefits of this work can be emphasized:

1. **Progress in Optoelectronics and Photonics**: The investigation of nonlinear optical properties and multi-photon phenomena in quantum nanostructures can facilitate the development of cutting-edge optoelectronic devices, such as high-performance optical switches and quantum well infrared photodetectors. These advancements are critical for increasing the speed, efficiency, and miniaturization of communication

technologies, potentially resulting in faster internet, improved data transmission, and enhancements in fiber-optic systems. These innovations could contribute to global connectivity, which in turn may drive economic growth and expand access to education and information, particularly in underserved areas.

2. **Impacts on Healthcare and Bioimaging**: The application of multi-photon bioimaging, as discussed in the research, offers transformative potential for medical diagnostics and imaging. These techniques enable highly detailed molecular-level imaging, which can aid in the early detection of diseases such as cancer. The heightened accuracy and sensitivity of these methods can lead to better diagnosis and treatment outcomes, ultimately reducing healthcare costs by promoting preventive care and more targeted therapies.
3. **Quantum Computing and Information Processing**: The exploration of external factors like electric and magnetic fields, combined with spin-orbit interactions in semiconductor nanostructures, is crucial for advancing quantum computing. Quantum dots and wires with customized spin characteristics can be used in spin-based transistors and filters, supporting the development of quantum computers. These computers have the potential to revolutionize industries such as cryptography, material science, and pharmaceutical research by addressing problems that are currently unsolvable by classical computers.
4. **Development of Energy-Efficient Technologies**: The research into the transport properties of quantum nanostructures, particularly in low-dimensional systems, could lead to the creation of energy-efficient electronic devices. This can result in reduced energy consumption in electronics like transistors and memory devices, which would have a significant impact on global energy demands. Such advancements are aligned with sustainability goals and could contribute to lowering carbon emissions.

5. **Educational and Research Contributions**: This study opens new avenues for both theoretical and experimental research in the fields of quantum physics, nanotechnology, and materials science. It has the potential to inspire future academic endeavors and drive innovation in the study of nanostructures, while also serving as a valuable educational resource for students and researchers. Over time, this could enhance scientific literacy and innovation, particularly in areas critical to the technological future.
6. **Spintronics and Future Electronics**: Spintronics, which leverages spin-related effects in quantum nanostructures, is a foundational component of next-generation electronics. These advancements could lead to faster, more reliable data storage devices that would benefit industries ranging from computing to entertainment. As spintronic devices are more energy-efficient than conventional electronics, their adoption could help reduce the ecological impact of technology, supporting broader sustainability efforts.

In summary, this research is positioned to drive technological innovation with far-reaching effects in healthcare, energy, computing, and communications. The potential to improve quality of life, foster sustainable technology, and enhance global connectivity underscores its broad social significance.

Physica B 629 (2022) 413649

Contents lists available at ScienceDirect

Physica B: Physics of Condensed Matter

journal homepage: www.elsevier.com/locate/physb

Effects of impurity factor on the physical and transport properties for $Ga_{1-x}Al_xAs$ quantum wire in the presence of Rashba spin-orbit interaction

Priyanka [a], Rinku Sharma [a,*], Manoj Kumar [b,**]

[a] Department of Applied Physics, Delhi Technological University, Delhi, 110042, India
[b] Department of Physics, Govt. College for Women, Jind, 126102, India

ARTICLE INFO

Keywords:
Quantum wire
Impurity factor
Rashba spin-orbit interaction (RSOI)
Energy spectrum
Ballistic conductance

ABSTRACT

There is a need to get familiarized with a systematic and precise approach to study the energy dispersion and ballistic conductance in a $Ga_{1-x}Al_xAs$ quantum wire. We have employed parabolic confinement in this work. The combined impacts of Rashba spin orbit interaction (RSOI), external electric field, magnetic field, and Aluminium concentration on energy dispersion and conductivity in a $Ga_{1-x}Al_xAs$ quantum wire have been explored. The Energy eigenvalues and eigenvectors are quantified using the diagonalization method and the transport properties are computed by Landuer-Bttiker formalism. It is noticed that the external electric field, magnetic field, Rashba spin-orbit interaction, and Aluminium concentration (impurity factor x) alter the energy spectra and conductivity. Hence, these parameters significantly affect the physical and transport properties.

1. Introduction

In recent times, the progress in Crystal growth techniques; like a metal-organic chemical-vapor deposition, create possibilities for fabricating profuse kinds of nanostructures viz. Quantum Dots (QDs), Quantum Wires (QWRs), and Quantum Well (QWs) [1,2]. A crucial role is played by the survey to check the dependency of physical properties for low-dimensional systems on external perturbation to develop tore investigation for QWRs [3–6]. Various studies have been found along with the exterior electric field, the magnetizing field also makes an impact on optical properties and transport properties in these systems [5,7,8].

Among these properties, transport properties play an important role. The explanation for transport properties is found by using a non-interacting electron model [9], in consonance with the Landuer-Büttiker formalism [10] in which the electrons get transferred from one reservoir to another when a small bias is applied across the channel. As they are confined in the channel transversely so they are distributed among different subbands according to Fermi-Dirac distribution. The number of modes of electron propagation completely specify the net conductance of a system and can be determined by the Fermi energy and energy spectrum. The experiments were accomplished independently by Yuriy et al. [11] and Quay et al. [9] that established a relation between energy dispersion and the conductance in a QWR. Using energy dispersion curves, they imposed that each subband contributes e^2/h to the ballistic conductance. We can predict transport properties with help of QWR due to peculiar properties shown in their band structures i.e., anticrossing and additional extrema of subband under the influence of external fields along with the spin-orbit interaction (SOI).

SOI influences the spintronic development considerably in low-dimensional semiconductor systems by utilizing electron spin for storing and hauling information. One of the most alluring spintronic devices is affirmed by Datta and Das [12] i.e., Spin polarised field-effect transistor (SFET) which may be rapidly switched, unlike conventional transistor. Two types of SOI are admissible for semiconductor Devices: Rashba spin-orbit interaction (RSOI) and Dresselhaus spin-orbit interaction (DSOI) [9–12]. The dearth of symmetry in bulk inversion brings the former into the spotlight while the latter makes an appearance from the unsymmetric behaviour of confining quantum well electric potential along its growing direction that creates a 2DEG on a narrow-gap semiconductor material surface. Since an external gate electrode [13–19] can tune RSOI. The impact of the RSOI on the ballistic conductance of the 2DEG and QWRs has been studied by Krstajic [20]. It is predictable, of researchers paying exceptional attention to spin-dependent transport [21–26]. Moreover, the sequel of the SOI and magnetic field influence transport characteristics of low-dimensional systems which restrain

* Corresponding author.
** Corresponding author.
E-mail addresses: rinkusharma@dtu.ac.in (R. Sharma), manojmalikdu@gmail.com (M. Kumar).

https://doi.org/10.1016/j.physb.2021.413649
Received 19 November 2021; Received in revised form 22 December 2021; Accepted 28 December 2021
Available online 3 January 2022
0921-4526/© 2022 Elsevier B.V. All rights reserved.

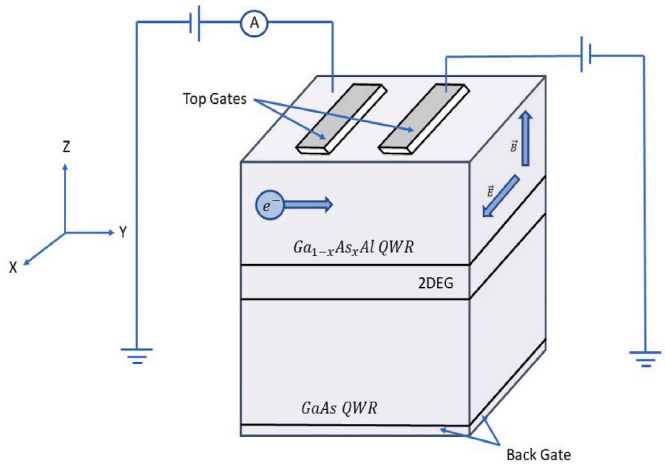

Fig. 1. Schematic view of the $Ga_{1-x}Al_xAs$ QWR within the presence of 2DEG, external electric and magnetic field.

movement of charge carriers in the 2DEG [27,28].

This has become quite essential to acknowledge the electronic as well as optical characteristics of impurities in the QWRs as physical, optical, and transport characteristics of low-dimensional devices are fabricated from such materials which are strongly affected due to the existence of the trivial impurities. In heterostructures, we can analyze the properties of impurities by using some constructive tools like intense laser field, electrostatic field, magnetic field, and hydrostatic pressure. Numerous studies have been carried out for discussion of QWRs hydrogenic-trivial impurities [29–33]. A minor impurity can enlarge the conductivity of a semiconductor by a few orders of magnitude. Addition of the impurities influences the electronic properties of bulk semiconductors which have been broadly recognized since the early stage of semiconductor science [34].

Since, the thermal, optical, and transport properties of semiconductor devices are firmly affected by impurities in QWRs. It has become crucial to examine the doped nanostructure. There is a flourishing interest in the research of transportation of electrons in recent times and electronics properties have been studied both theoretically [35–37] and experimentally [38,39]. To our apprehension, no evaluation of energy dispersion and transport properties of a $Ga_{1-x}Al_xAs$ QWRs under the hydrostatic pressure, temperature, electric field, and magnetic field have been done yet. The impetus behind this paper is to scrutinize the impacts of an external electrostatic field, magnetic field along with impurity factor on the physical and transport properties of $Ga_{1-x}Al_xAs$ QWRs using the diagonalization technique.

2. Theory

In Fig. 1, diagrammatic view of $Ga_{1-x}Al_xAs$ QWR is shown, for 1-D $Ga_{1-x}Al_xAs$ QWR harmonic potential is given by:

$$V(X) = \frac{1}{2}m^*(x,P,T)\omega_o^2 X^2, \tag{1}$$

where $m^*(x,P,T)$ is the effective mass with the dependence of x (also known as impurity factor) concentration of the Aluminium, pressure and temperature. For $Ga_{1-x}Al_xAs$ QWR the effective mass is described as [40]:

$$m^*(x,P,T) = m_o\left[1 + \frac{\pi^2(x)}{3}\left(\frac{2}{E_g{}^i(x,P,T)} + \frac{1}{E_g{}^i(x,P,T) + \Delta_o(x)}\right) + \delta_i\left(x\right)\right]^{-1}, \tag{2}$$

m_o is the mass for free electron, $\pi(x)$ and $\Delta_o(x)$ are known as inter-band matrix element and valence band spin-orbit coupling ($\Pi^2(x) = (28900 - 6290x)meV$) and $\Delta_o(x) = (341 - 66x)meV$). When remote-band effects are considered through $\delta_i(x)$ parameter given by:

$$\delta_i(x) = -3.935 + 0.488x + 4.938x^2, \tag{3}$$

In eq. (2) $E_g^i(x,P,T)$ is defined as an energy gap in the conduction band which is given by [41].

$$\widehat{H}_o = -\frac{1}{2m^*(x,P,T)}(\mathbf{p} + e\mathbf{A})^2 + \frac{1}{2}m^*(x,P,T)\omega_o^2 X^2 + \frac{1}{2}g^*\mu_B B\sigma_z + \frac{\alpha}{\hbar}[\sigma \times (\mathbf{p} + e\mathbf{A})]_Z, \tag{5}$$

$$E_g^i(x,P,T) = p_i + q_i x + r_i x^2 + s_i P - \frac{\beta_i T^2}{\gamma_i + T}. \tag{4}$$

where the values of parameters $p_i, q_i, r_i, s_i, \beta_i$ and γ_i are 1519.4 me, 1360 meV, 220 meV, 10.7 meV/kbar, 0.5405 meV/K and 204 K respectively. These values are obtained with help of photoluminescence measurement.

In effective-mass framework approximation, single electron Hamiltonian for a $Ga_{1-x}Al_xAs$ QWR in the manifestation of RSOI, under the impact of external electric and magnetic field is given as [42,43].

where **p** exists in eq (1) for the momentum of an electron, e is the electronic charge, g^* is known as Land e' factor. ω_o, μ_B and σ are known the oscillator frequency, Bohr magneton and Pauli matrices respectively, B is the intense magnetic field realistic in the Z-direction therefore vector potential **A** comes out to be $Bx\hat{j}$ due to symmetric gauge, last term in eq. (5) is known as RSOI Hamiltonian and α is the Rashba parameter.

When there is a presence of external electric field **E** along X-axis then the total Hamiltonian for this system is written as:

$$\widehat{H} = -\frac{1}{2m^*(x,P,T)}\left(p_X + (p_Y + eBX\ )^2 + \frac{1}{2}m^*(x,P,T)\omega_1^2 X^2 + eEX + \frac{1}{2}g^*\mu_B B\sigma_Z\frac{\alpha}{\hbar}[\sigma_X(p_Y + eBX) - \sigma_Y p_X)\right], \tag{6}$$

where $\omega_1 = (\omega_o^2 + \omega_c^2)^{\frac{1}{2}}$ known as effective cyclotron frequency and the cyclotron frequency is given by $\omega_c = \frac{eB}{m^*}$.If there is a translation along the length of the wire then Hamiltonian remain unchanged, therefore the

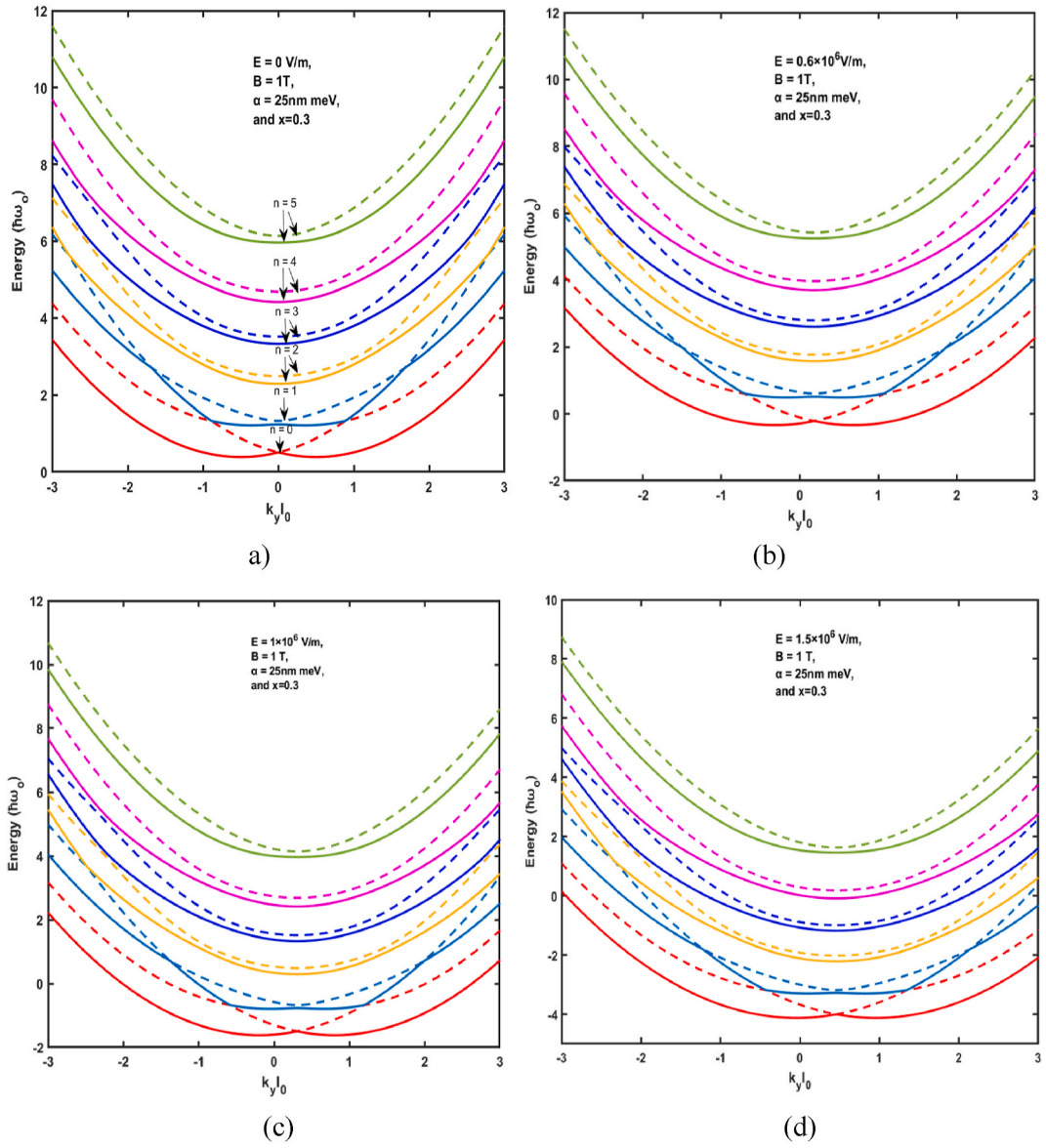

Fig. 2. The energy dispersion of the $Ga_{1-x}Al_xAs$ QWR at the magnetic field (B) = 1T, RSOI (α) = 25 nm meV and x = 0.3 for (a) E = 0V/m, (b) E = 0.6 $\times$ 10^6V/ m, (c) E = 1 $\times$ 10^6V/m, (d) E = 1.5. $\times$ 10^6V/m.

wavefunction is represented by:

$$\Psi(X,Y) = \varphi(X)\exp(ik_y Y), \tag{7}$$

where k_y is the propagation constant along Y-direction and $k_y = p_Y/\hbar$. So, we can write $\hat{H} = \hat{H}_q + \hat{H}_R$ where

$$\hat{H}_q = -\frac{p_X^2}{2m^*(x,P,T)} + \frac{1}{2}m^*(x,P,T)\omega_1^2(X-X_o)^2 - \frac{e^2E^2}{2m^*(x,P,T)\omega_1} + \frac{\omega_o^2\hbar^2 k_y}{\omega_1{}^2 2m^*(x,P,T)} - \frac{e^2EB\hbar k_y}{m^*(x,P,T)\omega_1} + \frac{1}{2}g^*\mu_B B\sigma_Z, \tag{8}$$

And

$$\hat{H}_R = \alpha\left(\sigma_X\left(k_y + \frac{eBX}{\hbar}\right) - i\sigma_Y\frac{d}{dX}\right). \tag{9}$$

where $X_o = -\left(\frac{eE}{m^*(x,P,T)\omega_1} + \frac{eB\hbar k_y}{m^{*2}(x,P,T)\omega_1}\right)$ is known as guiding centre coordinate.

The energy eigenvalues and eigenvectors for $\hat{H}_q$ is given as

$$\hat{H}_q\Psi_{n\sigma}(X) = E_{n\sigma}\Psi_{n\sigma}(X), \tag{10}$$

where

$$\Psi_{n\sigma}(X) = \frac{1}{\left(\sqrt{\pi}C_i 2^n n!\right)^{1/2}}H_n\left(\frac{X-X_o}{c_i}\right)\exp\left(-\frac{1}{2}\left(\frac{X-X_o}{c_i}\right)^2\right)\chi_\sigma. \tag{11}$$

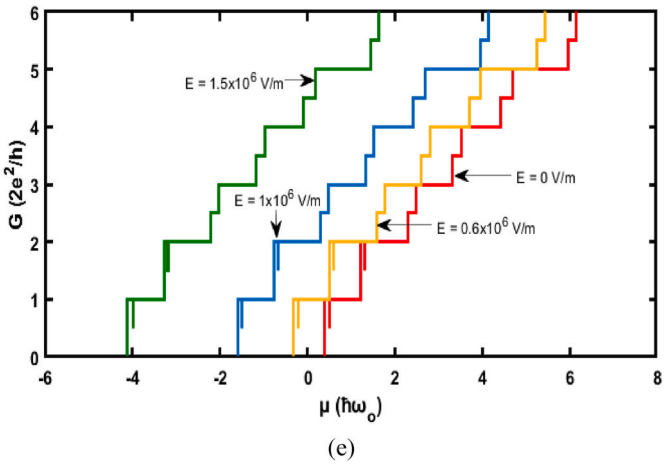

(e)

Fig. 3. The ballistic conductivity (G) for the energy dispersions given in Fig. 2(a–d).

with $C_i = \sqrt{\frac{\hbar}{m^*(x,P,T)\omega_1}}$ is the characteristic length of the harmonic oscillator, n = 0 to 5 and $\sigma = \pm$. $H_n(x)$ and χ_σ are the hermite polynomial and the spinor functions for spin down ($\chi_- = \begin{pmatrix} 0 \\ 1 \end{pmatrix}$) and for spin up ($\chi_+ = \begin{pmatrix} 1 \\ 0 \end{pmatrix}$) respectively and energy scales corresponding to the RSOI $\Delta_{so} = \frac{m^*\alpha^2}{2\hbar^2}$. A length scale has been established to characterise the strength of lateral confining potential $l_w = \sqrt{\frac{\hbar}{m^*\omega_o}}$.The energies eigenvalues of eq. (10) are

$$E_{n\sigma} = \hbar\omega\left(n + \frac{1}{2}\right) - \frac{e^2E^2}{2m^*(x,P,T)\omega_1} + \frac{\omega_o^2\hbar^2k_y}{\omega_1 2m^*(x,P,T)} - \frac{e^2EB\hbar k_y}{m^*(x,P,T)\omega_1} + \frac{1}{2}g^*\mu_B B\sigma_Z. \tag{12}$$

If we are expanding $\varphi(X) = \sum_{n\sigma} a_{n\sigma}\Psi_{n\sigma}(X)$, the Hamiltonian $'\hat{H}'$ eigenvalue equation can be written as:

$$\sum_{n\sigma} a_{n\sigma}(E_{n\sigma} - E)\Psi_{n\sigma}(X) + \sum_{n\sigma} a_{n\sigma}\hat{H}_R\Psi_{n\sigma}(X) = 0, \tag{13}$$

And via the orthogonality conditions, we have

$$(E_{n\sigma} - E)a_{n\sigma} + \sum_{n'\sigma'}\langle\Psi_{n\sigma}|\hat{H}_R|\Psi_{n'\sigma'}\rangle = 0, \tag{14}$$

where the 2nd term of the matrix elements of this equation are calculated as:

$$\langle n\sigma|\hat{H}_R|n'\sigma'\rangle = \alpha\left[\left(1 - \frac{\omega_c^2}{\omega_i}\right)k_y - \frac{\omega_c eE}{\hbar\omega_i}\right]\delta_{n,n'}\delta_{\sigma,\sigma'} + \frac{\alpha}{c_i}\left[\left(\frac{\omega_c}{\omega_i} + \sigma\right)\sqrt{\frac{n+1}{2}}\delta_{n,n'-1} + \left(\frac{\omega_c}{\omega_i} - \sigma\right)\sqrt{\frac{n}{2}}\delta_{n,n'-1}\right]\delta_{\sigma,-\sigma}. \tag{15}$$

After diagonalization of Eq. (14), we achieve the eigenfunction and the energy dispersion curve for this system.

The ballistic conductance of a nanostructure device is associated with two macroscopic electron reservoirs by ignoring the electron-electron interaction, which can be calculated with help of Landuer-B ü ttiker formalism [44]:

$$G = G_i\sum_{\beta\beta'} T_{\beta\beta'}, \tag{16}$$

where $T_{\beta\beta'}$ is known as transition probability from $|\beta$ state to $|\beta'$ state and $G_i = 2e^2/h$ is quantization constant. We follow Pershin and his colleagues [45,46] and accordingly at the end of QWR, a small bias ($\mu_l > \mu_r$) is applied between the contacts (where μ_l and μ_r chemical potentials). We have assumed the non-scattering and unity of the transition probability, conductance of this system can be obtained in following way [47]:

$$G = \frac{2e^2}{h}\sum_{n,s}\sum_{l}\alpha_l^{n,s} f\left(E_m^{n,s}\right), \tag{17}$$

In eq. (17), n is defined as a level of the states and s is the level of spin whereas $E_m^{n,s}$ is the energy of extremum point in energy spectra, and $f(E_m^{n,s})$ is known as Fermi-Dithe rac distribution function. $\alpha_l^{n,s}$ relates to −1 and +1 for a maximum and minimum point in the energy spectra respectively.

3. Result and discussion

In this present work, the energy dispersions and the ballistic conductance are described for $Ga_{1-x}Al_xAs$ quantum wire at distinct strengths of the magnetic field, external electric field, and impurity factor with $g^* = -0.44$, pressure = 15 kbar at room temperature.

This work aims to figure out the effect of energy dispersion and ballistic conductance with various strengths of an external electric field, magnetic field, RSOI, and impurity factor.

In Fig. 2(a–d), energy dispersion is represented as a function of $k_y l_o$ with $\alpha = 25$nm meV (RSOI factor), B = 1T (magnetic field) and x = 0.3(impurity factor). Here, all subsequent energy dispersion diagrams are given for more elaboration. In Fig. 2(a), two subbands are plotted for each energy level i.e., quasi spin-up (represented by solid line) and quasi spin-down (represented by dish line). Fig. 2(a) presents the dispersion curve in absence of an electric field, E = 0 V/m in which the lower two energy levels (where n = 0, 1) are anticrossing each other due to the mixing of intraband by spin split levels and the contribution of immense diagonal elements $\langle n\sigma|H_R^i|n\sigma\rangle$ [48]. This anticrossing may lead to anomalous conductance steps [41]. The presence of an electric field causes downward shifting of the energies and gives rise to a lateral shift along the $k_y l_o$-axis. Moreover, all spin branches descend towards lower energies as the electric field is increased. In Fig. 2(b–d), in which electric field is varied from 0.6×10^6V/m to 1.5×10^6V/m, the whole spectrum gets shifted downwards to lower energies. There is more downward shifting in the spectrum observed and this is called stark shifting.

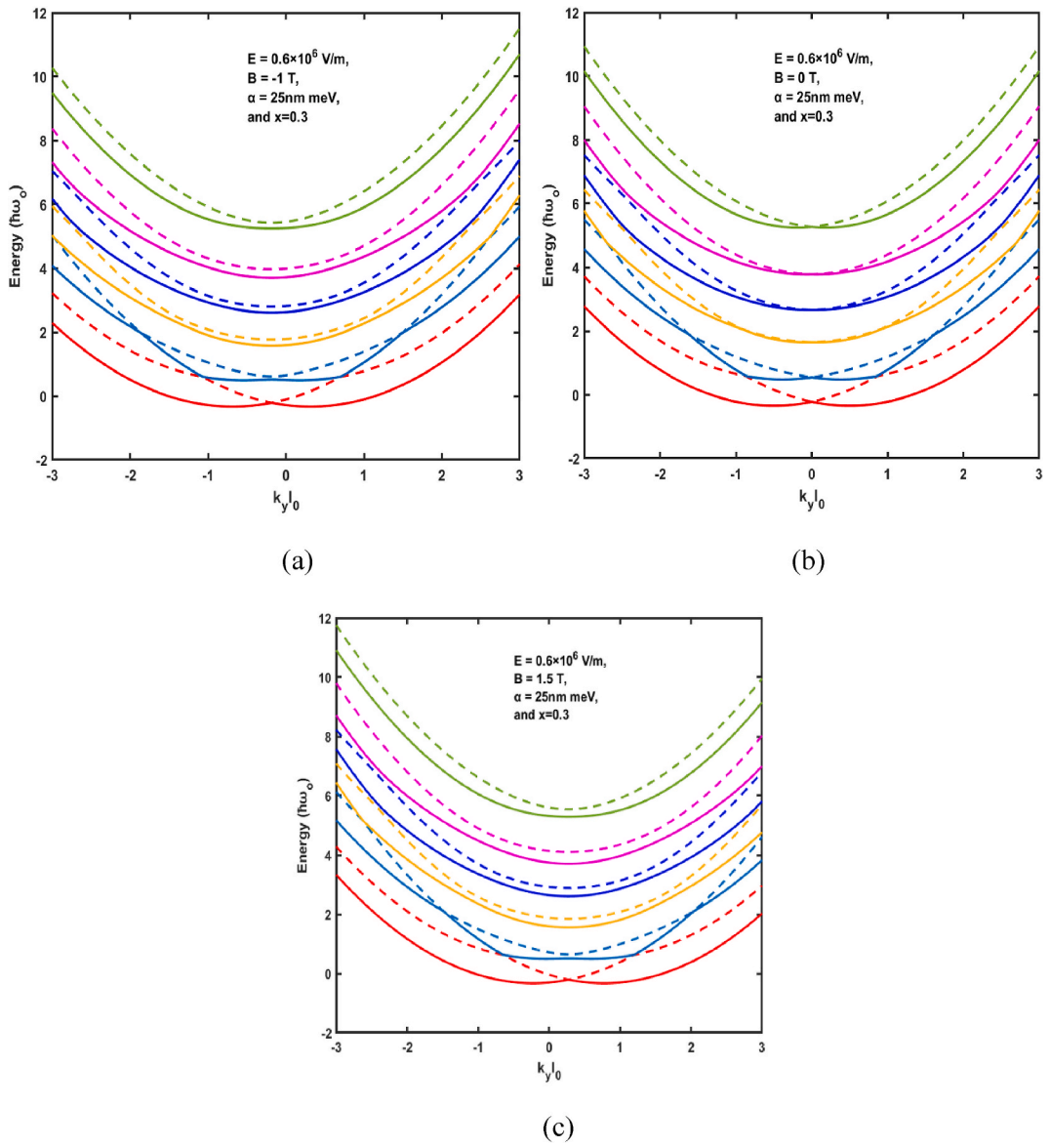

Fig. 4. The energy dispersion of the $Ga_{1-x}Al_xAs$ QWR at Electric field (E) = 0.6 × 10^6V/m, RSOI (α) = 25 nm meV and x = 0.3 for (a) B = −1 T, (b) B = 0 T, (c) B = 1.5 T.

Therefore, the contribution of the electric field to the energy dispersion is quadratic for downward shifts and linear for lateral displacements, as shown clearly in eq. (12). The creation of camel-back morphologies, crossing and anticrossing formations is determined by the interplay between RSOI and external fields, while the electric field has a more obvious effect at the weak coupling limit (α = 25 nm meV), as seen in Fig. 6(b)– (c).

Fig. 3, shows the ballistic conductance of the $Ga_{1-x}Al_xAs$ quantum wire as a function of the chemical potential for different strengths of electric field (E = 0, 0.6 × 10^6V/m, 1 × 10^6V/m, 1.5 × 10^6V/ m). The conductance shows a growing stepwise profile with integer conductance plateaus. This can be well understood with the dispersion curves. Fig. 2 (a–d), presents the energy spectrum with distinct strength of the electric field. These dispersion curves have parabolic forms and are formed in pairs. However, the two lowest energy subbands in Fig. 2(a–d) are not distinguished, they consist of two curves vertically offset by a small value. Every dispersion curve in this limit would have a two-fold degeneracy. Therefore, conductance would increase ($2e^2/h$), instead of ($2e^2/h$)/2 for a single quantum wire. This represents that the step height between two consecutive plateaus would be 1 in units of ($2e^2/h$). However, the splitting of the subbands causes the appearance of the narrow conductance plateaus with ($2e^2/h$)/2 as shown in Fig. 3. Their steps width reflects the magnitude of the subband split. The higher the subband index, the larger is the split of the subband.

In the ballistic conductance, each latest step visibly exhibits the 'turning on' of the latest mode (conducting channel) and an additional electron can travel along the wire. Ballistic conductance of quantum devices provides a new approach for designing spin filters and modulators [49]. Each sub-band has now a contribution of $2e^2$/h to the conductance due to the impact of the field on conductance, as observed e.g., in Ref. [50]. Firstly, we will get the contribution at the lowest minimum in Fig. 2(a–d) and the second contribution when chemical potential reaches the second minima of the same sub-band. When μ is further increased and passed through the local maximum point, the conductance will decrease by $2e^2$/h. The formation of conductance peaks is done, as shown in Fig. 3 [31]. If we compare the conductance steps with the chemical potential axis, the decrease in energy with the increase in strength of the external field can be easily observed. The anticrossing is observed at the lower level for n = 0 of the energy

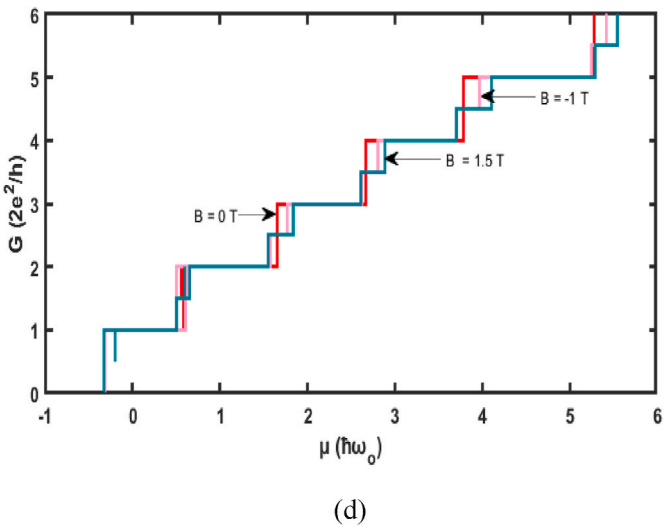

Fig. 5. The ballistic conductivity (G) for the energy dispersions given in Fig. 4(a–c).

dispersion curve as shown in Fig. 2(a–d). The presence of a camel-back formation in the energy dispersion with more than one extremum point creates narrower conductivity dips. This dip on conductance shows the steps of quantization which exhibit the monotonic increasing property, except the former.

Fig. 4(a–c), shows the impact on the curve of energy dispersion for various values of magnetic field and at E = 0.6 $\times 10^6$V/m and α = 25nm meV . When the magnetic field is applied (in z-direction) to the $Ga_{1-x}Al_xAs$ QWR, the symmetry of time reversal is broken. A complex spectrum is obtained due to the interaction between RSOI and Zeeman splitting. Therefore, we get the variation in energy separation for the various intensities of the applied magnetic field. When the direction of the magnetic field is reversed B = −1T (B_Z to $-B_Z$), a lateral shift in energy in the subbands along k_yl_o – axis is observed towards the lower value of k_yl_o shown in Fig. 4(a). And it is clearly seen that the gaps between the subbands are significantly dependent on the direction of applied magnetic field. This observation can help to tune the g-factor in such systems. In absence of a magnetic field i.e., B = 0T, we obtain energy dispersion with zero lateral shift and there is no spacing between the quasi spin-up and quasi spin-down bands at $k_yl_o = 0$ represented in Fig. 4(b). Consequently, Fig. 4(c) shows the presence of a positive magnetic field (B = 1.5T) that induces the shifting in the dispersion graph along the positive k_yl_o-axis. This results in an increased subband separation gap which is find out by the effective oscillator energy $\hbar\omega$, rather than the zero field $\hbar\omega$. Whereas, the interplay among the Zeeman splitting and the RSOI leads to rather complex level energy dispersion, resulting in variation of energy gaps between the succeeding subbands at high external field. For an applied magnetic field, the intermixing weakens in the energy range considered. We attribute this to the enhanced effective oscillator energy $\hbar\omega$ with reference to Δ_{so}. Fig. 5 displays that there are more propagating channels (in QWR) opened up with an increase in energy, so the G (conductivity) steps up in staircase shape. In presence of an uncertain magnetic field, there is 2-fold degeneracy i.e., state degeneracy and spin degeneracy. These propagating channels are opened up in pair with an increase in fermi-energy. Hence,

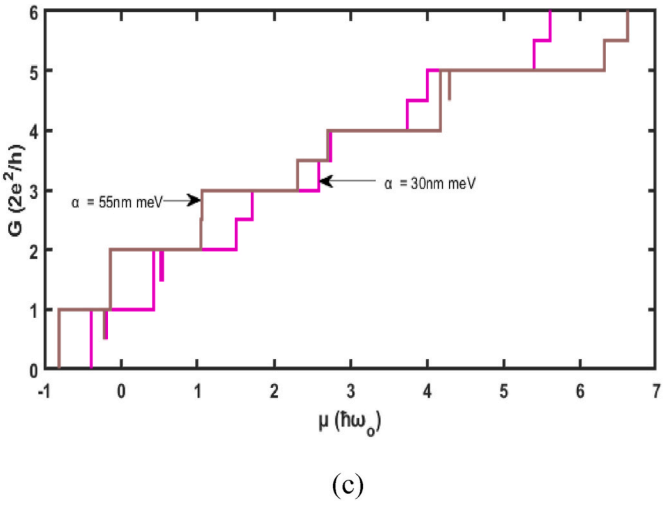

Fig. 7. The ballistic conductivity (G) for the energy dispersions given in Fig. 6 (a and b).

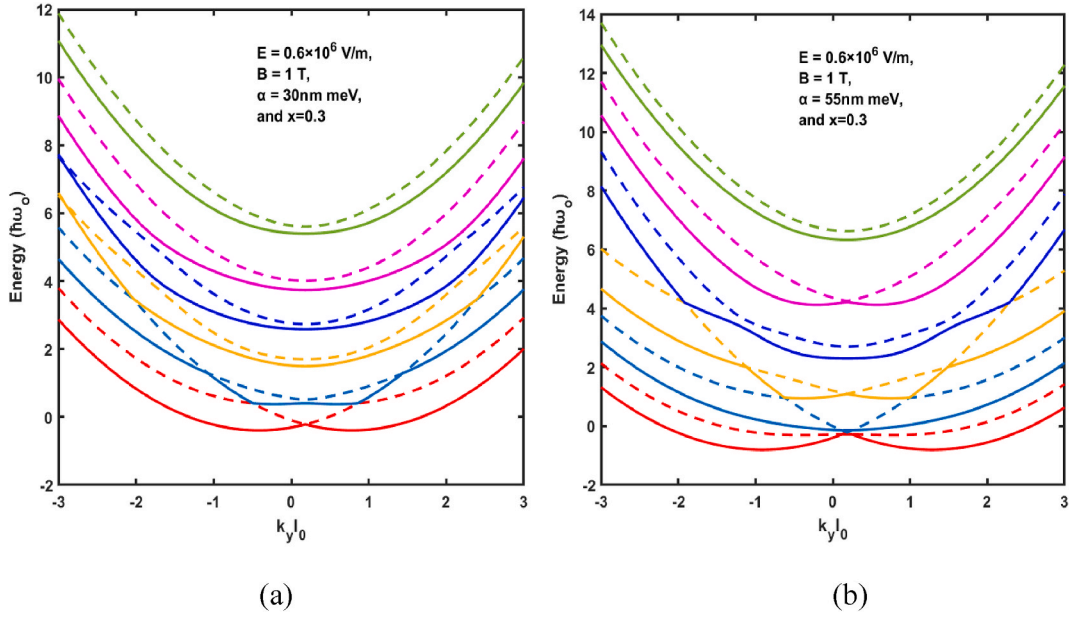

Fig. 6. The energy dispersion of the $Ga_{1-x}Al_xAs$ QWR at Electric field (E) = 0.6 $\times$ 10^6V/m, B = 1T and x = 0.3 for (a) α = 30 nm meV, (b) α = 55 nm meV.

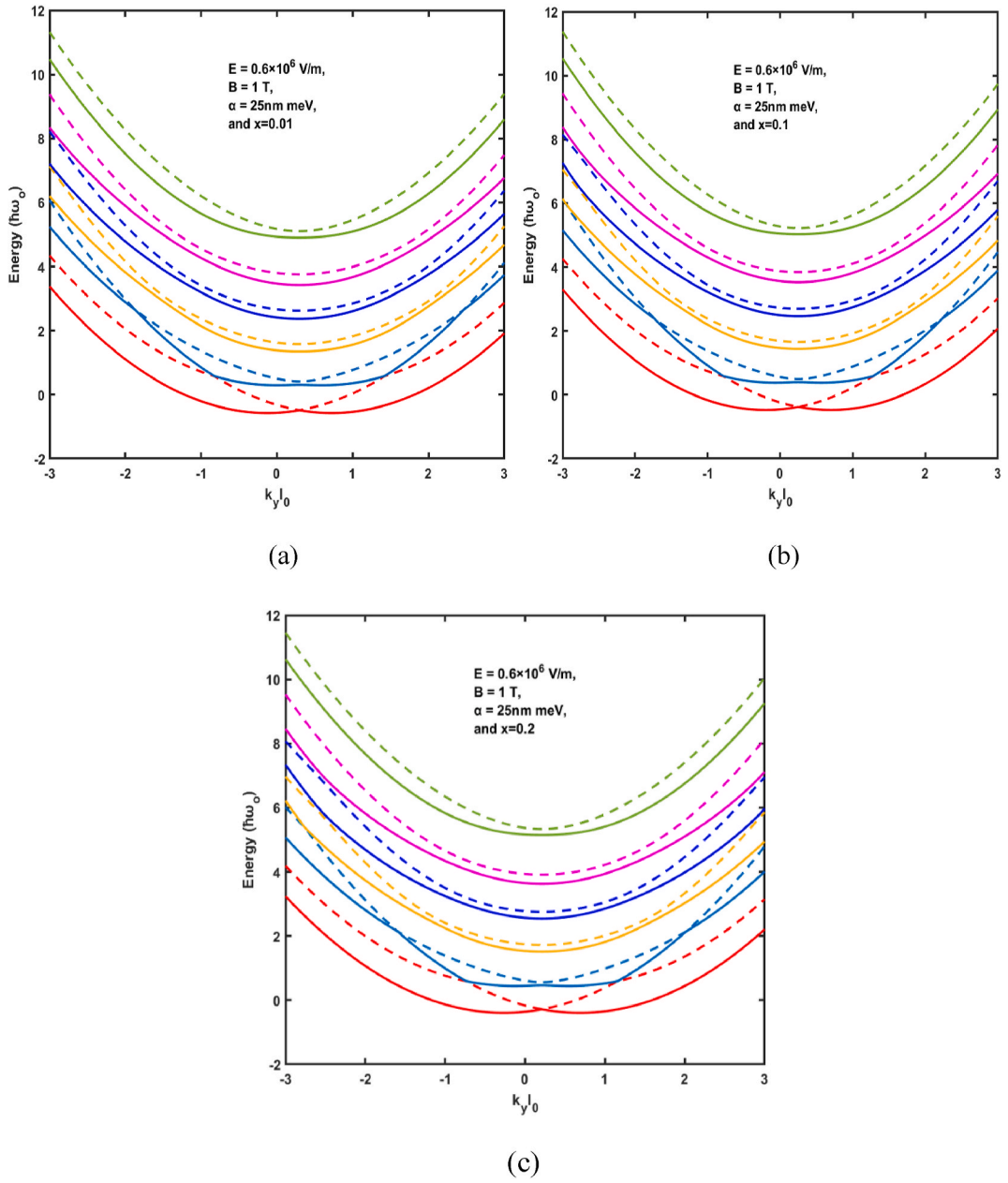

Fig. 8. The energy dispersion of the $Ga_{1-x}Al_xAs$ QWR at Electric field (E) = 0.6 × 10^6V/m, magnetic field (B) = 1T and RSOI (α) = 25 nm meV for (a) x = 0.01, (b) x = 0.1, (c) x = 0.2..

the conductance for weak magnetic induction (B = −1T, 0T) approaches 2($2e^2$/h), in place of 1($2e^2$/h) for a strong magnetic field (B = 1.5 T).

Fig. 6(a and b) shows the effects of various values of the RSOI on the spectrum of energy dispersion. The increment in SOI value from weak to strong (from α = 30 nm meV to 55 nm meV) causes the value superimposes the lower energies and consequently, a highly intricate energy spectrum is obtained (in Fig. 6(b)) [51–53]. For strong RSOI, (α = 55 nm meV) the anticrossings between the subbands turn out to be sharper resulting in a stronger intermixing of the levels due to the coupling between the spin spilt levels. The variation of conductance with chemical potential for the various value of RSOI is represented in Fig. 7. Due to the more complex energy dispersion curves for strong coupling as compared to weak coupling, the conductivity directly depends on the energy spectrum which exhibits more exceptional steps.

Fig. 8(a–c) shows, how the energy dispersion is modified by changing the impurity factor. From the visual comparison, we find the effect of the impurity factor. The spacing between the energy subbands increases when the concentration of Al in QWR is increased. There is a gradual increment in splitting. As a result, conductance also changes with respect to chemical potential (μ) as shown in Fig. 9. The extremum points located in energy subbands increase or decrease the conductance by e^2/h. With an increase in the Al concentration, the energy subbands show slight anomalies. Hence, the conductance shows generally a growth in stepwise profile with the integer conductivity.

Fig. 10 shows the conductivity as a function of chemical potential for GaAs QWR (that is QWR with zero impurity) and $Ga_{1-x}Al_xAs$ QWR. We can easily see that GaAs QWR require a lower chemical potential for conductivity as compared to $Ga_{1-x}Al_xAs$ QWR. Also, for two lower energy (n = 0, 1) states, conductance shows an increment of 2($2e^2$/h) for the QWR while for higher energy states, there is an increment in conductance by $2e^2$/h.

Thus, the change in the energy dispersion leads to the variation in transport properties. Therefore, the evaluation of conductance opens the door for understanding the microscopic transport procedure. Further, it

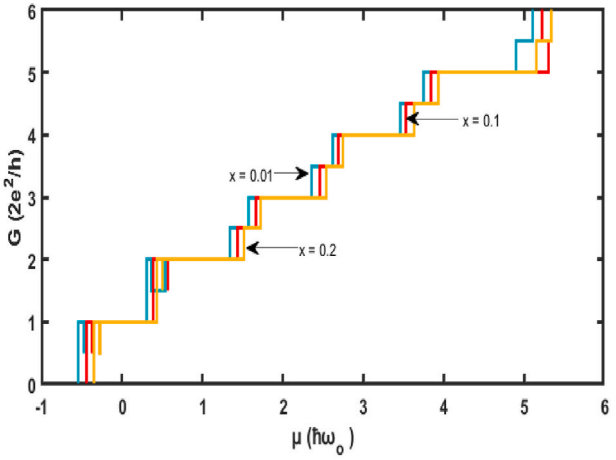

(d)

Fig. 9. The ballistic conductivity (G) for the energy dispersions given in Fig. 8(a–c).

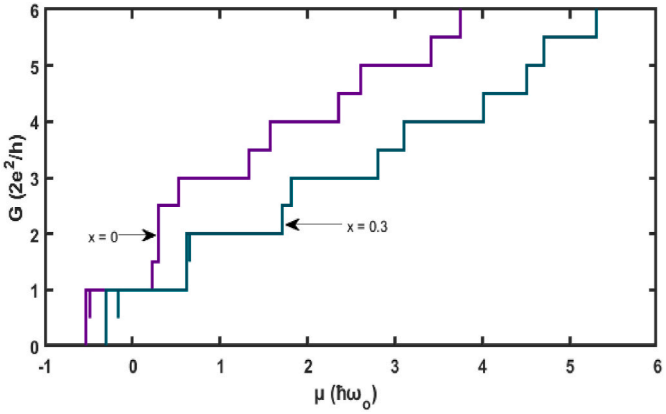

Fig. 10. Comparison between ballistic conductivity for the GaAs (when x = 0) QWR with the $Ga_{1-x}Al_xAs$ (at x = 0.3) QWR.

could be vital for constructing molecular and nanoscale electronic appliances.

4. Conclusion

In this paper, we have scrutinized the energy dispersion and ballistic conductance for Ga1-xAlxAs QWR. Collaborative impacts of the external electric field, magnetic field, SOI, as well as impurity factor on energy dispersions and ballistic conductance, have been investigated. The outcome of numerical calculation conveys that: The electric field causes the downward shifting in the spectrum of energy and ballistic conductivity steps as the chemical potential is increased. The magnetic field and SOI altered the energy spectrum by lateral shifting that caused camelback structures. The ballistic conductance of 1D QWR has significantly been influenced by the strengths of the external electric field, magnetic field, impurity concentration, and SOI. The extremum points in the spectrum of energy increase or decrease the conductivity steps by $2e^2/h$. The conductivity has generally a growth in stepwise profile by the factor of the integer conductivity, but due to the presence of exceptional formalism like subbands anticrossing, camelback structure, which includes more than one extremum point in the curve of energy dispersion resulted in the small trough or crest in steps of conductivity. These observations may lead to very interesting results and may be used to adjudicate the authentic character of nanostructures in transport properties and optical properties of 1D systems. To understand the microscopic transport mechanism, we need to analyze the conductance Eigen channels which are illustrated by our study in a meantime. It could perhaps be beneficial to design future molecular and nanoscale electronic devices [54].

Author contributions

Priyanka: Methodology, Software, Validation, Formal analysis, Data curation, Writing – original draft. Rinku Sharma: Resources, Investigation, Supervision, Writing – review & editing, Project administration. Manoj Kumar: Conceptualization, Formal analysis, Writing – review & editing, Visualization

Declaration of competing interest

The authors declare the following financial interests/personal relationships which may be considered as potential competing interests: Priyanka reports financial support was provided by University Grants Commission. Rinku Sharma reports was provided by Delhi Technological University. Priyanaka reports a relationship with University Grants Commission that includes: funding grants. Rinku Sharma reports a relationship with Delhi Technological University that includes: employment and funding grants. Manoj Kumar is employed by Govt College for Women, Jind, Department of Higher Education, Haryana.

Acknowledgment

Priyanka acknowledges the financial support by University Grants Commission and R. Sharma is thankful to the Delhi Technological University for the research facilities. We are thankful to Professor Man Mohan for valuable discussions regarding this problem.

References

[1] S. Ghajarpour-Nobandegani, M.J. Karimi, Effects of hydrogenic impurity and external fields on the optical absorption in a ring-shaped elliptical quantum dot, Opt. Mater. 82 (2018) 75–80, https://doi.org/10.1016/j.optmat.2018.05.045.
[2] S. Dahiya, S. Lahon, R. Sharma, Effects of temperature and hydrostatic pressure on the optical rectification associated with the excitonic system in a semi-parabolic quantum dot, Phys. E Low-dimens. Syst. Nanostruct. 118 (2020), https://doi.org/10.1016/j.physe.2019.113918.
[3] M. Royo, M. de Luca, R. Rurali, I. Zardo, A review on III-V core-multishell nanowires: growth, properties, and applications, J. Phys. Appl. Phys. 50 (2017), https://doi.org/10.1088/1361-6463/aa5d8e.
[4] E. Barrigón, M. Heurlin, Z. Bi, B. Monemar, L. Samuelson, Synthesis and applications of III-V nanowires, Chem. Rev. 119 (2019) 9170–9220, https://doi.org/10.1021/acs.chemrev.9b00075.
[5] K.M. Jiang, J. Yang, R. Zhang, H. Wang, Ballistic transport properties in spin field-effect transistors, J. Appl. Phys. 104 (2008), https://doi.org/10.1063/1.2970102.
[6] D. Csontos, U. Zülicke, Large variations in the hole spin splitting of quantum-wire subband edges, Phys. Rev. B Condens. Matter 76 (2007), https://doi.org/10.1103/PhysRevB.76.073313.
[7] Y. Sun, S.E. Thompson, T. Nishida, Physics of strain effects in semiconductors and metal-oxide-semiconductor field-effect transistors, J. Appl. Phys. 101 (2007), https://doi.org/10.1063/1.2730561.
[8] D. Grundler, Ballistic spin-filter transistor, Phys. Rev. B Condens. Matter 63 (2001), https://doi.org/10.1103/PhysRevB.63.161307.
[9] C.H.L. Quay, T.L. Hughes, J.A. Sulpizio, L.N. Pfeiffer, K.W. Baldwin, K.W. West, D. Goldhaber-Gordon, R. de Picciotto, Observation of a one-dimensional spin-orbit gap in a quantum wire, Nat. Phys. 6 (2010) 336–339, https://doi.org/10.1038/nphys1626.
[10] Y.v. Pershin, S.N. Shevchenko, I.D. Vagner, P. Wyder, Electronic transport through a nuclear-spin-polarization-induced quantum wire, Phys. Rev. B Condens. Matter 66 (2002) 1–5, https://doi.org/10.1103/PhysRevB.66.035303.
[11] Y.v. Pershin, J.A. Nesteroff, V. Privman, Effect of spin-orbit interaction and in-plane magnetic field on the conductance of a quasi-one-dimensional system, Phys. Rev. B Condens. Matter 69 (2004), https://doi.org/10.1103/PhysRevB.69.121306.
[12] J.C. Egues, G. Burkard, D. Loss, Datta-Das transistor with enhanced spin control, Appl. Phys. Lett. 82 (2003) 2658–2660, https://doi.org/10.1063/1.1564867.
[13] G. DRESSELHAUst, M. Tanenbautn, H.B. Briggs, Spin-Orbit Coupling Effects in Zinc Blende Structures*, 1936.
[14] Y. Ho Park, H.J. Kim, J. Chang, S. Hee Han, J. Eom, H.J. Choi, H. Cheol Koo, Separation of Rashba and Dresselhaus spin-orbit interactions using crystal

direction dependent transport measurements, Appl. Phys. Lett. 103 (2013), https://doi.org/10.1063/1.4855495.
[15] L. Meier, G. Salis, I. Shorubalko, E. Gini, S. Schön, K. Ensslin, Measurement of Rashba and Dresselhaus spin-orbit magnetic fields, Nat. Phys. 3 (2007) 650–654, https://doi.org/10.1038/nphys675.
[16] S.D. Ganichev, V.v. Bel'kov, L.E. Golub, E.L. Ivchenko, P. Schneider, S. Giglberger, J. Eroms, J. de Boeck, G. Borghs, W. Wegscheider, D. Weiss, W. Prettl, Experimental separation of Rashba and Dresselhaus spin splittings in semiconductor quantum wells, Phys. Rev. Lett. 92 (2004), https://doi.org/10.1103/PhysRevLett.92.256601.
[17] S. Antil, M. Kumar, S. Lahon, S. Dahiya, A. Ohlan, R. Punia, A.S. Maan, Influence of hydrostatic pressure and spin orbit interaction on optical properties in quantum wire, Phys. B Condens. Matter 552 (2019) 202–208, https://doi.org/10.1016/j.physb.2018.10.006.
[18] J.M. Kikkawa, D.D. Awschalom, Resonant Spin Amplification in N-type GaAs, 1998.
[19] J. Nitta, T. Akazaki, H. Takayanagi, T. Enoki, Gate Control of Spin-Orbit Interaction in an Inverted in 0.53 Ga 0.47 as in 0.52 Al 0.48 as Heterostructure, 1997.
[20] P.M. Krstajić, M. Pagano, P. Vasilopoulos, Transport properties of low-dimensional semiconductor structures in the presence of spinorbit interaction, Phys. E Low-dimens. Syst. Nanostruct. 43 (2011) 893–900, https://doi.org/10.1016/j.physe.2010.11.008.
[21] J. Nitta, F.E. Meijer, H. Takayanagi, Spin-interference device, Appl. Phys. Lett. 75 (1999) 695–697, https://doi.org/10.1063/1.124485.
[22] Q.F. Sun, J. Wang, H. Guo, Quantum transport theory for nanostructures with Rashba spin-orbital interaction, Phys. Rev. B Condens. Matter (2005) 71, https://doi.org/10.1103/PhysRevB.71.165310.
[23] C.L. Romano, S.E. Ulloa, P.I. Tamborenea, Level structure and spin-orbit effects in quasi-one-dimensional semiconductor nanostructures, Phys. Rev. B Condens. Matter (2005) 71, https://doi.org/10.1103/PhysRevB.71.035336.
[24] G. Liu, G. Zhou, A possible realization of spin filter using a quantum wire with Rashba spin-orbit coupling, J. Appl. Phys. 101 (2007), https://doi.org/10.1063/1.2512392.
[25] K.J. Thomas, J.T. Nicholls, M.Y. Simmons, M. Pepper, D.R. Mace, D.A. Ritchie, Possible Spin Polarization in a One-Dimensional Electron Gas, 1996.
[26] R.G. Pereira, E. Miranda, Magnetically controlled impurities in quantum wires with strong Rashba coupling, Phys. Rev. B Condens. Matter (2005) 71, https://doi.org/10.1103/PhysRevB.71.085318.
[27] F. Mireles, G. Kirczenow, Ballistic spin-polarized transport and Rashba spin precession in semiconductor nanowires, Phys. Rev. B Condens. Matter 64 (2001), https://doi.org/10.1103/PhysRevB.64.024426.
[28] M. Kumar, S. Lahon, P.K. Jha, S. Gumber, M. Mohan, Spin-orbit interaction effect on nonlinear optical rectification of quantum wire in the presence of electric and magnetic fields, Phys. B Condens. Matter 438 (2014) 29–33, https://doi.org/10.1016/j.physb.2013.12.044.
[29] S. M'Zerd, K. Rahmani, S. Janati, Y. Chrafih, I. Zorkani, A. Jorio, Stark effect of shallow donor impurities in HgS Inhomogeneous Quantum Dots, in: IOP Conference Series: Materials Science and Engineering, Institute of Physics Publishing, 2017, https://doi.org/10.1088/1757-899X/186/1/012015.
[30] L. Liu, J.J. Liu, Binding energy of ionized-donor-bound excitons in parabolic quantum-well wires in a magnetic field, J. Appl. Phys. 106 (2009), https://doi.org/10.1063/1.3211960.
[31] N. Raigoza, A.L. Morales, A. Montes, N. Porras-Montenegro, C.A. Duque, Stress effects on shallow-donor impurity states in symmetrical GaAs/AlxGa1 − xAs double quantum wells, Phys. Rev. B Condens. Matter 69 (2004), https://doi.org/10.1103/PhysRevB.69.045323.
[32] W. Xie, Impurity effects on optical property of a spherical quantum dot in the presence of an electric field, Phys. B Condens. Matter 405 (2010) 3436–3440, https://doi.org/10.1016/j.physb.2010.05.019.
[33] B. Çakır, Y. Yakar, A. Özmen, Linear and nonlinear absorption coefficients of spherical quantum dot inside external magnetic field, Phys. B Condens. Matter 510 (2017) 86–91, https://doi.org/10.1016/j.physb.2017.01.018.
[34] F. Bassanit, Electronic Impurity Levels in Semiconductors, 1974. http://iopscience.iop.org/0034-4885/37/9/001.
[35] C.A. Perroni, D. Bercioux, V.M. Ramaglia, V. Cataudella, Rashba quantum wire: exact solution and ballistictransport, J. Phys. Condens. Matter 19 (2007), https://doi.org/10.1088/0953-8984/19/18/186227.
[36] I.A. Kokurin, Effect of spin-orbit coupling on spectral and transport properties of tubular electron gas in InAs nanowires, Phys. E Low-dimens. Syst. Nanostruct. 74 (2015) 264–269, https://doi.org/10.1016/j.physe.2015.07.003.
[37] P.M. Krstajić, M. Pagano, P. Vasilopoulos, Transport properties of low-dimensional semiconductor structures in the presence of spinorbit interaction, Phys. E Low-dimens. Syst. Nanostruct. 43 (2011) 893–900, https://doi.org/10.1016/j.physe.2010.11.008.
[38] I. Cunha, L. Villegas-Lelovsky, V. Lopez-Richard, L.K. Castelano, Multichannel scattering mechanism behind the reentrant conductance feature in nanowires subject to strong spin-orbit coupling, Phys. Rev. B 102 (2020), https://doi.org/10.1103/PhysRevB.102.195423.
[39] K. Kolasiński, A. Mreńca-Kolasińska, B. Szafran, Transconductance and effective Landé factors for quantum point contacts: spin-orbit coupling and interaction effects, Phys. Rev. B 93 (2016), https://doi.org/10.1103/PhysRevB.93.035304.
[40] H.M. Baghramyan, M.G. Barseghyan, A.A. Kirakosyan, R.L. Restrepo, C.A. Duque, Linear and nonlinear optical absorption coefficients in GaAs/Ga 1-xAlxAs concentric double quantum rings: effects of hydrostatic pressure and aluminum concentration, J. Lumin. 134 (2013) 594–599, https://doi.org/10.1016/j.jlumin.2012.07.024.
[41] E. Reyes-Gómez, N. Raigoza, L.E. Oliveira, Effects of hydrostatic pressure and aluminum concentration on the conduction-electron g factor in GaAs-(Ga,Al)As quantum wells under in-plane magnetic fields, Phys. Rev. B Condens. Matter 77 (2008), https://doi.org/10.1103/PhysRevB.77.115308.
[42] S. Debald, B. Kramer, Rashba effect and magnetic field in semiconductor quantum wires, Phys. Rev. B Condens. Matter (2005) 71, https://doi.org/10.1103/PhysRevB.71.115322.
[43] N. Arunachalam, A. John Peter, C. Woo Lee, Pressure induced optical absorption and refractive index changes of a shallow hydrogenic impurity in a quantum wire, Phys. E Low-dimens. Syst. Nanostruct. 44 (2011) 222–228, https://doi.org/10.1016/j.physe.2011.08.019.
[44] R. Landauer, Spatial Variation of Currents and Fields Due to Localized Scatterers in Metallic Conduction, 1988.
[45] Y.v. Pershin, J.A. Nesteroff, V. Privman, Effect of spin-orbit interaction and in-plane magnetic field on the conductance of a quasi-one-dimensional system, Phys. Rev. B Condens. Matter 69 (2004), https://doi.org/10.1103/PhysRevB.69.121306.
[46] J.A. Nesteroff, Y.v. Pershin, V. Privman, Influence of nuclear spin polarization on quantum wire conductance, in: IEEE Transactions on Nanotechnology, 2005, pp. 141–147, https://doi.org/10.1109/TNANO.2004.837855.
[47] I.A. Kokurin, Determination of Rashba-coupling strength for surface two-dimensional electron gas in InAs nanowires, Solid State Commun. 195 (2014) 49–54, https://doi.org/10.1016/j.ssc.2014.07.002.
[48] M. Kumar, S. Lahon, P.K. Jha, M. Mohan, Energy dispersion and electron g-factor of quantum wire in external electric and magnetic fields with Rashba spin orbit interaction, Superlattice. Microst. 57 (2013) 11–18, https://doi.org/10.1016/j.spmi.2013.01.007.
[49] R. Rana, L. Balaghi, I. Fotev, H. Schneider, M. Helm, E. Dimakis, A. Pashkin, Nonlinear charge transport in InGaAs nanowires at terahertz frequencies, Nano Lett. 20 (2020) 3225–3231, https://doi.org/10.1021/acs.nanolett.9b05328.
[50] K.J. Thomas, J.T. Nicholls, M.Y. Simmons, M. Pepper, D.R. Mace, D.A. Ritchie, Possible Spin Polarization in a One-Dimensional Electron Gas, 1996.
[51] A. v Moroz, C.H.W. Barnes, Effect of the spin-orbit interaction on the band structure and conductance of quasi-one-dimensional systems, Phys. Rev. B 60 (1999) 271–285, https://doi.org/10.1103/PhysRevB.60.14272.
[52] B. Das, S. Datta, R. Reifenberger, Zero-field spin splitting in a two-dimensional electron gas, Phys. Rev. B 41 (1989) 8278–8287, https://doi.org/10.1103/PhysRevB.41.8278.
[53] J. Luo, H. Munekata, F.F. Fang, P.J. Stiles, Effects of inversion asymmetry on electron energy band structures in GaSb/InAs/GaSb quantum wells (n.d.), Phys. Rev. B 41 (1990) 7685–7693, https://doi.org/10.1103/PhysRevB.41.7685.
[54] X.-R. Zhang, X.-F. Peng, S.-H. Tan, M.-Q. Long, Ballistic electrical-thermal transport properties and their applications in graphene-nanoribbon-stacked heterojunctions, Phys. E Low-dimens. Syst. Nanostruct. 136 (2022) 115025, https://doi.org/10.1016/j.physe.2021.115025.

Physica B 648 (2023) 414402

Contents lists available at ScienceDirect

Physica B: Physics of Condensed Matter

journal homepage: www.elsevier.com/locate/physb

Effect of hydrostatic pressure and temperature on the ballistic conductance under the influence of Rashba spin-orbit coupling

Priyanka [a], Rinku Sharma [a,*], Manoj Kumar [b,**]

[a] Department of Applied Physics, Delhi Technological University, Delhi, 110042, India
[b] Department of Physics, Govt. College for Women, Jind, 126102, India

ARTICLE INFO

Keywords:
Rashba spin-orbit interaction
Hydrostatic pressure
Temperature
Energy dispersion and conductance

ABSTRACT

In semiconductors, the exploration of electron quantum transport on the nanoscale has become feasible due to the electric field as well as magnetic field impact. The existence of spin-orbit coupling in the quantum wire has set up a propitious stage for the development of apparatus for electron transportation. Here, we analyse the impact of hydrostatic pressure and temperature on the energy band structure as well as on the ballistic conductivity. The Energy eigenvalues and eigenvectors are found by using the diagonalization method and the ballistic conductance is computed by Landuer-B ü ttiker formalism. Also, we have studied the behaviour of energy concerning an external electric field, magnetic field and temperature. The system is expressed by parabolic confinement to the normal intense magnetic field and RSOI causes the collaborative impact of interior and exterior agents leading to downward/upward and lateral/vertical shifts in the dispersion. The oddity of the energy subbands results in oscillatory patterns in the ballistic conductance.

1. Introduction

The studies of spin-orbit interaction (SOI) have been growing interest in low-dimensional semiconductor devices made of III-V materials. The SOI is seen as an opportunity to control and manipulate the electron states through gate voltages [1]. Various research activities are activated by SOI on both theoretical and practical grounds, promoted by fundamental physics as well as application aspects [2,3]. Latterly, many papers have studied the effect of SOI along with the presence of the magnetic field and electric field for low-dimensional devices i.e., 2D, 1D and 0D nanostructures. In 2D nanostructures, the presence of SOI and external fields like electric and magnetic field change the optical, mechanical, optical and electronic properties. These changes help the finding pave the way for setting up the real application in optoelectronics [4,5]. Moreover, they have exclusive properties as well as excellent lubricity, chemical inertness and thermal conductivity [6]. Whereas, 0D nanostructures are enchantingly attractive in quantum-information properties due to their beneficial properties and 1D nanostructures are beneficial to be used in electro-optic devices and electronics. There are many researches theoretically and experimental in which electric, magnetic field and SOI play an important role in analysing the physical and electronic properties of 2D, 1D and 0D nanostructures [7–14]. The SOI may evince itself in a novel device either as a consequence of splitting of reversal symmetry of the entire structure, mentioned as Rashba spin-orbit interaction (SOI) term or because of insufficient reversal symmetry in the crystal structure, resorted to as Dresselhaus spin-orbit interaction (SOI) term [15]. For low dimensional nanostructure, spin-orbit plays an essential role in the physical properties and transport properties of the charge carrier [16] The consequences of Rashba SOI on the band structures spin accumulation and transport properties of quantum wire (QW) are researched by S. Debald and B. Kramer [17,18].

The pursuit of understanding the considerable effect due to electron spin on transportation properties has significantly captivated interest during the last few years. The description for transport properties like ballistic conductance quantisation is established by using a model of the non-interacting electron [19]. In which small biasing is exhausted over the channel then electrons start moving from one reservoir to another. On account of transverse confinement in the Channel of the device given by Landauer-B ü tricker formalism, the electrons are dispensed like fermi-distribution, amid various energy subdivisions of bands in the channel. Each of the energy subdivision bands gives the contribution of

* Corresponding author.
** Corresponding author.
E-mail addresses: rinkusharma@dtu.ac.in (R. Sharma), manojmalikdu@gmail.com (M. Kumar).

https://doi.org/10.1016/j.physb.2022.414402
Received 14 August 2022; Received in revised form 2 October 2022; Accepted 4 October 2022
Available online 15 October 2022
0921-4526/© 2022 Elsevier B.V. All rights reserved.

$2e^2/h$ to the conductance [20]. The experiments proficient independently by Yuriy et al. [21] and Quay et al. [22] gave a relation of energy dispersion with ballistic conductance. Using energy band structure, they inflict that each subband gives rise to $2e^2/h$ steps in the ballistic conductance. Some theoretical and experimental works explore the study of ballistic conductance under the presence of external fields like a magnetic field, electric field and Rashba SOI [10–12].

We know that outwardly restrained parameters like hydrostatic pressure and temperature are capable of manipulating the optical characteristics of quantum nanostructures. In a confined system, the electric band structure is altered due to hydrostatic pressure causing amendment in electron and hole actual masses, which results in numerous unusual optical as well as physical reactions [23–27]. Hydrostatic pressure and temperature have an impact on the semiconductor devices variables like energy gap, dielectric constant, effective mass, lattice vibration and so on. The hydrostatic pressure makes a great impact on the physical along with transport characteristics of QW. B. S. Ma et al. [28] examined that temperature also affects the physical properties of semiconductors. Also, a lot of work is done on the collaborative effect of hydrostatic pressure and temperature on the physical characteristics of semiconductor devices [29–33].

To scrutinize the properties in the field of spintronics devices further, we focus on the pressure and temperature's effect on the electronic energy spectrum, and ballistic conductance. Also, study the energy's behaviour with the electrostatic field, magnetic field and temperature. For this, we define parabolic confinement when QW is placed under external electric, intense magnetic field and also taking into account the presence of RSOI. Following is the consortium of our task. First of all, the system is described by analysing the strategy in a nutshell in Sec.2 and Sec.3 is dedicated to abstract of mathematical outcomes succeeded by a brief terminating segment.

2. Theory

We assume an electron-bound system for the GaAs quantum wire. The electron motion is confined only in x direction and the magnetic force field B is applied across QW along the z direction i.e. (0, 0, B) as shown in Fig. 1. Therefore, the analogous vector potential (**A**) in landau gauge can be written as Bx $\hat{j}$ .The Hamiltonian for a single electron is given by [17,34]

$$H=\frac{\left(p+e\overrightarrow{A}\right)^2}{2m_e^*(P,T)}+\frac{1}{2}m_e^*(P,T){\omega_{os}}^2(P)x^2+\frac{1}{2}gU_B\overrightarrow{\sigma}\bullet\overrightarrow{B}+H_R^j \tag{1}$$

where $\omega_{os}(\mathrm{P})$ is the oscillator strength,$m_e^*(P,T)$ is the pressure and temperature-dependent effective mass for an electron in Eq. (1). And g is known as Lande's g-factor, U_B is the Bohr magnetron and Pauli matrix is given by σ. For GaAs QW, $m_e^*\Gamma(P,T)$ is written as [35–38]

$$\mathrm{m_e^*(P,T)}=\left[1+E_P^\Gamma\left(\frac{2}{\mathrm{E_g^\Gamma(P,T)}}+\frac{1}{\mathrm{E_g^\Gamma(P,T)}+\Delta_0}\right)\right]^{-1}\mathrm{m_o}, \tag{2}$$

where $\mathrm{m_o}$ represents the free electron mass, $\Delta_0=0.341\mathrm{eV}$ & $E_P^\Gamma=7.51eV$ $\mathrm{E_g^\Gamma(P,T)}$ pressure and temperature-dependent energy band gap at Γ-point for GaAs QW, written as

$$\mathrm{E_g^\Gamma(P,T)}=E_g^\Gamma(0,0)-\frac{\alpha_i T^2}{T+204}+\beta_i P+\gamma_i P^2, \tag{3}$$

Here,

$E_g^\Gamma(0,0)=1.519eV, \alpha_i=5.405\times\frac{10^{-4}eV}{K}, \beta_i=1.26\times\frac{10^{-2}eV}{kbar}$ and γ_i $=3.771.26\times\frac{10^{-2}eV}{kbar^2}$.

For GaAs QW effective width is dependent on hydrostatic pressure, given by

$$\mathrm{W\ (P)=W\ (0)\ [1-2P\ (S_{11}\ +S_{12})]^{1/2}}, \tag{4}$$

Here, S_{11} and S_{12} are compliance tensor components of GaAs and their values are 1.16 $\times10^{-3}$ $\mathrm{kbar^{-1}}$ and -3.7 $\times10^{-4}$ $\mathrm{kbar^{-1}}$ respectively. W (0) is known as effective width at zero hydrostatic pressure. Confinement potential is related to effective width as

$$\mathrm{W\ (P)}=\sqrt{\frac{\hbar}{m_e^*(P,T)\omega_{os}(P),}} \tag{5}$$

In Eq. (1), H_R^j is the Hamiltonian term for Rashba SOI in presence of an external magnetic force field.

$$H_R^j=\frac{\alpha_R}{\hbar}\left(\overrightarrow{\sigma}\times\left(\overrightarrow{p}+e\overrightarrow{A}\right)\right) \tag{6}$$

where α_R the Rashba SOI factor and varied by the gate voltage.

When an external electric field in x-direction i.e., $\overrightarrow{E}=(0,\ 0,\ E)$ is applied to a quantum wire then the system's Hamiltonian transform from Eq. (1):

$$H_e=\frac{\left(p_x^2+\left(p_y+eBx\right)^2\right)}{2m_e^*(P,T)}+\frac{1}{2}m_e^*(P,T)\omega_{OS}^2(P)x^2+eEx+\frac{1}{2}gU_B\overrightarrow{\sigma}\bullet\overrightarrow{B}$$
$$+\frac{\alpha_R}{\hbar}\left(\sigma_x\left(p_y+eBx\right)-\sigma_y p_x\right). \tag{7}$$

Under translation, Hamiltonian remain unchanged along the wire and the Hamiltonian energy eigenstate is written as a solution of the plane wave as:

$$\Psi(x,y)=\varphi(x)\exp\left(ik_y y\right). \tag{8}$$

where k_y is the propagation constant for the plane wave in the y-direction. On substituting k_y instead of p_y, Reduces H_e into $H_e=H_e^j+H_R^j$ such that

$$H_e^j=\frac{p_x^2}{2m_e^*(P,T)}+\frac{1}{2}m_e^*(P,T)\omega^2(P)(x-x_i)^2-\frac{e^2E^2}{2m_e^*(P,T)\omega^2(P)}$$
$$+\frac{\omega_o^2(P)\hbar^2{k_y}^2}{\omega^2(P)2m_e^*(P,T)}-\frac{e^2EB\hbar k_y}{m_e^*(P,T)\omega^2(P)}+\frac{1}{2}gU_B\sigma_z B, \tag{9}$$

And

$$H_R^j=\alpha_R\left(\sigma_x\left(k_y+\frac{eBx}{\hbar}\right)-i\sigma_y\frac{d}{dx}\right) \tag{10}$$

where $\omega(P)=\sqrt{\omega_o^2(P)+\omega_c^2(P)}$ and $\omega_c(P)=\frac{eB}{m_e^*(P,T)}$ known as effective

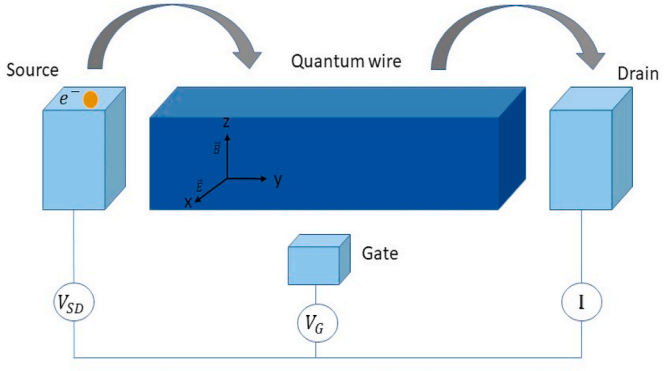

Fig. 1. Schematic view of the GaAs Quantum wire which is connected to drain and source reservoirs through tunnel barriers in the presence of electric and magnetic field.

cyclotron frequency and cyclotron frequency respectively and $x_i = -\left(\frac{eE}{m_e^*(P,T)\omega^2(P)} + \frac{eB\hbar k_y}{m_e^{*2}(P,T)\omega^2(P)}\right)$ the coordinate of the guiding centre for HO.

From Eq. (5), energy eigenvalues and eigenvectors of H_e^j are given as:

$$H_e^j \Psi_{n\sigma}(x) = E_{n\sigma}\Psi_{n\sigma}(x) \tag{11}$$

and

$$\Psi_{n\sigma}(x) = \frac{1}{\left(\sqrt{\pi}\, C_i 2^n n!\right)^{1/2}} H_n\left(\frac{x - x_i}{c_i}\right) exp\left(-\frac{1}{2}\left(\frac{x - x_i}{c_i}\right)^2\right)\chi_\sigma \tag{12}$$

With $C_i = \sqrt{\frac{\hbar}{m_e^*(P,T)\omega(P)}}$ is known characteristic length of the harmonic oscillator, n = 0, 1, 2 … and $\sigma = +$ or $-$. $H_n(x)$ is the Hermite polynomial and χ_σ is the spinor function for a spin down and spin up ($\chi_- = \begin{pmatrix} 0 \\ 1 \end{pmatrix}$ or $\chi_+ = \begin{pmatrix} 1 \\ 0 \end{pmatrix}$) respectively. The energies eigenvalues of Eq. (11) are

$$E_{n\sigma} = \hbar\omega\left(n + \frac{1}{2}\right) - \frac{e^2E^2}{2m^*(x,P,T)\omega_i^2} + \frac{\omega_o^2\hbar^2 k_y^{\,2}}{\omega_i^2 2m^*(x,P,T)} - \frac{e^2EB\hbar k_y}{m^*(x,P,T)\omega_i^2} + \frac{1}{2}g^*\mu_B B\sigma_z \tag{13}$$

As the lateral confining potential $l_o = \sqrt{\frac{\hbar}{m_e^*(P,T)\omega_o(P)}}$ defines by the length scale characterizing. Confining potential introduces energy scales $E_P = \hbar\omega_O(P)$ and Rashba SOI $\Delta_{SO} = \frac{m_e^*(P,T)\alpha^2}{2\hbar^2}$ The energy eigenvalues are shown in Fig. 2.

If we are expanding $\varphi(x) = \sum_{n\sigma} a_{n\sigma}\Psi_{n\sigma}(x)$, the Hamiltonian '$H_e$' eigenvalue equation can be written as:

$$\sum_{n\sigma} a_{n\sigma}(E_{n\sigma} - E)\Psi_{n\sigma}(x) + \sum_{n\sigma} a_{n\sigma}H_R^j\Psi_{n\sigma}(x) = 0, \tag{14}$$

$$(E_{n\sigma} - E)a_{n\sigma} + \sum_{n'\sigma'}\langle\Psi_{n\sigma}\left|H_R^j\right|\Psi_{n'\sigma'}\rangle = 0, \tag{15}$$

where the 2nd term of matrix elements of Eq. (11) is calculated as:

$$\langle n\sigma\left|H_R^j\right|n'\sigma'\rangle = \alpha\left[\left(1 - \frac{\omega_c^2(P)}{\omega^2(P)}\right)k_y - \frac{\omega_c(P)eE}{\hbar\omega^2(P)}\right]\delta_{n,n'}\delta_{\sigma,\sigma'} + \frac{\alpha}{c_i}\left[\left(\frac{\omega_c(P)}{\omega(P)} + \sigma\right)\sqrt{\frac{n+1}{2}}\,\delta_{n,n'-1} + \left(\frac{\omega_c(P)}{\omega(P)} - \sigma\right)\sqrt{\frac{n}{2}}\delta_{n,n'-1}\right]\delta_{\sigma,-\sigma}, \tag{16}$$

After diagonalization of Eq. (14), we obtain the eigenfunction, eigenvectors (shown in Fig. 3) and the energy dispersion of the subbands in GaAs QW for various values of pressure and temperature.

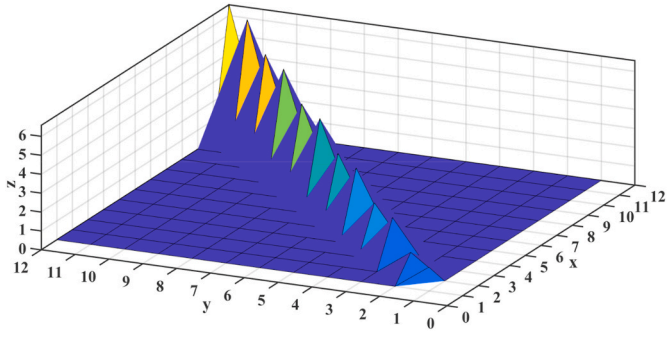

Fig. 2. Energy eigenvalues of GaAs QW when mass is dependent on pressure and temperature.

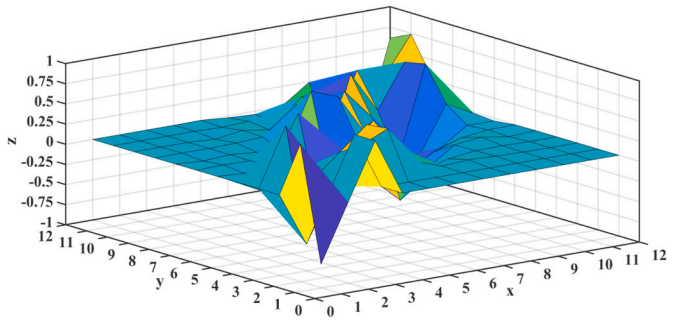

Fig. 3. Energy eigenvectors of GaAs QW when mass is dependent on pressure and temperature.

For the calculation of Ballistic conductance, we are using further a philosophized form of Landuer-B ü ttiker formula, which considers energy bands as erratic local exterior points and spin dependence is formulated as [39–42]

$$G' = \sum_{i,n} C_{i,n} f_o\left(\varepsilon_{i,k_n}\right), \tag{17}$$

where the aggregate is deliberated over the exterior points of all subbands. The quantity ε_{i,k_n} is the energy at the peak points $k_y = k_{i,n}$, $C_{i,n} = 1$ (or $C_{i,n}$ = -1) for a local energy extremum points for the given ith spin split subband. The association of physical conductance G with G' for spin-split subbands is given as

$$G = \left(\frac{2e^2}{h}\right)G'. \tag{18}$$

And G is known as ballistic conductance.

3. Result and discussion

Here, we have performed the numerical computation for GaAs Quantum wire with the mass dependence on temperature and pressure at the static electric field ($E = 0.6 \times 10^6$ V/m), magnetic field (B = 1 T) and Rashba SOI ($\alpha = 25$nm meV). In the residence of pressure and temperature in GaAs Quantum wire, we want to study the spectrum of the energies (in sec. A) and ballistic conductance's (G) behaviour (in sec. B) and we also demonstrate the energy dependence on external electric field (E), the intensity of magnetic field (B) and temperature of mass dependence at $k_y = 0$ (in sec. C).

3.1. *Section A. Energy spectra*

In this Sec., we focus on the energy dispersions curve for the various value of pressure and temperature. Fig. 4(a) shows the energy dispersion for 2 kbar pressure at temperature 300 K. In which there are some anti-crossing subbands structures (where solid line represents quasi spin-up state and dotted line presents quasi spin-down state) seen at lower energies state (n = 0,1) due to large value off-diagonal elements of Rashba spin-orbit contribution. And the separation between the subbands is non-uniform due to the effect of symmetric breaking when Rashba SOI and an intense magnetic field are applied at the same time [5]. Therefore, the contribution of magnetic field and Rashba SOI interaction gives rise to varying remarkable separation in spin-up and spin-down branches of the energy states. This separation is known as spin-orbit gap. The energy dispersion used in spintronics application for the confirmation of spin transport. This could be achieved either through direct detection of the spin current or through the detection of spin accumulation at the two ends of the device [43,44]. Fig. 4(b), there is shifting in two directions of energy dispersions due to the increment in the pressure from 2 kbar to 15 kbar. First is the laterally shift along the

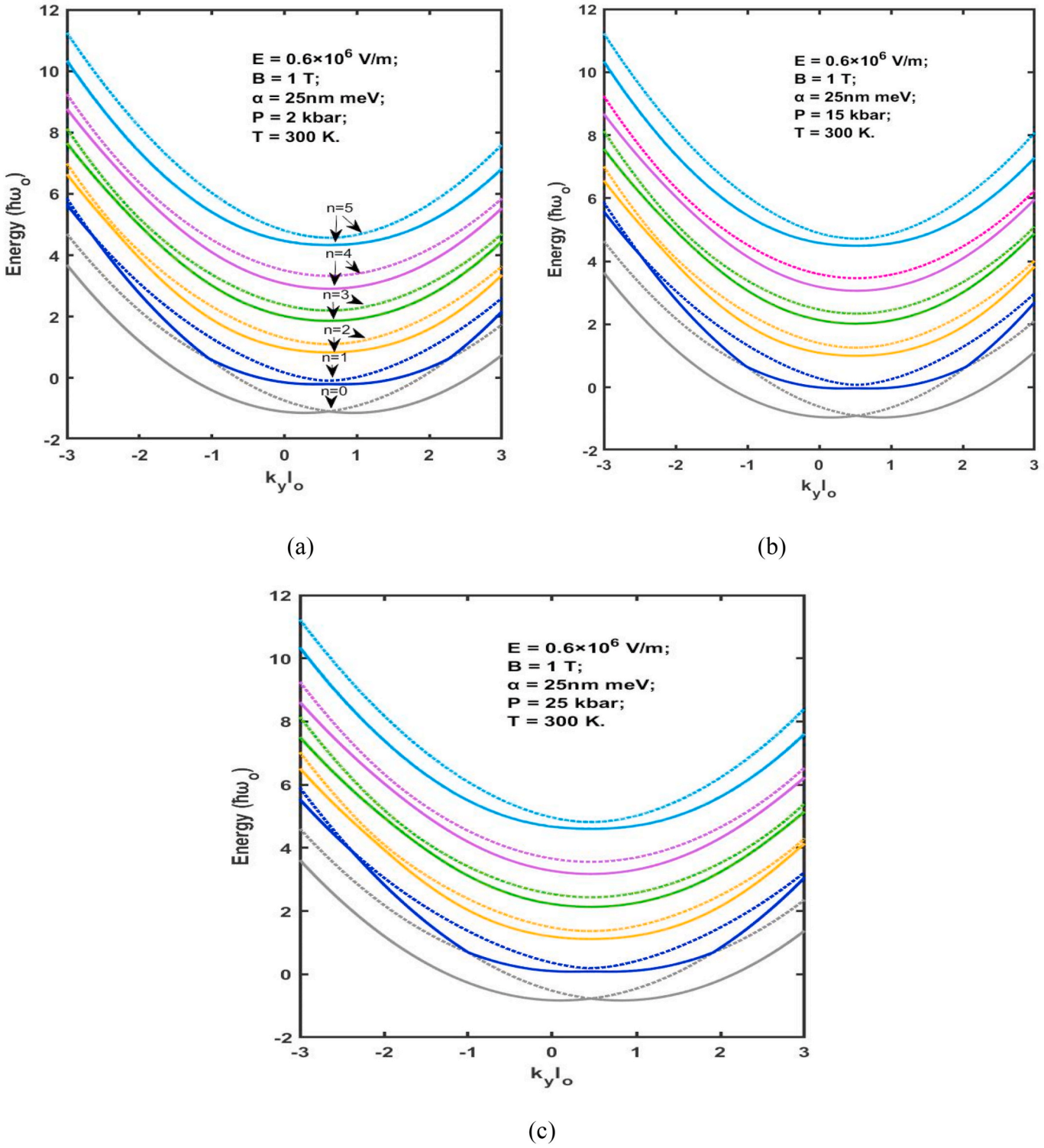

Fig. 4. Energy dispersion as a function of $k_y l_o$ potential at B = 1 T; E = 0.6 $\times 10^6$ V/m and Rashba SOI = 25 nm meV for (a) P = 2 kbar, (b) P = 15 kbar and (c) P = 25 kbar at temperature = 300 K.

negative $k_y l_o$ direction and the second shift in an upward direction (shown in Fig. 4(b)). As we increase the pressure by 25 kbar at temperature 100 K (shown in Fig. 4(c)), the shifting in the lateral direction and upward direction also increases. We observe from Fig. 4(a–c) that the energy spectrum shifts as the pressure increases. The reason for this shifting is the increase in the effective mass of the electron, Eq. (2), as the pressure increases. It is worth mentioning that by increasing the pressure, the wave function associated with the electron is more compressed and localized.

It is fruitful to examine the extent to which temperature and pressure of mass dependence interact to influence the system at this level. In Fig. 5, three energy dispersion curves are plotted for the distinct temperature at constant pressure (2 kbar). In the case of 300 K temperature (Fig. 5(a)), spin degeneracy is removed only for higher energies while intense anticrossing/crossings for states of least energy are visible. When the temperature rises from 300 K to 700 K, subbands get modified

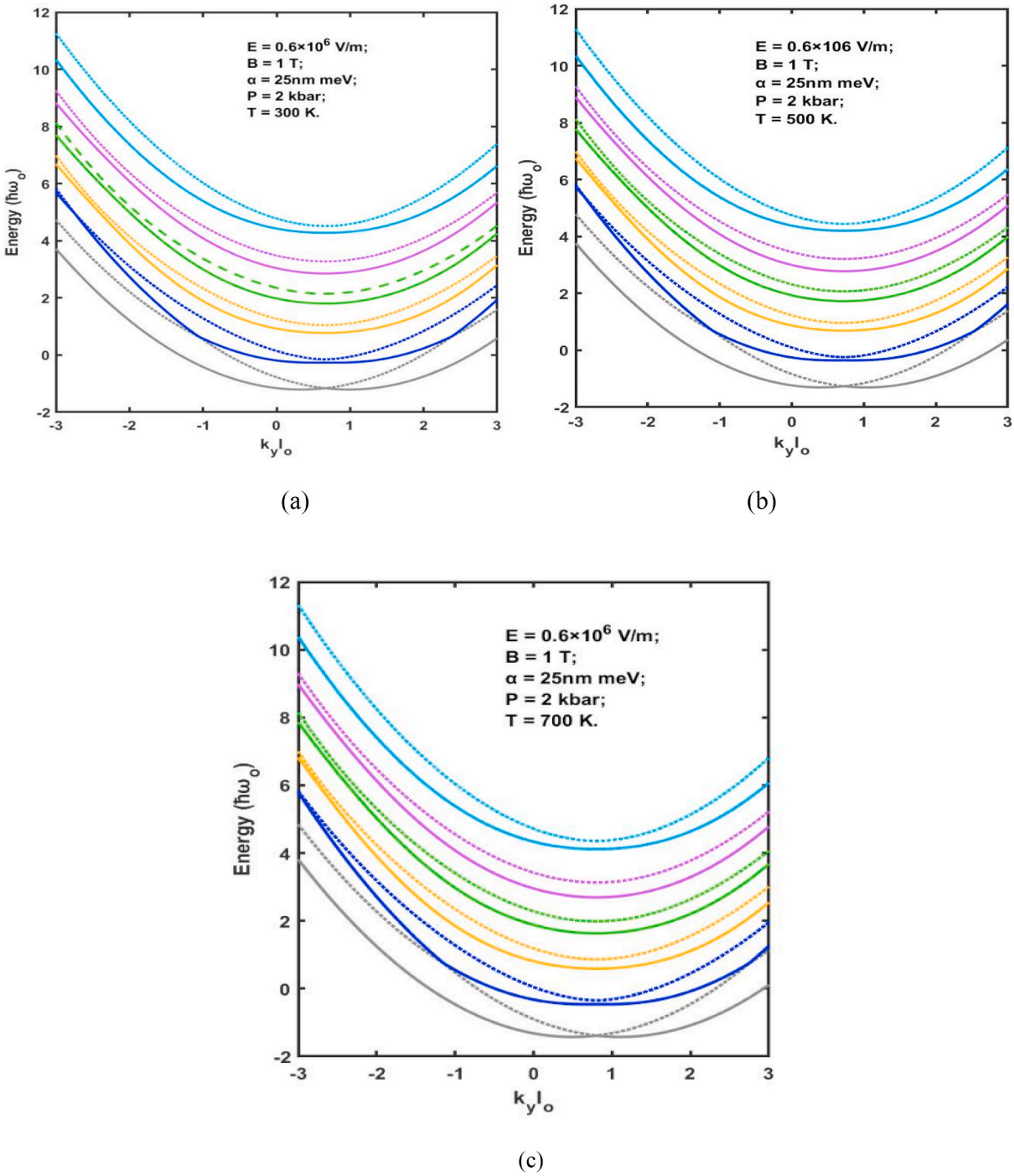

Fig. 5. Energy dispersion as a function of $k_y l_o$ at B = 1 T; E = 0.6 ×10^6 V/m and Rashba SOI = 25 nm meV (a) T = 300 K, (b) T = 500 K and (c) T = 700 K at Pressure = 2 kbar.

considerably by shifting in the downward direction and as well as in the lateral direction along the positive $k_y l_o$ axis (in Fig. 5(b-c)), the total shifting depends on the temperature values. Shifting is higher for a large value of the temperature of mass dependence.

3.2. ***Section B.*** *Ballistic conductance*

In this section, our aim is to find the impact of pressure and temperature on ballistic conductance. According to Landuer-B ü tter formalism, the conductivity of a ballistic GaAs quantum wire is associated with two electron reservoirs of macroscopic level (by ignoring the electron-electron reciprocation). And the extremum points in the energy subbands give rise to an increment or decrement in the conductance by $2e^2/h$. Increment in energy causes the opening of more propagating channels so the conductance steps up in the staircase shape. In Fig. 6 ballistic conductivity of GaAs quantum wire is related to chemical potential. When we apply pressure (2 kbar, 15 kbar and 25 kbar) the ballistic conductivity shows a stepwise increment. From Fig. 4(a–c) and Fig. 5(a–c), each minimum point and maximum point in the spectrum of energies provide increment and decrement of $2e^2/h$ to the ballistic conductance, respectively [39]. Each step in the ballistic conductance curve displays the 'turning on' of the latest mode called conducting

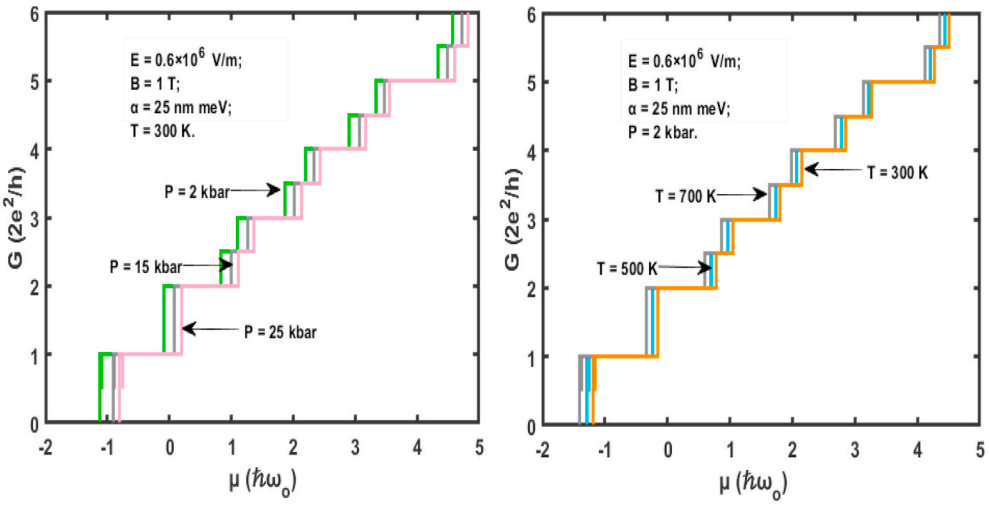

Fig. 6. Conductance (G) as a function of chemical potential (μ) for energy dispersions curve given in Fig. 4(a–c) and Fig. 5(a–c) respectively.

channel therefore an additional electron can move laterally. For designing modulators and spin filters, ballistic conductance offers a new approach. Each of the subbands contributes $2e^2/h$ to the conductance as a consequence of external field and conditions as observed in experimental research also e.g., in [45–47]The chemical potential grows as the energy bands are split; the first contribution in conductance comes from the lowest minimum in Fig. 4(a–c) and 5(a-c), and the second contribution comes when the chemical potential reaches the second minimum of the same subband. Whenever the chemical potential is further raised and passes through the local maximum point, the conductance will decrease by 2e2/h factor. The peaks in conductance are created by this mechanism, as shown in Fig. 6. Higher pressure requires higher chemical potential and it's vice-versa for temperature. The monotonic increasing characteristic is shown by the dips on ballistic conductance steps which are noticeable in energy spectra. This situation is more pronounced in lower energy states. When we differ in temperature and pressure then more than one extreme point is obtained in the energy state, as a result, narrow dips are induced in ballistic conductance steps (Fig. 6).

In Fig. 7, the variation of ballistic conductance with chemical potential is shown for two cases. Firstly, when temperature and pressure are 300 K and 2 kbar respectively. And secondly, when temperature and pressure both are zero. The ballistic conductance study helps in the manufacturing of electronic and spintronic devices and it also gives a new strategy for designing a spin filter [48].

3.3. *Section C. Energy as a function of E, B and temperature*

In Fig. 8, we imply that energy dispersion depends on the external electric field This is a sighting that negative and positive values of the external electrostatic field give rise to uniform structure and have the peak at zero electric fields. Furthermore, the subbands splitting inflate and all spin branches sink towards low energy states as the external field strength increases. This is evident that the system's efficacious configuration significantly alters the spectrum of energy. Consequently, in Fig. 9 we manifest the contrast of the energy subbands along the magnetic field and we observe that energies of all the spin branches increase when there is an increment in magnetic field intensity. Fig. 10 shows the energy dependence on the applied temperature for a lower energy state

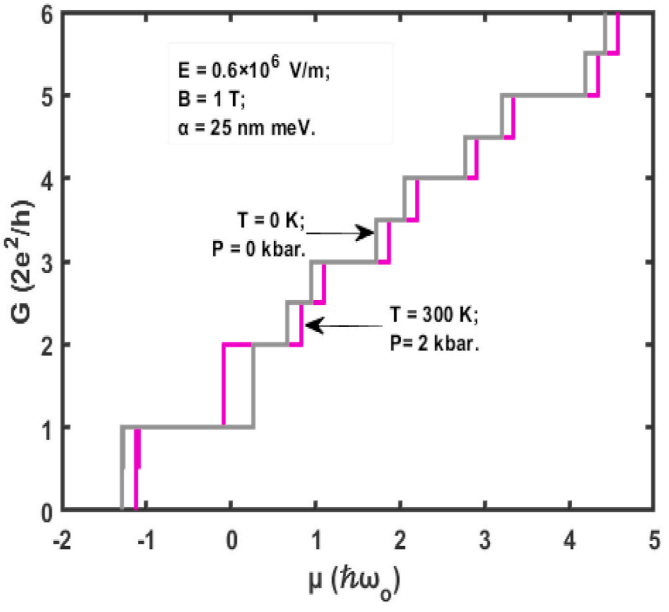

Fig. 7. Ballistic conductance as a function of chemical potential at B = 1 T; E = 0.6 $\times 10^6$ V/m and Rashba SOI = 25 nm meV when T = 0 K; P = 0 kbar and T = 300 K; P = 2 kbar.

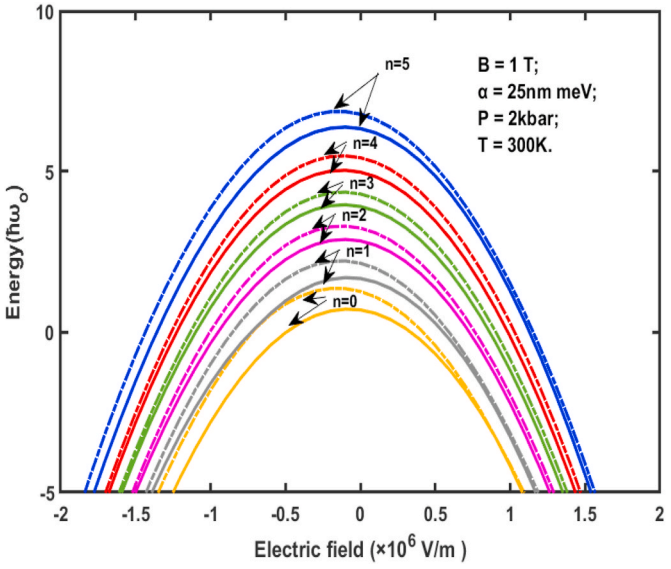

Fig. 8. The Energy dependence on the electric strength.

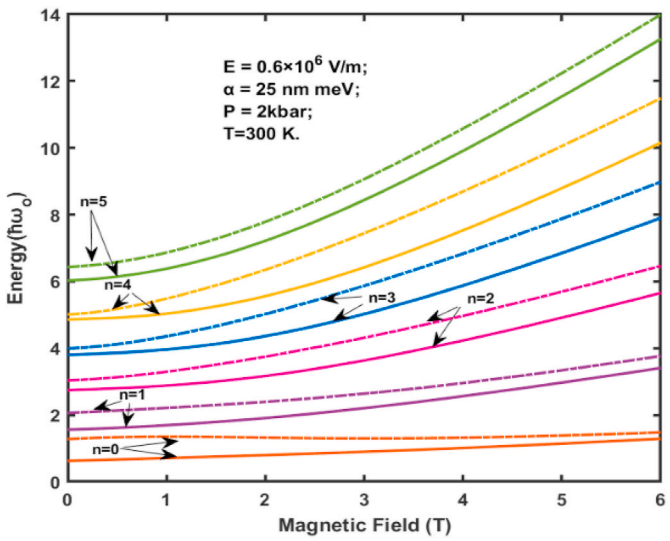

Fig. 9. The Energy dependence on the field magnetic field.

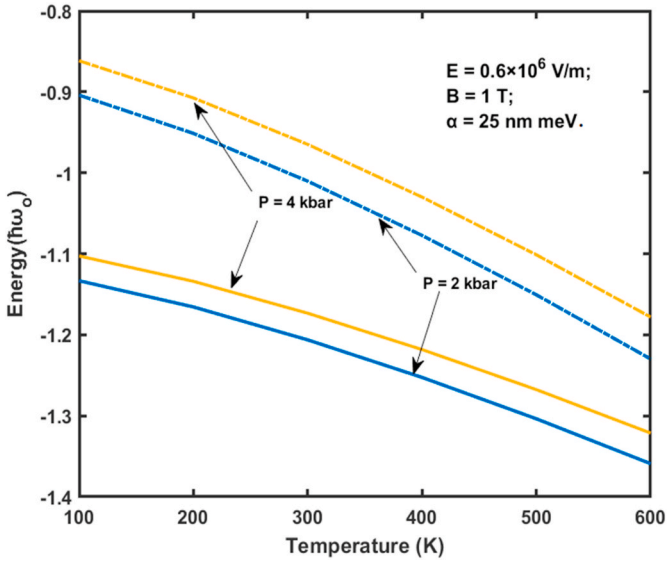

Fig. 10. The energy dependence on the temperature for lower energy state (n = 0).

(n = 0) at two fixed values of pressure of mass dependence i.e., 2 kbar and 4 kbar. We easily observe that the energy curves move towards lower energy states with a rise in the applied temperature of mass dependence. For pressure 4 kbar of mass dependence, the values of lower state energies are high as compared with energy values for pressure 2 kbar.

4. Conclusion

Hydrostatic pressure and temperature, the effect on the energy dispersions and ballistic conductance for a GaAs quantum wire is studied in this paper. The energy dispersions can be regulated by pressure and temperature of mass dependence according to the numerical results. Moreover, we conclude that ballistic conductance is sensitive to pressure and temperature of mass dependence. An anomaly is shown by the total conductance G for low energies due to the anticrossing of subbands. In addition, we study energy as a function of the external electric field, magnetic field and temperature of mass dependence which present regular patterns. In recent times, there are latest and enthralling viewpoints, as there is a logical relevance of conductance in topological insulators as well as Majorana fermions in hybrid superconductivity-semiconducting heterostructures, which are drawing attention enormously not merely in condensed matter community. In future, we assure prosperity in this area of investigation. The latest electronic and spin transport electronic devices will hold the market with a utility which will be associated with the physics of transport features. Alternatively, for the Majorana quasiparticle research case, conductance can overlay way for essential investigation for sake of inspecting unusual phenomenon which could be impressed by quantum simulators achieved in a system of solid state.

Credit author statement

Priyanka: Methodology, Software, Validation, Formal analysis, Data curation, Writing – original draft **Rinku Sharma**: Resources, Investigation, Supervision, Writing – review & editing, Project administration, **Manoj Kumar**: Conceptualization, Formal analysis, Writing – review & editing, Visualization.

Declaration of competing interest

The authors declare that they have no known competing financial interests or personal relationships that could have appeared to influence the work reported in this paper.

Data availability

No data was used for the research described in the article.

Acknowledgment

Priyanka acknowledges the financial support by University Grants Commission and R. Sharma is thankful to the Delhi Technological University for the research facilities. We are thankful to Professor Man Mohan for valuable discussions regarding this problem.

References

[1] J.C. Egues, G. Burkard, D. Loss, Rashba spin-orbit interaction and shot noise for spin-polarized and entangled electrons, Phys. Rev. Lett. 89 (2002), https://doi.org/10.1103/PhysRevLett.89.176401, 176401/1-176401/4.
[2] E.I. Rashba, A.L. Efros, Orbital mechanisms of electron-spin manipulation by an electric field, Phys. Rev. Lett. 91 (2003), https://doi.org/10.1103/PhysRevLett.91.126405.
[3] I. Žutić, J. Fabian, S. das Sarma, Spintronics: Fundamentals and Applications, 2004.
[4] P.T.T. Le, M. Yarmohammadi, Perpendicular electric field effects on the propagation of electromagnetic waves through the monolayer phosphorene, J. Magn. Magn Mater. 491 (2019), https://doi.org/10.1016/j.jmmm.2019.165629.
[5] P.T.T. Le, T.C. Phong, M. Yarmohammadi, β12-Borophene becomes a semiconductor and semimetal: via a perpendicular electric field and dilute charged impurity, Phys. Chem. Chem. Phys. 21 (2019) 21790–21797, https://doi.org/10.1039/c9cp04719k.
[6] P.T.T. Le, M. Davoudiniya, M. Yarmohammadi, Interplay of orbital hopping and perpendicular magnetic field in anisotropic phase transitions for Bernal bilayer graphene and hexagonal boron-nitride, Phys. Chem. Chem. Phys. 21 (2019) 238–245, https://doi.org/10.1039/c8cp05810e.
[7] S. Cao, C. Cao, S. Tian, J.H. Chen, Enhancement of spin-orbit coupling and magnetic scattering in hydrogenated graphene, Phys. Rev. B 104 (2021), https://doi.org/10.1103/PhysRevB.104.125422.
[8] H. Liu, T. Zhang, K. Wang, F. Gao, G. Xu, X. Zhang, S.X. Li, G. Cao, T. Wang, J. Zhang, X. Hu, H.O. Li, G.P. Guo, Gate-tunable spin-orbit coupling in a germanium hole double quantum dot, Phys Rev Appl 17 (2022), https://doi.org/10.1103/PhysRevApplied.17.044052.
[9] J. Sonehara, M. Kammermeier, D. Sato, D. Iizasa, U. Zülicke, S. Karube, J. Nitta, M. Kohda, Anisotropic spin dynamics in semiconductor narrow wires from the interplay between spin-orbit interaction and planar magnetic field, Phys. Rev. B 105 (2022), https://doi.org/10.1103/PhysRevB.105.094434.
[10] V.T. Pham, H. Yang, W.Y. Choi, A. Marty, I. Groen, A. Chuvilin, F.S. Bergeret, L. E. Hueso, I.v. Tokatly, F. Casanova, Large spin-charge interconversion induced by interfacial spin-orbit coupling in a highly conducting all-metallic system, Phys. Rev. B 104 (2021), https://doi.org/10.1103/PhysRevB.104.184410.
[11] M. Inglot, V.K. Dugaev, A. Dyrdał, J. Barnaś, Graphene with Rashba spin-orbit interaction and coupling to a magnetic layer: electron states localized at the

domain wall, Phys. Rev. B 104 (2021), https://doi.org/10.1103/PhysRevB.104.214408.
[12] H. Yang, Q. Wang, J. Fu, Interface involved Dresselhaus spin-orbit coupling in GaInAs/AlInAs heterostructures, Phys. Rev. B 104 (2021), https://doi.org/10.1103/PhysRevB.104.125426.
[13] S.M. Frolov, S. Lüscher, W. Yu, Y. Ren, J.A. Folk, W. Wegscheider, Ballistic spin resonance, Nature 458 (2009) 868–871, https://doi.org/10.1038/nature07873.
[14] Y. Sun, S.E. Thompson, T. Nishida, Physics of strain effects in semiconductors and metal-oxide-semiconductor field-effect transistors, J. Appl. Phys. 101 (2007), https://doi.org/10.1063/1.2730561.
[15] Y.A. Bychkov, E.I. Rashba, Phys. C (Amsterdam, Neth.): Solid State Phys. 17 6039 J. Phys. C: Solid State Phys (1984). http://iopscience.iop.org/0022-3719/17/33/015.
[16] D. Grundler, Ballistic spin-filter transistor, Phys. Rev. B Condens. Matter 63 (2001), https://doi.org/10.1103/PhysRevB.63.161307.
[17] S. Debald, B. Kramer, Rashba effect and magnetic field in semiconductor quantum wires, Phys. Rev. B Condens. Matter 71 (2005), https://doi.org/10.1103/PhysRevB.71.115322.
[18] R. Sharma M. Kumar Priyanka, Effects of impurity factor on the physical and transport properties for Ga1-xAlxAs quantum wire in the presence of Rashba spin-orbit interaction, Physica B (Amsterdam, Neth.) 629 (2022), https://doi.org/10.1016/j.physb.2021.413649.
[19] Y. Ho Park, H.J. Kim, J. Chang, S. Hee Han, J. Eom, H.J. Choi, H. Cheol Koo, Separation of Rashba and Dresselhaus spin-orbit interactions using crystal direction dependent transport measurements, Appl. Phys. Lett. 103 (2013), https://doi.org/10.1063/1.4855495.
[20] Y.v. Pershin, J.A. Nesteroff, V. Privman, Effect of spin-orbit interaction and in-plane magnetic field on the conductance of a quasi-one-dimensional system, Phys. Rev. B Condens. Matter 69 (2004), https://doi.org/10.1103/PhysRevB.69.121306.
[21] Y.v. Pershin, J.A. Nesteroff, V. Privman, Effect of spin-orbit interaction and in-plane magnetic field on the conductance of a quasi-one-dimensional system, Phys. Rev. B Condens. Matter 69 (2004), https://doi.org/10.1103/PhysRevB.69.121306.
[22] C.H.L. Quay, T.L. Hughes, J.A. Sulpizio, L.N. Pfeiffer, K.W. Baldwin, K.W. West, D. Goldhaber-Gordon, R. de Picciotto, Observation of a one-dimensional spin-orbit gap in a quantum wire, Nat. Phys. 6 (2010) 336–339, https://doi.org/10.1038/nphys1626.
[23] S. Zhang, R. Liang, E. Zhang, L. Zhang, Y. Liu, Magnetosubbands of semiconductor quantum wires with Rashba and Dresselhaus spin-orbit coupling, Phys. Rev. B Condens. Matter 73 (2006), https://doi.org/10.1103/PhysRevB.73.155316.
[24] F. Malet, M. Pi, M. Barranco, L. Serra, E. Lipparini, Exchange-correlation effects on quantum wires with spin-orbit interactions under the influence of in-plane magnetic fields, Phys. Rev. B Condens. Matter 76 (2007), https://doi.org/10.1103/PhysRevB.76.115306.
[25] F. Mireles, G. Kirczenow, Ballistic spin-polarized transport and Rashba spin precession in semiconductor nanowires, Phys. Rev. B Condens. Matter 64 (2001), https://doi.org/10.1103/PhysRevB.64.024426.
[26] F. Ungan, R.L. Restrepo, M.E. Mora-Ramos, A.L. Morales, C.A. Duque, Intersubband optical absorption coefficients and refractive index changes in a graded quantum well under intense laser field: effects of hydrostatic pressure, temperature and electric field, Physica B (Amsterdam, Neth.) 434 (2014) 26–31, https://doi.org/10.1016/j.physb.2013.10.053.
[27] Z. Zeng, C.S. Garoufalis, S. Baskoutas, G. Bester, Electronic and optical properties of ZnO quantum dots under hydrostatic pressure, Phys. Rev. B Condens. Matter 87 (2013), https://doi.org/10.1103/PhysRevB.87.125302.
[28] B.S. Ma, X.D. Wang, F.H. Su, Z.L. Fang, K. Ding, Z.C. Niu, G.H. Li, Photoluminescence from self-assembled long-wavelength InAs/GaAs quantum dots under pressure, J. Appl. Phys. 95 (2004) 933–938, https://doi.org/10.1063/1.1635988.
[29] L. Bouzaïene, R. ben Mahrsia, M. Baira, L. Sfaxi, H. Maaref, Hydrostatic pressure and temperature effects on nonlinear optical rectification in a lens shape InAs/GaAs quantum dot, J. Lumin. 135 (2013) 271–275, https://doi.org/10.1016/j.jlumin.2012.09.032.
[30] F. Segovia-Chaves, H. Vinck-Posada, The effect of the hydrostatic pressure and temperature on the defect mode in the band structure of one-dimensional photonic crystal, Optik 156 (2018) 981–987, https://doi.org/10.1016/j.ijleo.2017.12.037.
[31] L. Bouzaiene, H. Alamri, L. Sfaxi, H. Maaref, Simultaneous effects of hydrostatic pressure, temperature and electric field on optical absorption in InAs/GaAs lens shape quantum dot, J. Alloys Compd. 655 (2016) 172–177, https://doi.org/10.1016/j.jallcom.2015.09.181.
[32] W. Xie, Hydrostatic pressure and temperature effects of an excitondonor complex in quantum dots, Physica B (Amsterdam, Neth.) 407 (2012) 1134–1138, https://doi.org/10.1016/j.physb.2012.01.100.
[33] A. Sivakami, M. Mahendran, Hydrostatic pressure and temperature dependence of correlation energy in a spherical quantum dot, Superlattice. Microst. 47 (2010) 530–537, https://doi.org/10.1016/j.spmi.2009.12.010.
[34] J. Knobbe, T. Schäpers, Magnetosubbands of semiconductor quantum wires with Rashba spin-orbit coupling, Phys. Rev. B Condens. Matter 71 (2005), https://doi.org/10.1103/PhysRevB.71.035311.
[35] G. Rezaei, S. Shojaeian Kish, Linear and nonlinear optical properties of a hydrogenic impurity confined in a two-dimensional quantum dot: effects of hydrostatic pressure, external electric and magnetic fields, Superlattice. Microst. 53 (2013) 99–112, https://doi.org/10.1016/j.spmi.2012.09.014.
[36] E. Kasapoglu, F. Ungan, H. Sari, I. Sökmen, The hydrostatic pressure and temperature effects on donor impurities in cylindrical quantum wire under the magnetic field, Physica E Low Dimens Syst Nanostruct 42 (2010) 1623–1626, https://doi.org/10.1016/j.physe.2010.01.009.
[37] M.G. Barseghyan, A. Hakimyfard, S.Y. López, C.A. Duque, A.A. Kirakosyan, Simultaneous effects of hydrostatic pressure and temperature on donor binding energy and photoionization cross section in Pöschl-Teller quantum well, Physica E Low Dimens Syst Nanostruct 42 (2010) 1618–1622, https://doi.org/10.1016/j.physe.2010.01.008.
[38] U. Yesilgul, S. Şakiroğlu, E. Kasapoğlu, H. Sari, I. Sökmen, The effects of temperature and hydrostatic pressure on the photoionization cross-section and binding energy of impurities in quantum-well wires, Superlattice. Microst. 48 (2010) 106–113, https://doi.org/10.1016/j.spmi.2010.04.003.
[39] R. Arulmozhi, A.J. Peter, C.W. Lee, Optical absorption in a CdS/CdSe/CdS asymmetric quantum well, Chem. Phys. Lett. 742 (2020), https://doi.org/10.1016/j.cplett.2020.137129.
[40] Y.v. Pershin, J.A. Nesteroff, V. Privman, Effect of spin-orbit interaction and in-plane magnetic field on the conductance of a quasi-one-dimensional system, Phys. Rev. B Condens. Matter 69 (2004), https://doi.org/10.1103/PhysRevB.69.121306.
[41] B.H. Mehdiyev, A.M. Babayev, S. Cakmak, E. Artunc, Rashba spin-orbit coupling effect on a diluted magnetic semiconductor cylinder surface and ballistic transport, Superlattice. Microst. 46 (2009) 593–602, https://doi.org/10.1016/j.spmi.2009.08.009.
[42] G. Gumbs, A. Balassis, D. Huang, Energy bands, conductance, and thermoelectric power for ballistic electrons in a nanowire with spin-orbit interaction, J. Appl. Phys. 108 (2010), https://doi.org/10.1063/1.3493113.
[43] C.H.L. Quay, T.L. Hughes, J.A. Sulpizio, L.N. Pfeiffer, K.W. Baldwin, K.W. West, D. Goldhaber-Gordon, R. de Picciotto, Observation of a one-dimensional spin-orbit gap in a quantum wire, Nat. Phys. 6 (2010) 336–339, https://doi.org/10.1038/nphys1626.
[44] T. Koga, J. Nitta, T. Akazaki, H. Takayanagi, Rashba spin-orbit coupling probed by the weak antilocalization analysis in [formula presented] quantum wells as a function of quantum well Asymmetry, Phys. Rev. Lett. 89 (2002), https://doi.org/10.1103/PhysRevLett.89.046801.
[45] S. Kumar, K.J. Thomas, L.W. Smith, M. Pepper, G.L. Creeth, I. Farrer, D. Ritchie, G. Jones, J. Griffiths, Many-body effects in a quasi-one-dimensional electron gas, Phys. Rev. B Condens. Matter 90 (2014), https://doi.org/10.1103/PhysRevB.90.201304.
[46] B.H. Mehdiyev, A.M. Babayev, S. Cakmak, E. Artunc, Rashba spin-orbit coupling effect on a diluted magnetic semiconductor cylinder surface and ballistic transport, Superlattice. Microst. 46 (2009) 593–602, https://doi.org/10.1016/j.spmi.2009.08.009.
[47] C.H.L. Quay, T.L. Hughes, J.A. Sulpizio, L.N. Pfeiffer, K.W. Baldwin, K.W. West, D. Goldhaber-Gordon, R. de Picciotto, Observation of a one-dimensional spin-orbit gap in a quantum wire, Nat. Phys. 6 (2010) 336–339, https://doi.org/10.1038/nphys1626.
[48] Conductance for a Quantum Wire with Weak Rashba Spin-Orbit Coupling, 2005. http://iopscience.iop.org/0256-307X/22/12/049.

173 (2023) 207451

Contents lists available at ScienceDirect

Micro and Nanostructures

journal homepage: www.journals.elsevier.com/micro-and-nanostructures

Hydrogenic impurity effect on the optical properties of $Ga_{1-x}Al_xAs$ quantum wire under terahertz field

Priyanka [a], Rinku Sharma [a,*], Manoj Kumar [b,**], Pradumn Kumar [c]

[a] Department of Applied Physics, Delhi Technological University, Delhi, 110042, India
[b] Department of Physics, Govt. College for Women, Jind, 126102, India
[c] Department of Physics, University of Delhi, Delhi, 110021, India

ARTICLE INFO

Keywords:
Impurity factor
Quantum wire
Optical absorption coefficients
Second harmonic generation
Third harmonic generation

ABSTRACT

In this study, the effect of impurity factor on the optical absorption coefficients, refractive index changes, second harmonic generation, and third-harmonic generation for the intersubband transitions is explored between the electronic states of $Ga_{1-x}Al_xAs$ quantum wire initiated by the symmetric parabolic potential. The system is conquered by the presence of an intense electric field, magnetic field, and Rashba spin-orbit interaction. For the linear and non-linear optical absorption coefficients, refractive index, second harmonic generation, and third harmonic generation coefficient, the analytical expressions are obtained with the assistance of the compact density-matrix approach. The arithmetical outcomes illustrate the optical properties are significantly intuitive to the concentration of impurity and can be controlled by this parameter. The variation in the magnitude and position of peaks via impurity factor indicates the opportunity in the mechanism of optical non-linearity in the quantum wire and also, helps in the optical non-linearity tuning which has device application.

1. Introduction

In the few last years, low-dimensional nanostructures like: quantum dots, quantum wires, and quantum well have considerable devotion for their alluring potential applications in optical and laser technology [1–5]. In these nanostructures, the charge carrier having quantum confinement accompany the formation of energy states in the discrete form and enhance the density of states at definite energies which leads to variation in the optical spectra and helps in the evolution of novel properties. The optical properties viz. absorption spectra and refractive index changes (RICs) in the low-dimensional nanostructures take fascinated courtesy due to their high-level performance. One of the most arduously explored low-dimension nanostructures is quantum wire, especially in the theoretical and experimental research of the impurity effect on their optical properties [6–13]. Moreover, the tunability of the energy dispersion by the intense magnetic field, electric field, impurity factor, and Rashba spin-orbit interaction in the quantum wire has made a fruitful role in examining non-linear and linear properties for applications of novel devices [14,15].

A region of large potency is the spin-based phenomena in quantum wire for its profusion of the physically observable phenomena and has an encouraging future for spin-related electronic devices with a high degree of functionality, fast speed, and low power consumption [16–18]. Fortunately, spin physics in low-dimension nanostructures utilizes electron spin degree of freedom as a chunk of

* Corresponding author.
** Corresponding author.
E-mail addresses: rinkusharma@dtu.ac.in (R. Sharma), manojmalikdu@gmail.com (M. Kumar).

https://doi.org/10.1016/j.micrna.2022.207451
Received 26 August 2022; Received in revised form 9 November 2022; Accepted 17 November 2022
Available online 26 November 2022
2773-0123/© 2022 Published by Elsevier Ltd.

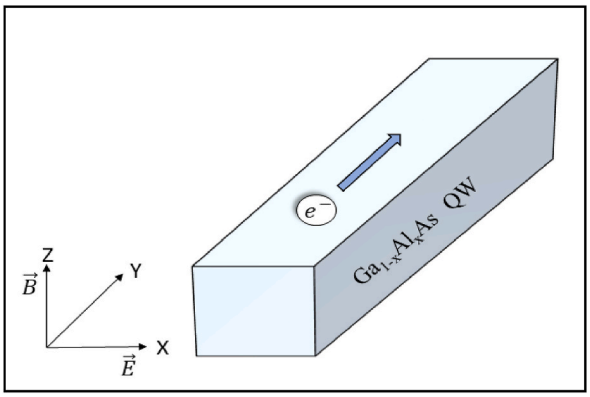

Fig. 1. The diagram of $Ga_{1-x}Al_xAs$ quantum wire within the existence of an external magnetic electric field, and Rashba SOI.

information instead of an electron-charge and assurance potential for imminent spin-based application devices that are smaller, faster, and more influential ergo those that are presently available. Specifically, the spin-orbit interaction (SOI) has fascinated enthusiasm as it permits optical spin detection and spin orientation. Moreover, SOI is assumed as an opportunity for controlling and manipulating the state of an electron via gate voltage. The type of SOI, eminent in a certain quantum wire heterostructure is the Rashba SOI. The Rashba SOI comes out in the picture due to the confinement potential which explains the quantum wire is a function perpendicular to the 2-dimension electron gas (2 DEG). This conjectures a structural inversion symmetry that easily can be tweaked by the external gate potential and also control the spin-related phenomena [19–23].

Although more study has been admiring to research the effect of Rashba SOI on the optical and physical properties of the quantum wire. The optical properties have been explored by lots of investigators in both theoretical and experimental [24–34]. Some external constraints like the intense electric field, magnetic field, Rashba SOI, impurity factor (x), etc play a significant role to influence the optical properties of quantum wire [35–38]. M. Santhi et al. [39] have vastly explored the effects of hydrogenic impurity on the linear and third-order nonlinear optical absorption coefficients (ACs), and third harmonic generation (THG) optical properties of GaAs/-GaAlAs quantum wire. However, when the electron is bound with the impurity atom within the presence of external perturbations shows rudimental character in grasping the electro-optical properties of hydrogenic impurities in nanostructures. The inclusion of hydrogenic impurities in nanostructures will excessively change the electrical and optical properties and affect the quantum device concert.

Martinez et al. [40] have explored the hydrostatic pressure and temperature effects on the hydrogenic impurity which relates cross-section of photoionization and impurity binding energy in $Ga_{1-x}Al_xAs/GaAs$ quantum wire. Zeiri et al. [41] discussed the linear and nonlinear susceptibility of self-organized in $GaN/Ga_{1-x}Al_xN$ quantum wire. Embroidering the energy dispersion is enthusiastic to yield the expedient optoelectronic device from the belief of confinement in the low-dimension nanostructures, transmission properties, and tunable emission are assumed to be significant features for them. Moreover, the optical properties are studied by many researchers.

With this motivation, the current work aims to represent the behavior of linear and third-order nonlinear optical (ACs), an absolute change in refractive index coefficients (RICs), second harmonic generation (SHG), and THG associated with the $Ga_{1-x}Al_xAs$ Quantum wire. The following is the work's alignment: In a nutshell, Section 2 represents the theoretical model of our system. The corresponding outcomes and discussion are noted in Section 3. Belatedly, Section 4 covers the study's foremost conclusions.

2. Theory

The Hamiltonian equation for $Ga_{1-x}Al_xAs$ quantum wire (shown in Fig. 1) under the influence of electric field (**E**) along X-direction, intense magnetic field (**B**) along Z-direction, and Rashba SOI, respectively is written by:

$$\widehat{H}_{oe} = -\frac{1}{2m_{e^*}(x,P,T)}(p_X + (p_Y + eBX)^2 + \frac{1}{2}m_{e^*}(x,P,T)\omega_{1e}^2 X^2 + eEX + \frac{1}{2}g^*\mu_B B\sigma_Z + \frac{\alpha}{\hbar}[\sigma_x(p_Y + eBX) - \sigma_Y p_X)] \quad (1)$$

Where p_X and p_Y represents the momentum component of an electron in X and Y direction. ω_{1e} is called effective cyclotron frequency. $\alpha,\ g^*, \mu_B, \sigma_X, \sigma_Y,$ and σ_z are known as Rashba SOI factor, Lande factor, Bohr magneton and Pauli matrices along x, y and z direction, respectively. $m_{e^*}(x,P,T)$ is known effective mass represented by [22]:

$$m_{e^*}(x,P,T) = m_o[(\frac{1}{\Delta_{oj}(x) + E_g^j(x,P,T)} + \frac{2}{E_g^j(x,P,T)})\frac{\Pi_j^2(x)}{3} + \delta_j(x) + 1]^{-1} \quad (2)$$

Here, m_o is known as free electron mass, x is used for impurity factor, $\Delta_{oj}(x)$ and $\Pi_j(x)$ are known as valence band spin-orbit coupling and inter-band matrix element, respectively $(\Pi_j^2(x) = (-6290x + 28900)meV$ and $\Delta_{oj}(x) = (-66x + 341)meV)$. When the remote-band effects are examined over $\delta_j(x)$ the parameter is given by Ref. [42]:

$$\delta_j(x) = 4.938x^2 + 0.488x - 3.935 \tag{3}$$

In eq. (2), $E_g{}^j(x, P, T)$ is called conduction band's an energy gap and is expressed via

$$E_g{}^j(x, P, T) = p_j + q_j x + r_j x^2 + s_j P - \frac{\beta_j T^2}{\gamma_j + T} \tag{4}$$

where the parameters' values $p_j, q_j, r_j, s_j, \gamma_j$and β_j are given by 1519.4 meV, 1360 meV, 220 meV, 10.7 meV/kbar, 204 K and 0.5405 meV/K, respectively. And the values of these parameters are determined with the assistance of photoluminescence.

Eq. (1) can be rewritten as write $\widehat{H}_{oe} = \widehat{H}_i + \widehat{H}_R$, where

$$\widehat{H}_i = -\frac{p_X^2}{2m_e{}^*(x, P, T)} + \frac{1}{2}m_e{}^*(x, P, T)\omega_{1e}^2(X - X_{oe})^2 - \frac{e^2E^2}{2m_e{}^*(x, P, T)\omega_{1e}{}^2} + \frac{\omega_o^2\hbar^2k_y{}^2}{\omega_{1e}{}^2 2m_e{}^*(x, P, T)} - + \frac{1}{2}g^*\mu_B B\sigma_Z \tag{5}$$

and

$$\widehat{H}_R = \alpha(\sigma_X(k_y + \frac{eBX}{\hbar}) - i\sigma_Y\frac{d}{dX}) \tag{6}$$

Where $X_{oe} = -(\frac{eE}{m_e{}^*(x,P,T)\omega_1{}^2} + \frac{eB\hbar k_y}{m_e{}^{*2}(x,P,T)\omega_1{}^2})$ is recognized as guiding centre coordinate.

For the complete solution within the presence of external fields and Rashba SOI. As a consequence of complex coupling in the $\widehat{H}_{oe}$, we assume that there is no analytic solution of the Schrödinger can be comes out, aside from the some trival limits. Consequently, we must solve the Schrödinger equation numerically to achieve an insight about the interplay of SOI. So, expanding the $\varphi(x) = \sum_{n\sigma} a_{n\sigma}\Psi_{n\sigma}(x)$, the Hamiltonian '$H_{oe}$' eigenvalue equation can be written as:

$$\sum_{n\sigma} a_{n\sigma}(E_{n\sigma} - E)\Psi_{n\sigma}(x) + \sum_{n\sigma} a_{n\sigma}\Psi_{n\sigma}(x) = 0 \tag{7}$$

$$(E_{n\sigma} - E)a_{n\sigma} + \sum_{n'\sigma'}\langle\Psi_{n\sigma}\,\widehat{H}_R\Psi_{n'\sigma'}\rangle = 0 \tag{8}$$

where the matrix elements' 2nd term of Eq. (8) is calculated as:

$$\langle n\sigma\widehat{H}_R n'\sigma'\rangle = \alpha[(1 - \frac{\omega_c^2}{\omega_{1e}{}^2})k_y - \frac{\omega_c eE}{\hbar\omega_{1e}{}^2}]\delta_{n,n'}\delta_{\sigma,\sigma'} + \frac{\alpha}{c_i}[(\frac{\omega_c}{\omega_{1e}} + \sigma)\sqrt{\frac{n+1}{2}}\,\delta_{n,n'-1} + (\frac{\omega_c}{\omega_{1e}} - \sigma)\sqrt{\frac{n}{2}}\delta_{n,n'-1}]\delta_{\sigma,-\sigma} \tag{9}$$

Now, our problem reduces to finding an appropriate numerical procedure for finding the various quantum states. The energies eigenvalues and their corresponding eigenvectors are obtained, and we can apply the analytical expressions via the perturbation method and density matrix approach for optical ACs, RICs and THG. For calculating these optical properties, we assume a circularly polarised electromagnetic (EM) field having incident photon frequency (ω) along the Z-direction, then the interaction within the system is given by [43,44]

$$\mathbf{E}(t') = \frac{E_0(t')}{\sqrt{2}}(\widehat{e}_X \pm \widehat{e}_Y) \tag{10}$$

Here, the terms $\widehat{e}_X$ and $\widehat{e}_Y$ represents unit vector for X and Y directions respectively, and $E_0(t')$ is

$$E_0(t') = E_0\cos(\omega t') = \widetilde{E}e^{-\omega t'} + \widetilde{E}e^{\omega t'} \tag{11}$$

Therefore, the system is excited through an electromagnetic field. By applying, the Bloch theorem for symmetry, for $\Psi_{nm,k}$ and $\Psi_{n'm',q'}$ states the dipole transition moment can be written

$$\langle\Psi_{nm,k}\,qX\Psi_{n'm',k'}\rangle = \delta_{k,k'}\langle\varphi_{n,m}qX\varphi_{n',m'}\rangle \tag{12}$$

Where δ is known as the Kronecker delta function.

With the help of a compact iterative procedure and density-matrix method, we will drive the mien of THG susceptibility for the 2D model of the isotropic harmonic oscillator. The term $\overline{\rho}$ represents the electron density matrix. And the time-dependent Liouville-equation is

$$\frac{\partial\overline{\rho}_{ij}}{\partial t} = \frac{1}{i\hbar}[H_o - qXE(t'), \overline{\rho}]_{ij} - \lceil_{ij}(\overline{\rho} - \overline{\rho}^{(o)})_{ij} \tag{13}$$

$\overline{\rho}^{(o)}$ is known as a density-matrix operator for an unperturbed system, $\lceil_{ij}$ called as phenomenological operator. It is hypothesized that $\lceil_{ij}$ is a diagonal matrix known as relaxation rate. Equation (13) can be resolved with the help of the standard iterative method [45] then

$$\overline{\rho}(t^{'}) = \sum_{n} \overline{\rho}^{(n)}(t^{'}) \tag{14}$$

with

$$\frac{\partial \overline{\rho}^{(n+1)}}{\partial t^{'}} = \frac{1}{i\hbar}\{[H_o, \overline{\rho}^{(n+1)}]_{ij} - i\hbar\lceil_{ij}\overline{\rho}_{ij}^{(n+1)}\} - \frac{1}{i\hbar}[qr, \overline{\rho}^{(n)}]_{ij}E(t^{'}) \tag{15}$$

The system's electronic polarization can also be expanded phenomenologically as an electric field series. Therefore, the three orders of electronic polarization P ($t^{'}$) are expressed by

$$P(t^{'}) = (\varepsilon_o\chi_{\omega}^{(1)}\widetilde{E}e^{-i\omega t^{'}} + \varepsilon_o\chi_o^{(2)}|\widetilde{E}|^2 + \varepsilon_o\chi_{2\omega}^{(2)}\widetilde{E}^2e^{-2i\omega t^{'}} + \varepsilon_o\chi_{3\omega}^{(3)}|\widetilde{E}|^2\widetilde{E}e^{-i\omega t^{'}} + \varepsilon_o\chi_{3\omega}^{(3)}\widetilde{E}^3e^{-3i\omega t^{'}}) + c.c. \tag{16}$$

Where $\chi_{\omega}^{(1)}, \chi_{2\omega}^{(2)}, \chi_o^{(2)}$ and $\chi_{3\omega}^{(3)}$ are the linear susceptibility, SHG, optical rectification, and THG, respectively. The ε_o is known as Vacuum dielectric constant. For nth-order electronic polarization is written by

$$P^{(n)}(t^{'}) = \frac{1}{V}Tr(\overline{\rho}^{(n)}qr) \tag{17}$$

The term V is used for volume of interaction and Tr (trace) represents the summation over diagonal elements of the matrix $\overline{\rho}$ qX. The trace (Tr) and susceptibility χ (ω) are correlated to absorption coefficient α (ω):

$$\alpha(\omega) = \omega\sqrt{\frac{\mu}{\varepsilon_r}}Im[\varepsilon_o\chi\ (\omega)] \tag{18}$$

Where ε_o and μ is known as the real part of the relative permittivity (ε_r) and permeability, respectively. Now, the linear and non-linear optical AC expression can be written as [46–49];

$$\alpha^{(1)}(\omega) = \hbar\omega\sqrt{\frac{\mu}{\varepsilon_r}}\ \frac{N_c\Gamma_{if}|M_{if}|^2}{\hbar^2\{(\omega_{fi}-\omega)^2 + {\Gamma_{if}}^2\}} \tag{19}$$

and

$$\alpha^{(3)}(\omega, I) = -\hbar\omega\sqrt{\frac{\mu}{\varepsilon_r}}\ \frac{I}{2\varepsilon_o n_r c} \times \frac{4N_c\Gamma_{if}|M_{if}|^2}{\hbar^4\{(\omega_{fi}-\omega)^2 + {\Gamma_{if}}^2\}} \times$$

$$[\frac{|M_{if}|^2}{(\omega_{fi}-\omega)^2 + {\Gamma_{if}}^2} + \frac{(M_{ff}-M_{ii})^2(3{\omega_{fi}}^2 - 4\omega_{fi}\omega)(\omega_{fi}^2 - \Gamma_{if}^2)}{4(\omega_{fi}^2 + \Gamma_{if}^2)\{(\omega_{fi}-\omega)^2 + {\Gamma_{if}}^2\}}] \tag{20}$$

In eq. (11), $\hbar\omega$ and I are the energy of incident photon and intensity of incident light respectively, N_c is the carrier density and n_r represents the refractive index of quantum wire material, Γ_{if} is called relaxation time & the subscript *i* and *f* are used for initial and final states. $\omega_{if} = (E_f - E_i)/\hbar$ is known as transition frequency (where, E_i and E_f is the energy for the initial and final state). M_{if} is known as transition matrix element and determined by $M_{if} = |\langle\varphi_i X\varphi_f\rangle|$.

The total optical absorption coefficient is written as [50–52].

$$\alpha_T(\omega, I) = \alpha^{(1)}(\omega) + \alpha^{(3)}(\omega, I) \tag{21}$$

The linear and third-order nonlinear refractive index for optical transitions are obtained by

$$\frac{\Delta n_r^{(1)}}{n_r} = \frac{N_c}{2n_r^2\varepsilon_o}\ \frac{|M_{if}|^2(\omega_{fi}-\omega)}{\hbar\{(\omega_{fi}-\omega)^2 + {\Gamma_{if}}^2\}} \tag{22}$$

$$\frac{\Delta n_r^{(3)}(\omega, I)}{n_r} = \frac{N_c}{2{n_r}^3\varepsilon_o}\ \frac{I\mu c|M_{if}|^2(\omega_{fi}-\omega)}{\hbar^3(\omega_{fi}-\omega)^2 + \Gamma_{if}^2} \times$$

$$[\frac{|M_{if}|^2}{(\omega_{fi}-\omega)^2 + \Gamma_{if}^2} + \frac{2\Gamma_{if}(M_{ff}-M_{ii})}{(\omega_{fi}-\omega)^2 + \Gamma_{if}^2} \times \{(\omega_{fi}-\omega)[\omega_{fi}(\omega_{fi}-\omega) + \Gamma_{if}^2] - \Gamma_{if}^2(2\omega_{fi}-\omega)\}] \tag{23}$$

The total refractive index is

$$\frac{\Delta n_r(\omega, I)}{n_r} = \frac{\Delta n_r^{(1)}}{n_r} + \frac{\Delta n_r^{(3)}(\omega, I)}{n_r} \tag{24}$$

And now, we focus on the SHG and THG (i.e., from the term of oscillating with 4 ω, we only cogitate the third-order contribution). With the help of the iterative method and compact density-matrix approach, the SHG and THG per unit volume are given as [12,53,54];

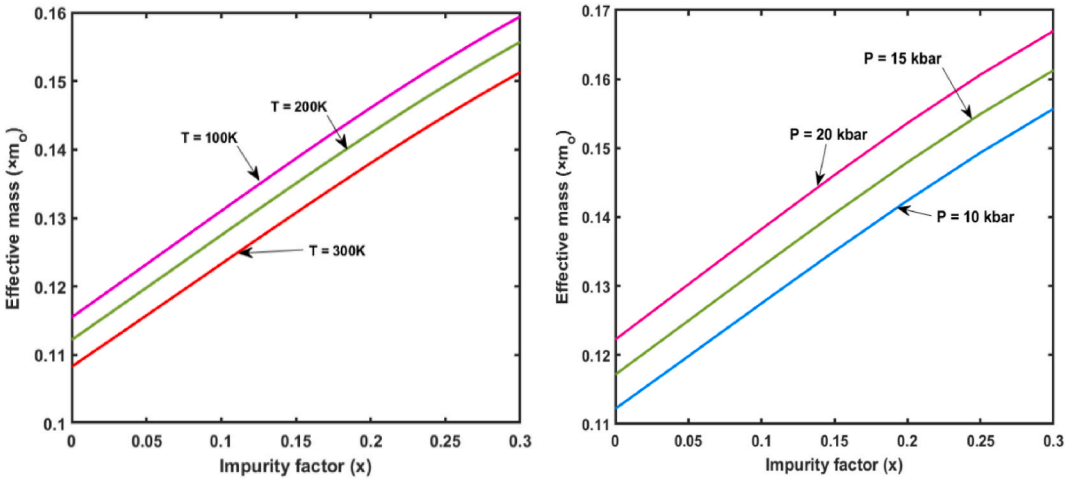

Fig. 2. (a) (b)
Effective mass variation with the hydrogenic impurity (x) for the $Ga_{1-x}Al_xAs$ quantum wire at T = 100 K, 200 K and 300 K.

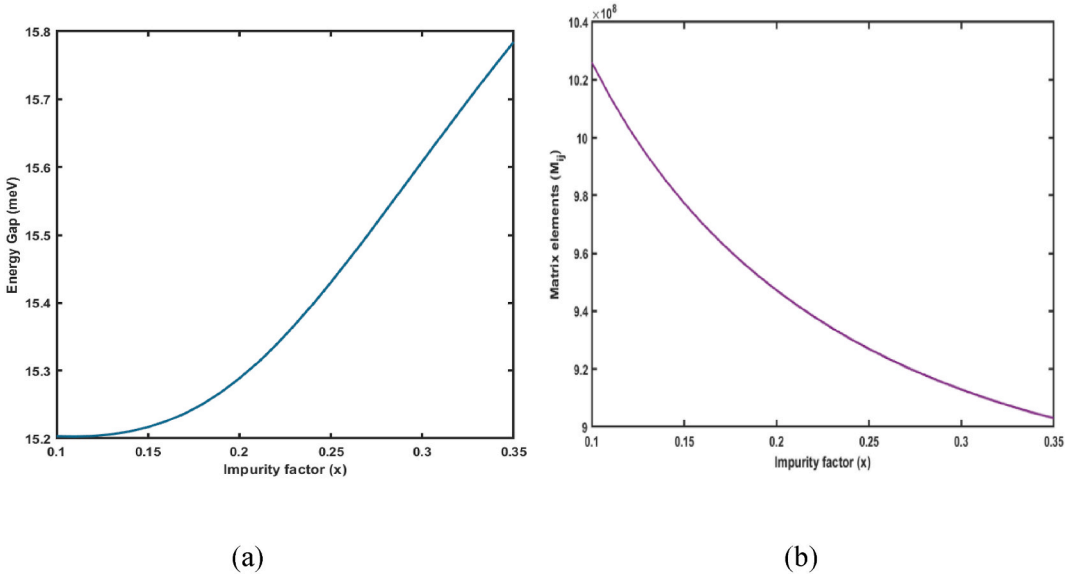

Fig. 3. (a) Energy gap between the two subsequent levels as a function of impurity factor (x), and (b) Matrix element as a function of impurity factor (x) for the $Ga_{1-x}Al_xAs$ quantum wire.

$$\chi_{2\omega}^{(2)} = -\frac{e^3 n_o}{\varepsilon_o \hbar^3} \frac{M_{12}M_{23}M_{31}}{(\omega - \omega_{21} + i\Gamma_{21})(2\omega - \omega_{32} + i\Gamma_{32})} \tag{25}$$

$$\chi_{3\omega}^{(3)} = -\frac{e^4 n_o}{\varepsilon_o \hbar^3} \frac{M_{12}M_{23}M_{34}M_{41}}{(\omega - \omega_{21} + i\Gamma_{21})(2\omega - \omega_{31} + i\Gamma_{31})(3\omega - \omega_{41} + i\Gamma_{41})} \tag{26}$$

The results and their implications are presented in the next section.

3. Result and discussion

In this investigation, the effects of hydrogenic impurity on the linear and the third-order nonlinear optical ACs, RICs, SHG, and THG in a typical $Ga_{1-x}Al_xAs$ within the presence 2-DEG have been studied. The physical constraints used for arithmetical computation are [12,55]: $n_o = 10^{16} cm^{-3}$, $n_r = 3.2$, $\Gamma_{12} = 1/T_{12}$ where $T_{12} = 0.2ps$ and (see Fig. 1)$\mu = 4\pi \times 10^{-7} Hm^{-1}$.

In Fig. 2 (a–b), the changes in the effective mass with the variation in impurity factor (x) for different values of temperature and pressure viz. 100 K, 200 K, and 300 K and 10 kbar, 15 kbar and 20 kbar respectively, are presented. As the impurity factor (x) increases,

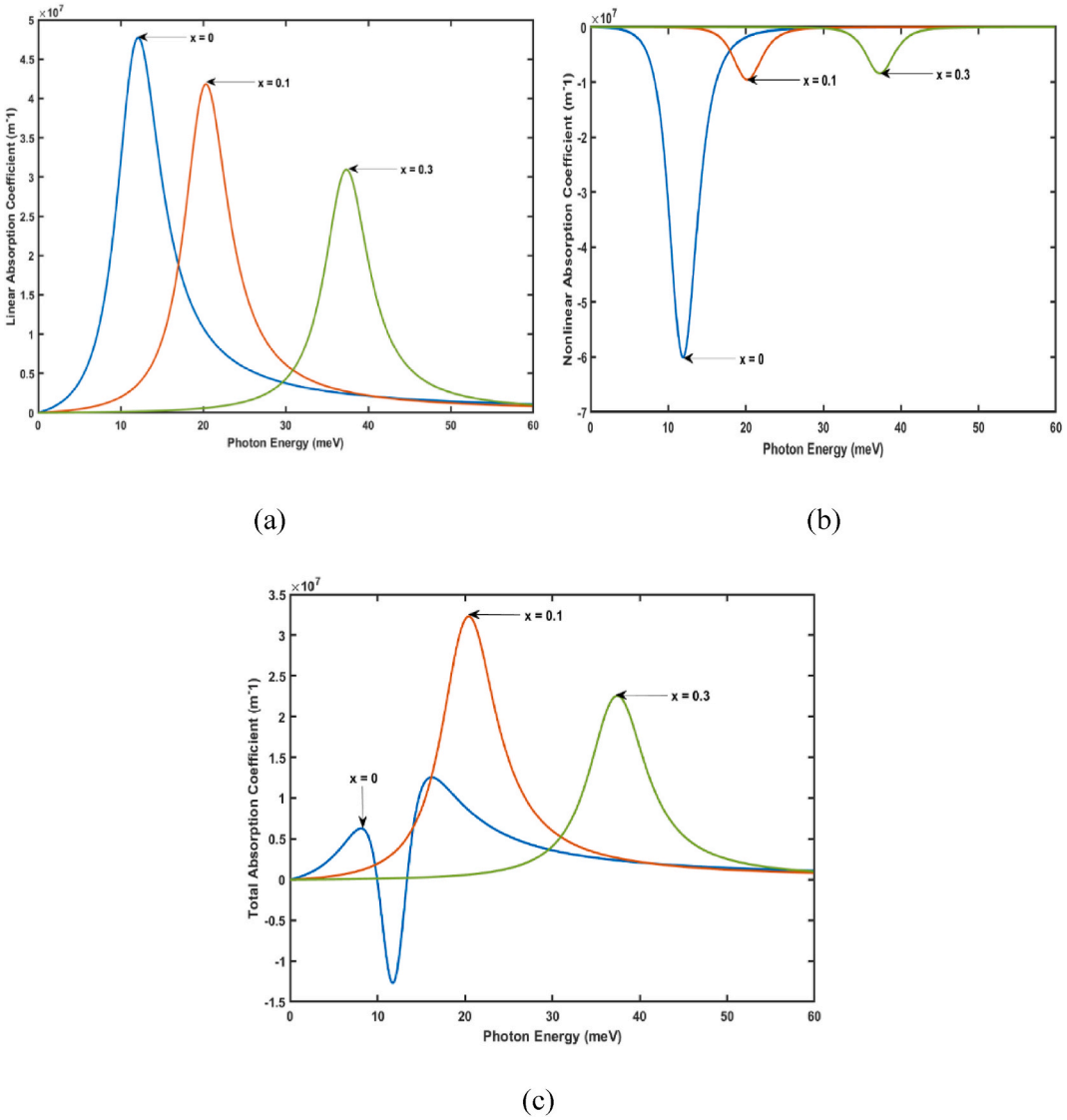

Fig. 4. (a)Linear optical ACs, (b) Third-order nonlinear optical ACs, and (c) total optical ACs as a function of Photon energy with the various values of the impurity.

the effective mass is also increased for each value of temperature and pressure. This is due to the strong dependence of impurity on the effective mass. When the impurity factor (x) is changed from 0 to 0.3, the behavior of the quantum wire in terms of effective mass is counter-intuitive when the rise in impurity factor probably enhances the effective mass. This nature helps in the study of the influences of hydrogenic impurity (x) on optical properties.

In Fig. 3 (a), energy gap variation with impurity factor (x) has been shown. As the hydrogenic impurity increases, the energy gap between the two subsequent levels is also increased. This enhancement in the energy gap due to impurity yields the change in optical properties of the $Ga_{1-x}Al_xAs$ quantum wire. Fig. 3 (b) shows the matrix elements variation with the impurity factor (x). The matrix elements reduce with an increment in hydrogenic impurity factor (x). From equations 19–25, we can easily see the dependence of matrix elements on the linear and third-order nonlinear ACs, RICs and THG therefore, when the matrix element changes these parameters also changes.

Fig. 4 (a–c), demonstrates the linear $\alpha^{(1)}$, the third-order nonlinear ACs $\alpha^{(3)}$ and the total optical ACs $\alpha^{(T)}$ as a function of the incident photon energy for the various value of the hydrogenic impurity factor (x). The magnetic field, electric field, Rashba SOI, and incident laser intensity are fixed at 1 T, 50 kV/m, 35 meV and 2.04 $\times$ $10^7 W/m^{-2}$, respectively. Generally, the $\alpha^{(1)}$ illustrations resonance at the zero thwarts which denotes when the energy difference between the subsequent states becomes cognate with an incident photon. Similarly, in the case of $\alpha^{(3)}$ with a negative sign. It is initiated that when the x is raised from 0.1 to 0.3, the maxims of $\alpha^{(1)}$ and $\alpha^{(3)}$ shows blue shifting. However, this effect is abetted via the decrement in the value of $\alpha^{(1)}$ and $\alpha^{(3)}$, with $\alpha^{(3)}$ entity effected

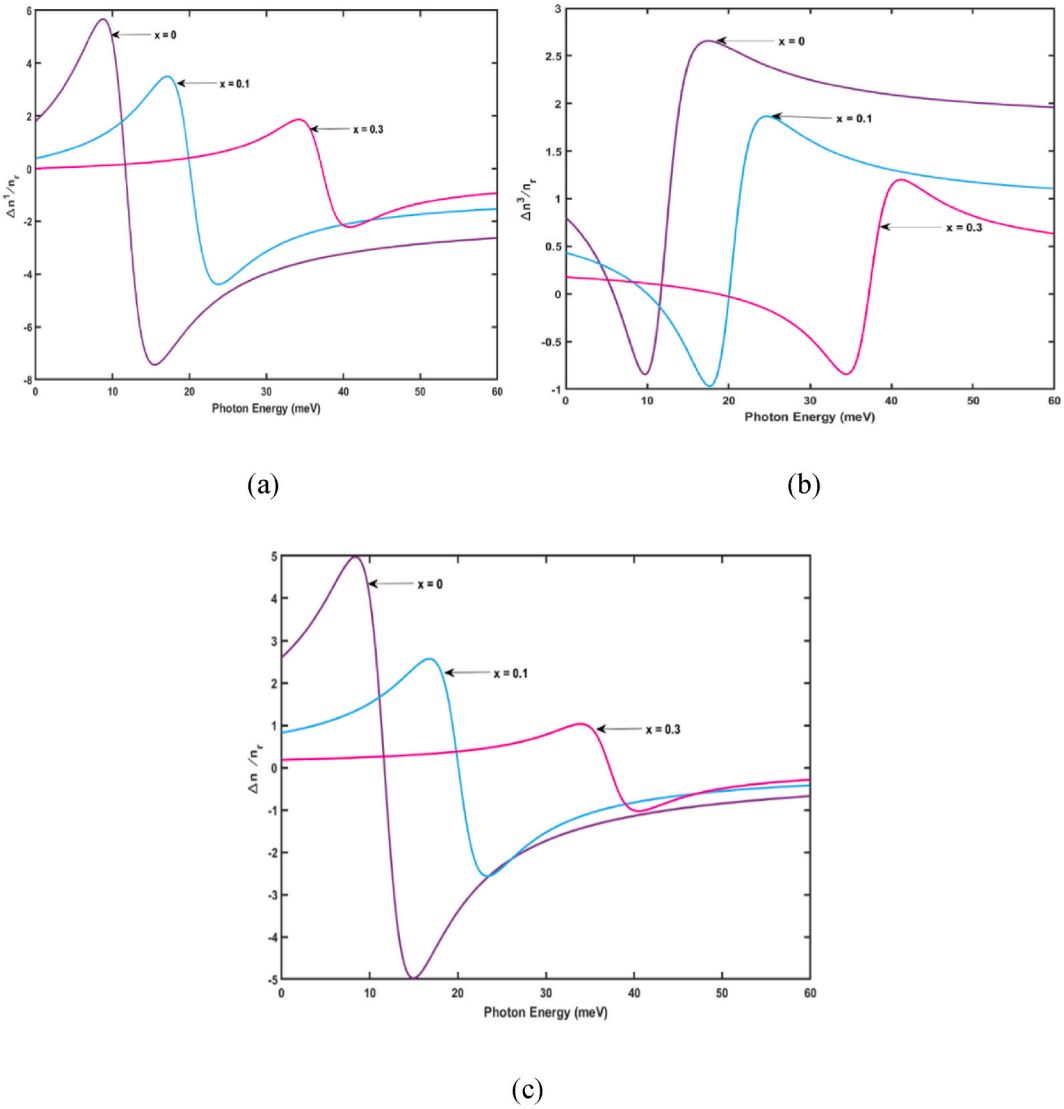

Fig. 5. (a)The linear RIC, non-linear RIC, and total RIC as a function of the incident photon energy for the various value of hydrogenic impurity.

firmly as compared to linear optical AC ($\alpha^{(1)}$). Whereas, the blue shifting takes place due to the enrichment in the energy gap between the subsequent states of energy which can easily be understood by Fig. 3 (a). This in turn consequences in further energy spacing between the ensuing states. Moreover, the impurity factor (x) effect on the $\alpha^{(3)}$ strongly as compared to $\alpha^{(1)}$ whose results illustrate the rare shape in the $\alpha^{(T)}$ curve. It can be noted that with an increment in the value of x there is a decrement in the height of peak maxims. This happened as a consequence of the small value of dipole matrix elements (M_{ij}) when the x rise. In accordance, with eq. (19) and eq. (20) the $\alpha^{(1)}$ and $\alpha^{(3)}$ resonant peaks values are proportional to $M_{12}^2 E_{12}$ and $M_{12}^4 E_{12}$, respectively. Therefore, the consequence of M_{12} is dominant, resulting in a decrease in the magnitude of the $\alpha^{(3)}$ term more than the $\alpha^{(1)}$. It is manifest that the $\alpha^{(1)}$, $\alpha^{(3)}$ and $\alpha^{(T)}$ peaks diminution and shifts in the direction of the higher energies as the impurity boosts.

In the optical studies of quantum wire, RICs play a significant role. In Fig. 5 (a–c), the linear, third order non-linear, and total RICs are plotted as a function of the incident photon energy for various hydrogenic impurity factor (x). As demonstrated from these plots, the linear RICs increase gradually with the incident photon energy and come to an extreme value. This brings out to the normal dispersion for any frequency of incident photo where $\frac{dn}{d\omega} > 0$. However, the energy of the photon approaches threshold energy, the dispersion $\frac{dn}{d\omega}$ in the RICs change its sign. At every resonant frequency of a quantum wire, this anomalous dispersion is defined by $\frac{dn}{d\omega} < 0$. In this area, photons are sturdily absorbed and behave like an absorption band. In Fig. 5 (a–c), the anomalous dispersion region moves towards large photon energies (i.e; blueshift) as a contrast to the low value of impurity factor cases. The root cause for the resonance shifting is an enhancement in the energy gap between the two electronic states among which an optical transition takes place. As the third-order nonlinear RIC has a negative sign therefore it takes an enfeebling effect on the total RIC. Therefore, it has been discovered

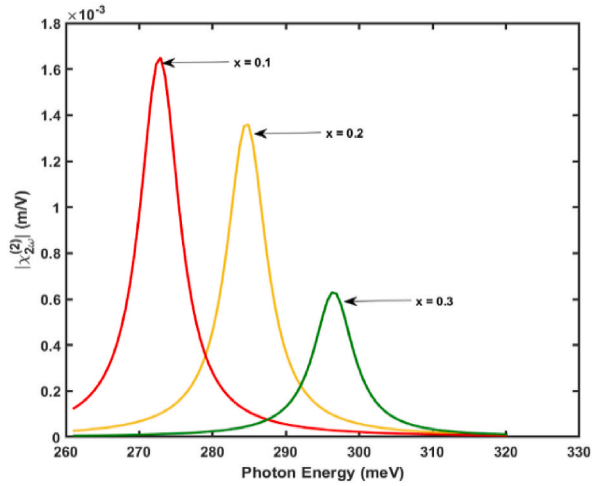

Fig. 6. SHG as a function of photon energy when x = 0.1, 0.2, and 0.3.

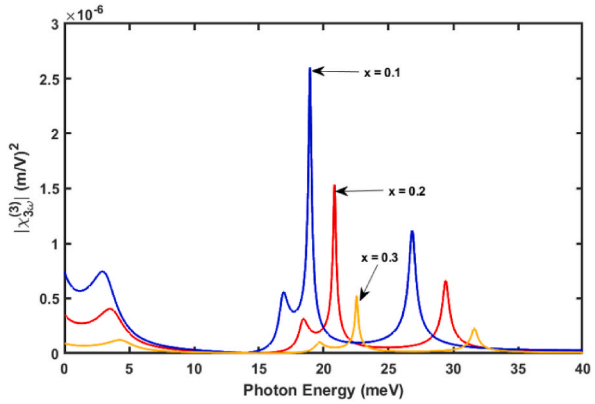

Fig. 7. THG as a function of incident photon energy for the various value of hydrogenic impurity.

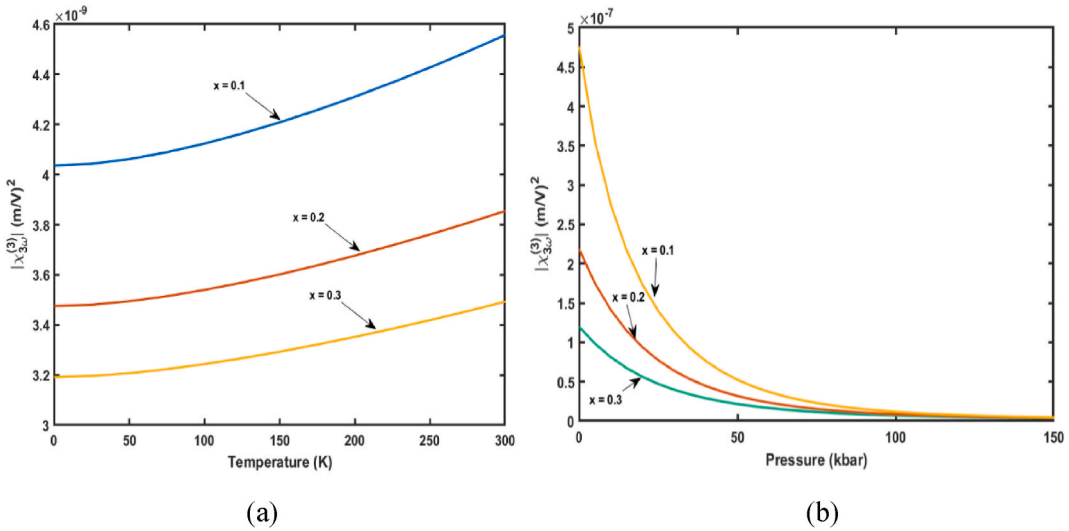

Fig. 8. (a) THG coefficient for the $Ga_{1-x}Al_xAs$ quantum wire as a function of hydrogenic temperature with x = 0.1, 0.2 and 0.3 at P = 15 kbar, and (b) THG coefficient as a function of pressure with x = 0.1, 0.2 and 0.3 at T = 300 K.

that the impurity, as a tunable parameter plays a significant role in supervising the optical properties of quantum wire.

Fig. 6, represents the SHG as a function of incident photon energy for the various value of impurity (x = 0.1, 0.2, and 0.3). It can be perceived from the plot that the resonant peaks of the SHG decrease and shift towards large value of photon energy (blue shift) when the impurity factor (x) increases. SHG figure has only one resonant peak due to the equally spaced energy spectrum. Additionally, the intensity in Fig. 6 is much larger with the comparison of resonant peaks in the situation of unequal spacing of the energy spectrum. The changes in the amplitude and position of the peaks are due to the change in the geometric factor of the quantum wire such as energy gap and matrix elements.

Fig. 7 shows that, for various values of the hydrogenic impurity factor x = 0, x = 0.1, and x = 0.3, the THG is plotted as a function of incident photon energy. For the low energy region, the triple resonance condition is not perfectly achieved due to the weaker confinement cause the energy separation between the states unequally and additionally, for high energy the transition energy between subbands decreases, and the overlaps of states will rise. When the hydrogenic impurity (x) is considered, the peaks of the THG coefficients show a blue shift. The magnitude of the peak for each curve reduces with the rise in impurity factor (x), due to allied with the product of matrix elements. This is due to the energy gap between two states containing hydrogenic impurity being larger than the energy gap between two states containing no hydrogenic impurity. This means that the THG drops and moves towards higher energies when the effect of impurity is taken into account.

The THG coefficient as a function of hydrogenic temperature and pressure when x = 0.1, 0.2, and x = 0.3 are illustrated in Fig. 8 (a) and (b), respectively. From Fig. 8 (a), it can be observed that as the temperature enhances there is an increment in height of the resonant peaks for x = 0.1, 0.2, and 0.3. When the hydrogenic impurity(x) rises from 0.1 to 0.3 the resonant peak amplitude reduces. In Fig. 8 (b), as the pressure enhances then the THG coefficient value decreases, unlike in the previous case. The enhancement in the impurity factor (x) parameter for supplementing values of P is reflected in the fall of the resonance peak amplitude. The amplitude of the resonant peak is calculated by the product of the transition matrix elements. These optical effects can be exploited as a probe for the precise mechanism such as optical nonlinearity in quantum wires and also, used in optical-magneto instruments.

4. . Conclusion

In this paper, we attention to the behavior of optical properties for the $Ga_{1-x}Al_xAs$ quantum wire and how its changes with the various value of hydrogenic impurity. The alteration in linear and third-order nonlinear optical ACs, RICs, SHG, and THG by the impurity factor under the presence of the intense magnetic field, electric field, and Rashba SOI are demonstrated. We experiential the energy gap and the dipole moment matrix element (M_{12}), are strongly affected by the hydrogenic impurity. Due to this optical ACs, RICs, SHG, and THG of the system change. It was noticed that the enhancement in hydrogenic impurity produces blue shifts in optical properties. However, hydrogenic impurity increases the energy gap and decreases the matrix elements, therefore as a result, the peaks of optical ACs, RICs, SHG, and third harmonic generation shift to higher photon energy. It is also concluded that the impurity factor can be explored as tunning tool for varying the optical properties via the introduction of spacing between the confined energy levels. It is presumed that impurity can show a significant role in the optical properties of semiconductor quantum wire. Therefore, the tunability and detuning of the terahertz laser in low-dimension nanostructure takes place due to the variation in hydrogenic impurity. These varieties of aspects would be beneficial for the evolution of tunable optoelectronic devices.

Declaration of competing interest

The authors declare that they have no known competing financial interests or personal relationships that could have appeared to influence the work reported in this paper.

Data availability

No data was used for the research described in the article.

Acknowledgment

Priyanka acknowledges the financial support from University Grants Commission and R. Sharma is thankful to the Delhi Technological University for the research facilities.

References

[1] E. Kasapoglu, F. Ungan, H. Sari, I. Sökmen, Binding energies of donor impurities in modulation-doped GaAs/AlxGa1−xAs double quantum wells under an electric field, Superlattice. Microst. 45 (2009) 618–623, https://doi.org/10.1016/J.SPMI.2009.02.011.

[2] R. Khordad, S.K. Khaneghah, Intersubband optical absorption coefficients and refractive index changes in a V-groove quantum wire, Phys. Status Solidi B 248 (2011) 243–249, https://doi.org/10.1002/pssb.201046348.

[3] Y.v Pershin, J.A. Nesteroff, V. Privman, Effect of spin-orbit interaction and in-plane magnetic field on the conductance of a quasi-one-dimensional system, Phys. Rev. B Condens. Matter 69 (2004), https://doi.org/10.1103/PhysRevB.69.121306.

[4] U. Yesilgul, F. Ungan, E. Kasapoglu, H. Sari, I. Sökmen, The linear and nonlinear intersubband optical absorption coefficients and refractive index changes in a V-shaped quantum well under the applied electric and magnetic fields, Superlattice. Microst. 50 (2011) 400–410, https://doi.org/10.1016/j.spmi.2011.08.002.

[5] S. Zhang, R. Liang, E. Zhang, L. Zhang, Y. Liu, Magnetosubbands of semiconductor quantum wires with Rashba and Dresselhaus spin-orbit coupling, Phys. Rev. B Condens. Matter 73 (2006), https://doi.org/10.1103/PhysRevB.73.155316.

[6] S. Zhang, R. Liang, E. Zhang, L. Zhang, Y. Liu, Magnetosubbands of semiconductor quantum wires with Rashba and Dresselhaus spin-orbit coupling, Phys. Rev. B Condens. Matter 73 (2006), https://doi.org/10.1103/PhysRevB.73.155316.

[7] W. Xie, The nonlinear optical rectification of a confined exciton in a quantum dot, J. Lumin. 131 (2011) 943–946, https://doi.org/10.1016/j.jlumin.2010.12.028.

[8] W. Xie, The nonlinear optical rectification coefficient of quantum dots and rings with a repulsive scattering center, J. Lumin. 143 (2013) 27–30, https://doi.org/10.1016/j.jlumin.2013.04.041.

[9] S. Lahon, M. Kumar, P.K. Jha, M. Mohan, Spin-orbit interaction effect on the linear and nonlinear properties of quantum wire in the presence of electric and magnetic fields, J. Lumin. 144 (2013) 149–153, https://doi.org/10.1016/j.jlumin.2013.06.054.

[10] R. Khordad, Optical properties of quantum wires: Rashba effect and external magnetic field, J. Lumin. 134 (2013) 201–207, https://doi.org/10.1016/j.jlumin.2012.08.047.

[11] R. Khordad, Optical properties of quantum wires: Rashba effect and external magnetic field, J. Lumin. 134 (2013) 201–207, https://doi.org/10.1016/j.jlumin.2012.08.047.

[12] R. Khordad, S. Tafaroji, Third-harmonic generation in a quantum wire with triangle cross section, Physica E Low Dimens Syst Nanostruct 46 (2012) 84–88, https://doi.org/10.1016/j.physe.2012.07.025.

[13] P.K. Jha, M. Kumar, S. Lahon, S. Gumber, M. Mohan, Rashba spin orbit interaction effect on nonlinear optical properties of quantum dot with magnetic field, Superlattice. Microst. 65 (2014) 71–78, https://doi.org/10.1016/j.spmi.2013.10.025.

[14] Y.Y. Zhang, G.R. Yao, Performance enhancement of blue light-emitting diodes with AlGaN barriers and a special designed electron-blocking layer, J. Appl. Phys. 110 (2011), https://doi.org/10.1063/1.3651393.

[15] T. Sugaya, K.Y. Jang, C.K. Hahn, M. Ogura, K. Komori, A. Shinoda, K. Yonei, Enhanced peak-to-valley current ratio in InGaAs/InAlAs trench-type quantum-wire negative differential resistance field-effect transistors, J. Appl. Phys. 97 (2005), https://doi.org/10.1063/1.1851595.

[16] I.Z. Utić′*utić′*, J. Fabian, S. das Sarma, Spintronics: Fundamentals and applications, Rev. Mod. Phys. 76, 323 (2004), https://doi.org/10.1103/RevModPhys.76.323.

[17] S. Datta, B. Das, Electronic analog of the electro-optic modulator, Appl. Phys. Lett. 56 (1990) 665–667, https://doi.org/10.1063/1.102730.

[18] M. Kumar, S. Lahon, P.K. Jha, M. Mohan, Energy dispersion and electron g-factor of quantum wire in external electric and magnetic fields with Rashba spin orbit interaction, Superlattice. Microst. 57 (2013) 11–18, https://doi.org/10.1016/j.spmi.2013.01.007.

[19] I.Z. Utić′*utić′*, J. Fabian, S. das Sarma, Spintronics: Fundamentals and applications, n.d.

[20] D. Ahn, S.L. Chuang, Calculation of linear and nonlinear intersubband optical absorptions in a quantum well model with an applied electric field, IEEE J. Quant. Electron. 23 (1987) 2196–2204, https://doi.org/10.1109/JQE.1987.1073280.

[21] M. Ahin, Third-order nonlinear optical properties of a one- and two-electron spherical quantum dot with and without a hydrogenic impurity, J. Appl. Phys. 106 (2009), https://doi.org/10.1063/1.3225100.

[22] K.J. Kuhn, G.U. Iyengar, S. Yee, Free carrier induced changes in the absorption and refractive index for intersubband optical transitions in AlxGa1-xAs/GaAs/AlxGa1-xAs quantum wells, J. Appl. Phys. 70 (1991) 5010–5017, https://doi.org/10.1063/1.349005.

[23] Y. bin Yu, K.X. Guo, Exciton effects on nonlinear electro-optic effects in semi-parabolic quantum wires, Physica E Low Dimens Syst Nanostruct 18 (2003) 492–497, https://doi.org/10.1016/S1386-9477(03)00190-5.

[24] J. Ganguly, S. Saha, S. Pal, M. Ghosh, Noise-driven optical absorption coefficients of impurity doped quantum dots, Physica E Low Dimens Syst Nanostruct 75 (2016) 246–256, https://doi.org/10.1016/j.physe.2015.09.027.

[25] S. Saha, S. Pal, J. Ganguly, M. Ghosh, Exploring optical refractive index change of impurity doped quantum dots driven by white noise, Superlattice. Microst. 88 (2015) 620–633, https://doi.org/10.1016/j.spmi.2015.10.021.

[26] I. Karabulut, S. Baskoutas, Linear and nonlinear optical absorption coefficients and refractive index changes in spherical quantum dots: Effects of impurities, electric field, size, and optical intensity, J. Appl. Phys. 103 (2008), https://doi.org/10.1063/1.2904860.

[27] G. Safarpour, A. Zamani, M.A. Izadi, H. Ganjipour, Laser radiation effect on the optical properties of a spherical quantum dot confined in a cylindrical nanowire, J. Lumin. 147 (2014) 295–303, https://doi.org/10.1016/j.jlumin.2013.11.053.

[28] B. Gisi, S. Sakiroglu, E. Kasapoglu, H. Sari, I. Sokmen, Spin-orbit interaction effects on the optical properties of quantum wires under the influence of in-plane magnetic fields, Superlattice. Microst. 86 (2015) 166–172, https://doi.org/10.1016/j.spmi.2015.06.046.

[29] A. Bouazra, S.A. ben Nasrallah, M. Said, Theory of electronic and optical properties for different shapes of InAs/In0.52Al0.48As quantum wires, Physica E Low Dimens Syst Nanostruct 75 (2016) 272–279, https://doi.org/10.1016/j.physe.2015.09.039.

[30] S. Sakiroglu, B. Gisi, Y. Karaaslan, E. Kasapoglu, H. Sari, I. Sokmen, Optical properties of double quantum wires under the combined effect of spin-orbit interaction and in-plane magnetic field, Physica E Low Dimens Syst Nanostruct 81 (2016) 59–65, https://doi.org/10.1016/j.physe.2016.02.048.

[31] N. Arunachalam, A. John Peter, C. Woo Lee, Pressure induced optical absorption and refractive index changes of a shallow hydrogenic impurity in a quantum wire, Physica E Low Dimens Syst Nanostruct 44 (2011) 222–228, https://doi.org/10.1016/j.physe.2011.08.019.

[32] C.v Nguyen, N.Ngoc Hieu, C.A. Duque, D. Quoc Khoa, N. van Hieu, L.van Tung, H.Vinh Phuc, Linear and nonlinear magneto-optical properties of monolayer phosphorene, J. Appl. Phys. 121 (2017), https://doi.org/10.1063/1.4974951.

[33] E. Kasapoglu, F. Ungan, C.A. Duque, U. Yesilgul, M.E. Mora-Ramos, H. Sari, I. Sökmen, The effects of the electric and magnetic fields on the nonlinear optical properties in the step-like asymmetric quantum well, Physica E Low Dimens Syst Nanostruct 61 (2014) 107–110, https://doi.org/10.1016/j.physe.2014.03.024.

[34] M.G. Barseghyan, A.A. Kirakosyan, C.A. Duque, Hydrostatic pressure,electric and magnetic field effects on shallow donor impurity states and photoionization cross section in cylindrical GaAs-Ga1-xAlxAs quantum dots, Phys. Status Solidi B 246 (2009) 626–629, https://doi.org/10.1002/pssb.200880516.

[35] L.E. Oliveira', L.M. Falicov, Energy Spectra of Donors and Acceptors in Quantum-Well Structures, Effect of spatially dependent screening, 1986.

[36] N. Porras-Montenegro, S.T. Pérez-Merchancano, A. Latgé, Binding energies and density of impurity states in spherical GaAs-(Ga,Al)As quantum dots, J. Appl. Phys. 74 (1993) 7624–7626, https://doi.org/10.1063/1.354943.

[37] A. Montes, C.A. Duque, N. Porras-Montenegro, Density of Shallow-Donor Impurity States in Rectangular Cross Section GaAs Quantum-Well Wires under Applied Electric Field, 1998. http://iopscience.iop.org/0953-8984/10/24/012.

[38] M.G. Barseghyan, M.E. Mora-Ramos, C.A. Duque, Hydrostatic pressure, impurity position and electric and magnetic field effects on the binding energy and photo-ionization cross section of a hydrogenic donor impurity in an InAs Pöschl-Teller quantum ring, Eur. Phys. J. B 84 (2011) 265–271, https://doi.org/10.1140/epjb/e2011-20650-7.

[39] M. Santhi, A. John Peter, C. Yoo, Hydrostatic pressure on optical absorption and refractive index changes of a shallow hydrogenic impurity in a GaAs/GaAlAs quantum wire, Superlattice. Microst. 52 (2012) 234–244, https://doi.org/10.1016/j.spmi.2012.04.020.

[40] J.C. Martínez-Orozco, M.E. Mora-Ramos, C.A. Duque, Electron-related optical properties in T-shaped AlxGa1−xAs/GaAs quantum wires and dots, Eur. Phys. J. B 88 (2015), https://doi.org/10.1140/epjb/e2015-60021-x.

[41] N. Zeiri, N. Sfina, S.A. ben Nasrallah, M. Said, Linear and non-linear optical properties in symmetric and asymmetric double quantum wells, Optik 124 (2013) 7044–7048, https://doi.org/10.1016/j.ijleo.2013.05.169.

[42] R. Sharma Priyanka, M. Kumar, Effects of impurity factor on the physical and transport properties for Ga1-xAlxAs quantum wire in the presence of Rashba spin-orbit interaction, Phys. B Condens. Matter 629 (2022), https://doi.org/10.1016/j.physb.2021.413649.

[43] R. Khordad, B. Mirhosseini, Optical properties of GaAs/Ga 1-xAl xAs ridge quantum wire: Third-harmonic generation, Opt Commun. 285 (2012) 1233–1237, https://doi.org/10.1016/j.optcom.2011.11.070.

[44] R. Khordad, Second and third-harmonic generation of parallelogram quantum wires: Electric field, Indian J. Phys. 88 (2014) 275–281, https://doi.org/10.1007/s12648-013-0414-1.

[45] G. Wang, Third-harmonic generation in cylindrical parabolic quantum wires with an applied electric field, Phys. Rev. B Condens. Matter 72 (2005), https://doi.org/10.1103/PhysRevB.72.155329.

[46] F. Rossi, E. Molinari, Coulomb-Induced Suppression of Band-Edge Singularities in the Optical Spectra of Realistic Quantum-Wire Structures, 1996.

[47] F. Zaouali, A. Bouazra, M. Said, A theoretical evaluation of optical properties of InAs/InP quantum wire with a dome cross-section, Optik (Stuttg 174 (2018) 513–520, https://doi.org/10.1016/j.ijleo.2018.08.101.
[48] S. Antil, M. Kumar, S. Lahon, S. Dahiya, A. Ohlan, R. Punia, A.S. Maan, Influence of hydrostatic pressure and spin orbit interaction on optical properties in quantum wire, Phys. B Condens. Matter 552 (2019) 202–208, https://doi.org/10.1016/j.physb.2018.10.006.
[49] R. Khordad, Optical properties of quantum wires: Rashba effect and external magnetic field, J. Lumin. 134 (2013) 201–207, https://doi.org/10.1016/j.jlumin.2012.08.047.
[50] M.J. Karimi, M. Hosseini, Electric and magnetic field effects on the optical absorption of elliptical quantum wire, Superlattice. Microst. 111 (2017) 96–102, https://doi.org/10.1016/j.spmi.2017.06.019.
[51] K. Chernoutsan, V. Dneprovskii, S. Gavrilov, V. Gusev, E. Muljarov, S. Romanov, A. Syrnicov, O. Shaligina, E. Zhukov, Linear and Nonlinear Optical Properties of Excitons in Semiconductor-Dielectric Quantum Wires, 2002. www.elsevier.com/locate/physe.
[52] V. Dneprovskii, E. Zhukov, V. Karavanskii, V. Poborchii, I. Salamatina, Nonlinear Optical Properties of Semiconductor Quantum Wires, 1998.
[53] R. Khordad, Second and third-harmonic generation of parallelogram quantum wires: Electric field, Indian J. Phys. 88 (2014) 275–281, https://doi.org/10.1007/s12648-013-0414-1.
[54] G. Wang, Third-harmonic generation in cylindrical parabolic quantum wires with an applied electric field, Phys. Rev. B Condens. Matter 72 (2005), https://doi.org/10.1103/PhysRevB.72.155329.
[55] N. Zeiri, A. Bouazra, S.A. ben Nasrallah, M. Said, Linear and nonlinear susceptibilities in GaN/Al x Ga1-xN quantum wire, Phys. Scripta 95 (2020), https://doi.org/10.1088/1402-4896/ab5b45.

Solid State Communications 366–367 (2023) 115155

Contents lists available at ScienceDirect

Solid State Communications

journal homepage: www.elsevier.com/locate/ssc

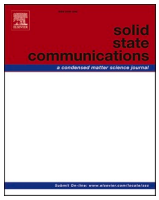

Impact of impurity on the non-linear and linear optical properties of $In_xGa_{1-x}As$ quantum dot

Priyanka, Rinku Sharma *

Department of Applied Physics, Delhi Technological University, Delhi, 110042, India

ARTICLE INFO

Communicated by: Y.E. Lozovik

Keywords:
Rashba spin-orbit coupling (RSOC)
Quantum dot
Third harmonic generation and absorption coefficients

ABSTRACT

In the current investigation, we emphasise the optical properties of the $In_xGa_{1-x}As$ quantum dot. In this esteem, we first estimate the energy levels and wavefunctions in the existence of impurity. Then, we focus on the impact of impurity on the absorption coefficients, refractive index changes, and third harmonic generation. It is found that the absorption coefficients, refractive index changes, and third harmonic generation peaks start to shift from their position with the decrement in the magnitude as the concentration of impurity enhances. As a consequence, it is cognizance that the concentration of impurity has a crucial role in the nanostructure optical properties.

1. Introduction

The impact of hydrogenic impurity on the physical, non-linear optical and transport properties of the low-dimensional semiconductor act as a major part in the demonstration of semiconductor physics on the account of the presence of impurity magnifying amend the performance of nanodevices [1,2]. In recent years, the hydrogenic impurity states in low-dimensional semiconductors, viz. Quantum dots, quantum wire and quantum well have been explored widely [3,4]. This investigation exposed that the optical properties and physical properties within the presence of hydrogenic impurity can be directly controlled by selecting the appropriate sizes, geometries, doping positions and materials. The inter-subband optical absorptions of low-dimensional semiconductors have engrossed vast interest in current years. The study indicates that the inter-subband optical absorptions (OAs) have large optical nonlinearity in nanodevices. Both the linear and nonlinear inter-subband OAs can be exploited for realistic applications in high-speed electro-optical devices and photodetectors. Furthermore, externally applied perturbations like electric, and magnetic fields and Rashba spin-orbit coupling (RSOC) are competent tools for scrutinising properties under the influence of impurity in low-dimensional semiconductors [5–7]. Whereas, the hydrogenic impurity, externally applied field and RSOC affects the optical properties of quantum dots have a great amount of interest for device applications and fundamental physics [8–12].

The impurity present in the semiconductor modifies the feast of the wave function, especially in strong spatial confinement. The external field and RSOC in the low-dimensional semiconductor break the symmetry of the system. As is well known, the RSOC and its consequence on the non-linear and linear optical properties of the quantum dot have sustained and persisted in the last decade. The RSOC arise due to structural inversion symmetry [13–15]. The strength of the RSOC depends on the external field and the characteristics of the material. In the realistic problem of optical properties of quantum dots, RSOC plays a vital role on account of their potential applications in quantum computers [16–18]. It is esteemed the spin of electrons plays a significant role in the spin phenomena namely spin relaxation, spintronics and quantum computer [19,20]. During the last eras, much research has investigated the optical properties and electronic of low-dimensional semiconductors under the presence of RSOC theoretically and experimentally [21–28].

Linear and nonlinear optical phenomena in semiconductors become enormously significant to design the photonic and electronic nanodevices applications like high-speed electro-optical modulators, laser amplifiers and so on [29]. As a result, much theoretical research has been done to recognize the exploitation of optical properties with different concentrations of impurity. However, the linear and nonlinear absorption coefficient (ACs), refractive index changes (RICs), and third harmonic generation (THG) are the most important property among optical properties of quantum dots [30–32]. Liu et al. focus on the cylindrical core-shell nanostructure's THG non-linear susceptibility under the existence electric field [33]. The electric field and hydrogenic impurity influence on the optical properties of the 3D quantum dots are

* Corresponding author.
E-mail address: rinkusharma@dtu.ac.in (R. Sharma).

https://doi.org/10.1016/j.ssc.2023.115155
Received 1 March 2023; Accepted 28 March 2023
Available online 1 April 2023
0038-1098/© 2023 Elsevier Ltd. All rights reserved.

studied by E. Sadeghi [34]. Linear and non-linear optical ACs and RICs based on the inter-subband optical transition of the quantum dots are also calculated in Refs. [35,36].

In this work, our purpose is to study the impact of impurity on the ACs, RICs and THG of the quantum dot underneath the influence of externally applied field and RSOC by numerical calculations. For this persistence, we find the wavefunctions and energy levels in the effective mass approximation numerically via the density matrix approach. The pattern of this paper is followed as: In Section 2, the calculation for energy eigenvalues and wave functions through the density matrix approach. In section 3, the result and discussion about $In_xGa_{1-x}As$ quantum dot are mentioned. In the end, we represent the conclusion part in section 4.

2. Theory

Consider the $In_xGa_{1-x}As$ quantum dot (seen in Fig. 1) with parabolic confinement potential under the presence of magnetic field along z-axis B = (0,0,B), therefore the symmetric gauge comes out to be A = (-y/2,x/2,0). The Hamiltonian for single electron mass is given by

$$H_i(r) = \frac{1}{2m_e(x,P,T)}(p+eA)^2 + \frac{1}{2}m_e(x,P,T)\omega_o\left(x^2+y^2\right) + \frac{1}{2}g^*\mu_B B\sigma_i \tag{1}$$

Here, p and A are the momentum and vector potential, ω_o is known as oscillator frequency, g^* is the Lande factor and σ_i is the Pauli spin matrix. $m_e(x,P,T)$ is the effective mass for $In_xGa_{1-x}As$ quantum dot expressed as [37,38]

$$m_e(x,P,T) = \mathrm{m_o}\left[7.51\left(\frac{1}{0.341+\mathrm{E_g}^i(x,\mathrm{P,T})}+\frac{2}{\mathrm{E_g}^i(x,\mathrm{P,T})}\right)+1\right]^{-1} \tag{2}$$

$\mathrm{m_o}$ is called free electron mass. $\mathrm{E_g}^i$ is the energy bandgap for the $In_xGa_{1-x}As$ given by

$$\mathrm{E_g}^i(x,\mathrm{P,T}) = \mathrm{E_g}^{GaAs}(P,T) + \left[\mathrm{E_g}^{InAs}(P,T) - \mathrm{E_g}^{GaAs}(P,T)\right]x - 0.475x(1-x) \tag{3}$$

Where $\mathrm{E_g}^{GaAs}(P,T) = qP - \frac{rT^2}{T+s} + \mathrm{E_g}^0$,

And $\mathrm{E_g}^{InAs}(P,T) = aP - \frac{bT^2}{T+c} + \mathrm{E_{gi}}^0$.

The parameters values: $\mathrm{E_g}^0 = 1.52$ eV (named as energy gap at P = 0 kbar and T = 0 K), q = 1.08 ×10^{-2} eV/kbar, r = 50.4 × 10^{-5} eV/K, and s = 204 K are the pressure coefficient and temperature coefficients, respectively for GaAs semiconductors. And $\mathrm{E_{gi}}^0 = 0.42$ eV (named as energy gap at P = 0 kbar and T = 0 K), a = 7.7 ×10^{-3} eV/kbar, b = 41.9 ×10^{-5} eV/K and c = 271 K are the pressure coefficient and temperature coefficients, respectively for InAs semiconductors.

When the RSOC is introduced in the system the total Hamiltonian becomes

$$H_T = \mathrm{p_e}^{2/(2\mathrm{m}}(\mathrm{x,P,T})\Big) + \frac{e}{m_e(x,P,T)}\boldsymbol{A}.\boldsymbol{p} + \frac{e^2A^2}{2m_e(x,P,T)} + \\ + \frac{1}{2}m_e(x,P,T)\omega_o\left(x^2+y^2\right) + \frac{1}{2}g^*\mu_B B\sigma_i + \frac{\alpha}{\hbar}[\sigma\times\boldsymbol{p}]_z + \frac{e\alpha}{\hbar}[\sigma\times\boldsymbol{A}]_z \tag{4}$$

The last two terms in eq. (4) corresponds to RSOC. In which α is known as the Rashba constant and σ is the electron spin. Moreover, the energy wave function and eigen energies correspond to eq. (4) are

$$\varphi_{nl\sigma} = \frac{1}{\sqrt{2\pi}}e^{il\varphi}R_{nl}(r)\chi_\sigma \tag{5}$$

and

$$E^T_{nl\sigma} = (2n+|l|+1)\hbar\Theta^2_\sigma + \frac{\hbar}{2}l\omega_c + \sigma\left(\frac{1}{2}g^*\mu_B B + l\alpha m_e(x,P,T)\omega_o^2\right) \tag{6}$$

Where $R_{nl}(r) = \frac{\sqrt{2}}{a}\sqrt{\frac{n!}{(n+|l|)!}}exp\left(-\frac{r^2}{2a^2}\right)\left(\frac{r^2}{a^2}\right)^{|l|/2}L_n^{|l|}\left(\frac{r^2}{a^2}\right)$, n = 0,1,2, …, and l = 0, ± 1, ± 2, …. A is the bohr radius ($a = \left(\frac{\hbar}{m_e(x,P,T)\omega_o}\right)^{1/2}$), and $\Theta^2_\sigma = \omega_o^2 + \frac{\omega_c^2}{4} + \frac{\sigma\alpha m_e(x,P,T)\omega_o^2\omega_c}{\hbar}$ with $\omega_c = \frac{eB}{m_e(x,P,T)}$ called cyclotron frequency. χ_σ is called the spinor function.

For the scheming of optical properties of the $In_xGa_{1-x}As$ quantum dot, the perturbation expansion and density matrix approach are used. The expression for the linear, nonlinear and total ACs are written as [39].

$$\alpha^{(1)}(\omega) = \omega\sqrt{\frac{\rho}{\rho_r}}\ \frac{\sigma_s\Gamma_{if}|M_{if}|^2}{\hbar\left\{(\omega_{fi}-\omega)^2+\Gamma_{if}{}^2\right\}} \tag{7}$$

And

$$\alpha^{(3)}(\omega,I) = -\hbar\omega\sqrt{\frac{\rho}{\rho_r}}\ \frac{I}{2\varepsilon_o n_r c}\times\frac{4\sigma_s\Gamma_{if}|M_{if}|^2}{\hbar^4\left\{(\omega_{fi}-\omega)^2+\Gamma_{if}{}^2\right\}}\times \\ \left[\frac{|M_{if}|^2}{(\omega_{fi}-\omega)^2+\Gamma_{if}{}^2}+\frac{(M_{ff}-M_{ii})^2\left(3\omega_{fi}{}^2-4\omega_{fi}\omega\right)\left(\omega_{fi}^2-\Gamma_{if}^2\right)}{4\left(\omega_{fi}^2+\Gamma_{if}^2\right)\left\{(\omega_{fi}-\omega)^2+\Gamma_{if}{}^2\right\}}\right] \tag{8}$$

The parameters used in Eqs. (7) and (8), ρ is known as permeability, ρ_r is the real part of permittivity and $\hbar\omega$ is the incident photon energy. I, σ_s and n_r are the intensity of incident light, carrier density and refractive index of the $In_xGa_{1-x}As$ quantum dot, respectively. Γ_{if} and ω_{if} named as relaxation time and transition frequency. $M_{if} = |\langle\varphi_i|r|\varphi_f\rangle|$ known as the transition matrix element. The total ACs are given by

$$\alpha_T(\omega,I) = \alpha^{(1)}(\omega) + \alpha^{(3)}(\omega,I) \tag{9}$$

The linear and non-linear RICs for the optical transition are written as [40].

$$\frac{\Delta n_r^{(1)}}{n_r} = \frac{\sigma_s}{2n_r^2\varepsilon_o}\ \frac{|M_{if}|^2(\omega_{fi}-\omega)}{\hbar\left\{(\omega_{fi}-\omega)^2+\Gamma_{if}{}^2\right\}} \tag{10}$$

$$\frac{\Delta n_r^{(3)}(\omega,I)}{n_r} = -\frac{\sigma_s}{2n_r{}^3\varepsilon_o}\ \frac{I\rho c|M_{if}|^2(\omega_{fi}-\omega)}{\hbar^3(\omega_{fi}-\omega)^2+\Gamma_{if}^2}\times \\ \left[\frac{|M_{if}|^2}{(\omega_{fi}-\omega)^2+\Gamma_{if}^2}+\frac{2\Gamma_{if}(M_{ff}-M_{ii})}{(\omega_{fi}-\omega)^2+\Gamma_{if}^2}\times\left\{(\omega_{fi}-\omega)\left[\omega_{fi}(\omega_{fi}-\omega)+\Gamma_{if}^2\right]-\Gamma_{if}^2(2\omega_{fi}-\omega)\right\}\right] \tag{11}$$

The total RICs represented as

$$\frac{\Delta n_r(\omega,I)}{n_r} = \frac{\Delta n_r^{(1)}}{n_r} + \frac{\Delta n_r^{(3)}(\omega,I)}{n_r} \tag{12}$$

For the oscillation with 4 ω, we consider a third-order contribution. Therefore, the THG per unit volume is obtained with the help of the density matrix approach, and written as [41]

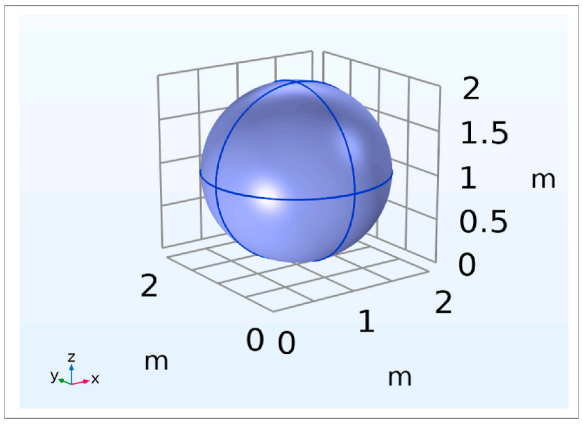

Fig. 1. $In_xGa_{1-x}As$ quantum dot systematic diagram.

$$\chi_{3\omega}^{(3)} = -\frac{q^4\vartheta}{\varepsilon_o\hbar^3}\frac{M_{12}M_{23}M_{34}M_{41}}{(\omega-\omega_{21}+i\Gamma_{21})(2\omega-\omega_{31}+i\Gamma_{31})(3\omega-\omega_{41}+i\Gamma_{41})} \quad (13)$$

Here, q and ϑ are known as the charge on an electron and electron density, respectively.

In the result section, the behaviour of the ACs, RICs and THG are studied.

3. Result

In this work, the impact of the hydrogenic impurity (x) on the ACs, RICs and THG of the $In_xGa_{1-x}As$ quantum dot under the influence of RSOC are examined. The constraints used in this paper are: $\vartheta = 10^{16}cm^{-3}$, $n_r = 3.2$, $\Gamma_{12} = 1/T_{12}$ where $T_{12} = 0.14ps$ and $\rho = 4\pi \times 10^{-7}Hm^{-1}$.

The linear, non-linear and total ACs of the $In_xGa_{1-x}As$ quantum dot with the different concentrations of the hydrogenic impurity (x = 0, 0.1, 0.2 and 0.3) are shown in Fig. 2(a–c), respectively. As it is easily noticeable that the position and magnitude of the peaks depend on the concentration of x. In such a way, the increase in the value of x the position of peaks towards a higher value of incident energies (blue shift) and the magnitude of peaks decreases. The blue shifting occurs as a consequence of an increment in the energy difference between the successive levels of the energy with the concentration of impurity. Moreover, the impurity (x) influences the total AC firmly as compared to the linear AC causing the erratic shape in the total AC. The magnitude

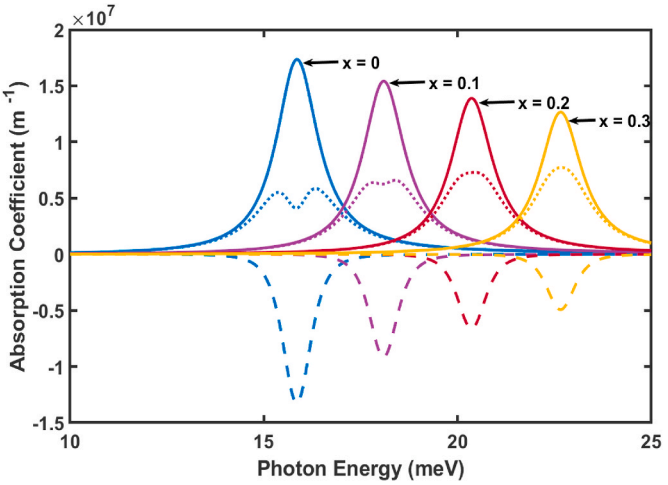

Fig. 2. Change of (a) linear, (b) non-linear, and (c) total ACs with the incident photon energy for x = 0, 0.1, 0.2 and 0.3.

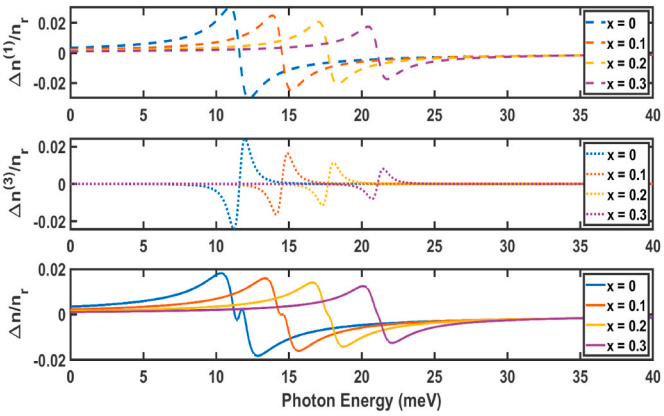

Fig. 3. Change of (a) linear, (b) non-linear, and (c) total RICs with the incident photon energy for x = 0, 0.1, 0.2 and 0.3.

decreases with the increment in the impurity happens on account of the small value of the dipole matrix element (M_{ij}). The linear and non-linear ACs depend on the $M_{12}^2E_{12}$ and $M_{12}^4E_{12}$, respectively present in eqs. (7) and (8). As the M_{12} is dominant the magnitude of the non-linear peak becomes larger than linear AC. It is obvious the linear, non-linear and total ACs peaks decrease and move towards higher energies as impurity increases.

Fig. 3 (a-c) represents the varation in the linear, non-linear and total RICs with the incident energy under the influence of impurity (x = 0, 0.1, 0.2 and 0.3). From the figure, the linear RIC start to rise with the incident photon energy and attains the maximum point which is called normal dispersion reason. Whenever the incident photon energy avenue the threshold energy, the sign of the $dn/d\omega$ vary and the anomalous dispersion occurs in the resonant frequency of the InxGa1-xAs quantum dot. With the concentration of the hydrogenic impurity, the resonant frequency moves towards a higher frequency (blue shift) with a decrement in the magnitude of the peaks. The nonlinear RIC eq. (11) contains a negative sign whereas the linear RIC eq. (10) have positive signs hence the total RIC is reduced by it. Thereby, the non-linear must be used for the high optical intensity devices.

In Fig. 4, the change in the THG with the photon energies under the impact of impurity (x = 0, 0.1, 0.2 and 0.3). With the concentration of the impurity (x), the peaks of the THG shift towards a high value of energies and indicate blue shifting. THG peak magnitude decreases with the increment in impurity as a consequence of matrix elements product. However, the gap between the two states becomes large when we introduce impurity into our system. Therefore, the THG peak reduces its

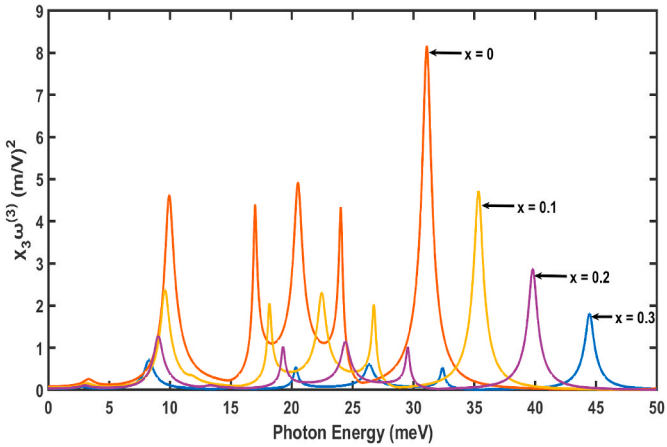

Fig. 4. Change of THG with the incident photon energy for x = 0, 0.1, 0.2 and 0.3.

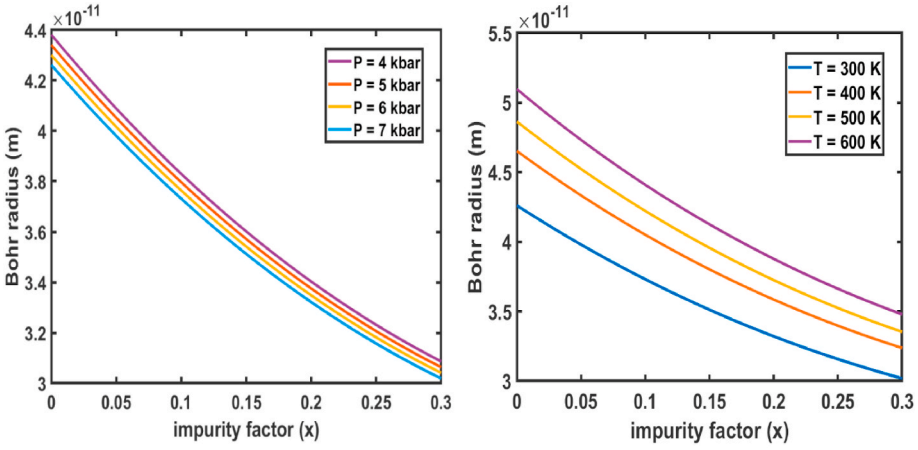

(a) (b)

Fig. 5. Bohr radius variation with the impurity at a different range of (a) pressure and (b) temperature.

magnitude and shifts towards higher photon energies as the impurity increases.

Fig. 5 shows the Bohr radius variation with different hydrogenic impurity factors for different values of pressure and temperature. It is observed that the Bohr radius decreases with increases in impurity due to mass dependence on the impurity factor. Whenever the pressure rises Bohr radius starts to decrease with the smaller value and vice versa for temperature rises as seen in Fig. 5 (a) and (b).

4. Conclusion

In this paper, the influence of hydrogenic impurity on the linear and non-linear optical properties of$In_xGa_{1-x}As$ quantum dot under the presence of an external applied field are demonstrated. It is observed that the dipole matrix elements and the transition energy both are strongly affected by the presence of impurities. Similarly, effects are shown in the case of RICs and THG. Hydrogenic impurity factor (x) inceases the energy gap between two states as a result, the peaks of ACs, RICs and THG shift towards higher incident energies. Whereas, impurity decreases the dipole matrix elements due to which the magnitude of the ACs, RICs and THG peaks decreases. Therefore, it was found that the impurity value caused the blue shifts and decrease in the peaks of linear and non-linear optical properties.

Declaration of competing interest

The authors declare that they have no known competing financial interests or personal relationships that could have appeared to influence the work reported in this paper.

Data availability

No data was used for the research described in the article.

Acknowledgement

Priyanka would like to acknowledge University Grants Commission (UGC) for the financial support. R. Sharma is grateful to Delhi Technological University (DTU) for the research facilities.

References

[1] L. Jiang, H. Wang, H. Wu, Q. Gong, S. Feng, External electric field effect on the hydrogenic donor impurity in zinc-blende GaN/AlGaN cylindrical quantum dot, J. Appl. Phys. 105 (2009), https://doi.org/10.1063/1.3080175.
[2] S.S. Li, J.B. Xia, Electronic structure and binding energy of a hydrogenic impurity in a hierarchically self-assembled GaAs Alx Ga1-x as quantum dot, J. Appl. Phys. 100 (2006), https://doi.org/10.1063/1.2358406.
[3] G. Rezaei, S. Shojaeian Kish, Linear and nonlinear optical properties of a hydrogenic impurity confined in a two-dimensional quantum dot: effects of hydrostatic pressure, external electric and magnetic fields, Superlattice. Microst. 53 (2013) 99–112, https://doi.org/10.1016/j.spmi.2012.09.014.
[4] E. Kasapoglu, H. Sari, I. Sökmen, Binding energy of impurity states in an inverse parabolic quantum well under magnetic field, Phys. B Condens. Matter 390 (2007) 216–219, https://doi.org/10.1016/j.physb.2006.08.016.
[5] F.K. Boz, S. Aktas, Magnetic field effect on the binding energy of a hydrogenic impurity in coaxial GaAs/AlxGa1-xAs quantum well wires, Superlattice. Microst. 37 (2005) 281–291, https://doi.org/10.1016/j.spmi.2005.01.004.
[6] C.A. Duque, A. Montes, A.L. Morales, Binding Energy and Polarizability in GaAs-(Ga,Al)As Quantum-Well Wires, 2001.
[7] E. Niculescu, A. Gearba, G. Cone, C. Negutu, Magnetic field dependence of the binding energy of shallow donors in GaAs quantum-well wires, Superlattice. Microst. 29 (2001) 319–328, https://doi.org/10.1006/spmi.2000.0895.
[8] yu X. li, J.J. Liu, X.J. Kong, The effect of a spatially dependent effective mass on hydrogenic impurity binding energy in a finite parabolic quantum well with a magnetic field, J. Appl. Phys. 88 (2000) 2588–2592, https://doi.org/10.1063/1.1286244.
[9] Y.J. Wang, Y.A. Leem, B.D. McCombe, X.G. Wu, F.M. Peeters, E.D. Jones, J.R. Reno, X.Y. Lee, H.W. Jiang, Strong three-level resonant magnetopolaron effect due to the intersubband coupling in heavily modulation-doped GaAs/AlxGa1-xAs single quantum wells at high magnetic fields, Phys. Rev. B Condens. Matter 64 (2001) 1613031–1613034, https://doi.org/10.1103/PhysRevB.64.161303.
[10] S. Paul, J.B. Roy, P.K. Basu, Empirical expressions for the alloy composition and temperature dependence of the band gap and intrinsic carrier density in GaxIn 1-xAs, J. Appl. Phys. 69 (1991) 827–829, https://doi.org/10.1063/1.348919.
[11] E.B. Al, F. Ungan, U. Yesilgul, E. Kasapoglu, H. Sari, I. Sökmen, Effects of applied electric and magnetic fields on the nonlinear optical properties of asymmetric GaAs/Ga1-xAlxAs double inverse parabolic quantum well, Opt. Mater. 47 (2015) 1–6, https://doi.org/10.1016/j.optmat.2015.06.048.
[12] E. Sadeghi, Electric field and impurity effects on optical property of a three-dimensional quantum dot: a combinational potential scheme, Superlattice. Microst. 50 (2011) 331–339, https://doi.org/10.1016/j.spmi.2011.07.011.
[13] R. Khordad, H. Bahramiyan, The second and third-harmonic generation of modified Gaussian quantum dots under influence of polaron effects, Superlattice. Microst. 76 (2014) 163–173, https://doi.org/10.1016/j.spmi.2014.09.036.
[14] J. Huser, M. Wagner, Energy Spectra of Two Electrons in a Harmonic Quantum Dot, 1991.
[15] P.K. Jha, M. Kumar, S. Lahon, S. Gumber, M. Mohan, Rashba spin orbit interaction effect on nonlinear optical properties of quantum dot with magnetic field, Superlattice. Microst. 65 (2014) 71–78, https://doi.org/10.1016/j.spmi.2013.10.025.
[16] I.Z. Utić*utić*, J. Fabian, S. das Sarma, Spintronics: Fundamentals and Applications, (n.d).
[17] D. Sanjeev Kumar, S. Mukhopadhyay, A. Chatterjee, Effect of Rashba interaction and Coulomb correlation on the ground state energy of a GaAs quantum dot with parabolic confinement, Physica E Low Dimens Syst Nanostruct 47 (2013) 270–274, https://doi.org/10.1016/j.physe.2012.10.030.
[18] S.S. Li, K. Chang, J.B. Xia, K. Hirose, Spin-dependent transport through Cd1−xMnxTe diluted magnetic semiconductor quantum dots, Phys. Rev. B Condens. Matter 68 (2003), https://doi.org/10.1103/PhysRevB.68.245306.
[19] J.E. Hirsch, Spin Hall Effect, 1999.
[20] S.A. Wolf, A.Y. Chtchelkanova, D.M. Treger, Spintronics-A Retrospective and Perspective, 2006. http://www.darpa.mil/dso/.

[21] M. Wierzbicki, Thermoelectric properties of magnetic configurations of graphene-like nanoribbons in the presence of Rashba and spin–orbit interactions, Physica E Low Dimens Syst Nanostruct 87 (2017) 220–227, https://doi.org/10.1016/j.physe.2016.10.033.
[22] H. Hassanabadi, H. Rahimov, L. Lu, C. Wang, Nonlinear optical properties of a three-electron quantum dot with account of the Rashba spinorbit interaction, J. Lumin. 132 (2012) 1095–1100, https://doi.org/10.1016/j.jlumin.2011.12.012.
[23] R. Khordad, Optical properties of wedge-shaped quantum dots under Rashba spin-orbit interaction, Int. J. Mod. Phys. B 31 (2017), https://doi.org/10.1142/S0217979217500552.
[24] S.A. Wolf, A.Y. Chtchelkanova, D.M. Treger, Spintronics-A Retrospective and Perspective, 2006. http://www.darpa.mil/dso/.
[25] H. Hassanabadi, H. Rahimov, L. Lu, C. Wang, Nonlinear optical properties of a three-electron quantum dot with account of the Rashba spinorbit interaction, J. Lumin. 132 (2012) 1095–1100, https://doi.org/10.1016/j.jlumin.2011.12.012.
[26] K. Premasiri, S.K. Radha, S. Sucharitakul, U.R. Kumar, R. Sankar, F.C. Chou, Y. T. Chen, X.P.A. Gao, Tuning Rashba spin-orbit coupling in gated multilayer InSe, Nano Lett. 18 (2018) 4403–4408, https://doi.org/10.1021/acs.nanolett.8b01462.
[27] T. Koga, J. Nitta, T. Akazaki, H. Takayanagi, Rashba spin-orbit coupling probed by the weak antilocalization analysis in [formula presented] quantum wells as a function of quantum well asymmetry, Phys. Rev. Lett. 89 (2002), https://doi.org/10.1103/PhysRevLett.89.046801.
[28] A. Gharaati, Lande g-factor in semiconductor cylinder quantum dots under magnetic fields and spin-orbit interaction, Solid State Commun. 258 (2017) 17–20, https://doi.org/10.1016/j.ssc.2017.04.013.
[29] L. Zhuang, L. Guo, S.Y. Chou, Silicon single-electron quantum-dot transistor switch operating at room temperature, Appl. Phys. Lett. 72 (1998) 1205–1207, https://doi.org/10.1063/1.121014.
[30] M. Kirak, S. Yilmaz, Third harmonic generation of spherical multilayered quantum dot: effects of quantum confinement, impurity, electric and magnetic fields, Appl. Phys. Mater. Sci. Process 128 (2022), https://doi.org/10.1007/s00339-022-05601-1.
[31] R.L. Restrepo, E. Kasapoglu, S. Sakiroglu, F. Ungan, A.L. Morales, C.A. Duque, Second and third harmonic generation associated to infrared transitions in a Morse quantum well under applied electric and magnetic fields, Infrared Phys. Technol. 85 (2017) 147–153, https://doi.org/10.1016/j.infrared.2017.06.005.
[32] H. Bahramiyan, Strain effect on the third-harmonic generation of a two-dimensional GaAs quantum dot in the presence of magnetic field and spin–orbit interaction, Indian J. Phys. 94 (2020) 789–796, https://doi.org/10.1007/s12648-019-01525-4.
[33] L. Liu, J. Li, G. Xiong, Studies of the third-order nonlinear optical susceptibility for in xGa1-xN/GaN cylinder quantum dots, Physica E Low Dimens Syst Nanostruct 25 (2005) 466–471, https://doi.org/10.1016/j.physe.2004.07.017.
[34] E. Sadeghi, Electric field and impurity effects on optical property of a three-dimensional quantum dot: a combinational potential scheme, Superlattice. Microst. 50 (2011) 331–339, https://doi.org/10.1016/j.spmi.2011.07.011.
[35] C.J. Zhang, K.X. Guo, Z.E. Lu, Exciton effects on the optical absorptions in one-dimensional quantum dots, Physica E Low Dimens Syst Nanostruct 36 (2007) 92–97, https://doi.org/10.1016/j.physe.2006.08.009.
[36] W. Xie, Linear and nonlinear optical properties of a hydrogenic donor in spherical quantum dots, Phys. B Condens. Matter 403 (2008) 4319–4322, https://doi.org/10.1016/j.physb.2008.09.021.
[37] P. Başer, I. Altuntas, S. Elagoz, The hydrostatic pressure and temperature effects on hydrogenic impurity binding energies in GaAs/InxGa1-xAs/GaAs square quantum well, Superlattice. Microst. 92 (2016) 210–216, https://doi.org/10.1016/j.spmi.2015.12.010.
[38] S. Paul, J.B. Roy, P.K. Basu, Empirical expressions for the alloy composition and temperature dependence of the band gap and intrinsic carrier density in GaxIn 1-xAs, J. Appl. Phys. 69 (1991) 827–829, https://doi.org/10.1063/1.348919.
[39] Priyanka, R. Sharma, M. Kumar, P. Kumar, Hydrogenic impurity effect on the optical properties of Ga1-xAlxAs quantum wire under terahertz field, Micro and Nanostructures 173 (2023), https://doi.org/10.1016/j.micrna.2022.207451.
[40] G. Rezaei, S. Shojaeian Kish, Linear and nonlinear optical properties of a hydrogenic impurity confined in a two-dimensional quantum dot: effects of hydrostatic pressure, external electric and magnetic fields, Superlattice. Microst. 53 (2013) 99–112, https://doi.org/10.1016/j.spmi.2012.09.014.
[41] R. Khordad, H. Bahramiyan, Optical properties of a GaAs cone-like quantum dot: second and third-harmonic generation, Opt Spectrosc. 117 (2014) 447–452, https://doi.org/10.1134/S0030400X14080165.

Physica B 659 (2023) 414845

Contents lists available at ScienceDirect

Physica B: Condensed Matter

journal homepage: www.elsevier.com/locate/physb

Impurity-modulated physical and transport properties in a $In_xGa_{1-x}As$ double quantum wire

Priyanka, Rinku Sharma *

Department of Applied Physics, Delhi Technological University, Delhi, 110042, India

ARTICLE INFO

Keywords:
Double quantum wire
Spin-orbit interactions
Impurity
Energy dispersion and ballistic conductance

ABSTRACT

In this study, we explore the influence of the temperature, hydrostatic pressure, and impurity on the energy spectrum, and ballistic conductivity of the $In_xGa_{1-x}As$ double QWR. The system is subject to the double-well anharmonic confinement potential under the existence of an intense magnetic field, electric field, Rashba and Dresselhaus SOIs. The energy eigenvalues and the ballistic conductance are calculated with the help of the diagonalization method and Landuer-B ü ttiker formalism, respectively. Moreover, the exploits of energy with the applied electric field, magnetic field, and temperature are also examined. The numerical result illustrates the influence of the temperature, hydrostatic pressure and impurity causing the shifting in the energy dispersion. The oddity in the energy dispersion catalyses the swinging patterns in the ballistic conductivity, and the alteration in the energy introduces the change in the conductance.

1. Introduction

The inspection of physical and transport properties of nanostructures viz. Quantum well (QW), quantum wire (QWR) and quantum dot (QD), have an intense curiosity for the high-performance devices over the past decades in their confining potential applications [1–3]. The scrutiny of the physical and transport properties of nanostructures like QW, QD and QWR, formed by the constrictive charge's motion in bulk structures, offers noteworthy participation to the sprouting invention technology of today. Restricting the motion of charge carriers develops the discrete energy dispersion consequently the optical properties of nanostructures modify [4,5]. The movement of the charge carriers is restricted by the confinement potential which is generally presumed as a harmonic oscillator, gaussian potential, and hard wall potential. Although, there is illustrious problem potential in physics and chemistry which is dealt with under the quartic-well potential and potential profile. Moreover, the double quartic-well potential has been used to illuminate some physical aspects like the occurrence of the doublet, and tunnelling with the help of semi-classical methods and quantum mechanics [6–8]. In this kind of study, energy eigenvalues have been calculated with the assistance of mainly variational perturbation method, WKB approximation etc. Therefore, some engrossing physical appearances of the double-well potential structures have been illustrated by many researchers' notable bulging of the subordinate energy eigenvalues for a system in which two-wells are effectively apart from each other [9,10]. Shi et al. illustrated the double QW structure with enough height potential barrier [11]. Moreover, there are many influences of external perturbative fields which deals with the transport and electronic phenomena related to coupled double-QW that have been focused theoretically [12–14] and experimentally [15–17]. Korepov and Liberman [18] have investigated the theory of two parallel QWs coupled by tunnelling within the existence of a perpendicular magnetic field. Lyo and his colleagues [19] examined the magnetoresistance, conductivity, and mobility of the coupled double-QW within the existence of an externally applied magnetic field. For window-coupled double-QW, the magneto-transport properties have been deliberated by Tang et al. [20].

Furthermore, there is a growing curiosity about the utilisation of the electron spin instead of its information processing and charge storage. The spin and charge of an electron have been used for information processing in the exploration of nanostructures recently. Most of the devices initiate the electron spin via spin-orbit interaction (SOI) [21–23]. The paradigmatic device among all the devices is the "spin field effect transistor" (SFET) designed by Datta Das [24]. Wherein the Rashba SOI helps in controlling the rotation of the electron spin when they pass through the device. Moreover, the Rashba SOI can be modulated by the gate voltage. This kind of interaction arises via the inversion asymmetry of the confining potential within two-dimensional electron gas (2DEG) [25]. Omitting Rashba SOI, the Dresselhaus interaction also

* Corresponding author.
E-mail address: rinkusharma@dtu.ac.in (R. Sharma).

https://doi.org/10.1016/j.physb.2023.414845
Received 4 December 2022; Received in revised form 13 March 2023; Accepted 27 March 2023
Available online 28 March 2023
0921-4526/© 2023 Published by Elsevier B.V.

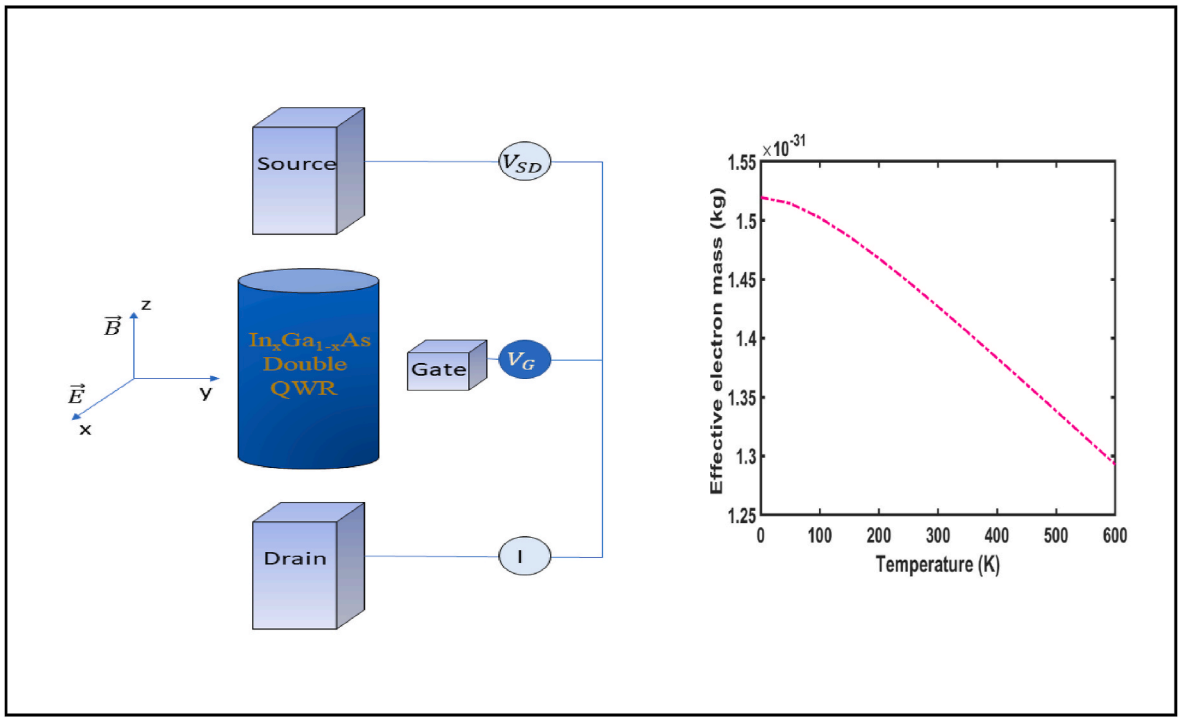

Fig. 1. Schematic view of the $In_xGa_{1-x}As$ double QWR which is coupled to the source and drain reservoirs via tunnel barriers under the presence of external fields and effective mass dependence on the temperature at P = 2 kbar & x = 0.3.

subsidizes the spin-orbit interaction. This classification of interaction arises in the crystal lattice structure due to the bulk inversion asymmetry and having the zinc blende structure. Dresselhaus interaction has two part which includes linear and the cubic term wise to wave vector (k) of an electron whereas, the cubic term is mainly avoided due to the effective linear term. Dresselhaus SOI strength is associated with the sample thickness [26,27]. There is a lot of research has been done along with the Rashba and Dresselhaus SOIs making an impact on the various properties of the nanostructures like physical, optical and transport properties [28–30].

Amid these properties, the transport properties show a pivotal role. The transport properties can be explained by the non-interacting model accordance with the Landuer-Büttiker formalism, the movement of charge carrier gets shifted from one reservoir to the other in the presence of a small biasing across the channel [30,31]. Whenever the electrons are confined in the channel along a transversal direction the distribution of electrons is done by the Fermi-Dirac distribution amongst different sub-bands. The number of modes for the propagation of electrons shows the net ballistic conductivity for the system which can be find out by the fermi-energy and the energy dispersion [32]. Quay et al. [33] established the connection between energy dispersion and the conductance of nanostructure devices. The energy dispersion executed that every sub-band subsidizes $2e^2/h$ to the ballistic conductivity. Moreover, the impact of externally applied fields, SOIs and other parameters like impurity, pressure and temperature on the transport properties of the nanostructure devices have been examined by many researchers [34–37].

The outwardly controlled parameters like temperature, hydrostatic pressure and impurity can manipulate the physical, optical, and electronic characteristics of nanostructures. In the quantum system, the energy spectrum and ballistic conductance can be shifted due to these parameters. As, the temperature, hydrostatic pressure and impurity influence the nanostructure devices' variables like effective mass, energy gap, lattice vibration, dielectric constant and so on [38–40]. Abundant studies have been explored for the discussion of the QWRs under the presence of temperature, pressure, and hydrogenic-trivial impurities. It has become vital to study the doped nanostructure [41,42].

In this current study, the influence of temperature, hydrostatic pressure, and impurity on energy dispersion and ballistic conductance in the presence of Rashba and Dresselhaus SOIs have been investigated. Moreover, we examine the energy exploits along the electric field, magnetic field, and temperature at x = 0 and 0.3. The paper is ordered in this way: Firstly, in section 2 we illustrate the theoretical framework. Formerly, in section 3 we describe the numerical result and discussion, and finally, the conclusion of the paper is represented in section 4.

2. Theory

A quasi-one-dimensional $In_xGa_{1-x}As$ double QWR is considered in which 2DEG and magnetic field applied along the x-y plane and z-direction, respectively. The $In_xGa_{1-x}As$ double QWR is confined by the double-well potential which is written by [43].

$$V(x) = \frac{1}{4}\rho\left(x^2 - \frac{\beta^2}{\rho}\right)^2. \quad (1)$$

Where ρ and β are the positive versatile structural parameters which help in adjusting the barrier's height between the wells and the width of the wells. Assume the double QWR is lie on the x-y plane and the electrons are allowed to move without any restrictions along the y-direction. The intense magnetic and electric field are applied along the z-direction (0, 0, B) and x-direction (E, 0, 0), respectively. The Hamiltonian for the single-particle electron under the occurrence of Rashba and Dresselhaus SOIs in double QWR is written as

$$H = \frac{1}{2m_e(x,P,T)}\left[p_x^2 + \left(p_y^2 + eBx\right)^2\right]\sigma_m + eEx\sigma + \frac{1}{2}g\mu_B B\sigma_z + H_R + H_D \quad (2)$$

Where $m_e(\mu, P, T)$ is known as the effective mass of an electron and having dependence on the impurity, pressure and temperature, e is the electron charge, p_x and p_y are the x and y-components of the momentum, respectively. σ_m is a 2 × 2-unit matrix. G is used for the Lande g-factor, μ_B is called Bohr magneton and σ_z is the Pauli matrix for z-component.

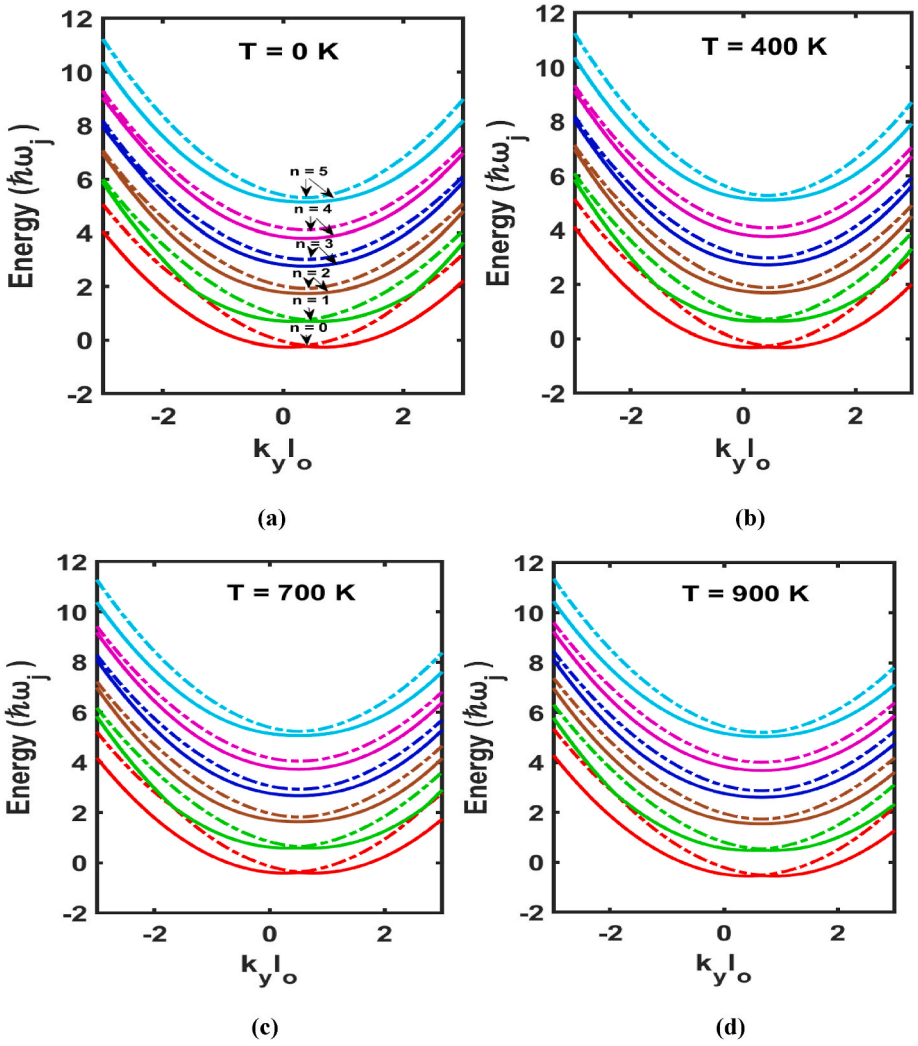

Fig. 2. Energy dispersion curve at the (a) T = 0 K, (b) T = 400 K, (c) T = 700 K, and (d) T = 900 K with P = 4 kbar.

The first and second terms in eq. (2) represents kinetic and confining potential contribution, respectively. Electric field contribution in energy and Zeeman energy splitting is given by the third and fourth terms in eq. (2). The last two terms are known as Rashba and Dresselhaus spin-orbit interaction terms. The expression for $m_e(x,P,T)$, H_R, and H_D are given by Ref. [44]:

$$m_e(x,P,T) = \mathrm{m_o}\left[1 + 7.51\left(\frac{2}{\mathrm{E_g}^j(x,\mathrm{P},\mathrm{T})} + \frac{1}{0.341 + \mathrm{E_g}^j(x,\mathrm{P},\mathrm{T})}\right)\right]^{-1} \quad (3)$$

$\mathrm{m_o}$ is the free electron mass, The energy bandgap ($\mathrm{E_g}^j$) for the $\mathrm{In_xGa_{1-x}As}$ in terms of x, P and T is:

$$\mathrm{E_g}^j(x,\mathrm{P},\mathrm{T}) = \mathrm{E_g}^{GaAs}(P,T) + \left[\mathrm{E_g}^{InAs}(P,T) - \mathrm{E_g}^{GaAs}(P,T)\right]x - 0.475x(1-x) \quad (4)$$

Where $\mathrm{E_g}^{GaAs}(P,T) = \mathrm{E_g}^0 + aP - \frac{bT^2}{T+c}$,

And $\mathrm{E_g}^{InAs}(P,T) = \mathrm{E_{gi}}^0 + uP - \frac{vT^2}{T+w}$.

The values of $\mathrm{E_g}^0 = 1.52$ eV (known as energy gap at P = 0 kbar and T = 0 K), a = 1.08 $\times 10^{-2}$ eV/kbar, b = 50.4 $\times 10^{-5}$ eV/K, and c = 204 K are the pressure coefficient, temperature coefficients, respectively for GaAs. And $\mathrm{E_{gi}}^0 = 0.42$ eV (known as energy gap at P = 0 kbar and T = 0 K), u = 7.7 $\times 10^{-3}$ eV/kbar, v = 41.9 $\times 10^{-5}$ eV/K and w = 271 K are the pressure coefficient, and temperature coefficients, respectively for InAs [45].

And,

$$H_R = \frac{\alpha_R}{\hbar}\left[\sigma_x\left(p_y + eBx\right) - \sigma_y p_x\right] \quad (5)$$

$$H_D = \frac{\alpha_D}{\hbar}\left[\sigma_y\left(p_y + eBx\right) - \sigma_x p_x\right] \quad (6)$$

Here α_R and α_D are the Rashba and Dresselhaus SOIs parameters. σ_x and σ_y are the Pauli matrix for x & y-component, respectively.

Moreover, as a result of the transitional invariance movement along the y-direction, the energy eigenfunctions of Hamiltonian in form of a plane wave are given by

$$\psi(x,y) = \varnothing(x)\exp\left(ik_y y\right) \quad (7)$$

Here, k_y is known as wave number for the plane wave. If the Hamiltonian in eq. (2) becomes separated in the x and y form, the Hamiltonian ($H = H_I + H_{II} + H_R + H_D$) are given by

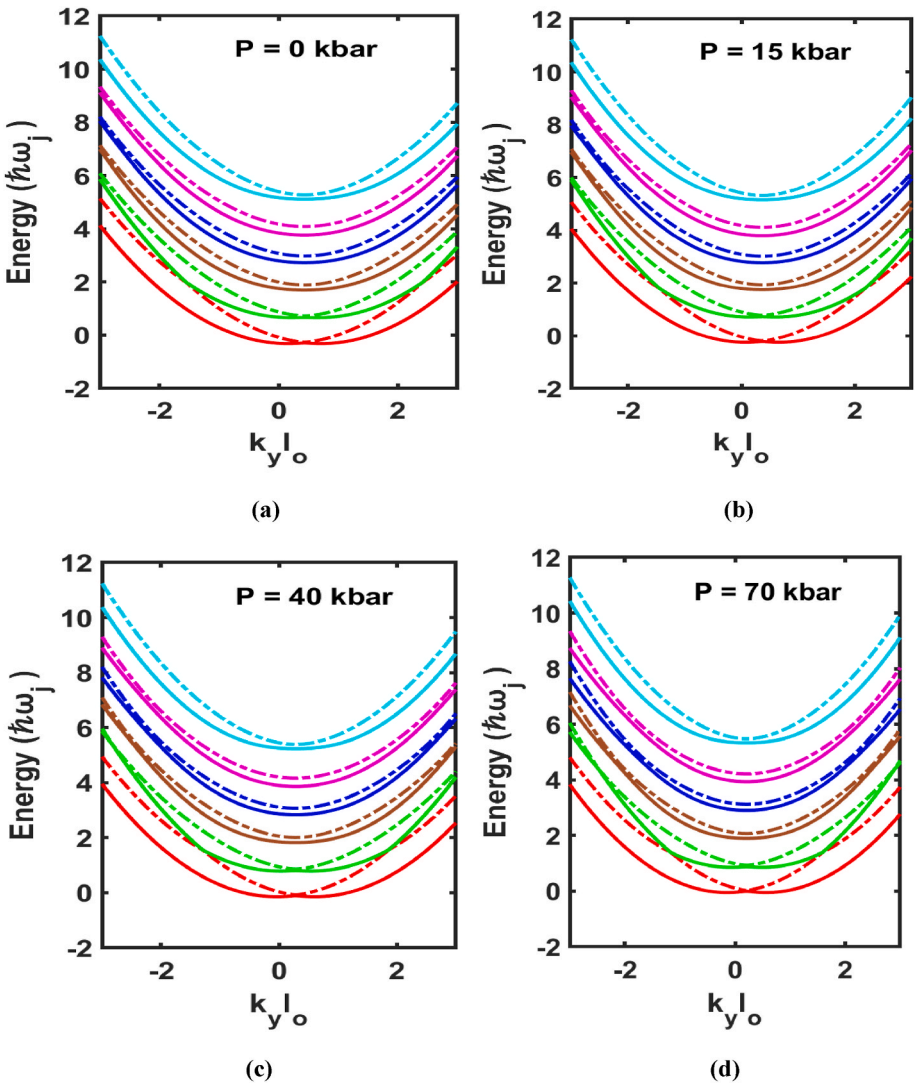

Fig. 3. Energy dispersion curve at the (a) P = 0 kbar, (b) P = 15 kbar, (c) P = 40 kbar, and (d) P = 70 kbar with T = 300 K.

$$H_I = \left[-\frac{\hbar^2}{2m_e(x,P,T)}\frac{d^2}{dx^2} + \frac{1}{2}m_e(x,P,T)\omega^2\left(x - x_j\right)^2 + \frac{\hbar^2 k_y^2}{2m_e(x,P,T)} - \frac{1}{2}m_e(x,P,T)\omega^2 x_j^2 \right]\sigma_m + \frac{1}{2}g\mu_B B\sigma_z$$

$$H_{II} = \left[-\frac{1}{2}\left(m_e(x,P,T)\omega_j^2 + \beta^2\right)x^2 + \frac{1}{4}\rho x^4 + \frac{1}{4}\frac{\mu^4}{\lambda}\right]\sigma_m$$

$$H_R = \alpha_R\left[\sigma_x\left(k_y + \frac{eB}{\hbar}x\right) + i\sigma_y\frac{d}{dx}\right]$$

$$H_D = \alpha_D\left[\sigma_y\left(k_y + \frac{eB}{\hbar}x\right) + i\sigma_x\frac{d}{dx}\right] \quad (8)$$

The variable introduced in the above equation is as follows: $\omega = \sqrt{\omega_j^2 + \omega_c^2}$ is known as effective oscillator frequency and $\omega_c = \frac{eB}{m_e(x,P,T)}$ is the cyclotron frequency. $x_j = -l_j\omega_{jw}^2(\omega_{cj} + el_jE/\hbar\omega_j)$ called guiding centre coordinate with the characteristic length $l_j = \sqrt{\hbar/\, m_e(x,P,T)\omega_j}$ and the diminutive $\omega_{jw} = \omega_j/\omega$, $\omega_{cj} = \omega_c/\omega_j$, and $k_o = l_j k_y$.

The eigenfunctions of Hamiltonian H_I achieve with the help of the Schrödinger equation $H_I\varphi_{n\sigma} = E_{n\sigma}^l\varphi_{n\sigma}$ are written as

$$\varphi_{m\sigma} = \frac{1}{\sqrt{l_j\sqrt{\pi}\omega_{jw}2^n n!}}H_n\left(\frac{x - x_j}{l_j\sqrt{\omega_{jw}}}\right)exp\left(-\frac{1}{2}\left(\frac{x - x_j}{l_j\sqrt{\omega_{jw}}}\right)^2\right)\chi_\sigma \quad (9)$$

With m = 0, 1, 2, 3, …and so on, $\sigma = \pm$, $H_n(x)$ is known as nth order of Hermite polynomial, χ_σ are the spinor function for the spin-up $\chi_+ = \begin{pmatrix}1\\0\end{pmatrix}$ and spin-down $\chi_- = \begin{pmatrix}0\\1\end{pmatrix}$ along z-direction. Eigenenergies for the H_I are given by

$$E_{n\sigma}^l = \frac{1}{\omega_{jw}}\left(n + \frac{1}{2}\right) + \frac{\omega_{jw}^2}{2}\left(k_j^2 - 2k_o\widetilde{E}\omega_{cj} - \widetilde{E}^2\right) \pm \frac{\Delta y}{2} \quad (10)$$

In recent work, we consider l_j as length scale and $\hbar\omega_j$ is the energy scale. $\widetilde{E} = el_jE/\hbar\omega_j$ and $\Delta y = g\mu_B B/\hbar\omega_j$ are the contribution of electric field

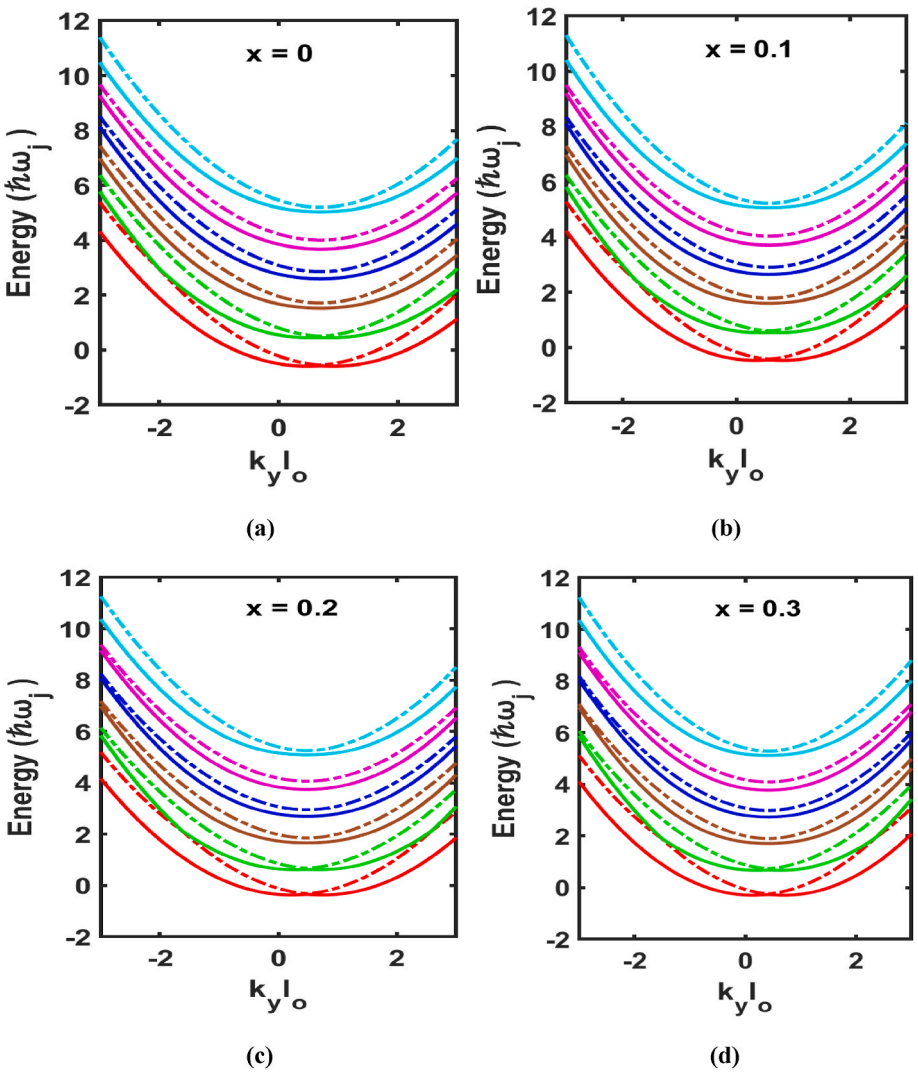

Fig. 4. Energy dispersion curve at the (a) x = 0, (b) x = 0.1, (c) x = 0.2, and (d) x = 0.3 with P = 4 kbar and T = 300 K.

and Zeeman energy in the scaled forms, respectively. As we expand $\varnothing(x) = \sum_{n,\sigma} A_{n\sigma}\varphi_{n\sigma}(x)$ in the form of H_I's eigenfunction therefore the Schrödinger equation corresponding to eq. (9) becomes

$$\left(E^{I}_{n\sigma} - E\right)A_{n\sigma} + \sum_{b,\sigma'=\sigma}(H_{II})^{\sigma\sigma'}_{nb}A_{b\sigma'} + \sum_{b,\sigma'\neq\sigma}(H_R)^{\sigma\sigma'}_{nb}A_{b\sigma'} + \sum_{b,\sigma'\neq\sigma}(H_D)^{\sigma\sigma'}_{nb}A_{b\sigma'} = 0 \tag{11}$$

Where $(H_{II})^{\sigma\sigma'}_{nb} = \langle\varphi_{n\sigma}|H_{II}|\varphi_{b\sigma'}\rangle$ and the matrix elements for this term are expressed as follows

$$(H_{II})^{\sigma\sigma'}_{nb} = P_{b4}\delta_{n.b-4} + P_{b3}\delta_{n.b-3} + P_{b2}\delta_{n.b-2} + P_{b1}\delta_{n.b-1} + P_0\delta_{n.b} + P_{a1}\delta_{n.b+1} + P_{a2}\delta_{n.b+2} + P_{a3}\delta_{n.b+3} + P_{a4}\delta_{n.b+4} \tag{12}$$

Where P factors in the above eq. are given by

$$P_{b4} = \frac{1}{16}\widetilde{\rho}\omega^2_{jw}\sqrt{(n+1)(n+2)(n+3)(n+4)}$$

$$P_{b3} = \frac{1}{4}\widetilde{\rho}\widetilde{x}_j\omega_{jw}\sqrt{2\omega_{jw}(n+1)(n+2)(n+3)}$$

$$P_{b2} = \frac{1}{4}\omega_{jw}\sqrt{(n+1)(n+2)}\left[\widetilde{\rho}\left(3\widetilde{x}_j^2 + \left(n+\frac{3}{2}\right)\right) - \left(1+\widetilde{\beta}^2\right)\right]$$

$$P_{b1} = \frac{1}{2}\widetilde{\rho}\sqrt{2\omega_{jw}(n+1)}\left[\widetilde{\rho}\left(\widetilde{x}_j^2 + \frac{3}{2}\omega_{jw}(n+1)\right) - \left(1+\widetilde{\beta}^2\right)\right]$$

$$P_0 = \frac{1}{4}\widetilde{\rho}\left[\widetilde{x}_j^4 + 3\omega_{jw}\widetilde{x}_j^2(2n+1) + \frac{\widetilde{\beta}^4}{\widetilde{\rho}^2}\right] + \frac{1}{4}\widetilde{\rho}\left[\frac{3}{2}\omega^2_{jw}\left(n^2+n+\frac{1}{2}\right)\right] - \frac{1}{2}\left(1+\widetilde{\beta}^2\right)\left[\widetilde{x}_j^2 + \omega_{jw}\left(n+\frac{1}{2}\right)\right],$$

$$P_{a1} = \frac{1}{2}\widetilde{x}_j\sqrt{2\omega_{jw}n}\left[\widetilde{\rho}\left(\widetilde{\beta}^2 + \frac{3}{2}\omega_{jw}n\right) - \left(1+\widetilde{\beta}^2\right)\right]$$

$$P_{a2} = \frac{1}{4}\omega_{jw}\sqrt{n(n-1)}\left[\widetilde{\rho}\left(3\widetilde{\beta}^2 + \left(n-\frac{1}{2}\right)\right) - \left(1+\widetilde{\beta}^2\right)\right]$$

$$P_{a3} = \frac{1}{4}\widetilde{x}_j\widetilde{\beta}\omega_{jw}\sqrt{2\omega_{jw}n(n-1)(n-2)}$$

$$P_{a4} = \frac{1}{16}\widetilde{x}_j\omega^2_{jw}\sqrt{n(n-1)(n-2)(n-3)}$$

With $\widetilde{x}_j = \frac{x_j}{l_j}$, $\widetilde{\beta} = \frac{\beta}{\sqrt{m_e(x,P,T)\omega_j}}$ and $\widetilde{\rho} = \frac{\rho}{\hbar\omega_j}$.

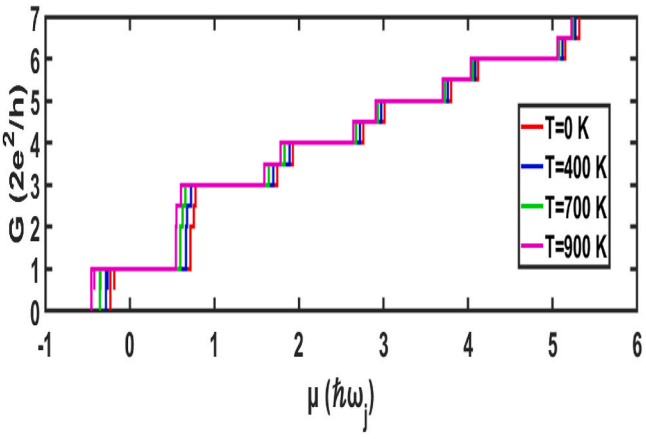

(a)

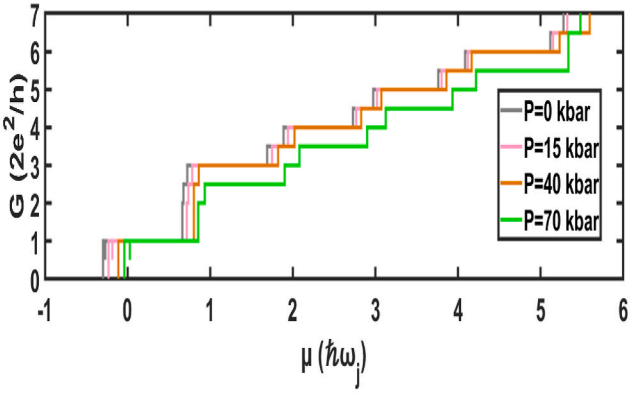

(b)

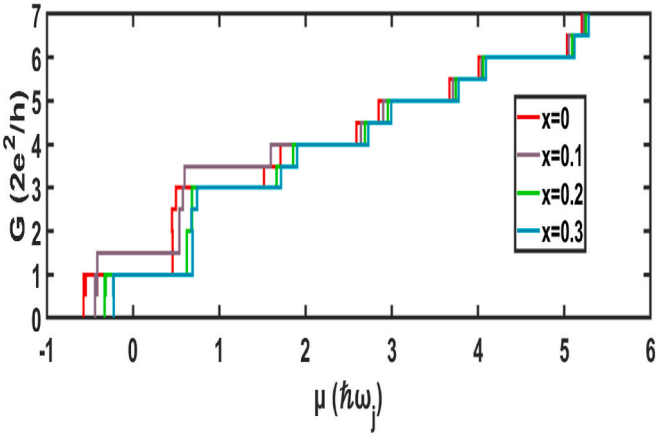

(c)

Fig. 5. (a–c). Ballistic Conductance (G) as a function of chemical potential (μ) for the energy dispersions plot shown in Fig. 2(a–c), Fig. 3(a–c), and Fig. 4(a–c) respectively.

The matrix element of Rashba and Dresselhaus Hamiltonian from eq. (12) $(H_R)_{nb}^{\sigma\sigma'} = \langle\varphi_{n\sigma}|H_R|\varphi_{b\sigma'}\rangle$ and $(H_D)_{nb}^{\sigma\sigma'} = \langle\varphi_{n\sigma}|H_D|\varphi_{b\sigma'}\rangle$, are given by

$$(H_R)_{nn}^{\pm\mp} = \sqrt{2\widetilde{\Delta}_R}\left[k_j\left(1-\omega_{cj}^2\omega_{jw}^2\right) - \omega_{cj}\omega_{jw}^2\widetilde{E}\right] \tag{13}$$

$$(H_R)_{nb}^{\pm\mp} = \sqrt{\frac{2\widetilde{\Delta}_R}{\omega_{jw}}}\left[\left(\omega_{cj}\omega_{jw}\pm 1\right)\sqrt{\frac{(n+1)}{2}}\delta_{n,b-1} + \left(\left(\omega_{cj}\omega_{jw}\mp 1\right)\sqrt{\frac{n}{2}}\delta_{n,b+1}\right]\right. \tag{14}$$

$$(H_D)_{nn}^{\pm\mp} = \mp i\sqrt{2\widetilde{\Delta}_D}\left[k_j\left(1-\omega_{cj}^2\omega_{jw}^2\right) - \omega_{cj}\omega_{jw}^2\widetilde{E}\right] \text{ and} \tag{15}$$

$$(H_R)_{nb}^{\pm\mp} = \mp i\sqrt{\frac{2\widetilde{\Delta}_D}{\omega_{jw}}}\left[\left(\omega_{cj}\omega_{jw}\mp 1\right)\sqrt{\frac{(n+1)}{2}}\delta_{n,b-1} + \left(\left(\omega_{cj}\omega_{jw}\pm 1\right)\sqrt{\frac{n}{2}}\delta_{n,b+1}\right]\right. \tag{16}$$

The scaled Rashba and Dresselhaus SOIs energies are defined as $\widetilde{\Delta}_R = \Delta_{SO}^R/\hbar\omega_j$ and $\widetilde{\Delta}_D = \Delta_{SO}^D/\hbar\omega_j$ with $\Delta_{SO}^R = m_e(x,P,T)\alpha_R^2/2\hbar^2$ and $\Delta_{SO}^D = m_e(x,P,T)\alpha_D^2/2\hbar^2$.

The energy function and energy dispersion relation of the $In_xGa_{1-x}As$ Double QWR under the existence of Rashba and Dresselhaus SOIs can be found by the diagonalization of eq. (11).

For the two microscopic electron reservoirs, the ballistic conductance is calculated with the help of the Landuer-B ü ttiker formalism [46]

$$G = G_j\sum_{\beta\beta'} T_{\beta\beta'} \tag{17}$$

Where, $T_{\beta\beta'}$ called the transition probability from the $|\beta\rangle$ state to $|\beta'\rangle$ state. The G_j is equal to the $2e^2/h$ which is known quantization constant. Considering at the end of the QWR a small bias is applied in between the contacts [47]. Also, assume the non-scattering condition with the unity transition probability. Therefore, the conductance for those systems is written as [48]:

$$G = \frac{2e^2}{h}\sum_{n,s}\sum_{l}\gamma_l^{n,s} f\left(E_m^{n,s}\right), \tag{18}$$

In above equation, n is the level states number, and s is the spin level, $E_m^{n,s}$ is the extremum's point energy, and $f(E_m^{n,s})$ is called Fermi-Dirac distribution function. $\gamma_l^{n,s}$ relays to +1 and −1 for the minimum and maximum points in the energy dispersion respectively.

3. Result

In this paper, the numerical constant for calculation of the physical and transportation properties follows as the structural parameter $\widetilde{\rho} = 1$, $\widetilde{\beta} = 1.5$, $\widetilde{\Delta}_R = 0.2$ and $\widetilde{\Delta}_D = 0.3$ considering the strong constant Rashba and Dresselhaus coupling limit by which tunnelling of an electron in the quantum wire is possible (see Fig. 1).

In Fig. 2, the energy dispersion plots for the variegated temperature i.e.; for T = 0 K, 400 K, 700 K and 900 K with B = 1 T, E = 0.6 × 10^6V/m, α = 25nm meV, and P = 4 kbar. For a better understanding, Here and all consequent energy dispersion is plotted with a different colour in which each energy level contains two sub-bands via two-fold degeneracy: one is presented by the solid line and another one is presented by the dashed line. All solid lines show the quasi spin-down and the dashed line show the quasi spin-up state. Fig. 2(a), shows the energy dispersion in the absence of temperature (T = 0 K), the dispersion curve not intertwined with all the branches at the $k_y = 0$ consequently the existence of the electric field, magnetic field, Rashba and Dresselhaus SOIs. Furthermore, the anti-crossing between the sub-bands is a consequence of the off-diagonal term present in the SOI energy contribution term. And the gap between the two sub-bands is non-uniform by the result of symmetric broken when we applied the magnetic field and SOIs field at the one-time [49]. So that the contribution of magnetic field and SOIs induces the notable separation among the quasi spin-down and spin-up sub-bands. The separation is called the spin-orbit gap. Moreover, the temperature enhances from T = 0 K – 400 K, cause downward (~0.1 $\hbar\omega_j$) and lateral shifting (~0.12) along the positive value of $k_y l_o$ in the energy dispersion as seen in Fig. 2(b). Further enhancement in the temperature (T = 400 K – 900 K) as represented in Fig. 2(b–d), give rise

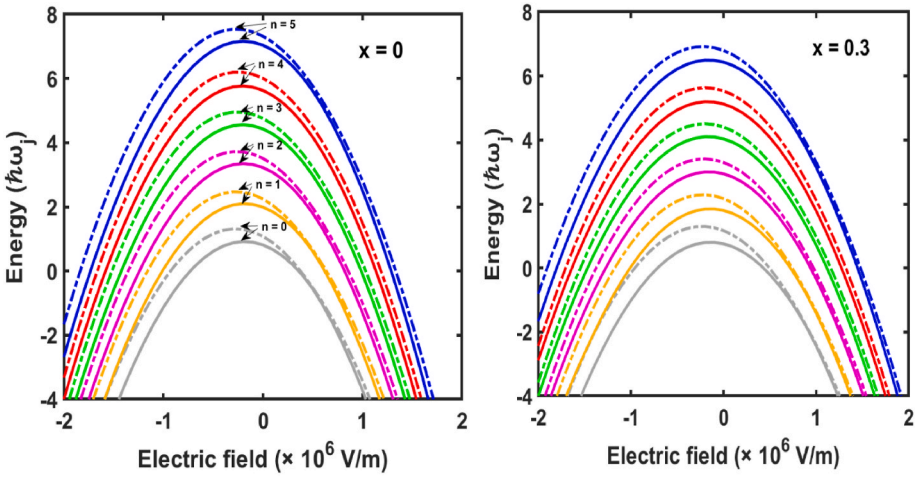

Fig. 6. Energy dependency on the Electric field at (a) x = 0 and (b) x = 0.3.

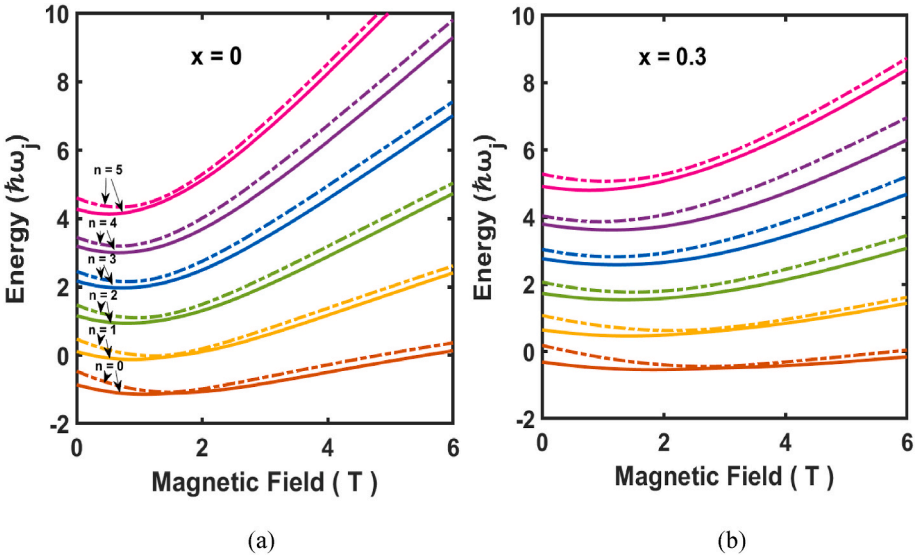

Fig. 7. Energy dependence on the Magnetic field at (a) x = 0 and (b) x = 0.3.

to more downward and laterally shifting due to the dependence of the mass on the temperature. We perceive from Fig. 2(a–d) that energy dispersion shifts as the temperature increase. The cause of these variations is the dependence of the effective mass of the electron on the temperature, given in Eq. (3). It is assistance citing that by enhancing the temperature, the wave function associated with the electron becomes more scattered.

Scrutiny of the $In_xGa_{1-x}As$ QWR with the external perturbation is influential for the administration of the physical and transport properties. And is fruitful to inspect the influence of the temperature and pressure on the dispersion curves. Therefore, in Fig. 3(a–d) we concentrate on the effect of pressure on energy dispersion with T = 300K.. When the pressure is enhanced from P = 0 – 70 kbar the energy dispersion shows two types of shifting first one is upward shifting (∼0.12 $\hbar\omega_j$) and the other one is laterally shifting (∼0.11) along the negative value of $k_y l_o$. The shifting in the energy dispersion with an increase in pressure determines the effective geometry of the QWR. The total shifting in the dispersion depends on the pressure values. Shifting is large when we provide high pressure in the system. Whereas, the interplay between the external fields and SOIs regulates the advent of camel-back shapes, anti-crossing and crossing formations.

To show the influence of impurity on energy dispersion, we begin the study of the energy dispersion in the absence of impurities after that we introduce and enhance the impurity in the system at P = 4 kbar and T = 300 K. It is shown from Fig. 4(a–d) that when the impurity is introduced the dispersion starts to shift upward and the negative value of $k_y l_o$. The separation between the sub-bands is used to determine the chemical potential value required for the conductance. And the anti-crossing in the dispersion generates a dip in the conductance curve. Therefore, the variation in the energy dispersion as a result of impurity produces the variation in the conductance also.

In Fig. 5(a–c), we represent the consequence of temperature, hydrostatic pressure, and impurity factor on the ballistic conductivity of the $In_xGa_{1-x}As$ double QWR. Following the Landuer-B $\ddot{u}$ tter formalism, the ballistic conductivity of a 1D nanostructure is linked with the two electrons reservoir at the microscopic level where we must neglect the electron-electron repulsion. Furthermore, the extreme points (maximum/minimum points) present in the energy spectrum cause the staircase structure (decrement/increment) in the conductance with the step size of $2e^2/h$. The increment in the energy spectrum opens more propagating channels due to which ballistic conductance has a staircase

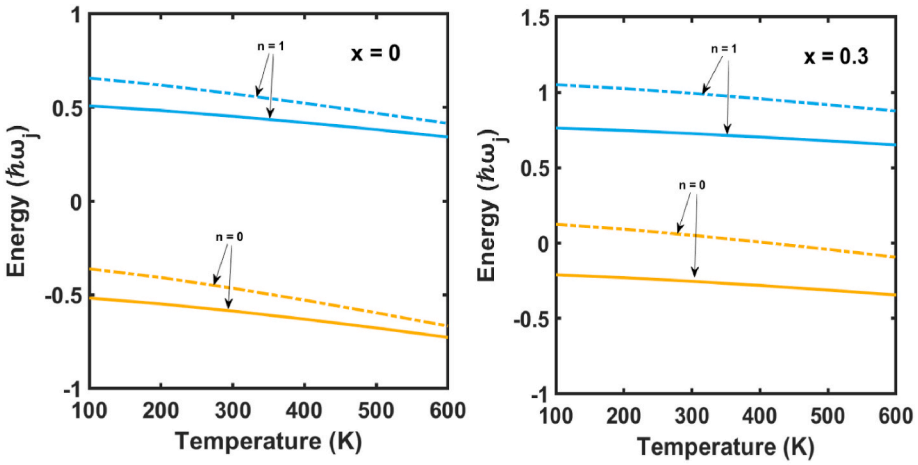

(a) (b)

Fig. 8. Energy dependency on the temperature at (a) x = 0 and (b) x = 0.3.

shape. From Fig. 2(a–d), 3(a-d) and 4(a-d), each extremum points in the energy dispersion create the decrement and increment of an integer $2e^2/h$ in the ballistic conductance [50]. Whenever the energy sub-bands split the conductance's chemical potential starts to grow. The foremost contribution in the conductivity arises from the lowest minimum point in these energy dispersion curves whereas, the second contribution arises due to the 2nd minimum point of the same sub-band. At each time when chemical potential passes through the local maximum points, the conductivity of the system decreases by the integer factor $2e^2/h$. The staircase structure is generated in Fig. 5(a–c) by using these mechanics. Therefore, when we provide the temperature: 0 K, 400 K, 700 K, and 900 K, the ballistic conductance is represented by the stepwise increment shown in Fig. 5(a). The temperature rise requires a low chemical potential for conductivity. Whereas, when we increase the pressure (P = 0 kbar – 70 kbar) and impurity (x = 0 to 0.3) higher value of chemical potential is required represented by Fig. 5(b and c).

In Fig. 6(a–b), the energy dispersion versus electric field plot is shown for x = 0 and 0.3. This is noticeable that the positive and negative values of the electric field give escalation to a uniform structure. Moreover, the splitting between the sub-bands bloat and whole the spin branches basin in the direction of the small energy states. Whenever we introduce impurity the energy plot with an electric field starts to shift in the downward direction. Subsequently, Fig. 7(a–b), represents the spectra of energy sub-bands with the magnetic field for the x = 0 and x = 0.3. It is observed that all the branches of the energy spectrum increase with the increment in the intense magnetic field. And when the impurity is introduced, the whole spectrum shifts towards high energy. Therefore, the confinement potential enhances with the separation between the sub-bands while lifting degeneracy in every sub-bands. Simultaneous, contribution of magnetic field and impurity familiarize the remarkable separation in spin-up and spin-down of the energy levels. Fig. 8(a–b), represents the energy necessity on the applied temperature for the x = o and 0.3. It is easily espied that the energy for the lower energy state (n = 0 and 1) starts decreasing with the rise in the temperature.

4. Conclusion

In this research, we focused on the energy spectrum and ballistic conductivity for the $In_xGa_{1-x}As$ QWR. The effect of temperature, hydrostatic pressure and SOIs fields along with the impurity on the energy spectrum and ballistic conductance have been examined. The results of our arithmetical scheming bear that: the variation in the temperature shifts the energy dispersion in the downward direction and the ballistic conductance steps along with the axis of chemical potential start shifting towards a lower value of chemical potential as a consequence of the reduction in energy with the rise in temperature easily noticeable. The effect of the variation in the pressure causes the upward shifting in the energy dispersion as a result conductivity of the QWR starts changing. Furthermore, the change in the impurity factor causes the variation in the energy dispersion and in the ballistic conductance of the $In_xGa_{1-x}As$ QWR. Whereas, the conductivity of the QWR is influenced by the strength of the externally applied field, confinement potential shape, SOIs and impurity concentration. The extremum points (maximum and minimum) in the energy dispersion create the changes (rise and deduction) in the steps of conductivity by the factor of $2e^2/h$. Moreover, the growth in the ballistic conductance has mainly in the form of a stepwise profile along with the integer conductivity, omitting the existence of abnormal formalism viz. Camelback-like structure, sub-bands anti-crossing generates numerous extreme points in the energy spectrum as a consequence of this the small dips, troughs or crests are created in the steps of ballistic conductance. The outcomes of these expedite significant results and are used for adjusting the characterisation of nanostructures, optical, physical, and transport properties of the QWR system. It is also useful for the manufacturing of nanoscale electronic devices, spin filters and future molecules. For a better understanding of the transport mechanism at microscopic level, we must securitize the Eigen channels of conductivity which is demonstrated by other studies in a meantime. Therefore, the study of transport properties of nanostructures has attracted vast activity due to high potentiality for the design of optoelectronic devices applications, spin filter and far infrared laser amplifiers, high-speed electrooptical modulators and photodetectors.

Author contributions

Priyanka: Methodology, Software, Validation, Formal analysis, Data curation, Writing – original draft, Conceptualization, Formal analysis, Writing – review & editing, Visualization; **Rinku Sharma**: Resources, Investigation, Supervision, Writing – review & editing, Project administration.

Declaration of competing interest

The authors declare that they have no known competing financial interests or personal relationships that could have appeared to influence the work reported in this paper.

Data availability

No data was used for the research described in the article.

Acknowledgement

Priyanka appreciates the financial help from the University Grants Commission and R. Sharma is grateful for the research facilities by Delhi Technological University.

References

[1] T. Sugaya, K.Y. Jang, C.K. Hahn, M. Ogura, K. Komori, A. Shinoda, K. Yonei, Enhanced peak-to-valley current ratio in InGaAs/InAlAs trench-type quantum-wire negative differential resistance field-effect transistors, J. Appl. Phys. 97 (2005), https://doi.org/10.1063/1.1851595.

[2] M.G. Barseghyan, A.A. Kirakosyan, C.A. Duque, Hydrostatic pressure,electric and magnetic field effects on shallow donor impurity states and photoionization cross section in cylindrical GaAs-Ga1-xAlxAs quantum dots, Phys. Status Solidi B 246 (2009) 626–629, https://doi.org/10.1002/pssb.200880516.

[3] M.G. Barseghyan, M.E. Mora-Ramos, C.A. Duque, Hydrostatic pressure, impurity position and electric and magnetic field effects on the binding energy and photo-ionization cross section of a hydrogenic donor impurity in an InAs Pöschl-Teller quantum ring, Eur. Phys. J. B 84 (2011) 265–271, https://doi.org/10.1140/epjb/e2011-20650-7.

[4] S. Banerjee, A. Dan, D. Chakravorty, Review Synthesis of Conducting Nanowires, (n.d).

[5] K.I. Kolokolov, S.D. Beneslavski, N.Y. Minina, A.M. Savin, Far-infrared intersubband absorption in p-type GaAs/AlxGa1−xAs single heterojunctions under uniaxial compression, Phys. Rev. B Condens. Matter 63 (2001), https://doi.org/10.1103/PhysRevB.63.195308.

[6] A.E. Sitnitsky, Exact Solution of Schr\"odinger Equation with Symmetric Double-Well Potential versus WKB: Accuracy for Ground State Splitting, 2018. http://arxiv.org/abs/1801.03733.

[7] E. Gildener, A. Patrascioiu, Pseudoparticle Contributions to the Energy Spectrum of a One-Dimensional System*, 1977.

[8] K.S.U. Kansanen, Theory for Polaritonic Quantum Tunneling, 2022. http://arxiv.org/abs/2204.13490.

[9] G. Thorgilsson, C.S. Tang, V. Gudmundsson, Time-dependent magnetotransport of a wave packet in a quantum wire with embedded quantum dots, Phys. Rev. B Condens. Matter 76 (2007), https://doi.org/10.1103/PhysRevB.76.195314.

[10] S.C. Arapan, M.A. Liberman, S.v. Korepov, B. Johansson, Conductance of a disordered double quantum wire in a magnetic field: boundary roughness scattering, Phys. Rev. B Condens. Matter 67 (2003) 11, https://doi.org/10.1103/PhysRevB.67.115328.

[11] J.-R. Shi, B.-Y. Gu, Magnetoconductance Oscillations of Two Parallel Quantum Wires Coupled through a Potential Barrier, 1997.

[12] Y. Karaaslan, B. Gisi, S. Sakiroglu, E. Kasapoglu, H. Sari, I. Sokmen, Electric and magnetic field modulated energy dispersion, conductivity and optical response in double quantum wire with spin-orbit interactions, Physics Letters, Section A: General, Atomic and Solid State Physics 382 (2018) 507–515, https://doi.org/10.1016/j.physleta.2017.12.018.

[13] N.R. Abdullah, C.S. Tang, V. Gudmundsson, Time-dependent magnetotransport in an interacting double quantum wire with window coupling, Phys. Rev. B Condens. Matter 82 (2010), https://doi.org/10.1103/PhysRevB.82.195325.

[14] G.R. Aizin, N.J.M. Horing, L.G. Mourokh, V.M. Kovalev, Current driven electromagnetic wave amplification by double quantum wire superlattice, J. Appl. Phys. 96 (2004) 4225–4232, https://doi.org/10.1063/1.1792807.

[15] N.R. Abdullah, C.S. Tang, V. Gudmundsson, Time-dependent magnetotransport in an interacting double quantum wire with window coupling, Phys. Rev. B Condens. Matter 82 (2010), https://doi.org/10.1103/PhysRevB.82.195325.

[16] B. Brun, F. Martins, S. Faniel, B. Hackens, G. Bachelier, A. Cavanna, C. Ulysse, A. Ouerghi, U. Gennser, D. Mailly, S. Huant, V. Bayot, M. Sanquer, H. Sellier, Wigner and Kondo physics in quantum point contacts revealed by scanning gate microscopy, Nat. Commun. 5 (2014), https://doi.org/10.1038/ncomms5290.

[17] S. Bandyopadhyay, W. Porod, Double Quantum Wire Aharonov-Bohm Interferometers For possible LN2 Temperature Operation, 1989.

[18] S. v Korepov, M.A. Liberman, Tunnel-coupled Double Quantum Wires in a Magnetic Field: Electron Scattering on Impurities and Boundary Roughness, 2002.

[19] L.W. Smith, W.K. Hew, K.J. Thomas, M. Pepper, I. Farrer, D. Anderson, G.A. C. Jones, D.A. Ritchie, Row coupling in an interacting quasi-one-dimensional quantum wire investigated using transport measurements, Phys. Rev. B Condens. Matter 80 (2009), https://doi.org/10.1103/PhysRevB.80.041306.

[20] C.S. Tang, V. Gudmundsson, Coherent magnetotransport spectroscopy in an edge-blocked double quantum wire with window and resonator coupling, Phys. Rev. B Condens. Matter 74 (2006), https://doi.org/10.1103/PhysRevB.74.195323.

[21] J.P. Heida, B.J. van Wees, J.J. Kuipers, T.M. Klapwijk, G. Borghs, Physical Review B 15, 1998. MAY 1998-I VOLUME.

[22] A.A. Burkov, A.S. Núñez, A.H. MacDonald, Theory of spin-charge-coupled transport in a two-dimensional electron gas with Rashba spin-orbit interactions, Phys. Rev. B Condens. Matter 70 (2004), https://doi.org/10.1103/PhysRevB.70.155308.

[23] X.F. Wang, P. Vasilopoulos, Magnetotransport in a two-dimensional electron gas in the presence of spin-orbit interaction, Phys. Rev. B Condens. Matter 67 (2003), https://doi.org/10.1103/PhysRevB.67.085313.

[24] A. Łusakowski, J. Wróbel, T. Dietl, Effect of bulk inversion asymmetry on the Datta-Das transistor, Phys. Rev. B Condens. Matter 68 (2003), https://doi.org/10.1103/PhysRevB.68.081201.

[25] A. Manchon, H.C. Koo, J. Nitta, S.M. Frolov, R.A. Duine, New Perspectives for Rashba Spin-Orbit Coupling, (n.d).

[26] D.v. Bulaev, D. Loss, Spin relaxation and anticrossing in quantum dots: Rashba versus Dresselhaus spin-orbit coupling, Phys. Rev. B Condens. Matter 71 (2005), https://doi.org/10.1103/PhysRevB.71.205324.

[27] M.K. Jana, R. Song, H. Liu, D.R. Khanal, S.M. Janke, R. Zhao, C. Liu, Z. Valy Vardeny, V. Blum, D.B. Mitzi, Organic-to-inorganic structural chirality transfer in a 2D hybrid perovskite and impact on Rashba-Dresselhaus spin-orbit coupling, Nat. Commun. 11 (2020), https://doi.org/10.1038/s41467-020-18485-7.

[28] R. Khordad, Optical properties of quantum wires: Rashba effect and external magnetic field, J. Lumin. 134 (2013) 201–207, https://doi.org/10.1016/j.jlumin.2012.08.047.

[29] V. Galitski, I.B. Spielman, Spin-orbit coupling in quantum gases, Nature 494 (2013) 49–54, https://doi.org/10.1038/nature11841.

[30] S. Pramanik, S. Bandyopadhyay, M. Cahay, Energy dispersion relations of spin-split subbands in a quantum wire and electrostatic modulation of carrier spin polarization, Phys. Rev. B Condens. Matter 76 (2007), https://doi.org/10.1103/PhysRevB.76.155325.

[31] Y.v. Pershin, S.N. Shevchenko, I.D. Vagner, P. Wyder, Electronic transport through a nuclear-spin-polarization-induced quantum wire, Phys. Rev. B Condens. Matter 66 (2002) 1–5, https://doi.org/10.1103/PhysRevB.66.035303.

[32] Y.v. Pershin, J.A. Nesteroff, V. Privman, Effect of spin-orbit interaction and in-plane magnetic field on the conductance of a quasi-one-dimensional system, Phys. Rev. B Condens. Matter 69 (2004), https://doi.org/10.1103/PhysRevB.69.121306.

[33] C.H.L. Quay, T.L. Hughes, J.A. Sulpizio, L.N. Pfeiffer, K.W. Baldwin, K.W. West, D. Goldhaber-Gordon, R. de Picciotto, Observation of a one-dimensional spin-orbit gap in a quantum wire, Nat. Phys. 6 (2010) 336–339, https://doi.org/10.1038/nphys1626.

[34] J.A. Nesteroff, Y.v. Pershin, V. Privman, Polarization of nuclear spins from the conductance of quantum wire, Phys. Rev. Lett. 93 (2004), https://doi.org/10.1103/PhysRevLett.93.126601.

[35] Y.v. Pershin, J.A. Nesteroff, V. Privman, Effect of spin-orbit interaction and in-plane magnetic field on the conductance of a quasi-one-dimensional system, Phys. Rev. B Condens. Matter 69 (2004), https://doi.org/10.1103/PhysRevB.69.121306.

[36] X.F. Wang, Spin transport of electrons through quantum wires with a spatially modulated Rashba spin-orbit interaction, Phys. Rev. B Condens. Matter 69 (2004), https://doi.org/10.1103/PhysRevB.69.035302.

[37] P. Dahan, I.D. Vagner, Nuclear spin relaxation rate of magnetic impurities in quantum Hall effect systems, Phys. Rev. B Condens. Matter 72 (2005), https://doi.org/10.1103/PhysRevB.72.115328.

[38] F. Segovia-Chaves, H. Vinck-Posada, The effect of the hydrostatic pressure and temperature on the defect mode in the band structure of one-dimensional photonic crystal, Optik 156 (2018) 981–987, https://doi.org/10.1016/j.ijleo.2017.12.037.

[39] L. Bouzaïene, R. ben Mahrsia, M. Baira, L. Sfaxi, H. Maaref, Hydrostatic pressure and temperature effects on nonlinear optical rectification in a lens shape InAs/GaAs quantum dot, J. Lumin. 135 (2013) 271–275, https://doi.org/10.1016/j.jlumin.2012.09.032.

[40] W. Xie, Impurity effects on optical property of a spherical quantum dot in the presence of an electric field, Physica B (Amsterdam, Neth.) 405 (2010) 3436–3440, https://doi.org/10.1016/j.physb.2010.05.019.

[41] E. Sadeghi, Electric field and impurity effects on optical property of a three-dimensional quantum dot: a combinational potential scheme, Superlattice. Microst. 50 (2011) 331–339, https://doi.org/10.1016/j.spmi.2011.07.011.

[42] E.B. Al, F. Ungan, U. Yesilgul, E. Kasapoglu, H. Sari, I. Sökmen, Effects of applied electric and magnetic fields on the nonlinear optical properties of asymmetric GaAs/Ga1-xAlxAs double inverse parabolic quantum well, Opt. Mater. 47 (2015) 1–6, https://doi.org/10.1016/j.optmat.2015.06.048.

[43] E. Gildener, A. Patrascioiu, Pseudoparticle Contributions to the Energy Spectrum of a One-Dimensional System*, 1977.

[44] P. Başer, I. Altuntas, S. Elagoz, The hydrostatic pressure and temperature effects on hydrogenic impurity binding energies in GaAs/InxGa1-xAs/GaAs square quantum well, Superlattice. Microst. 92 (2016) 210–216, https://doi.org/10.1016/j.spmi.2015.12.010.

[45] S. Paul, J.B. Roy, P.K. Basu, Empirical expressions for the alloy composition and temperature dependence of the band gap and intrinsic carrier density in GaxIn 1-xAs, J. Appl. Phys. 69 (1991) 827–829, https://doi.org/10.1063/1.348919.

[46] Y. Imry, R. Landauer, Conductance Viewed as Transmission, (n.d).
[47] G. Möller, R. Moessner, Magnetic multipole analysis of kagome and artificial spin-ice dipolar arrays, Phys. Rev. B Condens. Matter 80 (2009), https://doi.org/10.1103/PhysRevB.80.140409.
[48] I.A. Kokurin, Determination of Rashba-coupling strength for surface two-dimensional electron gas in InAs nanowires, Solid State Commun. 195 (2014) 49–54, https://doi.org/10.1016/j.ssc.2014.07.002.
[49] R. Sharma, M.Kumar Priyanka, Effect of hydrostatic pressure and temperature on the ballistic conductance under the influence of Rashba spin-orbit coupling, Physica B (Amsterdam, Neth.) 648 (2023), https://doi.org/10.1016/j.physb.2022.414402.
[50] B.H. Mehdiyev, A.M. Babayev, S. Cakmak, E. Artunc, Rashba spin-orbit coupling effect on a diluted magnetic semiconductor cylinder surface and ballistic transport, Superlattice. Microst. 46 (2009) 593–602, https://doi.org/10.1016/j.spmi.2009.08.009.